SYNTHESIS AND CHARACTERIZATION OF NOVEL METAL COMPLEXES AND THEIR INTERACTION WITH THERAPEUTIC BIOTARGETS

ABSTRACT

THESIS

SUBMITTED FOR THE AWARD OF THE DEGREE OF

Doctor of Philosophy

IN

CHEMISTRY

BY

Waddhaah Mohammed Abdulgaleel

Under the Supervision of

Prof. Sartaj Tabassum

DEPARTMENT OF CHEMISTRY
ALIGARH MUSLIM UNIVERSITY
ALIGARH (INDIA)

2012

Medicinal inorganic chemistry –a sub discipline of bioinorganic chemistry is one of the most rapidly developing areas of pharmaceutical research. This field gained momentum after the prototypical success story of platinum based anticancer drug cisplatin, cis diamminedichloro platinum(II), cis–[$Pt(NH_3)_2Cl_2$)] for treating solid cancers in particular, testicular, ovarian, small cell lung, head and neck cancers. Despite its success, there were serious concerns of this drug regarding its toxicity, intrinsic resistance, narrow spectrum of activity for phenotypes of cancer and patient compliance. Therefore, studies pertaining to essential metallo elements received much more attention in contrast to Pt, since the drugs designed and synthesized from endogenous metal ions may be less harmful and more prone to antiproliferative activity against tumors. Much of the attention has been laid towards the design of metal–based cancer chemotherapeutics, predominantly Cu(II), Co(II) and Zn(II) complexes (endogenously biocompatible metal ion which are present as integral part of the active site of metalloprotein and thus familiarize their coordination with human body's function) with active ligand pharmacophore. In particular, these metal complexes could efficiently bind and cleave DNA, thereby exert artificial nuclease activity. The development of artificial nucleases with improved efficiency and selectivity is in high demand and requires binuclear metal centers to achieve a synergistic effect in the process of substrate recognition and scission.

Additionally, it has been demonstrated that free radicals can damage proteins, lipids and DNA of bio–tissues, leading to increased rate of cancer. Redox behaviour of metal ion plays an important role in enzymatic activity and scavenge toxic ROS species. The superoxide radical anion; $O_2^{\cdot-}$ (a by product of normal cellular respiration) and protects cells from damage induced by reactive oxygen species (ROS). SOD catalyzes

disproportionates superoxide to dioxygen and hydrogen peroxide, which later on decomposes to water and dioxygen by catalase. Transition metal complexes have shown remarkable antioxidant and DNA–binding properties which have been proven effective in cancer chemotherapy. DNA–complex binding causes distortion of the helical structure and results in inhibition of DNA replication and transcription, thereby cell death. Ligand scaffolds are also considered important in muting the toxicity of the metallodrug as well tailored multifunctional ligands offer exciting possibilities by providing appropriate anchoring sites for the metal ions, matching the structural motif at the molecular target and restricting the geometry.

The specific delivery of a drug to their target cells may be achieved by the use of targeting groups or by tuning the chemical and physical characteristics of the drug or drug carrier, such as hydrophobicity and molecular size. Different types of macromolecules (liposomes, dendrimers, polyethylene glycol polymers, nanoparticles, and protein biomolecules) have been used as carrier molecules. In particular, HSA is the most multifunctional transport protein and plays an important role in the transport and deposition of a variety of endogenous and exogenous substances in blood. The interaction of metal ions with small peptides has been a subject of great interest for bioinorganic chemists. Copper is the center of the active site of various metalloproteins and plays vital role in biological processes like electron transfer, endogenous oxidative DNA damage associated with aging and cancer.

The thesis embodies the synthesis and characterization of new metallated chemical entities for use as antitumor agents. DNA is the primary cellular target for most of the chemotherapeutic agents therefore, preliminary *in–vitro* DNA binding profile of these

metal–based chemical entities were carried out by employing various bio–physical techniques. These studies are of paramount importance as the mode of binding to DNA gives an insight for the rationale of robust drug design. Our studies reveal that these complexes are capable of binding non–covalently to DNA and thereby they can act as efficient chemotherapeutic agents; however for the effective delivery of the potential drugs to the desired target, a strategy employing a protein carrier molecule is necessary to improve the pharmacokinetic profile of the drug or to target the drug to the pathogenic site addressing diseases. We have carried out binding studies with HSA to demonstrate specific targeted binding to the molecular DNA at the same time using HSA as a carrier protein.

The thesis is divided in six chapters which includes **Chapter I "Introduction"** giving a detail overview of literature relevant to this field and also helps to justify the objectives of the work done. **Chapter II** is **"Experimental"** where all details of methods and physical measurements employed in this work are given. **Chapter III–VI** embodies the molecular design, synthesis of novel metal–based potential chemotherapeutic agents and exploring their *in–vitro* binding propensity towards the specific target DNA and HSA at the molecular level.

Chapter III deals with the synthesis of the new dinuclear copper(II) complex as metallopeptide drug $[Cu_2(glygly)_2(ppz)(H_2O)_4]\cdot 2H_2O$ achieved by mixing stoichiometric amounts of Cu(II) nitrate trihydrate with glycyl glycine anion (glygly) followed by reaction with piperazine (pip) hexahydrate. Molecular structure of representative complex $[Cu_2(glygly)_2(ppz)(H_2O)_4].2H_2O$ was determined by single X ray crystallogrphically. The crystal obtained was monoclinic with space group P21/c. The *in vitro* DNA binding

studies of complex $[Cu_2(glygly)_2(ppz)(H_2O)_4].2H_2O$ with CT DNA were carried out by employing UV–vis, fluorescence and circular dichroism which reveal electrostatic interaction *via* groove binding mode. Complex $[Cu_2(glygly)_2(ppz)(H_2O)_4].2H_2O$ cleaves pBR322 DNA *via* an oxidative mechanism and strongly binds to the DNA minor groove. Furthermore, complex $[Cu_2(glygly)_2(ppz)(H_2O)_4].2H_2O$ exhibits significant inhibitory effect on the catalytic activity of topoisomerase I at a very low concentration, ~12.5 μM, additionally it behaves as an excellent SOD mimic (IC_{50} ~ 0.086 μM). The molecular docking technique was also utilized to ascertain the mechanism and mode of action towards the molecular target DNA and enzymes.

In the second part of **chapter III**, the interaction of new dinuclear copper(II) complex $[Cu_2(glygly)_2(ppz)(H_2O)_4].2H_2O$ with human serum albumin (HSA) was examined by means of fluorescence spectroscopy which revealed that complex $[Cu_2(glygly)_2(ppz)(H_2O)_4].2H_2O$ has a strong ability to quench the intrinsic fluorescence of HSA through static quenching pathway. The alterations of HSA secondary structure in presence of complex $[Cu_2(glygly)_2(ppz)(H_2O)_4].2H_2O$ were confirmed by UV–visible, FT–IR, CD and 3D fluorescence spectroscopy. The binding constants (K), and binding site number (n), corresponding thermodynamic parameters ΔG, ΔH and ΔS at different temperatures were also calculated. The molecular docking technique was utilized to ascertain the mechanism and mode of action towards the molecular target HSA, indicating that complex $[Cu_2(glygly)_2(ppz)(H_2O)_4].2H_2O$ was located to the entrance of site I by electrostatic and hydrophobic forces. Complex $[Cu_2(glygly)_2(ppz)(H_2O)_4].2H_2O$ showed efficient photo–induced HSA cleavage activity, indicating the involvement of hydroxyl radicals as the reactive species. Furthermore, the cytotoxicity of

$[Cu_2(glygly)_2(ppz)(H_2O)_4].2H_2O$ was examined on a panel of human cancer cell lines of different histological origins revealing moderate GI_{50} values specifically towards MIAPACA2, A498 and A549 cell lines. These results complement the previous biological studies for specific targeted metallopeptide, providing additional information about the possibility of transport and disposition in blood plasma.

Chapter IV describes synthesis of new water soluble complex $[Zn(glygly)(ssz)(H_2O)].6H_2O$ derived from dipeptide (glycyl glycine anion) and sulfasalazine (ssz) and its characterization by spectroscopic (IR, UV–vis, NMR, ESI–MS) and analytical methods. The *in vitro* DNA binding studies of complex $[Zn(glygly)(ssz)(H_2O)].6H_2O$ with CT DNA were carried out by employing various biophysical methods (UV–vis, Fluorescence and circular dichroism) and molecular docking technique which reveals strong electrostatic mode of binding, in addition to selective recognition towards the minor groove of DNA in A/T rich sequences. To gain further insight into the molecular recognition at the target site, interaction studies of complex $[Zn(glygly)(ssz)(H_2O)].6H_2O$ with nucleotide viz., 5′–TMP and 5′–GMP were carried out by UV–vis titration. This observation was validated by ^1H and ^{31}P NMR with 5′–TMP which implicate the preferential selectivity of $[Zn(glygly)(ssz)(H_2O)].6H_2O$ towards N3 of thymine. Complex $[Zn(glygly)(ssz)(H_2O)].6H_2O$ was accessible to minor groove of DNA and cleaved pBR322 DNA *via* hydrolytic pathway, the hydrolytic cleavage mechanism of the complex $[Zn(glygly)(ssz)(H_2O)].6H_2O$ was supported by evidence from DNA religation employing T4 DNA ligase assay. The significance of such studies provides the rationale for design of novel metal–based drugs with

proven pharmacokinetic properties that could overcome the intrinsic or acquired resistance of several tumors to platinum drugs and role of metal ions in enzyme catalysis. In the second part of **chapter IV**, [Cu(glygly)(ssz)(H_2O)].6H_2O complex derived from dipeptide (glycyl glycine anion) and sulfasalazine (ssz) was synthesized and characterized by elemental analysis (CHN), molar conductance measurements and spectroscopic methods (IR, UV–vis, ESI–MS). The complex [Cu(glygly)(ssz)(H_2O)].6H_2O is water soluble, covalent in nature and possess octahedral geometry around Cu(II) metal ion. The interaction of complex [Cu(glygly)(ssz)(H_2O)].6H_2O with human serum albumin (HSA) was investigated under physiological condition in Tris–HCl buffer solution at pH 7.4 by employing fluorescence, CD and FTIR spectroscopic and molecular docking technique. The fluorescence titration results revealed that the complex [Cu(glygly)(ssz)(H_2O)].6H_2O strongly quench the intrinsic fluorescence of HSA through a static quenching procedure. Binding constants (K_b) and the number of binding sites ($n \approx 1$) were calculated using modified Stern–Volmer equations. The thermodynamic parameters ΔG at different temperatures were calculated subsequently the value of ΔH and ΔS was also calculated which revealed that the hydrophobic and hydrogen bonding interactions play a major role in HSA–complex [Cu(glygly)(ssz)(H_2O)].6H_2O association. The distance r between donor (HSA) and acceptor (complex) was obtained according to fluorescence resonance energy transfer and the alterations of HSA secondary structure induced by complex [Cu(glygly)(ssz)(H_2O)].6H_2O were confirmed by FT–IR and CD measurements. Our results provide valuable information to understand the mechanistic pathway of drug delivery and to pharmacological behavior of drug.

Chapter V deals with the synthesis of new series of transition metal complexes $[Cu_2(bipy)_2(im)_2(pip)(NO_3)_2].2NO_3$, $[Zn_2(bipy)_2(im)_2(pip)].4Cl$ and $[Ni_2(bipy)_2(im)_2(pip)].4Cl$ derived from 2,2'–bipyridyl (bipy), imidazole (im) and piperazine (pip). The proposed structure of the complexes was formulated on the basis of elemental analysis and other spectroscopic data (IR, ^1H and ^{13}C NMR, EPR, UV–vis, ESI–MS and TGA). The proposed geometry of Cu(II) complex was distorted square pyramidal while square planar geometry was observed for Ni(II) and Zn(II) metal ions . The X–ray powder diffraction (XRPD) confirmed the crystalline nature for the complexes. The *in vitro* DNA binding studies of these complexes $[Cu_2(bipy)_2(im)_2(pip)(NO_3)_2].2NO_3$, $[Zn_2(bipy)_2(im)_2(pip)].4Cl$ and $[Ni_2(bipy)_2(im)_2(pip)].4Cl$ were carried out by employing UV–vis, fluorescence and circular dichroism which revealed that the complexes bind to CT–DNA by electrostatic groove binding mechanism. The binding affinity of these complexes, the intrinsic binding constant K_b were determined and followed the order $[Cu_2(bipy)_2(im)_2(pip)(NO_3)_2].2NO_3$ > $[Zn_2(bipy)_2(im)_2(pip)].4Cl$ > $[Ni_2(bipy)_2(im)_2(pip)].4Cl$. Therefore, the interaction study of $[Cu_2(bipy)_2(im)_2(pip)(NO_3)_2].2NO_3$ complex was carried out with 5'– guanosine monophosphate nucleotide (5'–GMP) by absorption titration and further validated by ^1H, ^{13}C and ^{31}P NMR spectroscopy. From gel electrophoretic mobility assay, the complex $[Cu_2(bipy)_2(im)_2(pip)(NO_3)_2].2NO_3$ displayed efficient cleavage activity of plasmid pBR322 DNA followed by conversion of Form I (supercoiled DNA) to Form II (nicked circular DNA) and ultimately leading to the formation of linearized Form III with increasing concentrations of the complex. The complex $[Cu_2(bipy)_2(im)_2(pip)(NO_3)_2].2NO_3$ exhibited remarkable ability to affect DNA double

strand scission in hydrolytic cleavage manner. SOD activity exhibited the high superoxide dismutase activity (IC_{50}~0.28 μM) of complex $[Cu_2(bipy)_2(im)_2(pip)(NO_3)_2].2NO_3$ due to cooperation of two Cu(II) centers in close proximity, acting in concord in free radical binding and electron transfer or due to a vacant coordination site that permits the bonding of superoxide anion and the influence of ligand on SOD activity.

Chapter VI embodies synthesis of new series of bis–macrocyclic complexes derived from salicylaldehyde derivative ligand (O,O′–bis{5–{(1E)–(2hydroxyphenyl)methylene] amino}–2–hydroxybenzoic acid) (**L**) and its characterization by spectroscopic, analytical and visualization techniques. The crystalline nature of the complexes were authenticated by X–ray powder diffraction (XRPD) measurements. The *in vitro* DNA binding studies of complexes $[Cu_2(L)_2].2NO_3$, $[Ni_2(L)_2]$ and $[Sn_2(L)_2.4Cl]$ were carried out by absorption titrations, fluorescence, NMR and circular dichroism, which revealed that the noncovalent mode of binding by electrostatic interaction *via* phosphate backbone of the DNA double helix. To quantify the extent of DNA binding, the intrinsic binding constant K_b were determined and follows the order $[Cu_2(L)_2].2NO_3 > [Ni_2(L)_2] > [Sn_2(L)_2.4Cl] >$ [L]. Interaction between complex $[Cu_2(L)_2].2NO_3$ and pBR322 DNA was investigated by agarose gel electrophoresis, noticeably, the Cu(II) complex $[Cu_2(L)_2].2NO_3$ exhibited an outstanding ability to affect DNA double strand scission through hydrolytic pathway.

SYNTHESIS AND CHARACTERIZATION OF NOVEL METAL COMPLEXES AND THEIR INTERACTION WITH THERAPEUTIC BIOTARGETS

THESIS

SUBMITTED FOR THE AWARD OF THE DEGREE OF

Doctor of Philosophy

IN

CHEMISTRY

BY

Waddhaah Mohammed Abdulgaleel

Under the Supervision of

Prof. Sartaj Tabassum

DEPARTMENT OF CHEMISTRY
ALIGARH MUSLIM UNIVERSITY
ALIGARH (INDIA)

2012

Dedicated

to

My Beloved

Parents,

wife,

son

&

Supervisor

Prof. Sartaj Tabassum
Department of Chemistry
Aligarh Muslim University
Aligarh-202002, India

Phone No. 0571-2703893
Mob: 91-9358255791
E-mail: tsartaj62@yahoo.com

Certificate

The work embodied in this thesis entitled **"Synthesis and Characterization of novel metal complexes and their interaction with therapeutic biotargets"** is the result of original researches carried out by **Mr. Waddhaah Mohammed Abdulgaleel** under my supervision and is suitable for the award of Ph.D. degree.

Prof. Sartaj Tabassum

CONTENTS

Acknowledgements

In the name of "Allah, Most Gracious, Most Merciful"

All praise and thanks to Almighty Allah for letting me to accomplish this research endeavor. During this long and eventful journey I have had a vigorous training to excellence in research, to move forward with investigations in depth and in particular, i have learned a lot about myself. To say it has been a learning experience is a vast understatement, i will remember everything I have learned here and use it to guide me through the rest of my days.

My heartfelt emotions which cannot be expressed in words are for my most respected teacher and supervisor **Prof. Sartaj Tabassum** for his proficient guidance, incessant encouragement, incredible patience and constructive critiques. His skills as an innovative and an accomplished researcher, ebullient scientific attitude, good organizing ability, enthusiasm, inspiration and his great efforts to explain things clearly and simply, served to give me a sense of direction in research and life in general.

Much gratitude is extended to **Dr. (Mrs) Farukh Arjmand** for so generously sharing her knowledge and expertise. Her thoughtful advice and deep insight into the work are extremely valuable in getting through the difficult times, whenever the problems got difficult.

At this juncture of my life i wish to thank my beloved parents, my wife and my son **Mohammad** for their inspiration and the innumerable sacrifices, the unmatched love, sincerity and for encouraging me to accomplish this task and provided me the self-confidence.

The biggest thanks belong to **Mohd. Afzal** for their sound advice, good company, and fruitful discussions and of course to the wonderful moments we had together. I would like to express my appreciation for my lab colleague **Mehvish Zaki**, who read the multiple drafts of the entire document and pointed out the mistakes politely. Special thanks to my friend **Rashid Y. Kamal** (MSc. lab) for help me.

I gratefully acknowledge **Dr Rizwan. H. Khan** and **G. Rabani** Interdisciplinary Biotechnology unit for CD, thermal denature experiments and 3D fluorescence facility. Thanks to **Mr. Avtar Singh** at Regional Sophisticated Instrumentation Center Punjab University Chandigarh who facilitated me to carry my experiments in his laboratory.

I would also acknowledge the support and love of my dear brothers **Fahed**, **Amjed** and **Kamal** and my dear uncles **Abdulrahman**, **Waddee**, **Khalil and Abdumoeen** for all the strength and support they have given me during my Ph.D. My special thanks are reserved for my uncle **Shamsi** and my brothers **Labib**, **Mohammed** and **Ibrahim** to support me also.

I am extremely fortunate to have encouraging affectionate and loving parents and siblings whose blessings, inspiration, discipline and love gave me the spirit, energy to walk through the tough times; in particular my brothers and sisters cannot be forgotten for cheering me up and making me smile always in difficult circumstances.

Waddaah

Waddaah Mohammed Abdulgaleel

Publications
&
Conferences

Publications

1. Molecular drug design, synthesis and structure elucidation of a new specific target peptide based metallo drug for cancer chemotherapy as topoisomerase I inhibitor. Sartaj Tabassum, **Waddhaah M. Al-Asbahy**, Mohd. Afzal, Farukh Arjmand and Vivek Bagchi, **Dalton Transaction**, (2012), **41**, 4955.
2. Interaction and Photo–induced Cleavage Studies of Copper based Chemotherapeutic Drug with Human Serum Albumin: Spectroscopic and Molecular Docking Study. Sartaj Tabassum, **Waddhaah M. Al-Asbahy**, Mohd. Afzal, Farukh Arjmand, Rizwan H. Khan, **Molecular BioSystems,** (2012), **8**, 2424.
3. Synthesis, characterization and interaction studies of copper based drug with Human Serum Albumin (HSA): spectroscopic and molecular docking investigations. Sartaj Tabassum, **Waddhaah M. Al-Asbahy**, Mohd. Afzal, Farukh Arjmand, **Journal of Photochemistry and Photobiology B: Biology,** (2012), **114**, 132.
4. DNA binding and cleavage studies of new sulfasalazine–derived dipeptide Zn(II) complex: Validation for specific recognition with 5′–TMP. Sartaj Tabassum, **Waddhaah M. Al-Asbahy**, Mohd. Afzal, Manal Shamsi, Farukh Arjmand, **Journal of Luminescence**, (2012), **132**, 3058.

International Conferences

- EICC-1: First EuChemMS Inorganic Chemistry conference, 11-14 April 2011, Manchester, UK.
- MedChem 2011 UK-India conference, organizing by the Royal Society of Chemistry (RSC) and IICT, 25-26 Feb. 2011, Hyderabad, India.

Abstract

Medicinal inorganic chemistry –a sub discipline of bioinorganic chemistry is one of the most rapidly developing areas of pharmaceutical research. This field gained momentum after the prototypical success story of platinum based anticancer drug cisplatin, cis diamminedichloro platinum(II), cis–[$Pt(NH_3)_2Cl_2$)] for treating solid cancers in particular, testicular, ovarian, small cell lung, head and neck cancers. Despite its success, there were serious concerns of this drug regarding its toxicity, intrinsic resistance, narrow spectrum of activity for phenotypes of cancer and patient compliance. Therefore, studies pertaining to essential metallo elements received much more attention in contrast to Pt, since the drugs designed and synthesized from endogenous metal ions may be less harmful and more prone to antiproliferative activity against tumors. Much of the attention has been laid towards the design of metal–based cancer chemotherapeutics, predominantly Cu(II), Co(II) and Zn(II) complexes (endogenously biocompatible metal ion which are present as integral part of the active site of metalloprotein and thus familiarize their coordination with human body's function) with active ligand pharmacophore. In particular, these metal complexes could efficiently bind and cleave DNA, thereby exert artificial nuclease activity. The development of artificial nucleases with improved efficiency and selectivity is in high demand and requires binuclear metal centers to achieve a synergistic effect in the process of substrate recognition and scission.

Additionally, it has been demonstrated that free radicals can damage proteins, lipids and DNA of bio–tissues, leading to increased rate of cancer. Redox behaviour of metal ion plays an important role in enzymatic activity and scavenge toxic ROS species. The superoxide radical anion; $O_2^{\cdot-}$ (a by product of normal cellular respiration) and protects cells from damage induced by reactive oxygen species (ROS). SOD catalyzes

disproportionates superoxide to dioxygen and hydrogen peroxide, which later on decomposes to water and dioxygen by catalase. Transition metal complexes have shown remarkable antioxidant and DNA–binding properties which have been proven effective in cancer chemotherapy. DNA–complex binding causes distortion of the helical structure and results in inhibition of DNA replication and transcription, thereby cell death. Ligand scaffolds are also considered important in muting the toxicity of the metallodrug as well tailored multifunctional ligands offer exciting possibilities by providing appropriate anchoring sites for the metal ions, matching the structural motif at the molecular target and restricting the geometry.

The specific delivery of a drug to their target cells may be achieved by the use of targeting groups or by tuning the chemical and physical characteristics of the drug or drug carrier, such as hydrophobicity and molecular size. Different types of macromolecules (liposomes, dendrimers, polyethylene glycol polymers, nanoparticles, and protein biomolecules) have been used as carrier molecules. In particular, HSA is the most multifunctional transport protein and plays an important role in the transport and deposition of a variety of endogenous and exogenous substances in blood. The interaction of metal ions with small peptides has been a subject of great interest for bioinorganic chemists. Copper is the center of the active site of various metalloproteins and plays vital role in biological processes like electron transfer, endogenous oxidative DNA damage associated with aging and cancer.

The thesis embodies the synthesis and characterization of new metallated chemical entities for use as antitumor agents. DNA is the primary cellular target for most of the chemotherapeutic agents therefore, preliminary *in–vitro* DNA binding profile of these

metal–based chemical entities were carried out by employing various bio–physical techniques. These studies are of paramount importance as the mode of binding to DNA gives an insight for the rationale of robust drug design. Our studies reveal that these complexes are capable of binding non–covalently to DNA and thereby they can act as efficient chemotherapeutic agents; however for the effective delivery of the potential drugs to the desired target, a strategy employing a protein carrier molecule is necessary to improve the pharmacokinetic profile of the drug or to target the drug to the pathogenic site addressing diseases. We have carried out binding studies with HSA to demonstrate specific targeted binding to the molecular DNA at the same time using HSA as a carrier protein.

The thesis is divided in six chapters which includes **Chapter I "Introduction"** giving a detail overview of literature relevant to this field and also helps to justify the objectives of the work done. **Chapter II** is **"Experimental"** where all details of methods and physical measurements employed in this work are given. **Chapter III–VI** embodies the molecular design, synthesis of novel metal–based potential chemotherapeutic agents and exploring their *in–vitro* binding propensity towards the specific target DNA and HSA at the molecular level.

Chapter III deals with the synthesis of the new dinuclear copper(II) complex as metallopeptide drug $[Cu_2(glygly)_2(ppz)(H_2O)_4]\cdot 2H_2O$ achieved by mixing stoichiometric amounts of Cu(II) nitrate trihydrate with glycyl glycine anion (glygly) followed by reaction with piperazine (pip) hexahydrate. Molecular structure of representative complex $[Cu_2(glygly)_2(ppz)(H_2O)_4].2H_2O$ was determined by single X ray crystallogrphically. The crystal obtained was monoclinic with space group P21/c. The *in vitro* DNA binding

studies of complex $[Cu_2(glygly)_2(ppz)(H_2O)_4].2H_2O$ with CT DNA were carried out by employing UV–vis, fluorescence and circular dichroism which reveal electrostatic interaction *via* groove binding mode. Complex $[Cu_2(glygly)_2(ppz)(H_2O)_4].2H_2O$ cleaves pBR322 DNA *via* an oxidative mechanism and strongly binds to the DNA minor groove. Furthermore, complex $[Cu_2(glygly)_2(ppz)(H_2O)_4].2H_2O$ exhibits significant inhibitory effect on the catalytic activity of topoisomerase I at a very low concentration, ~12.5 μM, additionally it behaves as an excellent SOD mimic (IC_{50} ~ 0.086 μM). The molecular docking technique was also utilized to ascertain the mechanism and mode of action towards the molecular target DNA and enzymes.

In the second part of **chapter III**, the interaction of new dinuclear copper(II) complex $[Cu_2(glygly)_2(ppz)(H_2O)_4].2H_2O$ with human serum albumin (HSA) was examined by means of fluorescence spectroscopy which revealed that complex $[Cu_2(glygly)_2(ppz)(H_2O)_4].2H_2O$ has a strong ability to quench the intrinsic fluorescence of HSA through static quenching pathway. The alterations of HSA secondary structure in presence of complex $[Cu_2(glygly)_2(ppz)(H_2O)_4].2H_2O$ were confirmed by UV–visible, FT–IR, CD and 3D fluorescence spectroscopy. The binding constants (K), and binding site number (n), corresponding thermodynamic parameters ΔG, ΔH and ΔS at different temperatures were also calculated. The molecular docking technique was utilized to ascertain the mechanism and mode of action towards the molecular target HSA, indicating that complex $[Cu_2(glygly)_2(ppz)(H_2O)_4].2H_2O$ was located to the entrance of site I by electrostatic and hydrophobic forces. Complex $[Cu_2(glygly)_2(ppz)(H_2O)_4].2H_2O$ showed efficient photo–induced HSA cleavage activity, indicating the involvement of hydroxyl radicals as the reactive species. Furthermore, the cytotoxicity of

$[Cu_2(glygly)_2(ppz)(H_2O)_4].2H_2O$ was examined on a panel of human cancer cell lines of different histological origins revealing moderate GI_{50} values specifically towards MIAPACA2, A498 and A549 cell lines. These results complement the previous biological studies for specific targeted metallopeptide, providing additional information about the possibility of transport and disposition in blood plasma.

Chapter IV describes synthesis of new water soluble complex $[Zn(glygly)(ssz)(H_2O)].6H_2O$ derived from dipeptide (glycyl glycine anion) and sulfasalazine (ssz) and its characterization by spectroscopic (IR, UV–vis, NMR, ESI–MS) and analytical methods. The *in vitro* DNA binding studies of complex $[Zn(glygly)(ssz)(H_2O)].6H_2O$ with CT DNA were carried out by employing various biophysical methods (UV–vis, Fluorescence and circular dichroism) and molecular docking technique which reveals strong electrostatic mode of binding, in addition to selective recognition towards the minor groove of DNA in A/T rich sequences. To gain further insight into the molecular recognition at the target site, interaction studies of complex $[Zn(glygly)(ssz)(H_2O)].6H_2O$ with nucleotide viz., 5′–TMP and 5′–GMP were carried out by UV–vis titration. This observation was validated by ^{1}H and ^{31}P NMR with 5′–TMP which implicate the preferential selectivity of $[Zn(glygly)(ssz)(H_2O)].6H_2O$ towards N3 of thymine. Complex $[Zn(glygly)(ssz)(H_2O)].6H_2O$ was accessible to minor groove of DNA and cleaved pBR322 DNA *via* hydrolytic pathway, the hydrolytic cleavage mechanism of the complex $[Zn(glygly)(ssz)(H_2O)].6H_2O$ was supported by evidence from DNA religation employing T4 DNA ligase assay. The significance of such studies provides the rationale for design of novel metal–based drugs with

proven pharmacokinetic properties that could overcome the intrinsic or acquired resistance of several tumors to platinum drugs and role of metal ions in enzyme catalysis. In the second part of **chapter IV**, [Cu(glygly)(ssz)(H_2O)].6H_2O complex derived from dipeptide (glycyl glycine anion) and sulfasalazine (ssz) was synthesized and characterized by elemental analysis (CHN), molar conductance measurements and spectroscopic methods (IR, UV–vis, ESI–MS). The complex [Cu(glygly)(ssz)(H_2O)].6H_2O is water soluble, covalent in nature and possess octahedral geometry around Cu(II) metal ion. The interaction of complex [Cu(glygly)(ssz)(H_2O)].6H_2O with human serum albumin (HSA) was investigated under physiological condition in Tris–HCl buffer solution at pH 7.4 by employing fluorescence, CD and FTIR spectroscopic and molecular docking technique. The fluorescence titration results revealed that the complex [Cu(glygly)(ssz)(H_2O)].6H_2O strongly quench the intrinsic fluorescence of HSA through a static quenching procedure. Binding constants (K_b) and the number of binding sites ($n \approx 1$) were calculated using modified Stern–Volmer equations. The thermodynamic parameters ΔG at different temperatures were calculated subsequently the value of ΔH and ΔS was also calculated which revealed that the hydrophobic and hydrogen bonding interactions play a major role in HSA–complex [Cu(glygly)(ssz)(H_2O)].6H_2O association. The distance *r* between donor (HSA) and acceptor (complex) was obtained according to fluorescence resonance energy transfer and the alterations of HSA secondary structure induced by complex [Cu(glygly)(ssz)(H_2O)].6H_2O were confirmed by FT–IR and CD measurements. Our results provide valuable information to understand the mechanistic pathway of drug delivery and to pharmacological behavior of drug.

Chapter V deals with the synthesis of new series of transition metal complexes $[Cu_2(bipy)_2(im)_2(pip)(NO_3)_2].2NO_3$, $[Zn_2(bipy)_2(im)_2(pip)].4Cl$ and $[Ni_2(bipy)_2(im)_2(pip)].4Cl$ derived from 2,2'–bipyridyl (bipy), imidazole (im) and piperazine (pip). The proposed structure of the complexes was formulated on the basis of elemental analysis and other spectroscopic data (IR, ^1H and ^{13}C NMR, EPR, UV–vis, ESI–MS and TGA). The proposed geometry of Cu(II) complex was distorted square pyramidal while square planar geometry was observed for Ni(II) and Zn(II) metal ions . The X–ray powder diffraction (XRPD) confirmed the crystalline nature for the complexes. The *in vitro* DNA binding studies of these complexes $[Cu_2(bipy)_2(im)_2(pip)(NO_3)_2].2NO_3$, $[Zn_2(bipy)_2(im)_2(pip)].4Cl$ and $[Ni_2(bipy)_2(im)_2(pip)].4Cl$ were carried out by employing UV–vis, fluorescence and circular dichroism which revealed that the complexes bind to CT–DNA by electrostatic groove binding mechanism. The binding affinity of these complexes, the intrinsic binding constant K_b were determined and followed the order $[Cu_2(bipy)_2(im)_2(pip)(NO_3)_2].2NO_3$ > $[Zn_2(bipy)_2(im)_2(pip)].4Cl$ > $[Ni_2(bipy)_2(im)_2(pip)].4Cl$. Therefore, the interaction study of $[Cu_2(bipy)_2(im)_2(pip)(NO_3)_2].2NO_3$ complex was carried out with 5'– guanosine monophosphate nucleotide (5'–GMP) by absorption titration and further validated by ^1H, ^{13}C and ^{31}P NMR spectroscopy. From gel electrophoretic mobility assay, the complex $[Cu_2(bipy)_2(im)_2(pip)(NO_3)_2].2NO_3$ displayed efficient cleavage activity of plasmid pBR322 DNA followed by conversion of Form I (supercoiled DNA) to Form II (nicked circular DNA) and ultimately leading to the formation of linearized Form III with increasing concentrations of the complex. The complex $[Cu_2(bipy)_2(im)_2(pip)(NO_3)_2].2NO_3$ exhibited remarkable ability to affect DNA double

strand scission in hydrolytic cleavage manner. SOD activity exhibited the high superoxide dismutase activity (IC_{50}~0.28 μM) of complex $[Cu_2(bipy)_2(im)_2(pip)(NO_3)_2].2NO_3$ due to cooperation of two Cu(II) centers in close proximity, acting in concord in free radical binding and electron transfer or due to a vacant coordination site that permits the bonding of superoxide anion and the influence of ligand on SOD activity.

Chapter VI embodies synthesis of new series of bis–macrocyclic complexes derived from salicylaldehyde derivative ligand (O,O′–bis{5–{(1E)–(2hydroxyphenyl)methylene] amino}–2–hydroxybenzoic acid) (**L**) and its characterization by spectroscopic, analytical and visualization techniques. The crystalline nature of the complexes were authenticated by X–ray powder diffraction (XRPD) measurements. The *in vitro* DNA binding studies of complexes $[Cu_2(L)_2].2NO_3$, $[Ni_2(L)_2]$ and $[Sn_2(L)_2.4Cl]$ were carried out by absorption titrations, fluorescence, NMR and circular dichroism, which revealed that the noncovalent mode of binding by electrostatic interaction *via* phosphate backbone of the DNA double helix. To quantify the extent of DNA binding, the intrinsic binding constant K_b were determined and follows the order $[Cu_2(L)_2].2NO_3 > [Ni_2(L)_2] > [Sn_2(L)_2.4Cl] >$ [L]. Interaction between complex $[Cu_2(L)_2].2NO_3$ and pBR322 DNA was investigated by agarose gel electrophoresis, noticeably, the Cu(II) complex $[Cu_2(L)_2].2NO_3$ exhibited an outstanding ability to affect DNA double strand scission through hydrolytic pathway.

Abbreviations

CD	circular dichroism
CT DNA	calf thymus DNA
DMF	dimethylformamide
DMSO	dimethylsulfoxide
EPR	electron parmagentic resonance
ESI	electrospray ionization
EthBr	ethidium bromide
EtOH	ethanol
gly gly	glycyl glycine
GMP	guanosine monophosphate
HSA	human serum albumin
IL	intraligand
IR	infra red
L	Schiff base ligand of salicylaldehyde and 5–aminosalicylic acid and further reacted with the linker–ligand 1,2–dibromo–ethane.
LMCT	ligand to metal charge transfer
LNT	liquid nitrogen temperature
MeOH	methanol
NBT	nitroblue tetrazolium
NMR	nuclear magnetic resonance
pip	piperazine
R	correlation coefficient
SDS	sodium dodecyl sulphate
SOD	Superoxide Dismutase
ssz	sulfasalazine
TCNE	tetracyanoethylene
TMP	thymidine monophosphate
tris	tris(hydroxymethyl)aminomethane
UV	ultra-violet

CHAPTER I

Introduction

Introduction

Medicinal inorganic chemistry has emerged as a new discipline of inorganic chemistry after the serendipitous discovery of the antitumor activity of cisplatin cis–$[Pt(NH_3)_2Cl_2]$ for therapeutic use (Figure 1a) [1–6], Gd(III) complexes as magnetic resonance imaging contrast agents (e.g. Dotaram) and ^{99}Tc complexes in cardiovascular imaging (e.g. Cardiolyte) (Figure 1b) [7–13]. Coordination complexes offer a diverse arena and their applications in medicine encompass cancer chemotherapy [14,15], antimicrobial agents [16–18], anti HIV–AIDS drugs [19, 21], anti–hypertensive, etc [22].

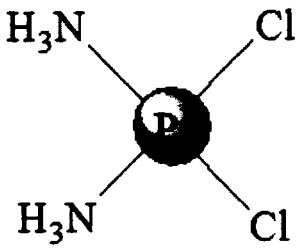

(a)

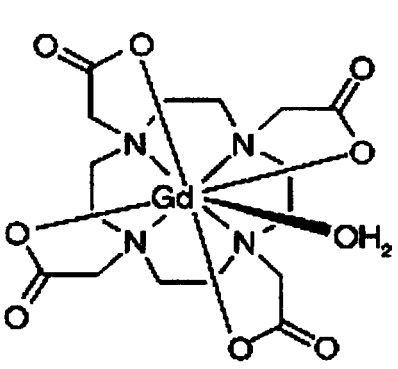

Dotaram

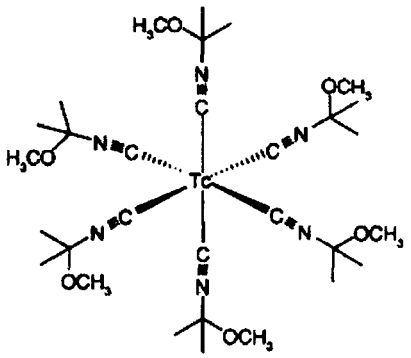

Cardiolyte

(b)

Figure 1. *Representative metallopharmaceuticals that are clinically used (a) as chemotherapeutic and (b) as MRI imaging agents.*

The use of metal–based therapeutic agents can be traced back to 3500 BC when copper was used to sterilize water by Egyptians and gold was used in the variety of medicines in Arabia and China. Gold–based drugs (sodium aurothiomalate and aurothioglucose) were employed for rheumatoid arthritis since twentieth century [23]. This implication was extended for modern medicine in 1985, when an orally bioavailable monomeric gold(I) phosphine drug (Auranofin) was introduced for rheumatoid arthritis. A curious connection between the discovery of a new precious element and its quick application into the medicinal armamentarium has been witnessed [24].

However, one of the major medical breakthrough for metal–based drugs was the discovery of potent antitumor activity of cisplatin. Cisplatin was approved for clinical use in 1978 and has become first line therapy for the treatment of testicular cancers. Platinum drugs are now widely used for the treatment the solid malignances, although they pose several serious limitations *viz.,* systemic toxicity, drug resistance, non–selective reactions with a variety of biomolecules such as proteins and phospholipids [25–29].

Optimization of platinum drugs was carried out by designing targeted Pt drugs. The targeting strategy uses selective transport of functionalized drug molecules recognized by receptor highly or only expressed on the surface of cancers cells [30–31], leaving healthy or normal cells unaffected. It has been estimated that approximately half the patients being treated for cancers today by chemotherapy receive a platinum compound. Nevertheless, these complexes do not serve the beneficial purpose or healing effect owing to their serious short comings and major drawbacks *viz.*, systemic toxicity (such as nephrotoxicity, myelotoxicity, ototoxicity, hematological toxicity), anaphylactic reactions, gastrointestinal disorders, tumor cell resistance induced by chemotherapeutic

agents [32]. Therefore considerable effort has been now focused on the development of new anticancer drugs based on non–platinum metal complexes [33].

Transition metals offer potential advantages over the common organic–based drugs, which include a wide range of coordination numbers and geometrics, accessible redox states, electron shuttling thermodynamic and kinetic stability [34]. Metal complexes are more appealing for design of new lead therapeutic drugs as metals play an important role in the chaperoning and delivery of drugs away from the sides where they exert most toxicity and toward their sites of activity [35, 36] (Figure 2). Transition metal complexes can undergo ligand exchanges; thus they can serve as prodrug, where ligand substitution can activate the metal complexes toward binding to target molecules [37].

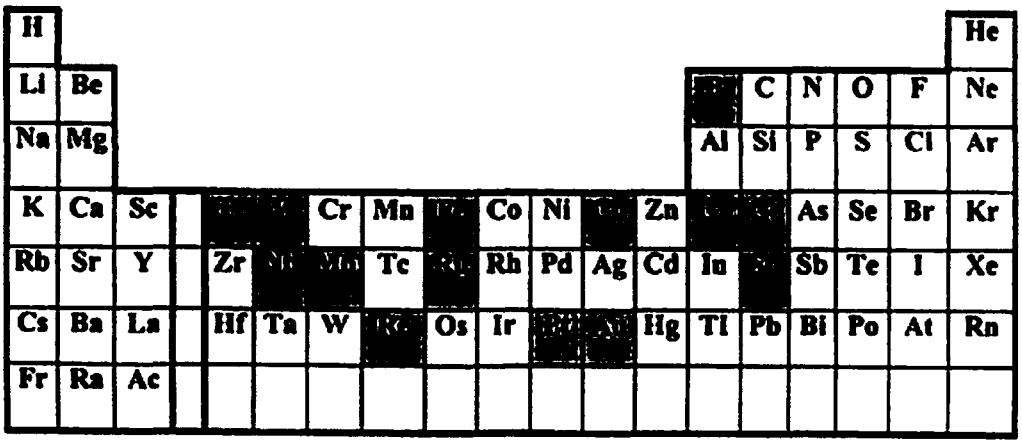

Figure 2. *Early–transition, late–transition and main–group metals and metalloids, which are known to form compounds that exhibit antitumor activity.*

The choice of metal ions and its oxidation state can be decisive in regulating the immediate *in vivo* response to metal–based chemotherapeutic agents. Most transition metal ions bind in site selective manner at physiological pH and generally bind to the most accessible N7 position of guanine or N3 of adenine in the DNA double helix [38].

Deoxyribonucleic acid (DNA), an inherently chiral molecule is a polymorphic structure with polyanionic nucleotide chains and sugar phosphate backbone [39]. The asymmetric D–ribose and D–2–deoxyribose units contain several stereogenic centers, whose configuration is important in overall DNA structure. It is well known that DNA does not exist in a three–dimensional structure, but can adopt different conformations which are defined both locally and macroscopically by different structural parameters (Figure 3). Double stranded DNA commonly adopts a right–handed helical conformation that of B– and the A–form, however, they differ in the conformation of the sugar (C2'–endo for B–DNA and C3'–endo for A–DNA, and in helical parameters). It was discovered that certain sequences of DNA have the propensity to undergo conformational transitions to left handed helical form termed as Z–DNA [40]. Z–DNA, first described in the late 1970s, is a left handed helical form of DNA in which the double helix wind to the left in a zig–zag pattern. DNA containing alternating purine and pyrimidine repeat tracts has the potential to adopt this non–B structure *in vivo* under physiological conditions. In a Z–DNA structure, the purines are inverted and in the syn–conformation, while the pyrimidines remain in the anti–conformation; as a result, the pyrimidine nucleotide must rotate to maintain the Watson–crick base–pairing. Such alternating syn–anticonformation drives the DNA backbone into a zig–zag shape. The major groove essentially disappears in a Z–DNA conformation, while the minor groove remains and maintains its narrow character, corresponding to the B–DNA structure [41].

A large percentage of the chemotherapeutic anticancer drugs currently used fall into the category of DNA–binding drugs, which interact with DNA duplex by any of the three general binding modes which have been thoroughly characterized from a structural point

of view. DNA intercalators [42], groove binders [43], and covalent binders [44–47] (Figure 4), with some peculiarities within each general category, may be cytotoxic and thus therapeutic either by direct interaction with DNA or by inhibition of topoisomerase enzymes (preventing DNA relaxation) [48].

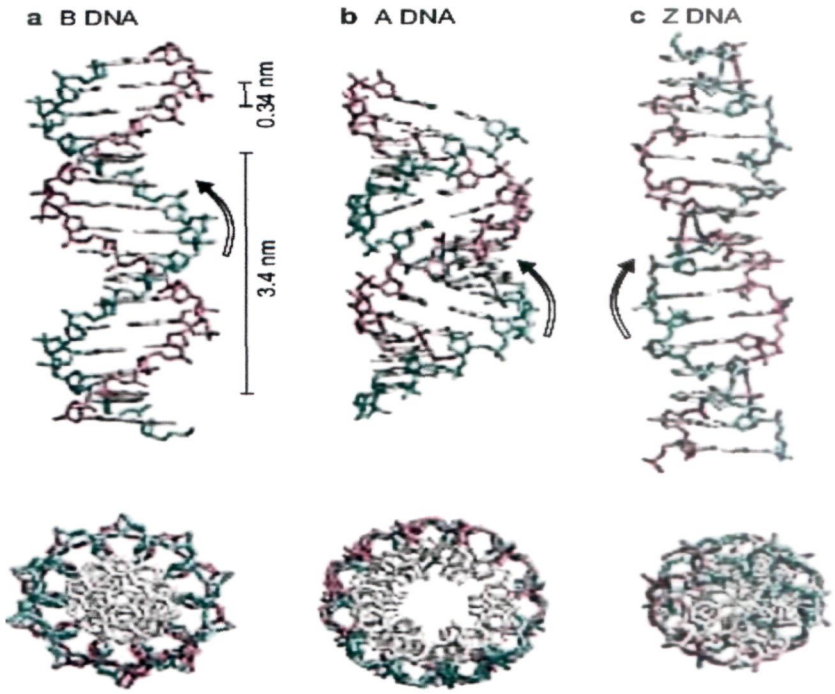

Figure 3. *Different conformational variations of DNA structure.*

In eukaryotic cells, DNA is stored in its supercoiled duplex form and its arranged on supramolecular structures that are stabilized by ancillary proteins. However, during activation toward processes such as replication and transcription, this stable storage complex is rearranged and the DNA may form structures that differ from Watson–Crick–induced B–DNA duplex [49]. Many classical DNA–intercalators have been tested as antitumor drugs [50], but their use is limited by the lack of specificity and frequent side effects. However, combinations of intercalators with groove binders, intercalators and molecules that form covalent adduct with DNA. Interestingly, few new classes of

compounds in these categories have been identified and reported. The combination of binding modes has several potential advantages over molecules binding in a single mode.

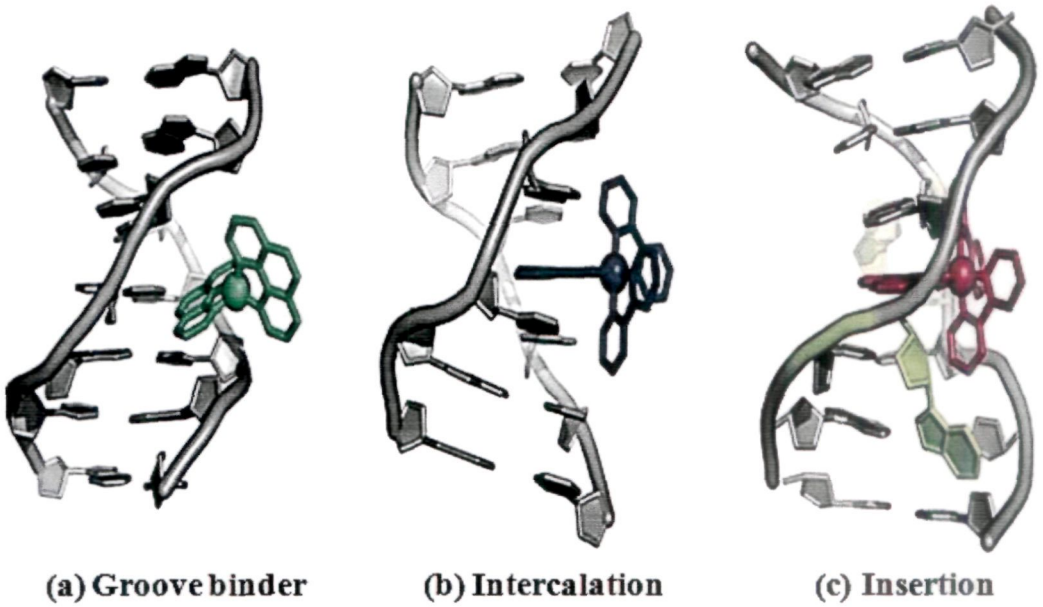

Figure 4. *The three binding modes of metal complexes with DNA: (a) groove binding, (b) intercalation and (c) insertion.*

Firstly, the stability of ligand–DNA complexes is expected to improve by the multiple interactions. In addition, the combination of covalent binding with non–covalent recognition represents an entropic advantage over molecules that do not localize covalently to the DNA. Furthermore, most molecules only have weak preference for a certain sequence, and binding to several alternative sites often occurs [51–57].

Cancer is defined as an abnormal cell behavior including irregular and rapid proliferation at the cellular level [58]. Cancer is caused by mutation of cellular genes that control cell growth and division [59]. The current treatment for cancer primarily includes surgery and chemotherapy, however, chemotherapy is used as mainstay due to its ability to cure widespread malignancies or metastatic cancers alone or in combination with radiotherapy [60]. The drugs used to treat cancer are often named as anticancer drugs. However, the

drug is referred to as an antitumor agent if it is targeted against a malignant tumor. A malignant tumor is the result of the proliferation of the abnormal cancer cell, which generally spreads to distant parts of the body by the blood or lymph and consequently evolves into new cancer cells. This process is named metastasis [61].

All living cells (including cancer cells) contain genetic information necessary for replication and survival. When a cell is divided, its DNA is reproduced. Hence, one of the most approaches has been to inhibit the growth of cancer cells by disrupting the flow of their genetic information [62]. Almost all of the currently used agents exert their mode of action by the inhibition of DNA synthesis, direct chemical damage to the genomic DNA, or some alternative means of inhibiting the mechanics of cell division. DNA has been therefore, considered to be the major primary target for the action of a large number of currently used anticancer agents [63].

Metal–based pharmaceuticals can be arranged into seven categories depending on the function of the metal and ligand moieties according to Hambley et al [64]: i) the metal complex is active in its inert form, ii) the metal complex is active in its reactive form, iii) the metal serves as a radiation enhancer, iv) the compound contains a radioactive metal, v) the metal or its biotransformation product is active, vi) ligand is biologically active, and vii) only a fragment of the complex is active. Transition metals have demonstrated remarkable cytotoxicity in cell culture or antitumor activity. Iron is biologically most significant metal ion and recently an organometallic compound (Ferrocifen), an analog of tamoxifen, an antagonist of the estrogen receptor (widely used in the clinic for the treatment of hormone dependent breast cancers) was discovered indicating a distinguished mode of antiproliferative action (Figure 5a) [65]. Because Ru derivative

does not show the same cytotoxicity profile, it was assumed that redox properties of ferrocene played an important role.

A prodrug approach for the inhibition of enzymes by cobalt complexes has been explored by Hambley et al [66]. Their strategy involves the complexation of matrix metalloproteinase (MMP) inhibitor to a Co(III) complex for selective delivery of MMP to tumor (Figure 5b). The prodrug is activated by a bio–reduction pathway producing a labile Co(II) complex, which results in the release of the MMP inhibitor [67].

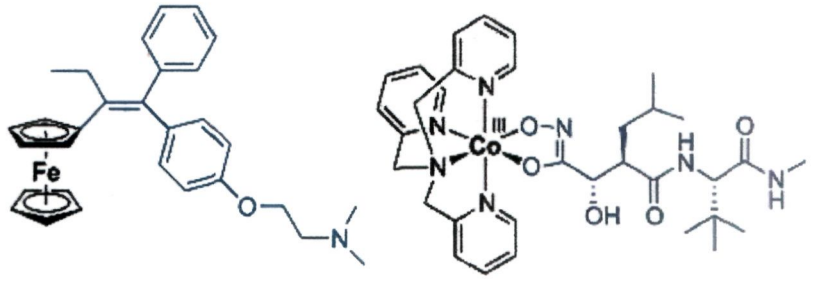

(a) **(b)**

Figure 5. *(a) Ferrocifen, a ferrocene derivative of tamoxifen, shown in blue. The third phenyl ring in tamoxifen is replaced by ferrocene and (b) Co(III) complex with marimastat.*

The chemistry of copper is attractive for the development of hypoxia selective drugs, because Cu has two oxidation states and the reduction potential in accessible within the cellular potential range [68]. Recently, the 'Tirapazamine' ligand was employed as a hypoxic cytotoxin for use with radioactive Cu, combining the antitumor activity of the copper complex with its radioactivity, the ^{64}Cu or ^{67}Cu isotopes with bis (thiosemicarbazone) and bis (salicylaldimine) ligands showed hypoxic selectivity against Chinese hamster ovary cancer cells [69]. Complexes with nitrogen mustard based as cyclen, cyclem and tacn are cytotoxic against leukemia cells. Cu(II) complex with

1,4,7,10–tetraazacyclododecane, (Figure 6) exhibited good aqueous stability and, *in vitro* 24–fold increased cytotoxicity under hypoxic conditions vs. oxic conditions [70].

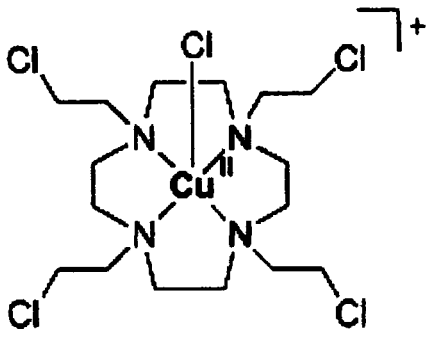

***Figure** 6. Cu(II) complex for releasing nitrogen mustards based on cyclen.*

In such complexes the tunable redox properties of the metal ion and ligand modifications can be exploited to control biological action. Ligand loss during reduction in hypoxic cancer tissue can activate metal complexes for binding to target molecules. Furthermore, as for Co and Cu, the loss of the ligand in a reductive environment can also trigger the release of an active species, a molecule that would have shown systemic toxicity if not bound to the deactivating metal center [64].

Zinc is the second most prominent trace metal in the human body and plays an important role in regulating the cellular response to DNA damage, including cell cycle arrest and the induction of apoptosis [71,72]. The deficiency of zinc may cause growth effects and disorders of the central nervous system [73–75]. In the literature, diverse zinc complexes with biological activity are reported [76], but drugs with zinc complexes are used for the treatment of Alzheimer diseases [77] and others showing antibacterial [78], anti–convulsant [79], anti–diabetic [80] anti–inflammatory [81], anti–microbial [82] and anti–proliferative, anti–tumor [83] activity were structurally characterized.

A Tarushi et al [84] has described the synthesis and characterization of mononuclear zinc complex with first–generation quinoline antibacterial drug oxolinic acid in the absence or in presence of N–donor heterocyclic ligand bipyridyl. In the complex, oxolinic acid was found bound to Zinc(II) *via* ketone oxygen and a carboxylate oxygen. The biological activity of the complexes was evaluated by their ability to bind to CT DNA by employing UV and fluorescence optical methods. Interaction of the complexes with DNA has shown that $Zn(oxo)_2(py)_2$ exhibits the highest K_b value, which was comparable to the K_b value with EB. EB (3, 8–Diamino–5–ethyl–6–phenyl–phenanthridinium bromide) is a phenanthridine fluorescence dye and is a typical indicator of intercalation [85]. It can form soluble complexes with nucleic acids emitting intense fluorescence in presence of CT DNA due to intercalation of the planar phenanthridinium ring between adjacent base pairs on the double helix [86]. The changes observed in the spectra of EB on its binding to CT DNA are used for the interaction study between DNA and metal complexes [87].

Recently, a novel organotin complex 1–{(2–hydroxyethyl)amino}–2–amino–1,2–dideoxy–D–glucose triphenyltin(IV) (GATPT) (Figure 7), a sugar based apoptosis inducer was synthesized by our research group [88]. GATPT was tested for its cytotoxic properties against SY5Y, PC–12 and N2A neuronal tumor cell lines. GATPT induced significant apoptosis in the PC–12 cell line characterized by DNA fragmentation and chromosome condensation. Treatment of PC–12 cells with GATPT resulted in a dramatic up–regulation of Bax and Bak and down–regulation of the anti–apoptotic factor Bcl–2. Apoptotic induction by GATPT was shown to be mediated in a p53–dependent manner and loss of p53 impaired the release of cytochrome c from mitochondria to cytosol. Caspase–3 was found to be indispensable for the GATPT triggered apoptosis signaling

pathway. Furthermore, *in vivo* studies using a nude mice model revealed that GATPT exhibits significant antiproliferative activity against tumor development with minimal cytotoxicity.

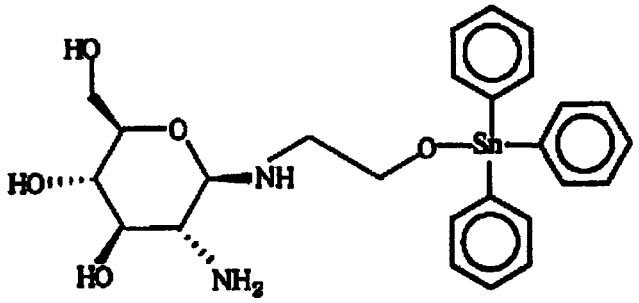

***Figure** 7. Molecular structure of GATPT.*

Tailored multifunctional ligands for metal based medicinal drugs offer many exciting possibilities including targeting specific tissues, membrane receptors, or endogenous molecules and can play an integral role in modulating the potential toxicity of a metallodrugs [89]. Recent advances in ligand design have resulted in potent antitumor compounds that are active in cisplatin resistant cell lines, and also include additional features to allow for an increased understanding of the mechanism of action of drug. In addition, the carrier ligands may also affect bio–distribution and recognition of DNA adducts by repair enzymes, regulatory and DNA binding proteins.

Recently, Dolenc et al [90] have designed and synthesized a series of novel desmuramyldipeptides for therapeutically useful muramyldipeptide (MDP) analogs. The MDP is an immune–amplifier and modulator of immune reaction, rather than an immune stimulant *per se* [91]. Some desmuramylpeptides were able to enhance the host defense against microbial infections as well as exhibit strong antiviral activity and remarkable antitumor potency [92–97]. LK–409 (7–oxooctanoyl–L–Ala–D–isoglutamine) and LK–

410 (N–(trans–2–(2'–acetylaminocyclohexyloxy)acetyl)–L–alanyl–D–glutaminic acid) (Figure 8) stimulated the macrophages in a dose–dependent manner to produce superoxide radicals and significantly accelerated the differentiation of mouse B lymphocytes in plaque forming cells [98].

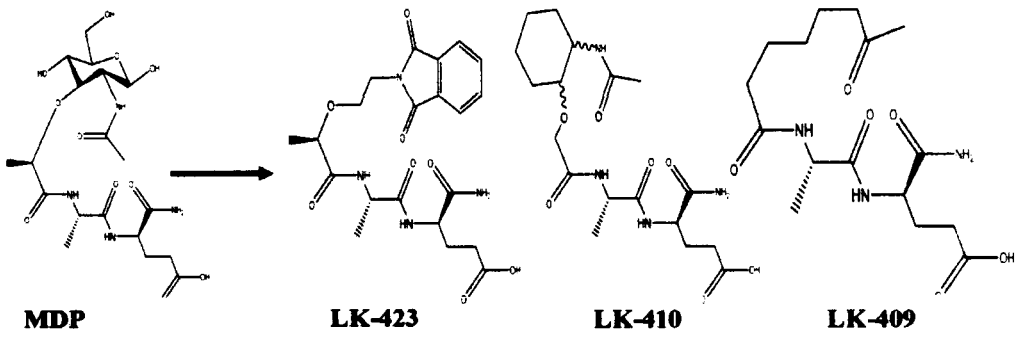

Figure 8. *Design of novel desmuramyldipeptide analogs.*

Furthermore, a phthalimido desmuramyldipeptide compound, LK–423 (N–[2–(2–phthalimidoethoxy)acetyl]–L–alanyl–D–glutamic acid), proved to be the most promising analog and was selected for further study to develop as an anti–inflammatory agent [99–101].

Peptides play important roles as hormones, enzyme inhibitors, neurotransmitters, and immune modulators in living systems and therefore, are expected to play significant role in the treatment of many diseases *viz.*, cancer, AIDS, Alzheimer's disease, malaria and as antimicrobials. Recently, it has been reported that some peptide derivatives show antitumor activity with little toxicity against non–malignant cells either by triggering apoptosis [102] or by forming ion channels/pores [103]. Furthermore, some peptides were found to be cytotoxic against MDR cancer cells [104,105]. Advantages of Peptides over other ligands are biocompatibility, non–toxicity, enantiomeric purity, and water solubility. An improved understanding of protein–DNA

interaction would find application in the design of repressors, transcription factors, and nucleases with altered sequence selectivity.

Metals may be directly bound into peptides and have been used for DNA selective recognition and/or cleavage [106–108]. It was reported that peptide functionalization of polypyridyl ruthenium(II) [109] or rhodium(III) [110,111] metallo–intercalators improved the selectivity of the parent intercalators, with similar effects observed by conjugating minor groove binders with short peptides that mimic natural protein motifs [112]. Thus, the metal complex serves to deliver the peptide to the DNA recognition site. This approach offers the opportunity to explore site–specific recognition of DNA by small peptides where residues may be varied in a systematic and well–defined fashion.

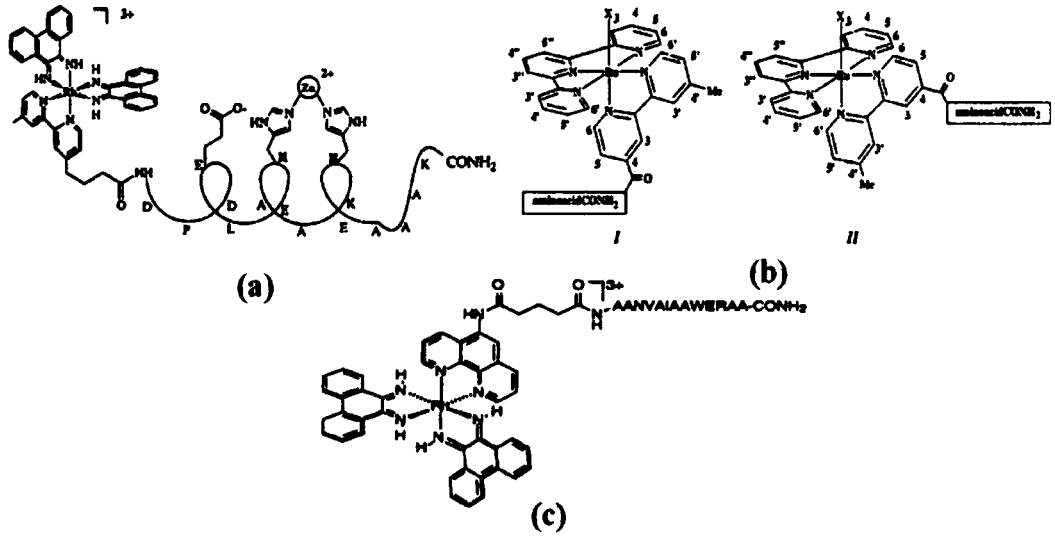

Figure 9. *(a) Metal–peptide conjugate [Rh(phi)$_2$bpy'–Peptide] (b) Structures of the positional isomers of the ruthenium oligopyridine complexes with conjugated amino acids and (c) Structures of the positional isomers of the ruthenium oligopyridine complexes with conjugated amino acids.*

Cowan et al have studied the single– and double–strand DNA cleavage efficiency of Cu(II)– and Ni(II)–Lys–Gly–His–derived (ATCUN) metallopeptides binding motif of

proteins (Figure 10) and its impact of the positioning of charged Lys side chains and their stereochemistry on metal reduction potentials and DNA cleavage reactivity [113].

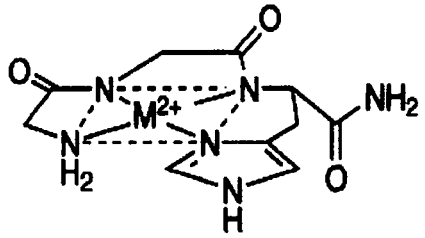

Figure 10. *Structure of M(II)• Gly–Gly–His.*

Since, ATCUN binding motifs of proteins occur naturally in the albumins and others native proteins, these metallotripeptide particularly Cu(II)•Gly-Gly-His was found active against Ehrlich ascites tumor cells [114]. It has been shown to induce DNA cleavage when activated with ascorbate [115], this system also effects DNA strand scission as a synthetic [116] or biosynthetic appendage to DNA binding proteins [117]. Enrique J. Baran and coworkers [118] have synthesized a new copper(II) complexes of stoichiometry [Cu(L–dipeptide)].nH_2O, containing dipeptide ligands L–alanine– L–isoleucine, L–alanine– L–threonine and L–alanine– L–tyrosine (Figure 11).

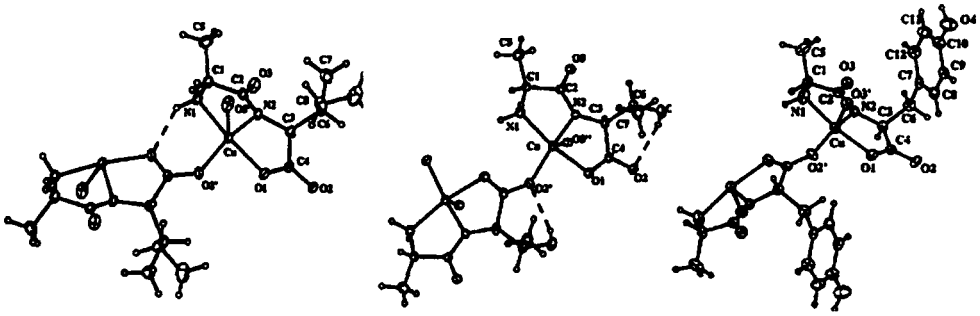

(a) *(b)* *(c)*

Figure 11. *Structure of (a) Cu(ala–ile), (b) Cu(ala–thr) and (c) Cu(ala–tyr) complexes.*

The single crystal X–ray studies of the all complexes show the same elongated square pyramidal coordination, being equatorially cis coordinated by a N_2O_2 arrangement of

ligand atoms and axially by a carbonyl oxygen atom. Furthermore, comparative superoxide dismutases (SOD)–like activity were investigated for all complexes. These studies demonstrated that, only Cu(ala–phe) complex (Table 1) revealed activity which was close to the ranges that were clinically interesting [119], due to the different dihedral angles subtended between the equatorial CuN_2O_2 planes, and it could be responsible for changes the overall environment around the active metal center due to differences in the stoichiometry of the dipeptides.

Table 1. *Cu(II) concentration required to yield 50% inhibition in SOD–assays*

Complex	Concentration (M)	$[Cu]_{complex}/[Cu]_{SOD}$
Cu(ala–ile)	3.30×10^{-4}	32353
Cu(ala–thr)	9.90×10^{-5}	9705
Cu(ala–tyr)	2.52×10^{-4}	24706
Cu(ala–val)	2.37×10^{-4}	23235
Cu(ala–phe)	1.49×10^{-5}	1461
Cu/SOD	1.02×10^{-8}	–

The results indicate that the chelated dipeptide ligand help to anchor copper metal ion and their spatial arrangement, often modulate very precisely and specifically the biological response of a metallic center [120, 121].

Sulfa drugs have attracted special attention for their therapeutic importance as they were used against a wide spectrum of bacterial ailments [122–129]. Also, some sulfa drugs were used in the treatment of cancer, malaria, leprosy and tuberculosis [126]. Recently, Borrás et al [130] have synthesized three dinuclear and one mononuclear copper(II)–1,10–phenanthroline ternary complexes, $[Cu(L1)(phen)(OH)]_2$ (**a**), $[Cu(L2)(phen)(OH)]_2.3H_2O$ (**b**), and $[Cu(L4)_2(phen)(H_2O)]$ (**c**), with thiadiazole sulfonamide derivative ligands: HL1 (N–(5–ethyl–1,3,4–thiadiazol–2–yl) naphthalene–1–sulfonamide), HL2 (N–(5–ethylthio)–1,3,4–thiadiazol–2–yl)–4–

methylbenzenesulfonamide), HL3 (N–(5–ethyl–1,3,4–thiadiazol–2–yl) benzenesulfonamide) and HL4 (N–(5–ethyl–1,3,4–thiadiazol–2–yl)–4–methyl–benzenesulfonamide) and their pUC18 plasmid DNA cleavage activity were investigated in the presence of reactive oxygen intermediate (Figure 12).

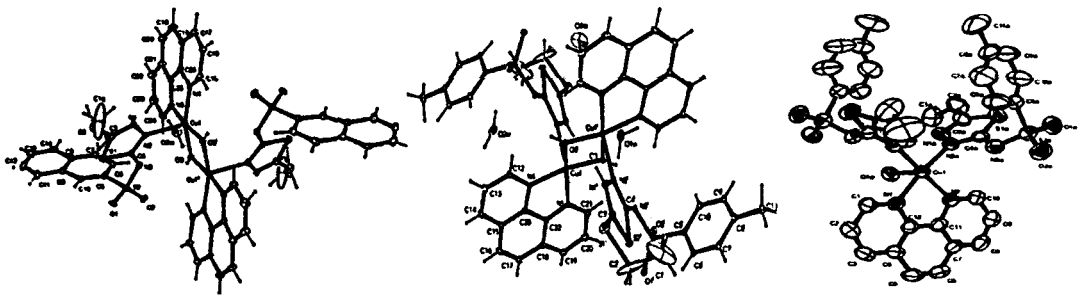

(a) *(b)* *(c)*

Figure 12. *The ORTEP drawing of mononuclear unit of (a) [Co(HL1)(H_2O)$_2$], (b) [Cu(HL2)(H_2O)$_2$] and (c) [Cu(L4)$_2$(phen)(H_2O)].*

The condensation of primary amines with carbonyl compounds was first reported by Schiff and since then condensation products are referred to as Schiff bases [131]. Several Schiff base complexes were found to inhibit tumor growth [132]. A few structurally characterized amino acid derived Schiff bases and their metal complexes were reported [133–136]. Schiff base are considered as 'privileged ligands' as they bind with different metal ion in various oxidation states [137].

Ghosh et al [138] has synthesized Schiff–base ligand; [L^1 = N,N′–bis((pyridine–2–yl) phenylidene)–1,3–diaminopropan–2–ol] and their Cu(II)complex [Cu(L^1)Cl](ClO_4).CH_3OH (Figure 13), and their interaction studies with calf thymus DNA (CT DNA) were validated by using absorption and emission spectral studies.

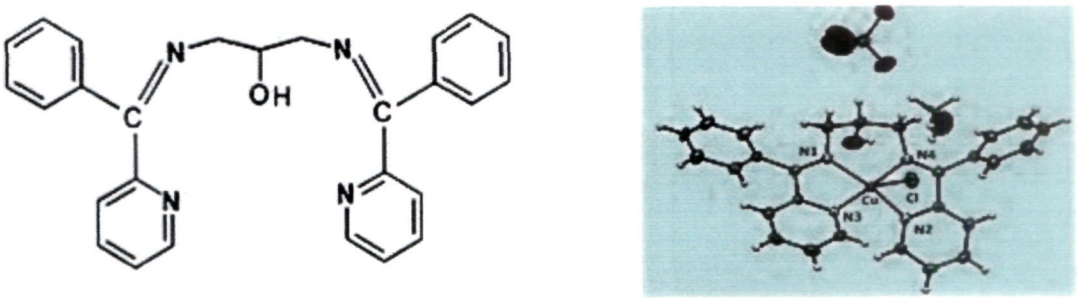

Figure 13. *Schematic diagrams of ligand (N,N'-bis((pyridine-2-yl)phenylid ene)-1,3-diaminopropan-2-ol) (left) and its copper(II) complex (right).*

DNA and enzymes involved in replication and transcription represent the most targeted bioreceptors for small molecules and a target for the control of gene expression. Most anticancer drug bind to DNA and proteins either in a reversible or irreversible manner suggesting a direct relationship between their interactions with macromolecules, hence, leading to their therapeutic effect. Numerous reports in literature are available for the binding studies using various biophysical techniques.

H.–J. Yu et al [139] has carried out DNA binding studies of two ruthenium(II) complexes [Ru(bipy)2(mitatp)]+2 and [Ru(bipy)2(nitatp)]+2 where mitatp = 5-methoxy-isatino[1,2-b]-1,4,8,9-tetraazatriphenylene and nitatp = 5-nitro-isatino[1,2-b]-1,4,8,9-tetraazatriphenylene) by employing absorption spectroscopy, fluorescence spectroscopy, DNA melting experiments and gel mobility shift assays.

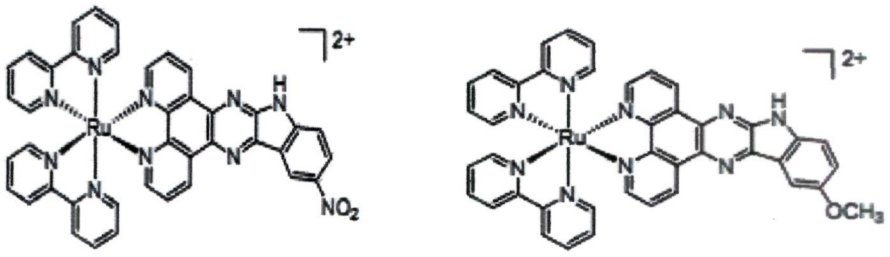

$[Ru(bipy)_2(mitatp)]^{+2}$ $[Ru(bipy)_2(nitatp)]^{+2}$

Figure 14. *Structure of the ruthenium(II) complexes.*

For metallo–intercalators, DNA–binding is associated with hypochromism and a red shift in the MLCT and ligand bands [140]. The absorption spectra of $[Ru(bipy)_2(mitatp)]^{+2}$and $[Ru(bipy)_2(nitatp)]^{+2}$in the absence and presence of CT DNA (at a constant concentration of complexes, [Ru]= 20 μM) has been depicted in figure 15 [139]. Upon increasing concentration of DNA, both complexes exhibited pronounced hyperchromism, along with a modest bathochromic shift.

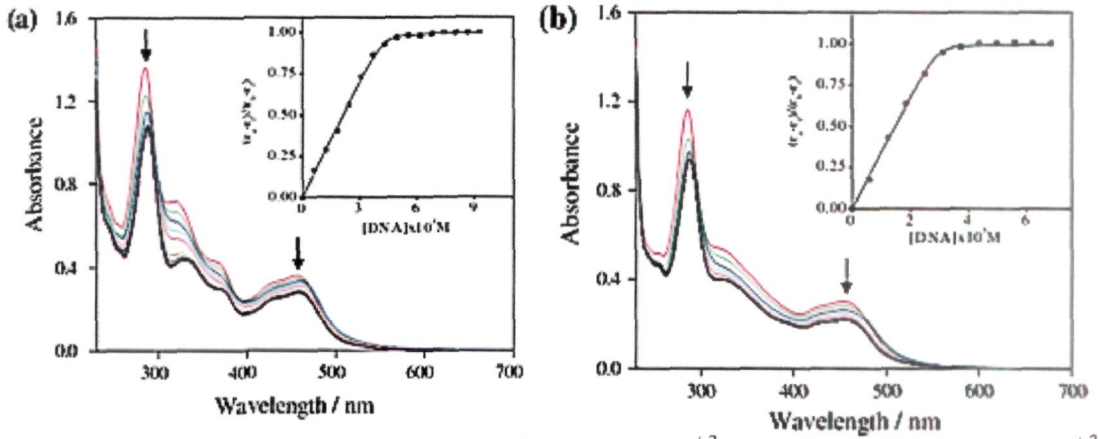

Figure 15. *Absorption spectra of (a) $[Ru(bipy)_2(nitatp)]^{+2}$ and (b) $[Ru(bipy)_2(mitatp)]^{+2}$ in the presence of an increasing amount of CT DNA. [Ru] = 20 μM. Inset:$(\varepsilon_a-\varepsilon_f)/(\varepsilon_b-\varepsilon_f)$ vs. [DNA], and the non linear fit curve.*

Similar hypochromicity was reported for [Ru(phen)2(dppz)]+, implying binding to DNA through intercalation of the dppz ligand (dipyrido[3,2-a:2',3'-c]phenazine) [141].

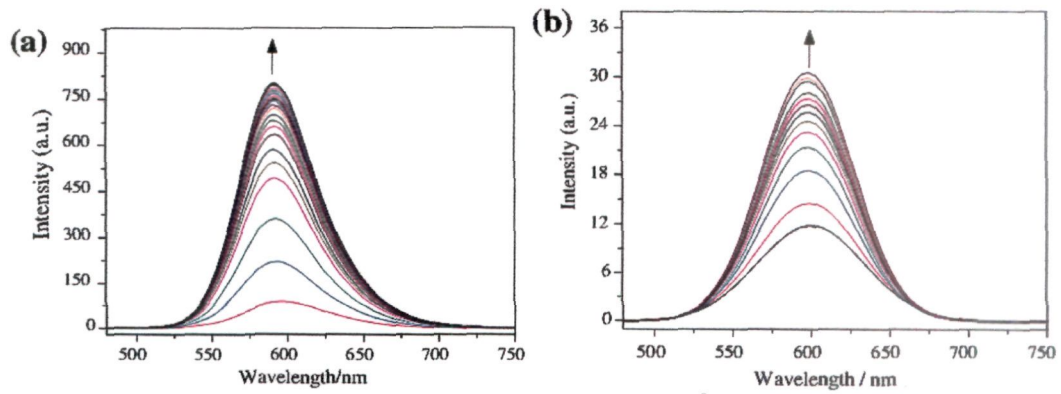

Figure 16. *Emission spectra of (a) $[Ru(bipy)_2(nitatp)]^{+2}$ and (b) $[Ru(bipy)_2(mitatp)]^{+2}$ in Tris–HCl buffer in the absence and presence of CT DNA. Arrow shows the intensity change upon increasing DNA concentrations. [Ru] = 5 μM.*

The intrinsic binding constants "K" and binding site "n" derived for $[Ru(bipy)_2(mitatp)]^{+2}$and $[Ru(bipy)_2(nitatp)]^{+2}$ complexes were (8.38 ± 0.3) × 10^6 M^{-1} (n=1.06 ± 0.01 bp) and (1.07 ± 0.4) × 10^7 M^{-1}(n=0.73 ± 0.01 bp), respectively. The K values were comparable to the known DNA intercalator (1.04 × 10^7 M^{-1}) [142].

The luminescence titration experiments carried out in aqueous solution. As shown in figure 16, upon addition of CT DNA, revealed increase in emission intensity was observed for both complexes. This implies that both complexes exhibited strong interaction with DNA, since the hydrophobic environment inside the DNA helix reduces the accessibility of water molecules to the complex and the complex mobility is restricted at the binding site, leading to decrease of the vibrational modes of relaxation.

Z.–W. Mao et al [143] has studied the CD spectral characteristics of CT DNA in the absence and presence of complexes $[Cu(L1)(ClO_4)](ClO_4).0.5H_2O$ and $[Cu(L2)(H_2O)](ClO_4)_2.H_2O$ (L1= 2–benzyl–1,3–bis(aminoethylthio) propane and L2= 2–(4–butylben–zyl)–1,3bis(aminoethylthio)propane) (Figure 17).

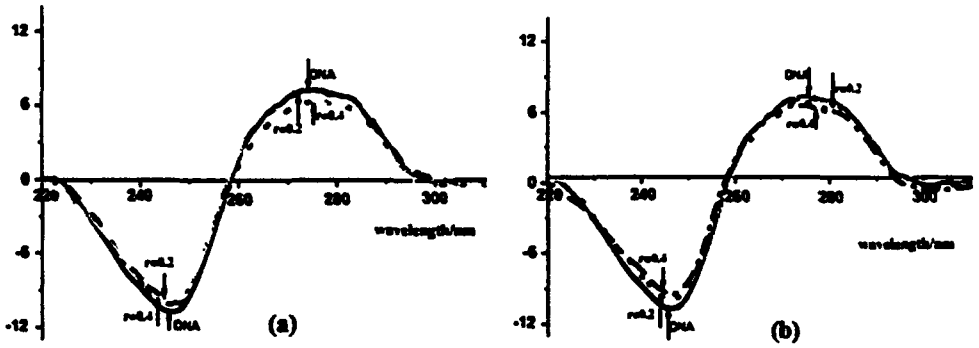

Figure 17. *CD spectra of CT–DNA (1.0 x10^{-4} M) in the absence and the presence of $[Cu(L1)(ClO_4)](ClO_4).0.5H_2O$ (a) and $[Cu(L2)(H_2O)](ClO_4)_2.H_2O$ (b) at ratio [complex]/[DNA] = 0.2, 0.4 in 5 mM Tris–50 mM NaCl aqueous buffer solution (pH 7.5).*

Upon addition of increasing concentrations of $[Cu(L1)(ClO_4)](ClO_4).0.5H_2O$ and $[Cu(L2)(H_2O)](ClO_4)_2.H_2O$, both positive and negative bands show slight change, which implies a non–intercalative mode between DNA and complexes. Since, the cationic core of $[Cu(L1)(ClO_4)](ClO_4).0.5H_2O$ and $[Cu(L2)(H_2O)](ClO_4)_2.H_2O$ could exert a strong electrostatic attraction to the anionic phosphate backbone of DNA, consistent with the electrostatic binding mode [144].

There has been considered interest in DNA endonucleolytic cleavage reactions that are activated by metal complexes [145,146] thus, DNA mobility shift assay were carried out to investigate the ability of complexes to interact with plasmid DNA. Change in the electrophoretic mobility of plasmid DNA on agarose gel is commonly taken as evidence for direct DNA–metal interactions. Alteration of the DNA structure cause retardation in the migration of supercoiled, and slight increase in the mobility of open circular DNA to a point where both forms comigrate. Impairment of DNA function results in the inhibition of replication and transcription processes and, eventually, if the DNA lesions are not rapidly and properly repaired, it results in cell death. Metal–DNA interaction cause alteration in the structure of DNA, where upon the mobility of supercoiled DNA decreases and the migration of open–circular DNA slightly increase at the comigration junction of both forms [147]. When a circular plasmid DNA is subjected to agarose gel electrophoresis, the fastest migration will be observed for supercoiled form (Form I). If one strand is cleaved, the supercoils will be relax to produce a slower moving open circular form (Form II). If both strands cleaved, a linear form (Form III) will be generated that migrates in between [148]. One of the illustrative examples of concentration dependent pBR322 DNA cleavage of $[Cu(Pyimpy)(ClO_4)(Cl)]$ (Pyimpy = 1-phenyl-1-

(pyridin-2- yl)-2-(pyridin-2-ylmethylene)hydr azine) was presented by Ghosh et al [149], enhancement of DNA cleavage activity was observed due to variation of incubation time (Figure 18, lane 10–14). Furthermore, nuclease activity of [Cu(Pyimpy)(ClO_4)(Cl)] in presence of H_2O_2 or 2–mercaptoethanol increased the cleavage activity, followed by complete conversion of SC form to NC and LC form of DNA (Figure 19, lane 7, 8).

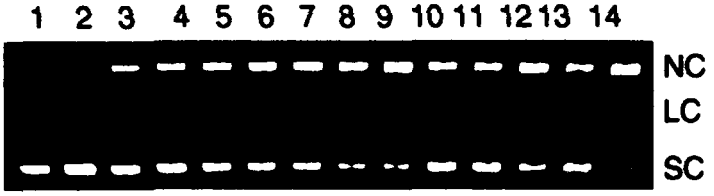

Figure 18. *Gel electrophoresis showing the cleavage of supercoiled pBR322 DNA (100ng) by complex [Cu(Pyimpy)(ClO_4)(Cl)] . Incubated at 37 °C for 1.5 h. lane 1, DNA control; lane 2 DNA + 10% DMF; lanes 3– 9, DNA + [Cu(Pyimpy)(ClO_4)(Cl)] = 10, 25 40, 50, 60, 80, 100 μM respectively; lanes 10 –14, DNA + [Cu(Pyimpy)(ClO_4)(Cl)] (100 μ M) + incubation time 5, 15, 30, 60 and 90 min respectively.*

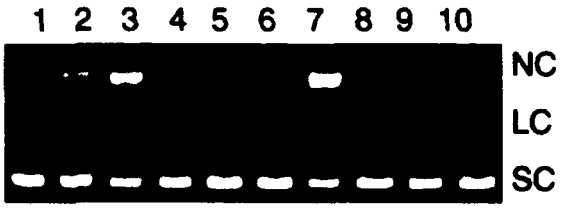

Figure 19. *Gel electrophoresis showing the cleavage of supercoiled pBR322 DNA (100 ng) by complex [Cu(Pyimpy)(ClO_4)(Cl)] (50 μM) in presence of radical scavenger s (20 mM). lane 1,DNA; lane 2, DNA + $Cu(ClO_4)_2 \cdot 6H$ 2O (100 μM); lane 3, DNA + [Cu(Pyimpy)(ClO_4)(Cl)] (50 μM); lane 4 –10, DNA + [Cu(Pyimpy)(ClO_4)(Cl)] (50 μM) + DMSO, ethanol , urea, catalase (1U), D_2O, L-histidine, NaN_3, respectively.*

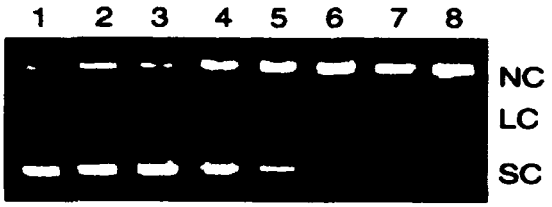

Figure 20. *Gel electrophore sis separations showing the cleavage of supercoiled pBR322 DNA (100 ng) by complex [Cu(Pyimpy)(ClO_4)(Cl)] in presence of H_2O_2 and BME. Incubated at 37 °C for 1.5 h.(a) lane 1, DNA control; lane 2, DNA + H_2O_2 (400 μM); lane 3, DNA + BME (400 μ M); lanes 4– 6, DNA + [Cu(Pyimpy)(ClO_4)(Cl)]= 25, 50, 100 μM; respectively, lane 7, DNA + [Cu(Pyimpy)(ClO_4)(Cl)] (50 μM) + H_2O_2 (200 μM); lane 8, DNA + [Cu(Pyimpy)(ClO_4)(Cl)] (50 μM) + BME (200 μM).*

Involvement of reactive oxygen species (hydroxyl radical, superoxide ion, singlet oxygen and hydrogen peroxide) in nuclease activity could be diagnosed by monitoring the quenching of DNA cleavage in the presence of radical scavengers in solution [150]. The hydroxyl radical scavengers like DMSO, ethanol and urea showed the complete inhibition of nuclease activity (Figure 20, lane 4–6). These results suggested that hydroxyl radicals may be involved in the cleavage process. Addition of singlet oxygen scavengers like L–histidine and NaN_3 (Figure 20, lane 9, 10) showed complete inhibition of nuclease. So these results suggested that $^1O_2$ or any other singlet oxygen–like entity may participate in the DNA strand scission. However, nuclease activity was not enhanced in presence of D_2O (Figure 20, lane 8). Probable participation of hydrogen peroxide was excluded due to enhancement of nuclease activity upon addition of catalase (Figure 20, lane 7). On the basis of these observations, it was concluded that complex [Cu(Pyimpy)(ClO_4)(Cl)] generated reactive oxygen species (ROS) which were responsible for nuclease activity.

The SOD activity of [Cu(Phimp)(H_2O)]$_2$(ClO_4) and [Cu(Phimp)(AOc)]$_2$ were determined by using the xanthine/xanthine oxidase by monitoring the reduction of nitro blue tetrazolium (NBT) with $O_2^{\cdot-}$ generated xanthine/xanthine oxidase system [151]. The rate of absorption change was determined and the concentration required to produce 50% inhibition (IC_{50}) was calculated by graphing the rate of NBT reduction (along Y–axis) versus the concentration of the test solution (along Y–axis) (Figure 21). The complexes [Cu(Phimp)(H_2O)]$_2$(ClO_4) and [Cu(Phimp)(AOc)]$_2$ showed IC_{50} values 11.20 and 8.31, respectively.

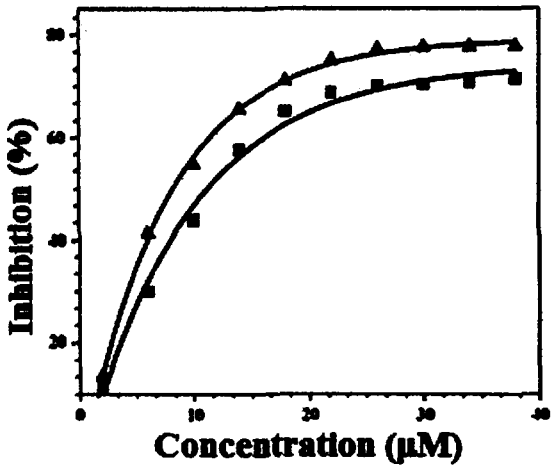

Figure 21. *Effect of complexes $[Cu(Phimp)(H_2O)]_2(ClO_4)$ (▲) and $[Cu(Phimp)(AOc)]_2$ (■) on the inhibition of the reduction. Incubation time was 5 min.*

Most of the drugs exert their cytotoxic effect and thereby therapeutic effect by direct interaction with DNA or by inhibition of topoisomerases (preventing DNA relaxation) Thus, new light has been shed on the discovery of metal–based drugs that inhibit enzymatic activities or even target protein directly. There are many reviews which highlight some exciting results published recently on the development of metal as enzyme inhibitors for potential therapeutic applications [152]. Topoisomerase–I (Topo I) is one of the nuclear enzymes that control the topology of DNA by triggering single–stranded breaks, passing the other strand through the cutting site and religating the cut strand [153]. These topoisomerases are important in DNA replication and transcription. Topo I inhibitors have been reported to be among the most widely used clinical drugs for treatment of cancer [154]. To determine catalysis or by altering the apparent topological state of DNA, the DNA strand passage assay was performed [155]. Chao et al [156] have investigated the Topo I inhibitory activity of $[Ru(bpy)_2(bfipH)](ClO_4)_2$ and $[Ru(phen)_2(bfipH)](ClO_4)$ (bfipH = 2–(benzofuran–2yl)imidazo[4,5–f], phen = 1,10 phenanthroline) by gel electrophoresis. Both complexes inhibited the ability of Topo I to

relax negatively supercoiled plasmid DNA (IC_{50} is ~17 μM for complex $[Ru(bpy)_2(bfipH)](ClO_4)_2$ and ~8 μM for complex $[Ru(phen)_2(bfipH)](ClO_4)_2$). These findings imply that these complexes block the DNA strand passage event of the enzyme, and can serve as catalytic inhibitors of Topo I.

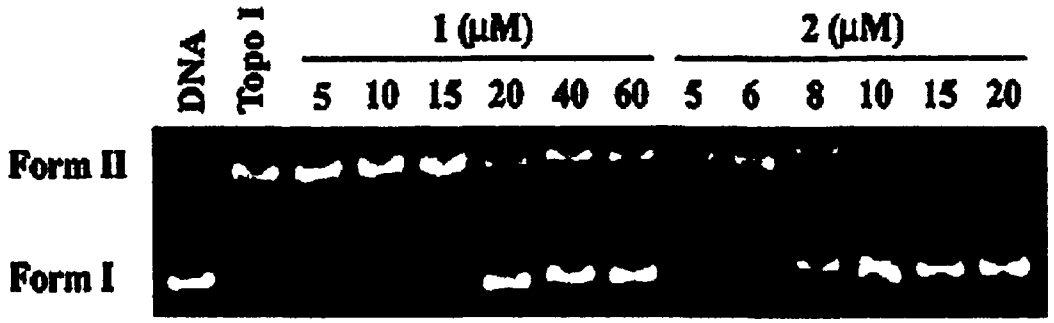

Figure 22. *Effects of different concentrations of complexes $[Ru(bpy)_2(bfipH)](ClO_4)_2$ and $[Ru(phen)_2(bfipH)](ClO_4)_2$ on the activity of DNA topoisomerase–I (Topo I) activity.*

As shown in Figure 23, the rate of Topo I–catalyzed DNA supercoiling in the presence of the Ru(II) complexes was lower than the rate of EB, which was identical to the rate of Topo I–catalyzed DNA relaxation in the absence of drug. These findings suggest that complexes $Ru(bpy)_2(bfipH)](ClO_4)_2$ and $[Ru(phen)_2(bfipH)](ClO_4)_2$ were catalytic inhibitors of topoisomerase–I.

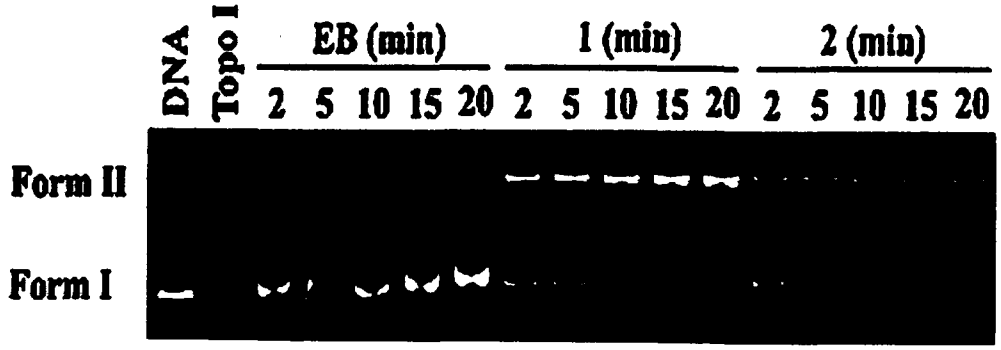

Figure 23. *The time dependence of Topo I DNA strand passage assays in the presence of ethidium bromide (EB) and complexes $[Ru(bpy)_2(bfipH)](ClO_4)_2$ and $[Ru(phen)_2(bfipH)](ClO_4)_2$.*

Griffith et al [157] have analysed the docking poses of the two most active compounds, NSC0674004 (4–Chloro–2–mercapto–5–methyl–N–[5–amino–1–(quinoxalin–2–yl))–1,2,4–triazol–3–yl}benzenesulphonamide) and NSC0039875 (sodium 3–amino–4–chloro–9,10–dioxoanthracene–2–sulfonic acid), and compared to the docking pose of Scutellaprostin G (Figure 24, views down the DNA axis in A to C, and from the major groove in D).

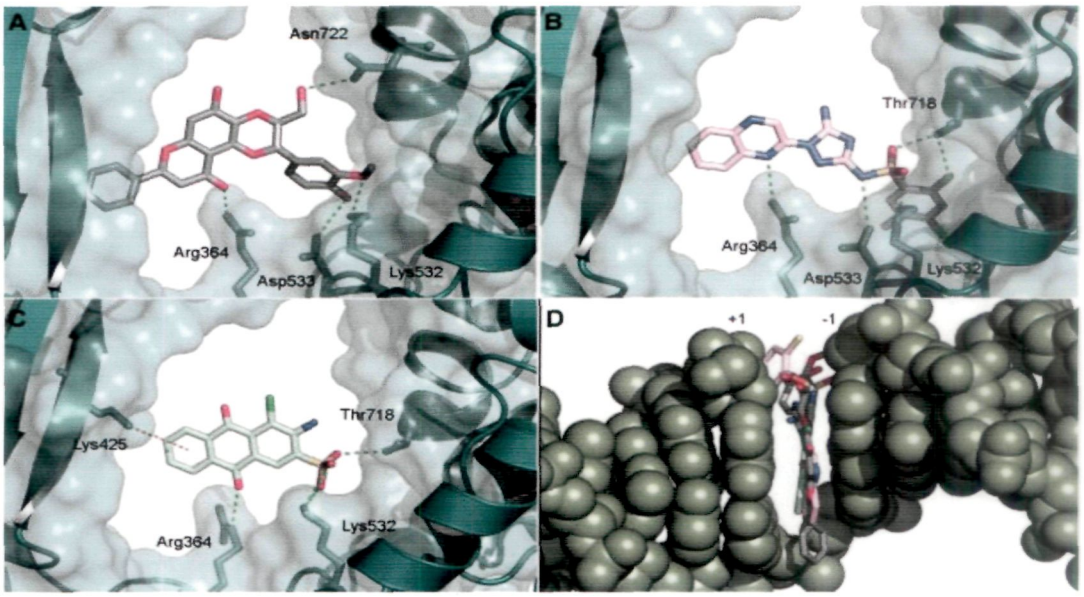

Figure 24. *Interactions between protein side chains and docked ligand: (A) Scutellaprostin G (B) NSC 0674004 (C) NSC 0039875 and (D) Overlay of docking poses of Scutellaprostin G (gray carbons), NSC 0674004 (pink carbons) and NSC 0039875 (green carbons) within the DNA cleavage site.*

Analysis and superimposition of the docking poses revealed that the three compounds intercalate between the DNA base pairs at the cleavage site, each providing three aromatic rings for extensive base pair stacking, and form hydrogen bonds to the side chains of the Topo1 residues Arg364 and Lys532.

The X–ray structure shows that active–site cavity of bovine CuZnSOD is ~15 Å deep and 12 Å wide near the protein surface and narrows to ~3 Å at the catalytic copper [158],

which has a solvent–exposed surface area of ~5Å^2 (Figure 25a). English et al has performed the docking studies of well–known chelator EDTA into the active–site channel of bovine CuZnSOD (Figure 25b). This implies that EDTA's carboxylate groups can coordinate to the active–site copper without reorganization of groups in the active–site cavity. Furthermore, the concentration of positive electrostatic potential (blue) around the cavity should promote binding of anionic ligands in the cavity [159,160].

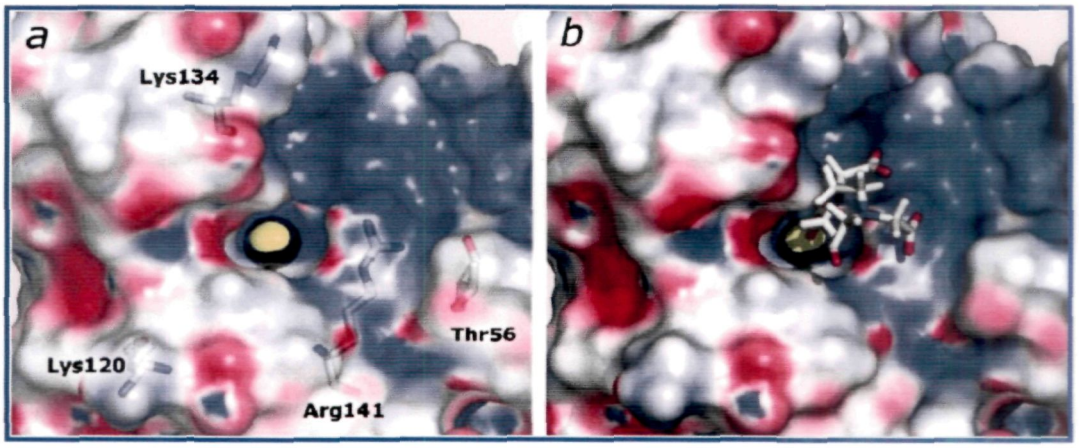

Figure 25. *Docking of EDTA into the active–site channel of bovine CuZnSOD. (a) Molecular surface and electrostatic potential map (blue, positive; red, negative) of the active–site channel of CuZnSOD and (b) Docking of the EDTA molecule into the active–site channel demonstrates that a carboxylic group of EDTA can access the active–site copper.*

Human serum albumin (HSA) is emerging as a versatile protein carrier for drug targeting and for improving the pharmacokinetic profile of peptide or protein based drugs [161]. It is a transport protein per se trafficking fatty acids, metal ions (Ca^{+2}, Zn^{+2}, Cu^{+2}) bilirubin, high binding drugs such as benzodiazepines, antibiotics, anti–inflamatory drugs, antianesthetic or platinum and gold complexes (cisplatin and ornophin) within the body. The main role of HSA is to maintain the osmotic blood pressure and to scavenge free radicals as an antioxidant. It is an attractive macromolecular carrier, due to its lack of toxicity and immunogenicity make it an ideal candidate for drug delivery.

X–ray structure analysis of HSA (which appeared in Brookhaven data bank) depicted in Figure 26 showed an ellipsoid shape consisting three domains, I, II and III. The binding sites for metabolic substrate and diagnostic as well as therapeutic drugs have been extensively studies and reviewed [162].

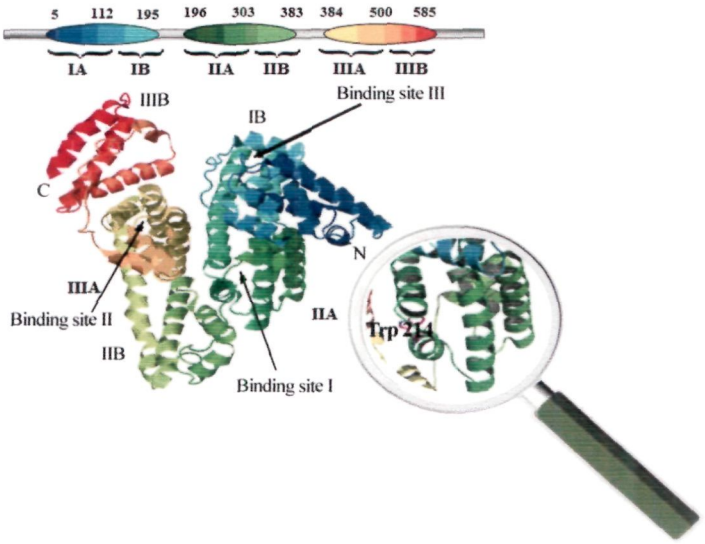

Figure 26. *Modeling of X–ray crystallographic structure of HSA (PDB ID: 1h9z). The domains and subdomains were displayed with different color, the every subdomain and classical binding site were marked in the corresponding location.*

The specific delivery of a drug to cancer cells may be achieved by the use of targeting groups or by tuning the chemical and physical characteristics of the drug or drug carrier, such as hydrophobicity and molecular size [163]. In particular, human serum albumin (HSA) is known to accumulate in tumors, being taken up by tumor cells at increased levels compared to normal cells because of enhanced tumor vascular permeability and prolonged retention time in the tumor interstitium due to the obstruction of lymphatic drainage, and has been exploited as the carrier conjugate of various anticancer drugs such as chlorambucil, doxorubicin, and paclitaxel [164,165]. Different types of macromolecules (liposomes, dendrimers, poly(ethylene glycol) polymers, nanoparticles,

and protein biomolecules) have been used as carrier molecules [166]. There are number of peer–reviewed articles on albumin and drug carriers and number of citation has essentially doubled from ~250 to ~500 citations between 2002 and 2010 (Figure 27) [167].

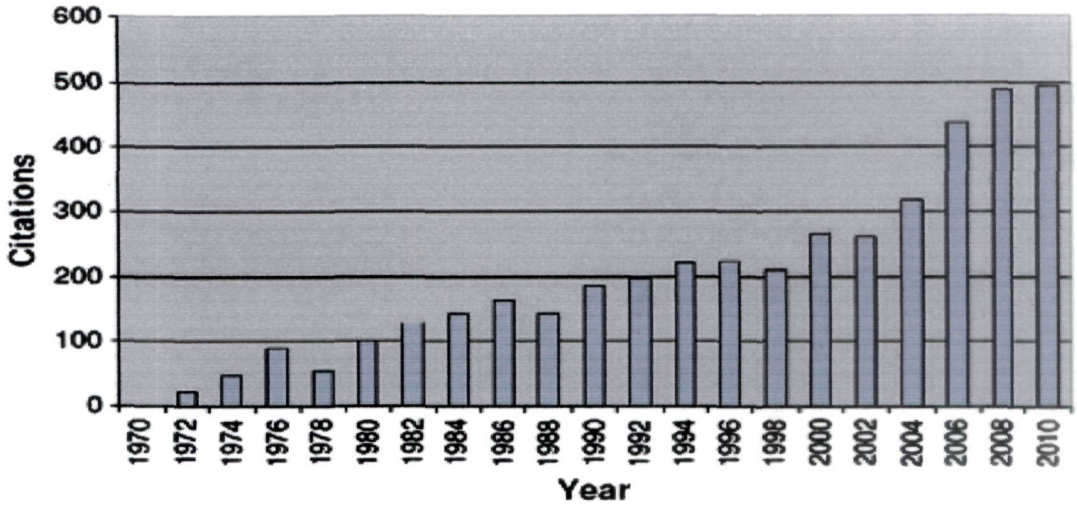

Figure 27. *Literature survey — impact of albumin on drug delivery: number of citations in PubMed combining the key word "albumin" with " drug carrier" from 1970 to 2010 dis–played as 2–year intervals.*

The interactions of drugs with protein results in the formation of a stable drug–protein complex, which can exert important effect on the distribution, free concentration and metabolism of the drug in the blood stream [168]. Therefore, drug binding to proteins such as HSA has become an important determinant of pharmacokinetics, restricting the unbound concentration and affecting distribution and elimination [169]. Although the unbound drug is regarded as the therapeutically active fraction that exerts its effect on the molecular target within cells and tissues–are three fold: (i) The half–life, clearance and tissue distribution of the vast majority of low–molecular weight drugs are so fast (in the order of minutes or at the most a few hours) that the fraction of the drug that is

actually protein–bound in the plasma is very small or sometimes negligible; (ii) The binding constants of the drug for albumin are generally low (K_d<10^6M) so the drug displays a very rapid pharmacokinetic–pharmacodynamic equilibration time; (iii) As a consequence, protein–binding of a drug measured in an isolated non–dynamic system outside of the body can but often does not correlate with other pharmacokinetic parameters such as plasma half–life, clearance, area under the curve (AUC), or volume of distribution [170].

Due to the susceptibility of therapeutic peptides to degradation by peptidases, lack of bioavailability and distribution to the target site, recent efforts have concentrated on improving their pharmacokinetic profile making use of albumin binding strategies. HSA has proved as an attractive molecular carrier due to its non–toxic, non–immunogenicity and availability in pure form. Chlorambucil, Paclitaxel conjugated to HSA exhibited cytotoxicity comparable to that of parent drugs *in vitro* but are less toxic *in vivo* [171]. Similarly conjugate RAPTA ($[Ru^{II}(\eta6\text{–arene})(pta)Cl_2]$) moieties were developed with carrier protein molecules such as rHSA for passive drug targeting [172].

Many drugs and other small bioactive molecules bind reversibly to albumin and other serum components that then function as carriers. Serum albumin often increases the apparent solubility of hydrophobic drug in plasma and modulate their delivery to cells *in vitro* and *in vivo*. The subsequent increase of the concentration of released drug may lead to serious drug–drug interaction. Therefore, a very high affinity to HSA is undesirable in potential drugs. Thus studying the binding phenomena will be important in providing basic information on the pharmacological actions, bio–transformation, and bio–distribution, etc. The interactions between plasma proteins and drug molecules such as

daunorubicin [173], 5–fluorouracil [174] have been explored by means of fluorescence spectra, UV spectra and CD spectra [175].

In recent years, novel methods such as fluorescence spectroscopy, UV–vis spectrophotometry, circular dichroism (CD) spectroscopy, Raman spectroscopy, nuclear magnetic resonance (NMR), electrochemistry, equilibrium dialysis, attenuated total reflectance–Fourier transform infrared (ATR–FT–IR), resonance light scattering (RLS), capillary electrophoresis, high–performance liquid chromatography and chemiluminescence [176–180] have been developed in the study of interactions between small molecules and HSA. Measurement of quenching of albumin's natural fluorescence is an important method to study its interaction with substances because of its high sensitivity, rapidity and ease of implementation.

Chen et al has explored the binding of antineoplastic drug oxaliplatin (Figure 28A) with HSA by the fluorescence quenching method [181].

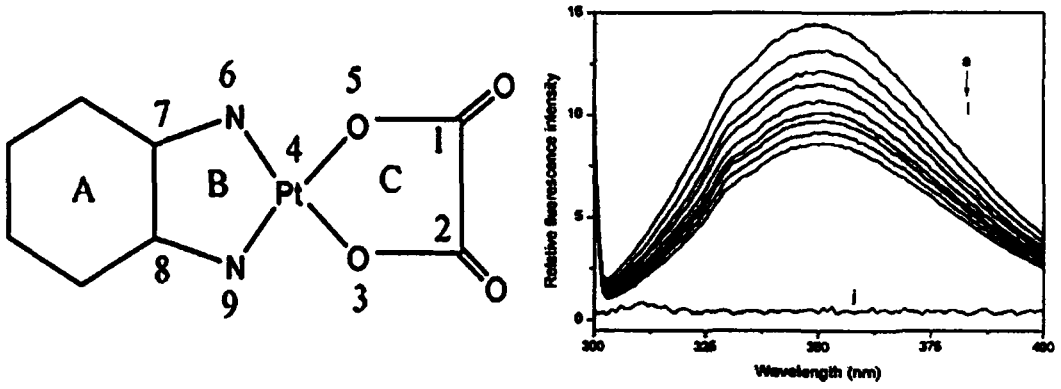

(A) (B)

Figure 28. *(A) Molecular structure of oxaliplatin and (B) Fluorescence spectra of HSA with various concentrations of oxaliplatin at 298 K (pH 7.40). (a) 3.0 μM HSA and (b)–(i) 3.0 μM HSA in the presence of 3.33, 6.67, 10.0, 13.33, 16.67, 20.0, 23.33, and 26.67× 10^{-5} M oxaliplatin; (j) 3.32 μM oxaliplatin.*

Fluorescence spectroscopy is a powerful method to study molecular interactions involving proteins. By measuring the intrinsic fluorescence quenching of HSA, the accessibility of quenchers to the fluorophore groups of HSA can be estimated. As shown in Figure 28B, there was no fluorescence emission for oxaliplatin at the range measured and the fluorescence intensity of HSA decreased gradually with the increase of oxaliplatin concentration without changing the emission maximum and shape of the peaks. These results indicated that there were interactions between oxaliplatin and HSA [182]. The fluorescence quenching effect was due to the formation of non–fluorescent complexes [183].

The circular dichroism spectroscopy is an important tool to understand the binding of drug to HSA. The CD spectra of HSA exhibit two negative bands at 208 and 222 nm, which are characteristic features of α–helical structure of proteins [184]. As evident from Figure 29, the band intensities of HSA at 208 and 222 nm decreased with negative cotton effect by the binding of oxaliplatin without causing any significant shift of the peaks, which indicated the considerable changes in the protein secondary structure. The α–helical content of HSA decreased while the increase of the disorder structure content in the HSA [185]. The α–helical content of HSA was calculated and the results exhibited a reduction of α–helical structures from 57.53 to 52.76 at a molar ratio of HSA to oxaliplatin 1:2.

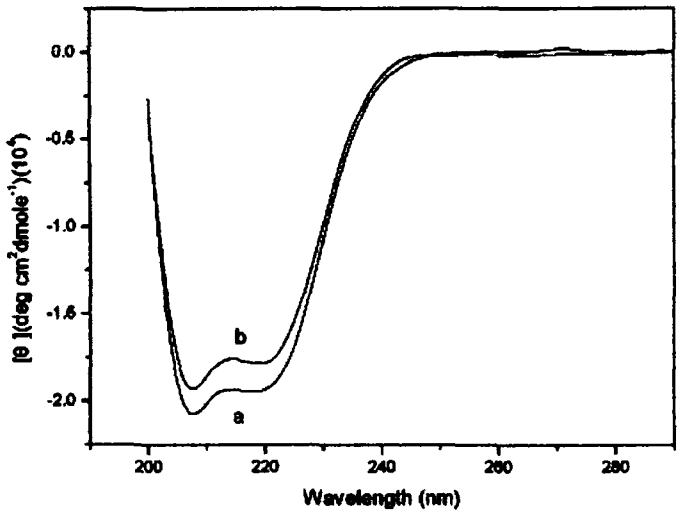

Figure 29. *CD spectra of the HSA–oxaliplatin system. (a) 3.0 μM HSA in Tris–HCl buffer and (b) 3.0 μM HSA in the presence of 6.0 μM oxaliplatin.*

The FT–IR spectra of free HSA and oxaliplatin–bound form of HSA with its difference absorption spectrum (Figure 30). The spectrum in Figure 30a was obtained by subtracting the absorption of the Tris–HCl from the spectrum of the protein solution. The spectrum in Figure 30a was obtained by subtracting the absorption of the oxaliplatin–free form from that of the oxaliplatin–bound form. Infrared spectra of proteins exhibited a number of the amide bands, which represent different vibrations of the peptide moiety. Among these amide bands of the protein, the protein amide I in the region 1600–1700 cm^{-1} (mainly C=O stretch) and amide II band in the region 1500–1600 cm^{-1} (C–N stretch couple with N–H bending mode) both have a relationship with the secondary structure of protein, and the amide II band absorbance intensity has been reported to be proportional to the amount of protein absorbed, and is believed not to be very sensitive to the conformation of the protein [186].

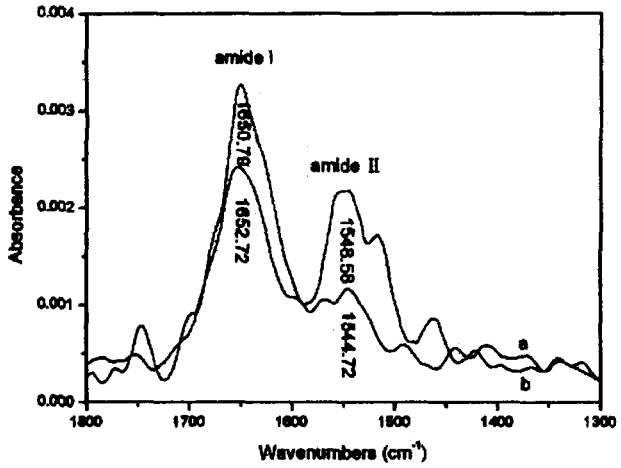

Figure 30. *FT–IR spectra and different spectra of HSA: (a) FT–IR spectrum of HSA in Tris–HCl buffer (pH 7.40) and (b) FT–IR difference spectrum of HSA obtained by subtracting the spectrum of the oxaliplatin–free form from that of the oxaliplatin–bound form in the region of 1800–130 0 cm^{-1}, [HSA] = 3.0 × 10^{-5} M, [oxaliplatin] = 6.0 × 10^{-5} M, pH 7.40, T =298 K.*

As shown in Figure 30, the peak position of amide I a band has changed from 1650.79 to 1652.72 cm^{-1}, which indicated that the secondary structure of the protein has been changed after oxaliplatin was added. These results also indicated that oxaliplatin interacted with the C=O and C–N groups in the protein polypeptides. The HSA–oxaliplatin complexes caused the rearrangement of the polypeptide carbonyl hydrogen bonding network and finally the reduction of the protein α–helical structure.

Fluorescence resonance energy transfer (FRET) is useful for measuring the distance between the donor fluorophore and acceptor *in vitro* and *in vivo* [187]. Seetharamappa et al monitored the distance r between donor (Trp–214) and acceptor carbamazepine (Figure 31A) according to (FRET) [188].

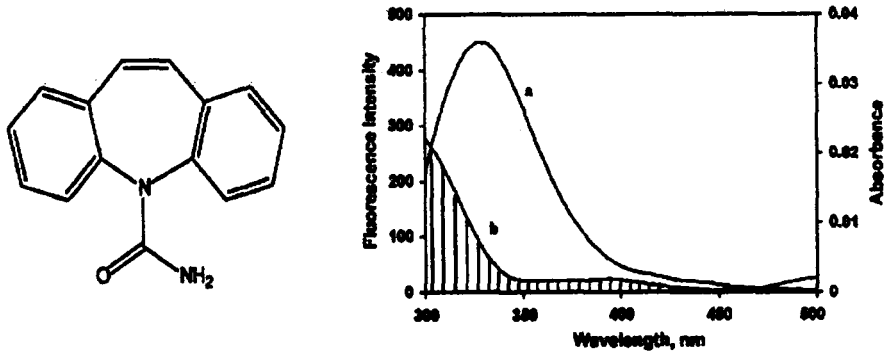

(A) (B)

Figure 31. *(A) Structure of carbamazepine (CBZ) and (B) The overlap of fluorescence emission spectrum of HSA (a) with the UV absorption spectrum of CBZ and (b) [CBZ] = [HSA] = 5 μM.*

It is a non–destructive spectroscopic method that can be employed to monitor the proximity and relative angular orientation of the donor and acceptor. Transfer of energy may take place through a direct electrodynamic interaction between the primarily excited molecule and its neighbors [189]. As shown in Figure 31B, the overlap of the fluorescence spectrum of HSA with the absorption spectrum of carbamazepine (CBZ). Electronic absorption spectroscopy is a reliable tool to understand the morphological changes in secondary structure of HSA *via* complex formation between drug and HSA. The UV absorption spectra of CBZ, HSA and CBZ–HSA are shown in Figure 32. The absorbance of HSA increased regularly with increase in the concentration of CBZ. Moreover, the maximum peak position of CBZ–HSA was observed to be shifted slightly towards higher wavelength region.

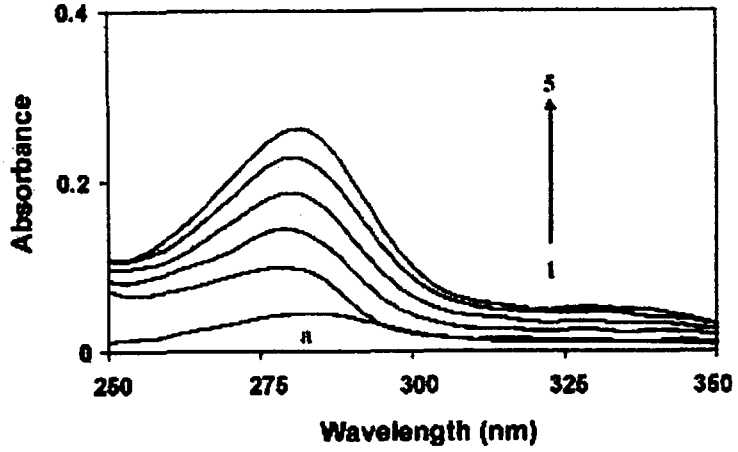

Figure 32. *UV–vis absorption spectra of 5 μM HSA (1) in presence of increasing concentration of CBZ (1) 0, (2) 5, (3) 10, (4) 15 and (5) 20μM. (a) Indicates 5 μM of CBZ only.*

This change in λ_{max} indicated the change in polarity around the tryptophan residue and the change in peptide strand of HSA molecules and hence the change in hydrophobicity. This indicated that the binding between carbamazepine and HSA molecule has led to changes in protein conformation [190].

The 3D fluorescence spectroscopy is a newly emerged analytical technique that can provide more detailed information about the conformational changes of proteins. One of the example illustrating the interaction of PPB (1–Picolyl–1H–benzo[d]imidazole) with HSA was reported by Zhuo et al [191]. As shown in figure 33, the fluorescence intensity of peak a increased with the addition of PPB. This is due to the formation PPB–HSA when PPB was added. The fluorescence intensity of peak b decreased markedly and the maximum emission wavelength of the peak was changed following the addition of PPB. Peak c was the second–ordered scattering peak ($\lambda_{em}=2\lambda_{ex}$). Analyzing from the intensity changes of peak a and peak b revealed that the binding of PPB to HSA induced some conformational and micro–environmental changes in HSA [192,193].

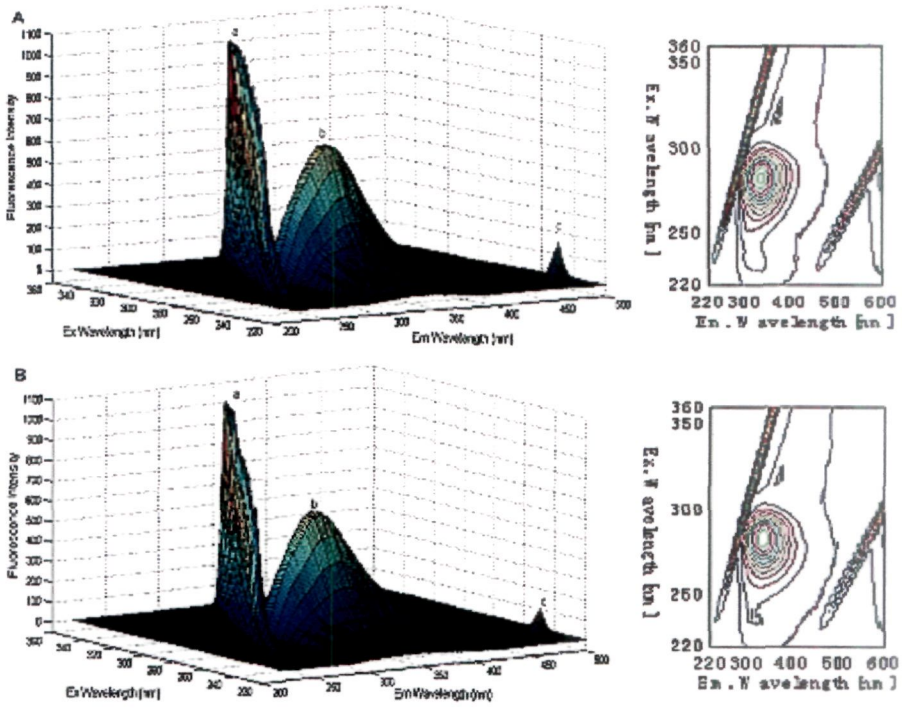

Figure 33. *Three–dimensional fluorescence spectra of HSA (A) and HSA–PPB system (B).*$C_{(HSA)}$*: (A) 3 μM, (B) 3 μM;* $C_{(PPB)}$*: (A) 0, (B) 6 μM.*

Table 2. *3D Fluorescence Spectral Parameters of HSA in the Absence and Presents of PPB*

Peak	HSA			HSA–PPB		
	Peak position $\lambda_{ex}/\lambda_{em}$ (nm/nm)	Δλ (nm)	Intensity	Peak position $\lambda_{ex}/\lambda_{em}$ (nm/nm)	Δλ (nm)	Intensity
Peah a	250/250–360/360	0	59.40–999.13	250/250–360/360	0	68.52–999.78
Peak b	280/334	58	628.232	280/338	54	600.174

There is a considerable interest in the development of synthetic chemical proteases that are activated by radical–generating metal complex [194,195]. Such chemical proteases can be utilized for breaking large proteins into smaller fragments that are more amenable to sequencing. One of the examples illustrated by Ferreira et al [196], in which the copper(II) complexes (Figure 34) were incubated with HSA for 30 min at 37 °C,

exhibited extensive carbonyl group formation, only in the case of complex $[Cu(isaepy)_2]^{+2}$.

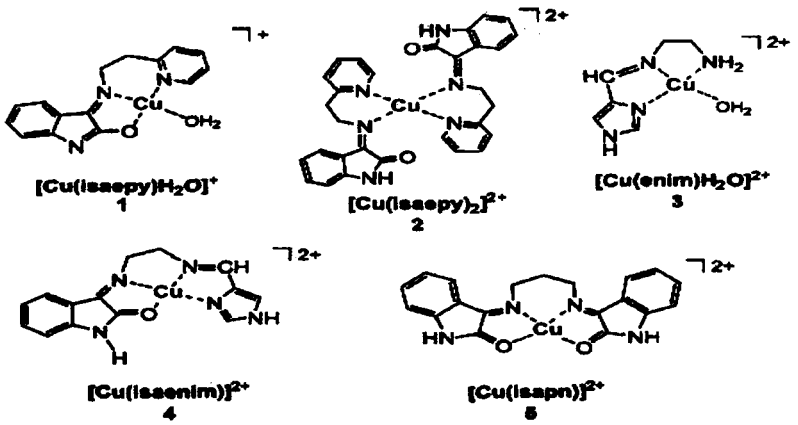

Figure 34. *Structures of the studied copper(II) complexes with oxindole–Schiff base ligands.*

However, in the presence of hydrogen peroxide all the complexes exhibited an increased level of protein oxidation (Figure 35a), depending on the ligand, in the order: $[Cu(isaepy)_2]^{2+}$ >> $[Cu(isapn)]^{2+}$ > $[Cu(isaepy)H_2O]^{+}$ ≈ $[Cu(isaenim)]^{2+}$ > $[Cu(enim)H_2O]^{2+}$ > $[Cu(H_2O)_4]^{2+}$.

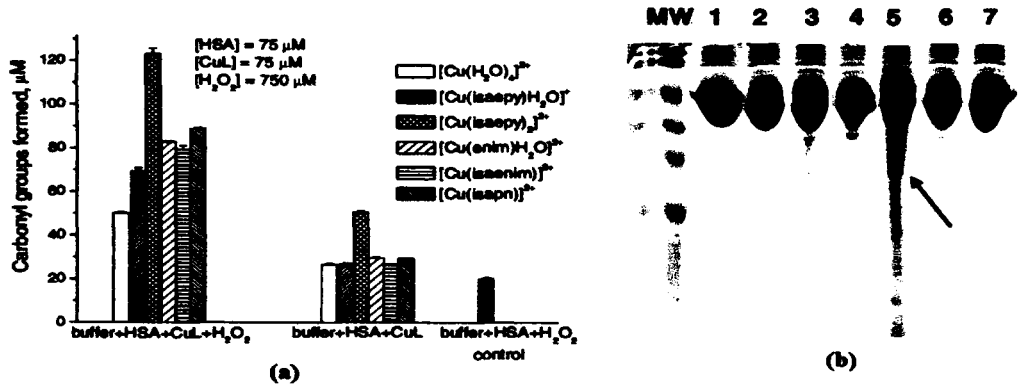

Figure 35. *(a) Carbonyl group formation in HSA protein (75 μM) after incubation with copper(II) complexes (75 μM), in the absence and in the presence of H_2O_2 (750 μM), for 30 min, at 37 °C and (b) SDS–PAGE showing HSA fragmentation treated with H_2O_2,in phosphate buffer 50 mM, pH 7.4. Lane 1: HSA; Lane 2: HSA + $[Cu(H_2O)_4]^{2+}$; Lane 3: HSA+ $[Cu(isapn)]^{2+}$; Lane4: HSA + $[Cu(isaepy)H_2O]^{+}$; Lane 5: HSA+ $[Cu(isaepy)_2]^{2+}$; Lane 6: HSA +$[Cu(enim)H_2O]^{2+}$; Lane 7: HSA + $[Cu(isaenim)]^{2+}$.*

Present Work

To explore the biological activities including antioxidant, DNA binding, topoisomerase–I inhibition and cytotoxicity, new metallopeptide based dinuclear copper(II) complex $[Cu_2(glygly)_2(ppz)(H_2O)_4]\cdot 2H_2O$ derived from glycyl glycine anion (glygly) and piperazine (ppz) was synthesized by employing *de novo* synthetic strategy which was thoroughly characterized by spectroscopic (IR, EPR, UV–vis, ESI–MS) and analytical methods. The structural elucidation of the complex was done by elemental analysis, spectroscopic methods and single crystal X–ray diffraction. The ligand scaffold was designed to modulate the toxicity, intrinsic resistance factors that exist in present cancer drugs. The single crystal X–ray analysis revealed the complex crystallizes as monoclinic crystal system with space group P21/c and contains two six coordinated Cu(II) centers bridged by piperazine ligand, which adopted a chair–shape conformation at the equatorial site. The interaction with CT DNA in Tris–HCl buffer was studied by various biophysical methods *viz.*, electronic absorption titrations fluorescence and circular dichroism. DNA cleavage activity employing agarose gel electrophoresis was also carried out examine the scission activity of the complex. A plasmid DNA cleavage assay was used to investigate the effect of complex on the activity of human Topo I by agarose gel electrophoresis. Superoxide dismutase activity of the complex was assayed by using its ability to inhibit the reduction of nitroblue tetrazolium, NBT, at 560 nm by superoxide ions produced by the xanthine–xanthine oxidase system. In vitro antitumor activity of the complex was screened against 9 different human carcinoma cell of different histological origin. The molecular docking technique was also utilized to ascertain the mechanism and mode of action towards the molecular target DNA and enzymes. Understanding the Topo I

inhibitory activity and DNA binding modes *viz.*; covalent or non–covalent plays a pronounced influence on the efficacy of a drug or chemical entity as a potential drug. However, the efficient passages of drugs into cells remain a major hurdle in anticancer drug delivery to the molecular target. In this regard, the interaction studies of complex with HSA were performed to elucidate the mechanism and mode of action at the molecular target. The interaction between complex and HSA was investigated by employing different spectroscopic techniques (UV–vis, fluorescence, CD, FTIR and 3D–fluorescence measurements) in accordance with molecular docking technique. Photo–induced degradation of HSA was carried out by employing SDS–PAGE analysis with increasing concentrations of complex. This work embodies the design of new specific target metallopeptide drug as potential chemotherapeutic agent *via* topoisomerase–I inhibition, also providing additional information about their possibilities of transport and disposition in blood plasma and contribute to the molecular design of novel synthetic protein photo–degradation agents. In an another attempt, complexes $[Zn(glygly)(ssz)(H_2O)].6H_2O$ and $[Cu(glygly)(ssz)(H_2O)].6H_2O$ were synthesized by reacting glycyl glycine anion (glygly) and sulfasalazine (ssz) followed drop wise addition of KOH. These complexes were thoroughly characterized by various spectroscopic techniques *viz.*, IR, UV–vis, ^{1}H, ^{13}C, NMR, EPR and elemental analysis and XRPD measurement. The interaction of Zn(II) complex with CT DNA was carried out by employing various biophysical methods such as UV–vis absorption, fluorescence and CD spectroscopy and molecular docking technique. A concentration dependent cleavage activity with pBR322 DNA was carried out by using agarose gel electrophoresis experiments in order to determine the mechanistic pathway for DNA cleavage. On the

other hand, interaction of Cu(II) complex with HSA was carried out by employing fluorescence, CD and FTIR measurement in accord with molecular docking technique.

A new series of transition metal complexes $[Cu_2(bipy)_2(im)_2(pip)(NO_3)_2].2NO_3$, $[Zn_2(bipy)_2(im)_2(pip)].4Cl$ and $[Ni_2(bipy)_2(im)_2(pip)].4Cl$ were synthesized to modulate the therapeutic profile to overcome inherent resistance and exhibit fewer side effects. *In vitro* DNA binding studies of all complexes were carried out to evaluate binding propensity towards DNA which demonstrate that $[Cu_2(bipy)_2(im)_2(pip)(NO_3)_2].2NO_3$ binds more avidly and readily to DNA in comparison to $[Zn_2(bipy)_2(im)_2(pip)].4Cl$ and $[Ni_2(bipy)_2(im)_2(pip)].4Cl$ complexes. To gain further insight into the molecular recognition at the target site, UV–vis titrations of complex $[Zn_2(bipy)_2(im)_2(pip)].4Cl$ with 5′–TMP and5′–GMP was carried out and validated by ^1H and ^{31}P NMR. The DNA cleavage and SOD activity was measured for complex $[Cu_2(bipy)_2(im)_2(pip)(NO_3)_2].2NO_3$.

New bis–macrocyclic complexes $[Cu_2(L)_2]$, $[Ni_2(L)_2]$ and $[Sn_2(L)_2.4Cl]$ derived from Schiff base (L) of salicylaldehyde and 5–aminosalicylic acid and further reacted with the linker–ligand 1,2–dibromo–ethane. The proposed structures of these dinuclear complexes were consistent with the data obtained from elemental analysis, molar conductance, IR, EPR, UV–vis, ESI–MS, ^1H, ^{13}C and ^{119}Sn NMR spectroscopy and XRPD measurement confirm its crystalline nature. The interaction studies of the complexes with CT DNA were carried out by using UV–vis absorption, emission, CD and NMR (^1H and ^{31}P) spectroscopy. DNA cleavage studies of complex $[Cu_2(L)_2]$ was carried out in absence and presence of external agents (activators, radical scavengers and groove binders).

CHAPTER II

Experimental

CHAPTER II

EXPERIMENTAL METHODS

1. Materials

2. Characterization techniques

2.1 Infrared spectroscopy

2.2 Ultra–violet and visible spectroscopy

2.3 Nuclear magnetic resonance spectroscopy

2.4 Electron paramagnetic resonance spectroscopy

2.5 Mass spectroscopy

2.6 C, H, N elemental Analyzer

2.7 X–ray powder diffraction analysis (XRPD)

2.8 Single crystal X–ray crystallography

2.9 Molar conductance measurements

2.10 Thermal gravimetric analysis (TGA)

3. DNA and HSA binding studies

3.1 Absorption spectral studies

3.2 Fluorescence spectral studies

3.3 Circular dichroism spectral studies

3.4 Three- dimensional fluorescence spectral studies

4. Gel electrophoresis

4.1 Agarose-Gel Electrophoresis for DNA

4.2 SDS-PAGE (sodium dodecyl sulfate polyacrylamide gel electrophoresis) for HSA

5. Topoisomerase I inhibition assay

6. Religation experiment with T4 DNA ligase enzyme

7. *In vitro* antitumor studies

8. Measurement of SOD like activity

9. Molecular docking studies

1. Materials

$Zn(NO_3)_2.6H_2O$, $CuCl_2.2H_2O$ and $ZnCl_2$.(anhydrous) (Rankem), $NiCl_2.6H_2O$(BDH), $SnCl_4.5H_2O$ (Lancaster), $Cu(NO_3)_2.3H_2O$ (Fisher Scientific), Glycylglycine (Loba chemie), Salicylaldhyde (Alfa Aesar), 1,2 dibromoethane and 1,10–Phenanthroline (merck), 5–aminosalcylic acid (Fluka), Sulfasalazine, Piperazine hexahydrate, 2,2'–Bipyridyl, imdazole and Human Serum Albumin (fatty acid free, 99%) were purchased from Sigma, Tris(hydroxymethyl)aminomethane or Tris Buffer, Calf thymus DNA (CT DNA), Guanosine 5'–monophosphate disodium salt (5'–GMP) and Thymidine 5'–monophosphate (5'–TMP) were purchased from Fluka and were stored at −20 °C. 6X loading dye (Fermental Life Science), Agarose, Ascorbic acid, Sodium azide (NaN_3), DMSO, Superoxide dismutase (SOD), Methyl green, DAPI, Mercaptopropionic acid (MPA) (Sigma–Aldrich) and Super coiled plasmid DNA pBR322 (Genei) were utilized as received. SOD activity was determined by using superoxide dismutase activity kit II Cat.No.574601 (Calbiochem) according to the manufacturer's protocol. All reagents and solvents were of the best commercial grade and were used without further purification.

2. Characterization techniques

2.1 Infrared spectroscopy

Infra–red spectra of the ligands and complexes were recorded as KBr pellets on Interspec 2020 FTIR spectrometer. The formation of the ligands and complexes behavior has been ascertained by scanning their infrared spectra in 4000–400 cm^{-1}.

2.2 Ultraviolet and visible spectroscopy

The electronic spectral studies of metal complexes provide useful information about the stereochemistry, oxidation state of the metal ion and in suitable circumstances, the nature

of metal–ligand bond. Electronic spectra were recorded on UV–1700 PharmaSpec UV–vis spectrophotometer (Shimadzu). Data were reported in λ_{max}/nm.

2.3 Nuclear magnetic resonance spectroscopy

The nuclei of certain isotopes possess a mechanical spin or angular momentum. The NMR spectroscopy is concerned with nuclei having nuclear spin quantum number I = 1/2, example of which include ^{1}H, ^{13}C, ^{31}P and ^{119}Sn.

For a nucleus with I = 1/2, there are two values for the nuclear spin angular momentum quantum number $m_I = \pm 1/2$ which are degenerate in the absence of a magnetic field. However, in the presence of the magnetic field, this degeneracy is destroyed such that the positive value of m_I corresponds to the lower energy state and negative value to higher energy state separated by ΔE.

In an NMR experiment, one applies strong homogeneous magnetic field causing the nuclei to presses. Radiation of energy comparable to ΔE is then imposed with radio frequency transmitter equal to precision or Larmor frequency and the two are said to be in resonance. The energy can be transferred from the source to the sample. The NMR signal is obtained when a nucleus is excited from low energy to high energy state.

The ^{1}H, ^{13}C and ^{119}Sn NMR spectra were obtained on a Bruker DRX–400 spectrometer at 400 MHz, respectively operating at room temperature. Chemical shifts were reported on the δ scale in parts per million (ppm).

2.4 Electron paramagnetic resonance spectroscopy

Electron paramagnetic resonance (EPR) spectra of the Cu(II) complexes were obtained on a Varian E 112 EPR spectrometer using tetracyanoethylene (TCNE) as field marker.

The spectra were recorded for solid and solutions of the complexes in appropriate solvents at room temperature (RT) as well as at liquid nitrogen temperature (LNT).

2.5 Mass spectroscopy

Mass spectrometry is one of the most accurate microanalytical technique which requires only a few nano moles of the sample to obtain characteristic information regarding the molecular mass and to detect within a molecule the places at which it prefers to fragment from which the presence of recognizable group within the molecule can be deduced. Mass spectrometry is complementary to FT IR, NMR, UV–vis and EPR spectral techniques for structural identification of compounds.

ESI mass spectra is relatively routine technique for mass spectrometric analysis of inorganic and organometallic compounds whether charged or neutral but involves complication by redox, fragmentation and clustering processes in the study of metal complexes. ESI mass spectra were recorded on a Micromass Quattro II triple quadrupol mass spectrometer.

2.6 C, H, N and S elemental Analyzer

Carbon, hydrogen and nitrogen contents were determined using Carlo Erba Analyzer Model 1106. The visualization of spots on TLC plates was effected by exposure to iodine or spraying with 10% H_2SO_4 and charring and single spots of the products were observed which were different from those of the starting materials.

2.7 X–ray powder diffraction analysis (XRPD)

To obtain further evidence about the structure of the metal complexes, X–ray diffraction studies were performed on Rigaku Mini Flex II Instrument.

2.8 Single crystal X–ray crystallography

Single crystal X–ray structural studies of complex was performed on a Bruker SMART instrument equipped with CCD–based detector at 298 K using graphite monochromated Mo Kα radiation (λ= 0.71073 Å) [197]. Data collections and their refinement were evaluated by using the Bruker SMART software. The collected data were reduced by using the program SAINT, [198] and empirical absorption corrections were done using the SADABS [199]. The structure was solved by direct methods and refined with the full–matrix least squares techniques using SHELX–97 [200]. The positions of all atoms were obtained by direct methods. Anisotropic thermal parameter were assigned to all non–hydrogen atoms and the remaining hydrogen atoms were placed in geometrically constrained position and refined as riding atoms with a common fixed isotropic thermal parameter. ORTEP3 [201] was used to produce graphical representation.

2.9. Conductance measurements

The conductivity measurement is one of the simplest and easily available techniques used to study the nature of the complexes. It gives direct information regarding whether a given compound is ionic or covalent. For this purpose, the measurement of molar conductance (Λ_m), which is related to the conductance value in the following manner is made.

$$\Lambda_m = \frac{cell\ constant \times conductance}{concentration\ of\ solute\ expressed\ in\ mol\ cm^{-3}} \qquad (1)$$

Conventionally, solutions of 1 x 10^{-3} M strength are used for the conductance measurements. Molar conductances were measured at room temperature on a Digsun Electronic conductivity Bridge.

2.10. Thermal gravimetric analysis (TGA)

TGA was performed with a universal V3.8 B TA SDT Q600 Build 51 Thermal Analyzer under nitrogen atmosphere using alumina powder as reference material. The final thermolysis product of metal complex as metal oxides was studied.

3. DNA and HSA binding studies

All the experiments involving interaction of the complexes with CT DNA were conducted in buffer containing Tris(hydroxymethyl)aminomethane or Tris Buffer (0.01 M) adjusted to pH 7.2 with 4M hydrochloric acid. The CT DNA was dissolved in Tris HCl buffer and was dialyzed against the same buffer overnight. Solutions of CT DNA gave ratios of UV absorbance at 260 and 280 nm above 1.9:1, indicating that the DNA was sufficiently free of protein [202]. DNA concentration per nucleotide was determined by absorption spectroscopy using the molar absorption coefficient 6600 $dm^3 mol^{-1} cm^{-1}$ at 260 nm [203]. The stock solution was stored at 4 °C.

Human serum albumin of 1×10^{-3} M was prepared by dissolving protein in Tris–HCl buffer solution at pH 7.4. The protein concentration was determined spectrophotometrically using an extinction coefficient of 35219 $M^{-1} cm^{-1}$ at 280 nm [204]. Stock solution of complex (1×10^{-3} M) was prepared by dissolving complex in doubly distilled water. NaCl (analytical grade, 1M) solution was used to maintain the ionic strength of buffer at 0.1M, pH was adjusted to 7.4 by using HCl. Working standard solution was obtained by appropriate dilution of the stock solution.

3.1 Absorption spectral studies

3.1.1 Absorption spectral studies for DNA

These absorption spectral studies were performed on Shimadzu UV–1700 PharmaSpec UV–vis spectrophotometers. The intrinsic binding constant K_b of the complex to CT

DNA was determined from equation (2), through a plot of [DNA]/ ε_a–ε_f vs [DNA], where [DNA] represents the concentration of DNA, and ε_a, ε_f and ε_b the apparent extinction coefficient (A_{obs}/[M]), the extinction coefficient for free metal complex (M), and the extinction coefficient for the free metal complex (M) in the fully bound form, respectively. In plots of [DNA]/ε_a–ε_f vs. [DNA], K_b is given by the ratio of slope to intercept [205].

$$\frac{[DNA]}{\varepsilon_a - \varepsilon_f} = \frac{[DNA]}{\varepsilon_b - \varepsilon_f} + \frac{1}{K_b(\varepsilon_a - \varepsilon_f)} \qquad (2)$$

Absorption spectral titration experiments were performed by maintaining a constant concentration of the complex and varying the nucleic acid/nucleotide concentration. This was achieved by diluting an appropriate amount of the metal complex solutions and CT DNA/5'–GMP, 5'–TMP stock solutions while maintaining the total volume constant. This results in a series of solutions with varying concentrations of CT DNA/5'–GMP/5'–TMP but at constant concentration of the complex. The absorbance (A) was recorded after successive additions of CT DNA/5'–GMP/5'–TMP. While measuring the absorption spectra an equal amount of CT DNA/5'–GMP/5'–TMP was added to both the compound solution and the reference solution to eliminate the absorbance of the CT DNA/5'–GMP/5'–TMP itself.

3.1.2 Absorption spectral studies for HSA

The intrinsic binding constant K_b of the complex to HSA was determined from equation (3), through a plot of 1/A–A_o vs. 1/ $C_{complex}$, where A_o and A are the absorbance of HSA at 280 nm, in the absence and presence of complex, respectively. ε_{HSA} and ε_B are the molar extinction coefficient of HSA and the bound complex, respectively.

$$\frac{A_o}{A-A_o} = \frac{\varepsilon_{HSA}}{\varepsilon_B} + \frac{\varepsilon_{HSA}}{\varepsilon_B K_b} \cdot \frac{1}{C_{complex}} \qquad (3)$$

The double reciprocal plot of $1/A-A_o$ vs. $1/C_{complex}$ is linear and binding constant can be estimated from the ratio of intercept to the slope [206].

3.2 Fluorescence spectral studies

3.2.1 Fluorescence spectral studies for DNA

Emission intensity measurements were carried out using Hitachi F–2500 spectrofluorometer in a 1 cm path–length quartz cell. The emission spectrum is obtained by setting the excitation monochromator at the maximum excitation wavelength and scanning with emission monochromator. Often an excitation spectrum is first made in order to confirm the identity of the substance and to select the optimum excitation wavelength. Further experiments were carried out to gain support for the mode of binding of complexes with CT DNA.

Non–fluorescent or weakly fluorescent compounds can often be reacted with strong fluorophores enabling them to be determined quantitatively. On this basis molecular fluorophore EthBr was used which emits fluorescence in presence of CT DNA due to its strong intercalation. Quenching of the fluorescence of EthBr bound to DNA were measured with increasing amount of metal complexes as a second molecule and Stern–Volmer quenching constant K was obtained from the following equation (4) [207]:

$$I_o/I = 1 + Kr \qquad (4)$$

where r is the ratio of total concentration of complex to that of DNA and I_o and I are the fluorescence intensities of EthBr in the absence and presence of complex.

Binding constant K of the metal complexes was also determined from Scatchard equations (3) and (4) by employing emission titration [208,209]:

$$C_F = C_T(I / I_o - P)\ (1-P) \qquad (5)$$

$$r/C_F = K\ (n-r) \qquad (6)$$

where C_F is the free probe concentration, C_T is the total concentration of the probe added, I and I_0 are fluorescence intensities in presence and absence of CT DNA, respectively and P is the ratio of the observed fluorescence quantum yield of the bound probe to that of the free probe. The value P was obtained as the intercept by extrapolating from a plot of I/I_o vs 1/[DNA], r denotes ratio of C_B ($=C_T-C_F$) to the DNA concentration i.e., the bound probe concentration to the DNA concentration, K is the binding constant and C_F, is the free metal complex concentration and "n" is the binding site number. Emission intensity measurements were carried out using Hitachi F–2500 spectrofluorometer at room temperature.

3.2.1 Fluorescence spectral studies for HSA

Fluorescence measurements were carried out on Hitachi F–2500 fluorescence spectrophotometer in a 1 cm path–length quartz cell with the excitation and emission wavelength set at 280 and 300–400 nm, respectively. The intensity at 350 nm (Tryptophan) was used to calculate the binding constant (K). The fluorescence quenching of HSA at different temperatures (299, 308 and 318 K) were determined using the Stern–Volmer equation (7) [210]:

$$\frac{F_o}{F} = 1 + K_q \tau_o [Q] = 1 + K_{SV}[Q] \qquad (7)$$

where F_o and F are the fluorescence intensities in absence and presence of quencher, respectively, [Q] is the quencher concentration, and K_{SV} Stern–Volmer quenching constant, which can be written as

$$K_q = \frac{K_{SV}}{\tau_o} \qquad (8)$$

where K_q is the biomolecular quenching rate constant and τ_o is the average lifetime of the fluorophore (Trp–214) in absence of quencher and its value is around 10^{-8} s for most biomolecules [211]. Therefore, Equation (7) was applied to determine K_{SV} by linear regression of a plot of F_o/F vs [Q].

Calculation of binding constant

The binding constant was calculated from the modified Stern–Volmer equation (Equation (9)):

$$\frac{1}{[F_o - F]} = \frac{1}{F_o} + \frac{1}{K_b}\frac{1}{F_o}\frac{1}{Q} \qquad (9)$$

where K_b is the binding constant of complex with biomolecule which was calculated from the intercept and slope of slopes of the Lineweaver–Burk ($1/(F_o–F)$ versus $1/[Q]$) (intercept = $1/F_o$, slope = $1/K_bF_o$, so K_b = intercept/slope). Furthermore, the binding constant (K) and number of bound complex to HSA (n) were determined by plotting the double log graph of the fluorescence data using (Equation (10)):

$$\log\left[\frac{F_o - F}{F}\right] = \log K + n\log[Q] \qquad (10)$$

Determination of thermodynamic parameters

The thermodynamic parameters were calculated from the van't Hoff equation (Equation (11)):

$$\ln K = \frac{-\Delta H}{RT} + \frac{\Delta S}{R} \qquad (11)$$

where K is the Lineweaver–Burk static quenching constant at corresponding temperature and R is the gas constant, in which ΔH and ΔS of reaction was determined from the linear relationship between ln K and the reciprocal absolute temperature. Furthermore, the free energy change (ΔG) was calculated by the equation (12):

$$\Delta G = \Delta H - T\Delta S = -RT \ln K \qquad (12)$$

Calculations of energy transfer

According to Foster resonance energy transfer (FRET), the efficiency of energy transfer (E) is given by [212]:

$$E = 1 - \frac{F}{F_o} = \frac{R_o^{\,6}}{R_o^{\,6} + r_o^{\,6}} \qquad (13)$$

where F and F_0 are the fluorescence intensities of HSA in the presence and absence of quencher, r is the distance between acceptor and donor and R_0 is the critical distance when the transfer efficiency is 50%. The value of R_0 was calculated using the equation (14):

$$R_o^{\,6} = 8.78 \times 10^{-25} k^2 N^{-4} \phi J \qquad (14)$$

where k^2 is spatial orientation factor between the emission dipole of the donor and the absorption dipole of acceptor, N is the refractive index of the medium, ϕ is the fluorescence quantum yield of the donor and J is the overlap integral of the fluorescence emission spectrum of the donor and the absorption spectrum of the acceptor and calculated by equation (15):

$$J = \frac{\sum F(\lambda)\varepsilon(\lambda)\lambda^4 \Delta\lambda}{\sum F(\lambda)\Delta\lambda} \qquad (15)$$

where F(λ) is the corrected fluorescence intensity of the donor at wavelength λ and ε(λ) is the molar absorption coefficient of the acceptor at wavelength λ. Under the experimental condition, the value of K^2 =2/3, N =1.336, and ϕ = 0.188 [213].

3.3 Circular dichroism (CD) and Fourier Transform Infrared (FTIR) measurements.

CD spectra were measured on Jasco J–815–CD spectropolarimeter (Jasco, Japan) at room temperature using a 1 cm quartz cuvette. Measurements were taken at wavelengths between 200 and 250 nm. All observed CD spectra were baseline subtracted for buffer and the CD results were expressed in terms of MRE (mean residue ellipsticity) in deg cm^2 d mol^{-1} as Eq. (16):

$$MRE = \left[\frac{Observed CD(m\,\mathrm{deg})}{C_p n l \times 10} \right] \qquad (16)$$

where *Cp* is the molar concentration of the protein, *n* the number of amino acid residues (585) and *l* the path length (0.1 cm). The α–helical contents of free and combined HSA were calculated from the MRE value at 208 nm using the Eq. (17) as described by Basu et al [214]:

$$\alpha - helix(\%) = \left[\frac{-(MRE)_{208} - 4000}{33000 - 4000} \right] \times 100 \qquad (17)$$

where MRE_{208} is the observed MRE value at 208 nm, 4000 is the MRE of the β–form and random coil conformation cross at 208 nm, and 33000 is the MRE value of a pure α–helix at 208 nm.

Fourier Transform Infrared measurements carried out on an Interspec 2020 FTIR spectrometers were recorded in liquid phase in 400–4000 cm^{-1} range.

3.4 Three–dimensional (3D) fluorescence spectral studies

Three–dimensional fluorescence spectroscopy is a vigorous method for providing conformational and structural information of proteins. The outstanding advantage of three–dimensional fluorescence spectra is that the information regarding the fluorescence characteristics can be entirely acquired by simultaneously changing the excitation and emission wavelengths. The maximum emission wavelength and the fluorescence intensity of the residues have a close relation to the polarity of their micro–environment [215]. 3D–Fluorescence measurements were performed on an FL–4500 spectrofluorophotometer (Japan) under the following conditions: the emission wavelength scan range was recorded between 240 nm and 600 nm, the excitation wavelength scan range was recorded from 240 to 360 nm at 10 nm increments and other scanning parameters were just the same as the fluorescence quenching spectra.

4. Gel electrophoresis (Cleavage Studies DNA & HSA)

Cleavage experiments were performed with the help of Axygen electrophoresis supported by Genei power supply with a potential range of 50–500 Volts, visualized and photographed by Vilber–INFINITY gel documentation system.

4.1. Agarose–Gel Electrophoresis of DNA

The cleavage experiments of supercoiled pBR322 DNA (300 ng) in (5mM Tris–HCl, 50 mM NaCl), buffer at pH 7.4 was carried out using agarose gel electrophoresis. The samples were incubated for 1 hour at 37 °C. A loading buffer containing 25% bromophenol blue, 0.25% xylene cyanol, 30% glycerol was added and electrophoresis was carried out at 60 V for 1hour in Tris–HCl buffer using 1% agarose gel containing 1.0 μg/mL ethidium bromide. The DNA cleavage with added reductant was monitored as in

case of cleavage experiment without added reductant using agarose gel electrophoresis. The reaction were also monitored upon addition of various radical inhibitors such as sodium azide (NaN_3), DMSO, superoxide dismutase (SOD), distamycin, methyl green and mercaptopropionic acid (MPA). The samples were incubated for 45 minutes at 37 °C. The gel was visualized by photographing the fluorescence of intercalated ethidium bromide under a UV illuminator. The cleavage efficiency was measured by determining the ability of the complex to convert the supercoiled DNA (SC) to nicked circular form (NC) and linear form (LC).

4.2. SDS-PAGE (sodium dodecyl sulfate polyacrylamide gel electrophoresis) of HSA

Photo–induced protein cleavage experiments were performed following to the standard methods and practices previously adopted by Kumar and co–workers. [216]. The photo–induced protein cleavage studies were carried out using freshly prepared solution of HSA in 50 mM Tris–HCl buffer (pH 7.4). The protein solutions (15 μM) containing complex with increasing concentrations 100 to 250 μM were photo–irradiated at 365 nm for 20 min after 45 min incubation at 37 °C followed by SDS–PAGE analysis.

5. Topoisomerase I inhibition assay

DNA topoisomerase I, Human (Topo I) was purchased from CALBIOCHEM and was used without further purification. One unit of the enzyme was defined as completely relax 1 μg of negatively supercoiled pBR322 DNA in 30 min at 310 K under the standard assay conditions. The reaction mixture (30 μL) contained 35 mM Tris–HCl (pH 8.0), 72 mM KCl, 5 mM $MgCl_2$, 5 mM DTT, 2 mM spermidine, 0.1 mg/mL BSA, 0.25 μg pBR322 DNA, 2 Unit Topo I and complex sample. These reaction mixtures were incubated at 310 K for 30 min, and the reaction was terminated by addition of 4 μL of 5X buffer solution

consisting of 0.25% bromophenol blue, 4.5 % SDS and 45% glycerol. The samples were electrophoresed through 1% agarose in TBE at 30 V for 8h.

6. Religation experiment with T4 DNA ligase enzyme

The DNA religation experiments were performed using T4 DNA ligase enzyme to support the hydrolytic mechanism of DNA cleavage by following the standard DNA religation protocol [217]. The complex treated with pBR322 plasmid DNA (2 mg), ligation buffer of 1.5 mL in 10X, T4 ligase 1 mL (2 units) and 2.5 mL of H_2O were mixed and incubated at 4 °C for 1h. Subsequently, the samples were loaded on 1% agarose gel and visualized by staining with an ethidium bromide solution.

7. *In vitro* antitumor studies

The cell lines used for *in vitro* antitumor screening activity were, MIAPaCa–2 (Pancreatic), MCF–7, ZR–75–1 (Breast), SiHa (Uterine Cervix), Colo205, HCT15, SW620 (Colon), HOP–62, A549 (Lung), DWD (Oral), K562 (Leukemia), DU145, PC–3 (Prostate), A498 (Renal Cell), A2780 (Ovary), T24 (Urinary Bladder), U373MG (Astrocytoma), HT29 (colon adenocarcinoma grade II cell line) and Hela (Epithlial Carcinoma). G–adriamycin, standard anticancer drug was taken as control. These human malignant cell lines were procured and grown in RPMI–1640 medium supplemented with 10% Fetal Bovine Serum (FBS) and antibiotics to study growth pattern of these cells. The proliferation of the cells upon treatment with chemotherapy entities was determined using the Sulphorhodamine–B (SRB) semi–automated assay [218,219]. The dose response parameters such as growth inhibition 50% (GI_{50}), total growth inhibition (TGI) and lethal concentration 50% (LC_{50}) were calculated. GI_{50} is the concentration of drug required to decrease the cell growth to 50%, compared with that of the untreated cell number. TGI is

the concentration of drug required to decrease the cell growth to 100%, compared with that of the untreated cell number, during drug incubation. LC_{50} is the concentration of drug required to decrease the cell growth by 50% of the initial cell number prior to the drug incubation. Cells were seeded in 96 well plates at an appropriate cell density to give optical density in the linear range (from 0.5 to 1.8) and were incubated at 37 °C in CO_2 incubator for 24 hour. Stock solutions of the complexes were prepared as 100 mg/mL in DMSO and four dilutions i.e. 10 µL, 20 µL, 40 µL, 80 µL, in triplicates were tested, each well receiving 90 µL of cell suspension and 10 µL of the drug solution. Appropriate positive control (adriamycin) and vehicle controls were also run. The plates with cells were incubated in CO_2 incubator with 5% CO_2 for 24 hours followed by drug addition. The plates were incubated further for 48 hours. Termination of experiment was done by gently layering the cells with 50 µL of chilled 30% TCA (in case of adherent cells) and 50% TCA (in case of suspension cell lines) for cell fixation and kept at 4 °C for 1 h. Plates were stained with 50 µL of 0.4% SRB for 20 minutes. The bound SRB was eluted by adding 100 µL 10 mM Tris (pH 10.5) to each of the wells. The absorbance was read at 540 nm with 690 nm as reference wavelength. All experiments were repeated 3 times.

8. Measurement of SOD like activity

Superoxide dismutase (SOD)–like activity was investigated using Beauchamp and Fridovich's method – as improved by Imanari et al [220]. This method is based on the inhibitory effect of SOD on the reduction of nitrobluetetrazolium (NBT) by the superoxide anion generated by the xanthine/xanthine oxidase system. The assay was carried out in the assay buffer containing 50mM Tris HCl, pH 8.0, 0.1mM diethylene triamine penta acetic acid (DTPA) and 0.1mM hypoxanthine. Radical detector consists of a tetrazolium salt and is diluted by assay buffer. Similarly, the solutions of SOD

standards and xanthine oxidase were prepared in sample buffer consisting of 50mM Tris–HCl, pH 8.0. The complex was dissolved in its solvent and absorbance was reported for each set of concentrations after 15 minutes interval. Results were graphed as % inhibition of NBT reduction taken at various concentrations (0μM–20μM) for each complex on the study. IC_{50} values are reported equivalent concentrations (μM) to 1U bovine erythrocyte superoxide dismutase (native SOD).

9. Molecular docking studies

The rigid molecular docking studies were performed by using HEX 6.1 software [221], is an interactive molecular graphics program for calculating and displaying feasible docking modes of a pairs of protein, enzymes and DNA molecule. Structure of the complexes were sketched by CHEMSKETCH (http:// www.acdlabs.com) and convert it into pdb format from mol. Formate by OPEN BABEL (http:// www.vccclab.org/lab/babely). The coordinates of metal complex was taken from its crystal structure as a CIF file and was converted to the PDB format using Mercury software. The crystal structure of the B–DNA dodecamer $d(CGCGAATTCGCG)_2$ (PDB ID: 1BNA), native SOD (PDB ID: 1SXA), human–DNA–Topo I complex (PDB ID: 1SC7) and human serum albumin (PDB ID: 1h9z) were downloaded from the protein data bank (http://www.rcsb.org./pdb). All calculations were carried out on an Intel Pentium 4, 2.4 GHz based machine running MS Windows XP SP2 as operating system. Visualization of the docked pose has been done by using CHIMERA (http://www.cgl.ucsf.edu/chimera/) and PyMol (http://pymol.sourceforget.net/) molecular graphics program.

CHAPTER III (a)

Molecular drug design, synthesis and structure elucidation of new specific target peptide based metallo drug for cancer chemotherapy as topoisomerase I inhibitor

Synthesis

Synthesis of $[Cu_2(glygly)_2(ppz)(H_2O)_4].2H_2O$

To a stirred methanolic solution (15 ml) of $Cu(NO_3)_2.3H_2O$ (0.483g, 0.002mol) was added an aqueous solution of glycyl glycine (0.26g, 0.002mol) followed by drop wise addition of KOH (0.224g, 0.004mol) and pH of the resulting solution was adjusted between 8.0 – 12. This reaction mixture was stirred for ca 2 h at room temperature to obtain clear blue color solution. A methanolic solution (10 cm^3) of piperazine hexahydrate (0.194g, 0.001mol) was added to the above reaction mixture and stirred for 3h. The light blue colored solid precipitate was obtained and filtered off under vacuum, washed thoroughly with ice cold methanol and dried in vacuo over anhydrous $CaCl_2$ (Yield: 0.255g, 44%). Crystals suitable for X–ray analysis were collected after recrystallization from a mixture of $MeOH:H_2O$ (95:5) after several days at room temperature. m.p. 205 ± 2 °C (dec.). Anal. Calc. for $C_{12}H_{34}Cu_2N_6O_{12}$ (%): C, 24.79; H, 5.89; N, 14.45, Found: C, 24.64; H, 5.67; N, 14.85. Selected IR data on KBr/nujol, cm^{-1}: 3398 $\nu(NH_2+H_2O)$; 1602 $\nu(C=O)$; 1376 $\nu(C–N)$; 537 (Cu–O); 415 (Cu–N). Molar Conductance, Λ_M ($1\cdot10^{-3}$ M, H_2O): 20 $\Omega^{-1}cm^2$ mol^{-1} (Non–electrolyte). UV-vis absorption: (H_2O, 10^{-4} M), λ_{max}/nm ($\varepsilon/10^3$ M^{-1} cm^{-1}): 232 (1.50); 278 (4.70); 644 (2.50).

Results and Discussion

In order to enhance the specificity of the molecular recognition towards DNA helices and inhibition of the catalytic activity of many enzymes, new drug candidate, complex $[Cu_2(glygly)_2(ppz)(H_2O)_4].2H_2O$ was synthesized and characterized. The synthesis of new dinuclear copper(II) complex $[Cu_2(glygly)_2(ppz)(H_2O)_4].2H_2O$ was achieved by mixing stoichiometric amounts of Cu(II) nitrate trihydrate with glycyl glycine followed by the reaction with piperazine hexahydrate (Scheme 1).

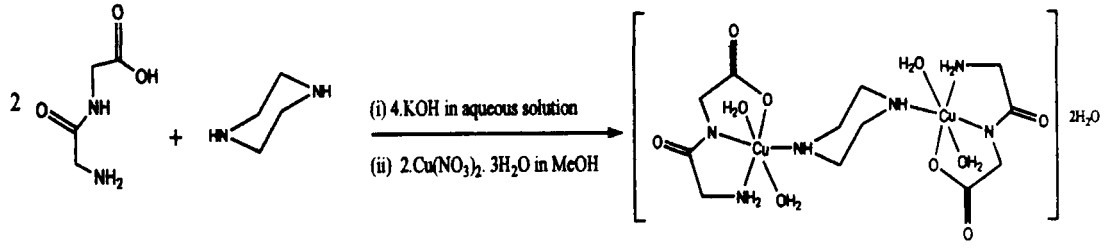

Scheme 1. *Synthesis scheme of* $[Cu_2(glygly)_2(ppz)(H_2O)_4].2H_2O$

The resulting complex $[Cu_2(glygly)_2(ppz)(H_2O)_4].2H_2O$ is stable towards air and moisture and readily soluble in H_2O. The complex was characterized by using elemental analysis, IR, UV–vis and EPR spectral studies. Molar conductance value of complex in H_2O (1×10^{-3} M) at 25 °C suggest its non–electrolyte nature (20 $\Omega^{-1}cm^2$ mol^{-1}). The formulation of the complex $[Cu_2(glygly)_2(ppz)(H_2O)_4].2H_2O$ was further confirmed by determination of the X–ray crystal structure.

X-ray structure of $[Cu_2(glygly)_2(ppz)(H_2O)_4].2H_2O$

The single crystal X–ray analysis reveals the complex $[Cu_2(glygly)_2(ppz)(H_2O)_4].2H_2O$ crystallizes as monoclinic crystal system with space group *P*21/*c*. An ORTEP view of the complex is illustrated in Figure 36, while selected bond lengths and bond angles are listed in Table 4. The packing diagram in the unit cell is shown in Figure 37. The $[Cu_2(glygly)_2(ppz)(H_2O)_4].2H_2O$ contains two six coordinated Cu(II) centers bridged by piperazine ligand, which adopted a chair–shape conformation at the equatorial site. Both Cu(II) centers are in a N_3O_3 coordination environment arranged in distorted octahedral geometries, as evidenced by all of the angles around them, which deviate from 180° and 90° (Table 4). The coordination sites around each Cu(II) centers is achieved by the terminal amino nitrogen (Cu(1)–N(2), 2.063 Å), the deprotonated peptide nitrogen (Cu(1)–N(2), 1.897 Å) and one of the carboxylate oxygen (Cu(1)–O(1), 2.017 Å) of the dipeptide and the fourth is ligated by the piperazine nitrogen (Cu(1)–N(3), 1.993 Å).

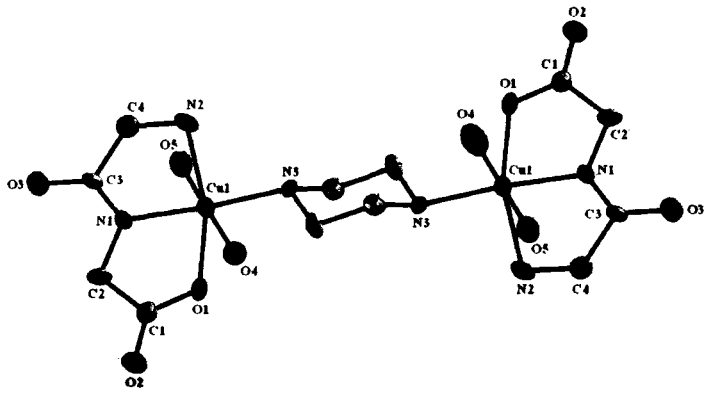

Figure 36. *ORTEP view of the $[Cu_2(glygly)_2(ppz)(H_2O)_4].2H_2O$ with atom numbering scheme. thermal ellipsoids are drawn at 50% probability level and solvent molecules were omitted for clarity.*

Besides these coordinations, the axial position is occupied by two oxygen atoms, O4 and O5 (Cu(1)–O(4), 2.381 Å, Cu(1)–O(5), 2.381 Å) provided by an aqua ligands. The Cu–N_{imine} distances (involving sp^2 N) are slightly shorter than the Cu–N_{amine} distances (involving sp^3 N) indicating that deprotonated nitrogen is more strongly coordinated to metal center than terminal amino group [222, 223]. On the other hand, the Cu–$O_{carboxylate}$ bond lengths exhibit smaller values than the Cu–O_{water}. The intramolecular Cu...Cu distance is near 6.803 Å, which is short as compared to 6.908 and 6.881 Å in previously reported chair–piperazine–bridged Cu_2 complexes [224]. As a consequence of small bite angles of N(1)–Cu(1)–N(2) and N(1)–Cu(1)–O(1) are 82.44° and 82.38°, respectively, is primarily responsible for distortion from the regular octahedral geometry. Whereas, the angle between N(1)–Cu(1)–N(3), N(3)–Cu(1)–O(1), N(3)–Cu(1)–N(2), O(1)–Cu(1)–N(2) and N(1)–Cu(1)–O(4) are 173.20°, 98.77°, 95.56°, 163.48° and 92.83°, respectively. The stability of the complex is reinforced by the intra–molecular interligand interaction (ppz) N3–H3···O2 (glygly) (2.079 Å; Figure 37). Thus, the molecular recognition pattern between the Cu(ppz) chelate and the glygly ligand was featured by the cooperative effect of the Cu(1)—N3(ppz) coordination bond and referred as interligand H–bond. Moreover,

it seems clear that such intra–molecular H–bond noticeably influences the molecular topology [225].

Table 3. Crystallographic data for the complex $[Cu_2(glygly)_2(ppz)(H_2O)_4].2H_2O$

Parameter	
CCDC No	CCDC 794697
formula	$C_{12}H_{34}Cu_2N_6O_{12}$
Fw (g mol^{-1})	581.55
cryst syst	Monoclinic
space group	*P*21/*c*
a (Å)	8.704(4)
b (Å)	10.611(5)
c (Å)	12.345(5)
α(deg)	90
β(deg)	105.085
γ(deg)	90
V($Å^3$)	1100(9)
Z	2
D_{calc} (Mg m^{-3})	1.754
μ (mm^{-1})	2.003
F(000)	604.0
crystal size (mm)	0.15 × 0.14 × 0.12
temp (K)	298(2)
measured reflns	9480
unique reflns	1943
θ range (deg)/ completeness (%)	2.42 to 25.00
no.of data/parameters/restraints	1943/172/0
GoF[a]	0.981
R^b[I>2σ(I)]	0.0418
$wR_2{}^b$(all data)	0.1006
largest diff. peak/hole (e.$Å^{-3}$)	0.478/–0.405

[a]GoF is defined as $\{\sum[w(F_0^2 - F_c^2)]/(n-p)\}^{1/2}$ where n is the number of data and p is the number of parameters. [b]$R = \{\sum\left\|F_0\right|-\left|F_c\right\|/\sum|F_0|, wR_2 = \{\sum w(F_0^2 - F_c^2)^2 / \sum w(F_0^2)^2\}^{1/2}$

Furthermore, it is believed that mode of coordination has a major influence on the conformational changes of a peptide molecule that influences its reactivity towards the receptor sites. So, complex formation plays significant role on the biological activity of

peptides where metal ions can be regarded as catalysts for many reactions and have been used for DNA selective recognition and/or cleavage.

Table 4. *Selected bond lengths (Å) and angles (°) for* $[Cu_2(glygly)_2(ppz)(H_2O)_4].2H_2O$

Bond lengths	(Å)
Cu(1) – N(1)	1.897(3)
Cu(1) – N(3)	1.993(3)
Cu(1) – O(1)	2.017(3)
Cu(1) – N(2)	2.063(3)
Cu(1) – O(4)	2.381(4)
Bond Angles	**(°)**
N(1) – Cu(1) – N(3)	173.20(15)
N(1) – Cu(1) – O(1)	82.38(13)
N(3) – Cu(1) – O(1)	98.77(13)
N(3) – Cu(1) – N(2)	82.44(15)
N(3) – Cu(1) – N(2)	95.56(15)
O(1) – Cu(1) – N(2)	163.48(13)
N(1) – Cu(1) – O(4)	92.83(14)
N(3) – Cu(1) – O(4)	93.89(14)
O(1) – Cu(1) – O(4)	89.36(15)
N(2) – Cu(1) – O(4)	97.85(17)

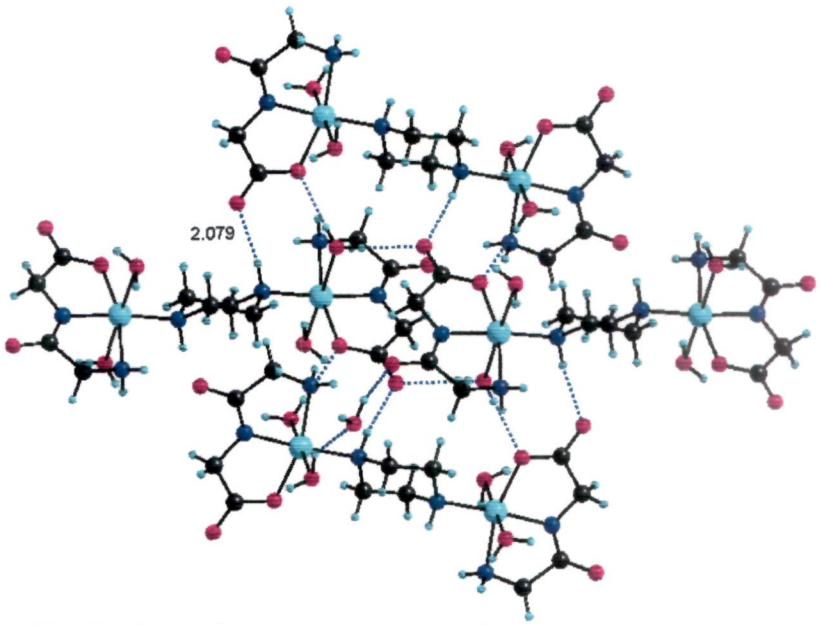

Figure 37. *The Packing diagram of* $[Cu(glygly)_2(ppz)(H_2O)_4].2H_2O$*, showing O–H interactions.*

Spectroscopic studies

Infrared spectra

The assignment of the IR bands of complex $[Cu_2(glygly)_2(ppz)(H_2O)_4].2H_2O$ was carried out in comparison to the IR spectra of the free dipeptide. The formation of complex was evidenced by the appearance of characteristic absorption bands at 3100–2950 cm^{-1}, 1625–1600 cm^{-1}, 1585–1550 cm^{-1} and 1393–1348 cm^{-1} which were attributed to $\nu_{as}(NH_3^+)$, $\delta(NH_3^+)$, $\nu_{as}(CO_2)$ and $\nu_s(CO_2)$, respectively. Disappearance of the $\nu_{as}(NH_3^+)$, and $\delta(NH_3^+)$ bands (associated with the zwitterions structure) in complex $[Cu_2(glygly)_2(ppz)(H_2O)_4].2H_2O$ was coupled with the appearance of broad band in the range 3398–3267 cm^{-1} assigned to the stretching vibrations of coordinated water molecules and terminal amino groups. The $\nu(CO)_{peptide}$ [amide I] band observed at ~1665 cm^{-1} in the free dipeptide was shifted to lower frequency at ~1602 cm^{-1} in complex $[Cu_2(glygly)_2(ppz)(H_2O)_4].2H_2O$ after complexation confirming the coordination of metal ion through O atom of deprotonated carboxylate group [226,227]. The bands around 1575 cm^{-1} and 1254 cm^{-1} observed in the free dipeptides attributed to amide II and III bands [due to $\delta(NH)+\nu(C–N)$ in compound containing neutral secondary peptide groups] were replaced by a new absorption band at 1376 cm^{-1} in complex $[Cu_2(glygly)_2(ppz)(H_2O)_4].2H_2O$. This is characteristic for deprotonated secondary peptide complex, since on removal of peptide proton the band becomes a pure C–N stretch [228]. The formation of complex $[Cu_2(glygly)_2(ppz)(H_2O)_4].2H_2O$ was also revealed by the presence of intense bands around ~ 415, ~537 cm^{-1} corresponding to Cu–N and Cu–O, respectively.

Electronic spectra

The electronic absorption spectrum of complex $[Cu_2(glygly)_2(ppz)(H_2O)_4].2H_2O$ in freshly prepared aqueous solutions was carried out in the region 200–1100 nm at room

temperature. The electronic spectra of free dipeptides displayed an intense absorption bands at 220 nm due to n→π* transition which was shifted to 232 nm upon coordination with Cu(II) metal ion, and has been assigned to N^-→Cu(II) ligand–to–metal charge transfer (LMCT) transition. A band at 278 nm was tentatively assigned to a COO^- →Cu(II) charge–transfer transition [229]. The low energy d–d band at 644 nm was assigned to $^2B_{1g}$→$^2B_{2g}$ transitions suggesting an octahedral geometry around Cu(II) metal ion [230], as deduced by EPR and validated by X–ray crystal structure.

EPR studies

The solid state X–band EPR spectra of the complex $[Cu_2(glygly)_2(ppz)(H_2O)_4].2H_2O$ was acquired at a frequency of 9.1 GHz under the magnetic field strength 3000±1000 Gauss using tetracyanoethylene (TCNE) as field marker at LNT (Figure 38). The complex exhibited an anisotropic spectrum with $g_{\|} = 2.19$ and $g_{\perp} = 2.06$ and $g_{av} = 2.08$ computed from the expression $g_{av}^2 = (g_{\|}^2 + 2g_{\perp}^2)/3$. These values are consistent with an octahedral geometry of copper with d^9 (Cu^{II}) configuration i.e. $(eg)^4$ $(a1g)^2$ $(b2g)^2$ $(b1g)^1$, occupied by an unpaired electron. The trend $g_{\|} > g_{\perp} > g_e$ (2.0023) reveals that the unpaired electron is localized in the $d_{x^2-y^2}$ orbital [231]. For a Cu(II) complex, $g_{\|}$ is a parameter sensitive enough to indicate covalence. For a covalent complex, $g_{\|} < 2.3$ and for an ionic environment, $g_{\|} = 2.3$ or more. In the present complex $g_{\|} < 2.3$ indicates an appreciable metal–ligand covalent character [232]. The exchange interaction parameter $G < 4$ (1.89), indicated considerable exchange interaction between the Cu(II) centers in the solid phase [233].

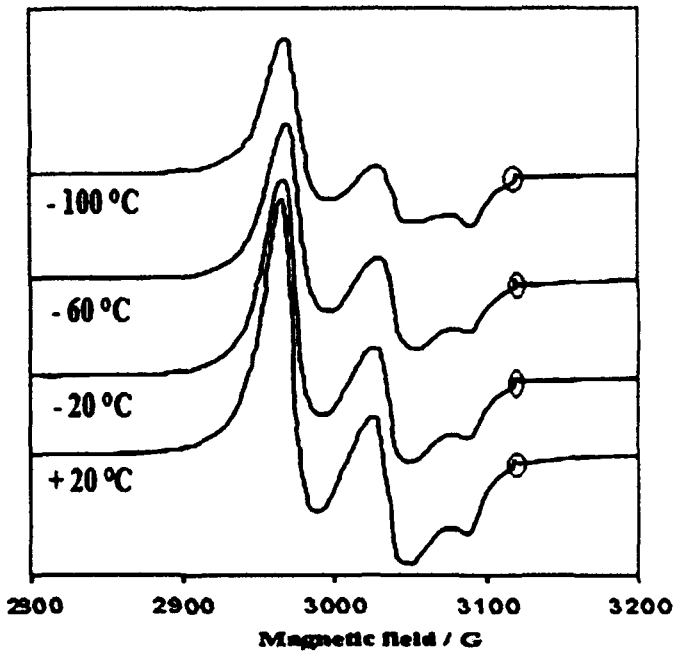

Figure 38. EPR spectra of complex $[Cu(glygly)_2(ppz)(H_2O)_4].2H_2O$ at variables temperature in solid state.

DNA binding studies

Electronic absorption titration

Electronic absorption spectroscopy is an effective method to examine the binding modes of complexes with DNA followed by the changes in the absorbance and shift in the wavelength. The absorption spectra of complex $[Cu_2(glygly)_2(ppz)(H_2O)_4].2H_2O$ in the absence and presence of CT DNA are shown in Figure 39. Binding of the complexes to DNA is expected to perturb the ligand centered transitions of complexes. Upon the addition of increasing amounts (0.067–0.33 x 10^{-4} M) of CT DNA to complex $[Cu_2(glygly)_2(ppz)(H_2O)_4].2H_2O$ of fixed concentration (0.067 x 10^{-4} M), there was an increase in the absorption intensity of complex $[Cu_2(glygly)_2(ppz)(H_2O)_4].2H_2O$ indicative of hyperchromism with no band shift. Hyperchromism with no shift in absorbance is consistent with groove binding, therefore in this complex it can be attributed to external contact (surface binding) with the duplex through hydrogen–

bonding interactions between coordinated –NH and $–NH_2$ with functional groups positioned on the edge of DNA bases which are accessible both in the major and minor grooves or due to strong binding of complex to CT DNA possibly via electrostatic interaction indicating DNA stabilization [234,235]. These results suggest the possibility of groove binding for the complex $[Cu_2(glygly)_2(ppz)(H_2O)_4].2H_2O$ to DNA and clearly rule out the intercalative binding of complex to DNA, as intercalation mode of binding leads to "hypochromism" in the spectral bands [236]. Since complex $[Cu_2(glygly)_2(ppz)(H_2O)_4].2H_2O$ possesses coordinated –NH– piperazine and amino functionality of dipeptide (glygly) which is quite likely to be engaged in hydrogen bonding with H–bond acceptor groups (the purine N(3) and pyrimidine O(2) at the floor of the groove walls). To assess the binding ability of the complex $[Cu_2(glygly)_2(ppz)(H_2O)_4].2H_2O$ with CT DNA, the intrinsic binding constant (K_b) value was calculated and found to be $2.14 \times 10^5\ M^{-1}$. The K_b value suggest that complex $[Cu_2(glygly)_2(ppz)(H_2O)_4].2H_2O$ has a strong binding affinity for CT DNA, which was further validated by molecular docking technique.

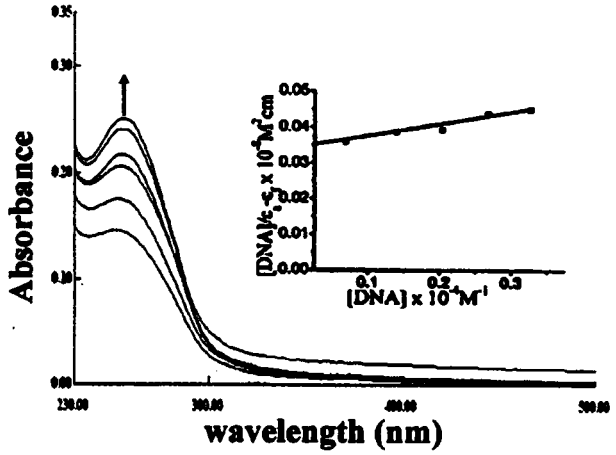

Figure 39. *Absorption spectral traces of complex $[Cu_2(glygly)_2(ppz)(H_2O)_4].2H_2O$ in 5mM Tris HCl/ 50 mM NaCl buffer at pH 7.2 upon addition of CT DNA. Inset: Plots of [DNA]/ ε_a–ε_f (M^2 cm) vs [DNA] for the titration of CT DNA with complexes ■, experimental data points; full lines, linear fitting of the data. [Complex] 0.67 x 10^{-4} M, [DNA] 0.067–0.33 x 10^{-4} M.*

Ethidium bromide displacement assay

No luminescence was observed for the complex $[Cu_2(glygly)_2(ppz)(H_2O)_4].2H_2O$ at room temperature in aqueous solution, in any organic solvent, or in presence of CT DNA. So, the binding of complex $[Cu_2(glygly)_2(ppz)(H_2O)_4].2H_2O$ with DNA can not be directly predicted through the emission spectra. Therefore, interaction of the complex $[Cu_2(glygly)_2(ppz)(H_2O)_4].2H_2O$ with DNA was carried out by the competitive binding experiment using ethidium bromide (EB) as a probe. EB does not show any appreciable emission in the buffer solution due to fluorescence quenching of the free EB by solvent molecules, while in presence of CT DNA, the fluorescence intensity of EB was highly enhanced due to its strong intercalation between the adjacent DNA base pairs [237]. The addition of a second DNA–binding molecule can quench the emission intensity of DNA–EB adduct by either replacing the EB and/or by accepting the excited–state electron of the EB through a photoelectron transfer mechanism [238] The addition of complex $[Cu_2(glygly)_2(ppz)(H_2O)_4].2H_2O$ to DNA pretreated with EB (Figure 40) caused significant reduction in emission intensities, which indicated that the complex $[Cu_2(glygly)_2(ppz)(H_2O)_4].2H_2O$ could bind to DNA through the groove binding mode releasing some EB molecules from the EB–DNA system [239]. The extent of reduction of the emission intensity gives a measure of the binding propensity of the complex $[Cu_2(glygly)_2(ppz)(H_2O)_4].2H_2O$ to CT DNA. According to the classical Stern–Volmer equation:

$$I_0/I = 1 + K_{SV}.r$$

where I_0 and I represent the fluorescence intensities in the absence and presence of the complex $[Cu_2(glygly)_2(ppz)(H_2O)_4].2H_2O$, respectively; r is the concentration ratio of the complex to DNA and K_{SV} used to evaluate the quenching efficiency is obtained as the slope of I_0/I versus r. The K_{SV} value for the complex $[Cu_2(glygly)_2(ppz)(H_2O)_4].2H_2O$

was found to be 2.15, indicating the strong affinity of the complex $[Cu_2(glygly)_2(ppz)(H_2O)_4].2H_2O$ to CT–DNA, consistent with the studies of absorption titrations.

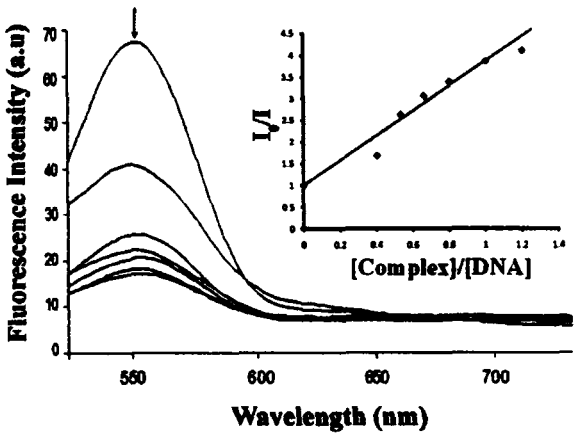

Figure 40. *Emission spectra of EB bound to DNA in the absence and presence complex* $[Cu_2(glygly)_2(ppz)(H_2O)_4].2H_2O$ *in 5 mM Tris–HCl/50 mM NaCl buffer. Arrows shows the intensity changes upon increasing concentration of the complex* $[Cu_2(glygly)_2(ppz)(H_2O)_4].2H_2O$. *Inset: Plots of* I_0/I *vs [complex]/[DNA]. (■) experimental data points; full lines, linear fitting of the data.*

Circular dichroism spectral study

CD spectroscopy is a useful technique in diagnosing changes in DNA morphology during drug–DNA interactions. The CD spectrum of CT DNA exhibits a positive band at 275 nm (UV: λ_{max}, 260 nm) due to base stacking and a negative band at 245 nm due to the right–handed helicity of B–DNA form which are quite sensitive to the mode of DNA interactions with small molecules. Simple groove binding and electrostatic interaction of the complexes with DNA shows less or no perturbation on the base stacking and helicity bands while intercalator enhances the intensities of both bands [240,241]. The interaction of the complex $[Cu_2(glygly)_2(ppz)(H_2O)_4].2H_2O$ with DNA induces a change in the CD spectrum of B DNA (Figure 41). The intensities of both the negative and positive bands decrease significantly (shifting to zero levels). This suggests that the DNA binding of the complex induces certain conformational changes, such as the conversion from a more B–like to a more C–like structure within the DNA molecule [242]. From the results of UV

absorption, fluorescence and CD spectroscopic studies, we conclude that the complex $[Cu_2(glygly)_2(ppz)(H_2O)_4].2H_2O$ binds avidly to CT DNA.

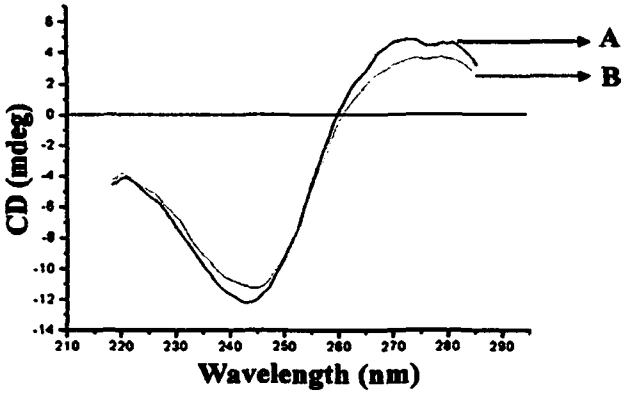

Figure 41. CD spectra of (A) CT DNA alone and (B) CT DNA in presence of complex $[Cu_2(glygly)_2(ppz)(H_2O)_4].2H_2O$ in 5 mM Tris–HCl/50 mM NaCl buffer at 25 °C. [Complex] 1.0 x 10^{-4} M, [DNA] 1.0 x 10^{-4} M.

DNA Cleavage Studies

Concentration dependent cleavage activity

In order to assess the chemical nuclease activity of $[Cu_2(glygly)_2(ppz)(H_2O)_4].2H_2O$ complex for DNA strand scission, pBR322 DNA was incubated with $[Cu_2(glygly)_2(ppz)(H_2O)_4].2H_2O$ complex under the reaction conditions. The cleavage reaction can be monitored by gel electrophoresis. When circular plasmid DNA is conducted by electrophoresis, the fastest migration will be observed for the supercoiled form (Form I). If one strand is cleaved, the supercoils will relax to produce a slower–moving nicked circular form (Form II). If both strands are cleaved, a linear form (Form III) that migrates between Form I and Form II will be generated.

The nuclease activity of the complex has been studied by agarose gel electrophoresis using supercoiled pBR322 plasmid DNA in a medium of 5 mM Tris–HCl/50 mM NaCl buffer solution (pH 7.2) in the absence of external agents. The cleavage reactions have been studied using different complex concentrations incubated at 310 K for 45 min as depicted in Figure 42. With increasing concentration of the complex

$[Cu_2(glygly)_2(ppz)(H_2O)_4].2H_2O$ (lanes 2–4), the amount of Form I of pBR322 DNA diminished gradually, whereas Form II increased. At the same time, when the concentration of complex $[Cu_2(glygly)_2(ppz)(H_2O)_4].2H_2O$ reached 25 μM, the linear Form III was manifested in the gel (lane 5), and the percentage of linear DNA increased with the increase of the concentration of complex $[Cu_2(glygly)_2(ppz)(H_2O)_4].2H_2O$. So, it is clear that cleavage of pBR322 DNA is highly dependent on metal ions concentration.

Figure 42. *Agarose Gel electrophoresis pattern for the cleavage of pBR322 supercoiled DNA (300 ng) by complex $[Cu_2(glygly)_2(ppz)(H_2O)_4].2H_2O$ at 310 K after 45 min of incubation; Lane 1, DNA control; Lane 2, 10 μM of $[Cu_2(glygly)_2(ppz)(H_2O)_4].2H_2O$ + DNA; Lane 3: 15 μM of $[Cu_2(glygly)_2(ppz)(H_2O)_4].2H_2O$ + DNA; Lane 4: 20 μM of $[Cu_2(glygly)_2(ppz)(H_2O)_4].2H_2O$ + DNA; Lane 5: 25 μM of $[Cu_2(glygly)_2(ppz)(H_2O)_4].2H_2O$ + DNA; Lane 6: 30 μM of 1 + DNA.*

DNA cleavage in presence of activators

To ascertain whether any adventitious agents present in the reaction mixture could account for the increased DNA degradation by complex $[Cu_2(glygly)_2(ppz)(H_2O)_4].2H_2O$. The nuclease efficiency of the copper(II) complexes is known to depend on the activators used for initiating the DNA cleavage. Thus, further activity of complex $[Cu_2(glygly)_2(ppz)(H_2O)_4].2H_2O$ was carried out with different activators *viz*; H_2O_2 as an oxidizing agent, ascorbate (Asc), 3–mercaptopropionic acid (MPA) and glutathione (GSH) as reducing agents. As shown in Figure 43 (Lane 2–5), the cleavage activity of complex $[Cu_2(glygly)_2(ppz)(H_2O)_4].2H_2O$ was significantly enhanced in presence of these activators and follows the order H_2O_2>MPA>Asc≈GSH. The complex $[Cu_2(glygly)_2(ppz)(H_2O)_4].2H_2O$ exhibited a significant DNA cleavage activity in the presence of H_2O_2.

The proposed mechanistic pathway proposed for the interaction of complex $[Cu_2(glygly)_2(ppz)(H_2O)_4].2H_2O$ with DNA in the presence of H_2O_2 has been illustrated below:

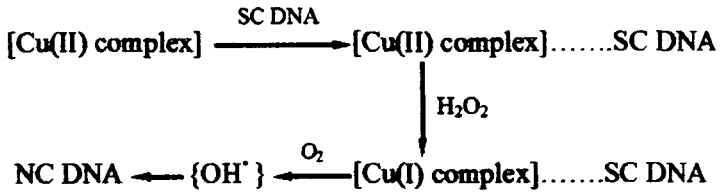

Reactive oxygen species responsible for DNA Cleavage

Copper complexes can cleave DNA both by hydrolytic and/or oxidative mechanisms. For the oxidative process, the complexes have been shown to react with molecular oxygen or hydrogen peroxide to produce a variety of active oxidative intermediates (reactive oxygen species or non–diffusible copper–oxene species) [243]. In order to gain information about the reactive oxygen species (ROS) which was responsible for the DNA cleavage catalyzed by the complex $[Cu_2(glygly)_2(ppz)(H_2O)_4].2H_2O$, reactions were carried out in the presence of typical scavengers such as hydroxyl radical scavengers (DMSO, EtOH), singlet oxygen quencher (NaN_3) and superoxide scavenger (SOD) under our experimental conditions. As shown in Figure 43, the DNA breakdown mediated by complex $[Cu_2(glygly)_2(ppz)(H_2O)_4].2H_2O$ was diminished in presence of DMSO (lane 6) and EtOH (lane 7), which indicated that the participation of hydroxyl radical in the oxidative DNA cleavage. Since, sodium azide had no significant effect on the DNA cleavage (lane 8). The participation of $^1O_2$ or singlet oxygen–like entities is ruled out [244]. On the other hand, DNA cleavage inhibited slightly in presence of SOD (lane 9), which demonstrate the involvement of superoxide radical anion ($O_2^{\bullet -}$) in DNA strand scission suggestive of oxidative cleavage mechanism [245]. From these results, we could

conclude that a Cu(I) species, superoxide O_2 and hydroxyl radical $OH^{\bullet}$ are the active species involved in the DNA strand scission.

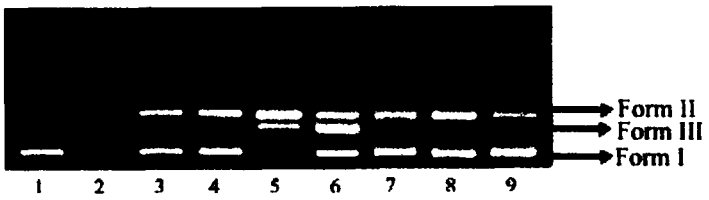

Figure 43. *Agarose Gel electrophoresis pattern for the cleavage of pBR322 supercoiled DNA (300 ng) by complex* $[Cu_2(glygly)_2(ppz)(H_2O)_4].2H_2O$ *in presence of different activating agents at 310 K after incubation for 45 min. Lane 1: DNA Control; Lane 2: 25 μM of* $[Cu_2(glygly)_2(ppz)(H_2O)_4].2H_2O$ *+* H_2O_2 *(0.4 M) + DNA; Lane 3: 25 μM of* $[Cu_2(glygly)_2(ppz)(H_2O)_4].2H_2O$ *+ MPA (0.4 M) + DNA; Lane 4: 25 μM of* $[Cu_2(glygly)_2(ppz)(H_2O)_4].2H_2O$ *+ GSH (0.4 M) + DNA; Lane 5: 25 μM of* $[Cu_2(glygly)_2(ppz)(H_2O)_4].2H_2O$ *+ ASc (0.4 M) + DNA; Lane 6: 25 μM of* $[Cu_2(glygly)_2(ppz)(H_2O)_4].2H_2O$ *+ DMSO (0.4 M) + DNA; Lane 7: 25 μM of* $[Cu_2(glygly)_2(ppz)(H_2O)_4].2H_2O$ *+ Ethyl alcohol (0.4 M) + DNA; Lane 8 : 25 μM of* $[Cu_2(glygly)_2(ppz)(H_2O)_4].2H_2O$ *+ sodium azide (0.4 M) + DNA; Lane 9 : 25 μM of* $[Cu_2(glygly)_2(ppz)(H_2O)_4].2H_2O$ *+ SOD (15 units) + DNA.*

DNA cleavage in presence of recognition elements (groove binding)

To determine the groove binding preference of $[Cu_2(glygly)_2(ppz)(H_2O)_4].2H_2O$ with pBR322 DNA, the supercoiled pBR322 DNA was treated with DNA groove binders such as DAPI (minor groove binding agent) and methyl green (major groove binding agent) prior to the addition of complex $[Cu_2(glygly)_2(ppz)(H_2O)_4].2H_2O$. As shown in Figure 44, DNA cleavage was inhibited in the presence of DAPI (lane 2). However, no apparent inhibition of DNA damage was observed in presence of methyl green (lane 3), suggesting that the complex has interaction with DNA through minor groove, which was further validated by molecular docking studies.

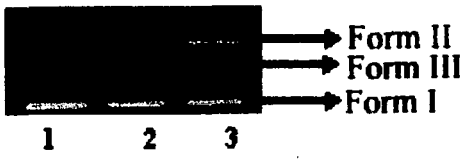

Figure 44. *Agarose Gel electrophoresis pattern for the cleavage of pBR322 supercoiled DNA (300 ng) by complex* $[Cu_2(glygly)_2(ppz)(H_2O)_4].2H_2O$ *in presence of DNA minor binding agent DAPI and major binding agent methyl green at 310 K after incubation for 45 min. Lane 1, DNA control; Lane 2, 25 μM of* $[Cu_2(glygly)_2(ppz)(H_2O)_4].2H_2O$ *+ DNA + DAPI (8 μM); Lane 3, 25 μM of* $[Cu_2(glygly)_2(ppz)(H_2O)_4].2H_2O$ *+ DNA+ methyl green (2.5 μL of a 0.01mg/ml solution).*

Topoisomerase I Inhibition

A plasmid DNA cleavage assay was used to investigate the effect of complex $[Cu_2(glygly)_2(ppz)(H_2O)_4].2H_2O$ on the activity of human Topo–I by agarose gel electrophoresis. This assay provides direct means of determining whether the drug affects the unwinding of a supercoiled (SC) duplex DNA to nicked open circular (NOC) and relaxed (R) DNA. When catalytic activity of topoisomerase I was assayed, complex $[Cu_2(glygly)_2(ppz)(H_2O)_4].2H_2O$ inhibited this process in a concentration–dependent manner [246]. As shown in Figure 45, supercoiled DNA was fully relaxed by the enzyme in the absence of complex $[Cu_2(glygly)_2(ppz)(H_2O)_4].2H_2O$ (Lane 2, Topo–I). However, upon increasing the concentration of complex $[Cu_2(glygly)_2(ppz)(H_2O)_4].2H_2O$ (5–12.5 μM), the levels of relaxed form were inhibited (Lane 3–6). At 12.5 μM the DNA relaxation effect caused by Topo–I was completely inhibited by complex $[Cu_2(glygly)_2(ppz)(H_2O)_4].2H_2O$. These observations suggest that complex $[Cu_2(glygly)_2(ppz)(H_2O)_4].2H_2O$ inhibits topoisomerase I catalytic activity due to the relatively strong DNA binding affinity of complex $[Cu_2(glygly)_2(ppz)(H_2O)_4].2H_2O$, which prevents the enzyme from efficiently binding to the DNA. Thus, the metal–based drug entity can exert its antitumor activity via topoisomerase I inhibition as it was found that most of the cancer cells (kidney, colon, prostate, ovary and esophagus) showed

significantly increased levels of topoisomerase, required for rapid and unchecked proliferation of cancer cells [247].

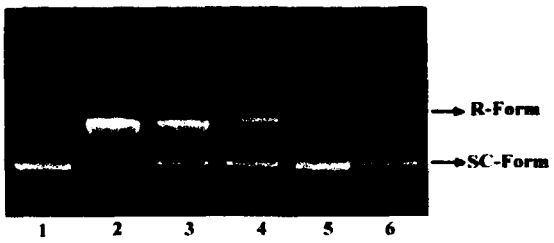

Figure 45. *Agarose Gel electrophoresis pattern showing effect of different concentration of complex* $[Cu_2(glygly)_2(ppz)(H_2O)_4].2H_2O$ *on the activity of DNA topoisomerase I (Topo–I); Lane 1, DNA control; lane 2, Topo–I + DNA; Lane 3, 5 μM of* $[Cu_2(glygly)_2(ppz)(H_2O)_4].2H_2O$ *+ DNA+ Topo–I; Lane 4: 7.5 μM of* $[Cu_2(glygly)_2(ppz)(H_2O)_4].2H_2O$ *+ DNA + Topo–I; Lane 5: 10 μM of* $[Cu_2(glygly)_2(ppz)(H_2O)_4].2H_2O$ *+ DNA + Topo–I; Lane 6: 12.5 μM of* $[Cu_2(glygly)_2(ppz)(H_2O)_4].2H_2O$ *+ DNA + Topo–I.*

Superoxide Dismutase Activity

Superoxide dismutase (SOD) is one of the most crucial enzymes in the defense system of organisms for its ability to protect cells from the damage of the toxic superoxide by catalyzing the dismutation of superoxide radicals effectively [248]. Therefore, it was interesting to investigate the SOD–like activity of this new dipeptide based binuclear Cu(II)–complex by using the xanthine–xanthine oxidase–nitroblue tetrazolium (NBT) assay. A plot (Figure 46) of NBT percent inhibition with an increase in concentration of complex $[Cu_2(glygly)_2(ppz)(H_2O)_4].2H_2O$, necessary to produce 50% inhibition (IC_{50}) of the reaction are presented in Table 5, together with the values found for the previously investigated dipeptide complexes and the one obtained with native SOD [249]. The IC_{50} value of complex $[Cu_2(glygly)_2(ppz)(H_2O)_4].2H_2O$ was found to be 0.086 μM, which is considered to be an excellent SOD mimic among the most active dipeptide complexes although it is somewhat less active than the IC_{50} value obtained for native enzyme (IC_{50} = 0.04 μM). In the enzyme, the flexible dipeptides together with piperazine ligand can

accommodate and stabilize the space structure of the protein and provide needed protons to the peroxide anion during the catalytic cycle. Since, the proton exchange between substrates and buffer is a rapid process in the small model systems; the buffer can directly transfer protons to peroxide anion in the mechanism [250].

$Cu(II) + O_2^{\cdot-} \rightleftharpoons Cu(I) + O_2$

$Cu(I) + O_2^{\cdot-} + 2H^+ \rightleftharpoons Cu(II) + H_2O_2$

Furthermore, the high superoxide dismutase activity of complex $[Cu_2(glygly)_2(ppz)(H_2O)_4].2H_2O$ may be possibly due to cooperation of two Cu(II) centers in close proximity, acting in concord in free radical binding and electron transfer.

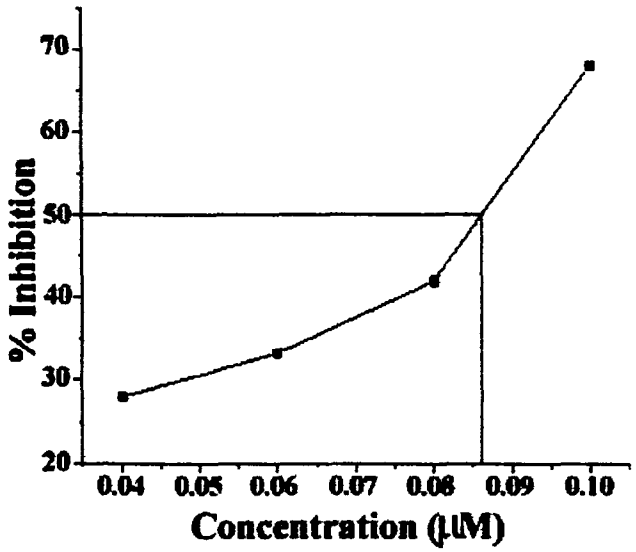

Figure 46. *A plot of percentage of NBT inhibition reduction with an increase in the concentration of complex* $[Cu_2(glygly)_2(ppz)(H_2O)_4].2H_2O$.

Table 5. *IC_{50} (μM) values of the complex $[Cu_2(glygly)_2(ppz)(H_2O)_4].2H_2O$, some of the dipeptide–based SOD mimicking compounds and the native Cu,ZnSOD enzyme*

Complexes	IC_{50} (μM)
$[Cu_2(glygly)_2(ppz)(H_2O)_4].\ 2H_2O$	0.086 (This work)
[Cu(ala–ile)]	330
[Cu(ala–thr)]	0.99
[Cu(ala–tyr)]	252
[Cu(ala–val)]	237
[Cu(ala–Phen)]	0.149
Native Cu,Zn–SOD	0.045

Molecular Docking

Molecular docking with DNA

Molecular docking techniques is an attractive scaffold to understand the Drug–DNA interactions in rational drug design, as well as in the mechanistic study by placing a small molecule into the binding site of the target specific region of the DNA mainly in a non–covalent fashion [251]. Targeting the minor groove of DNA through binding to a small molecule has long been considered as an important tool in molecular recognition of specific DNA–sequence [252].

In our experiment, rigid molecular docking (two interacting molecules were treated as rigid bodies) studies was performed to predict the binding modes of complex $[Cu_2(glygly)_2(ppz)(H_2O)_4].2H_2O$ with DNA duplex of sequence $d(CGCGAATTCGCG)_2$ dodecamer (PDB ID:1BNA) provide an energetically favorable docked pose that is shown in Figure 47. The results show that complex $[Cu_2(glygly)_2(ppz)(H_2O)_4].2H_2O$ interacts with DNA *via* electrostatic mode involving outside edge stacking interactions with the oxygen atom of the phosphate backbone of DNA. In this model, it is clearly

indicated that complex $[Cu_2(glygly)_2(ppz)(H_2O)_4].2H_2O$ fits snugly into the curved contour of the targeted DNA in the minor groove and is situated within G–C rich region thus, leads to van der Waals interaction and hydrophobic contacts with DNA functional groups that define the groove [253]. Moreover, the piperazine ring of the complex $[Cu_2(glygly)_2(ppz)(H_2O)_4].2H_2O$ arranged in a parallel fashion with respect to the deoxyribose groove walls of the DNA and was stabilized by hydrogen bonding (2.8–3.0 Å) between NH of piperazine with N3 and anomeric oxygen of deoxyribose of G16B and O2 of C10A with amino functionality of dipeptide (glygly), while the remaining amino group point outside the minor groove. The resulting relative binding energy of docked $[Cu_2(glygly)_2(ppz)(H_2O)_4].2H_2O$–DNA was found to be –256 $KJmol^{-1}$. This value was consistent with the high binding constant obtained from spectroscopic titration and groove binding in presence of minor groove binder DAPI and major groove binder MG from DNA cleavage studies.

Thus, we can conclude that there is a mutual complement between spectroscopic techniques and molecular modeling, which can provide valuable information about the mode of interaction of the complex with DNA and the conformation constraints for adduct formation.

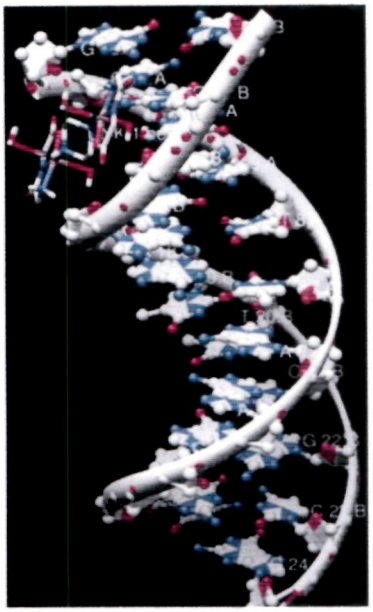

Figure 47. *Molecular docked model of complex* $[Cu_2(glygly)_2(ppz)(H_2O)_4].2H_2O$ *showing chemically significant hydrogen–bonding interactions into adjacent C:G base pairs from minor side with DNA dodecamer duplex of sequence* $d(CGCGAATTCGCG)_2$ *(PDB ID: 1BNA).*

Molecular docking with Topoisomerase I

In order to further rationalize the observed Topo–I inhibitory assay with complex $[Cu_2(glygly)_2(ppz)(H_2O)_4].2H_2O$, molecular docking studies were performed to understand the binding mode of complex $[Cu_2(glygly)_2(ppz)(H_2O)_4].2H_2O$ with human–DNA–Topo–I complex (PDB ID: 1SC7) as depicted in Figure 48. The X–ray crystallographic structure of the human–DNA–Topo I complex was retrieved from Protein Data Bank in which Topo I is bound to the oligonucleotide sequence 5′–AAAAAGACTTsX–GAAAATTTTT–3′, where's' is 5′– bridging phosphorothiolate of the cleaved strand and 'X' represents any of the four bases A, G, C or T. The phosphoester bond of G12 in 1SC7 was rebuilt and SH of G11 on the scissile strand was changed to OH [254]. The resulting docked model with minimum relative binding energy –299 $KJmol^{-1}$ speculate that the complex $[Cu_2(glygly)_2(ppz)(H_2O)_4].2H_2O$ intercalated between the purine ring of G11 (+1) and pyrimidine ring of T10 (–1) in the minor groove

on the scissile strand and C112 and A113, on the non–scissile strand, parallel to the plane of base pairs without having hydrogen bonds with the enzyme (Figure 49), subsequently leading to inhibitory effect on topoisomerase I [255]. Furthermore, DNA intercalating force was much more important than hydrogen bonding of the ligand to the surrounding amino acids residues of the protein, or to the base pairs [256]. So, we can concluded that the complex occupies the topoisomerase binding site which may suppress the association of topoisomerase with DNA, thus influencing the topoisomerase inhibition activity or form stable complex with DNA and have a high potential to act as DNA–targeting anticancer drugs [257].

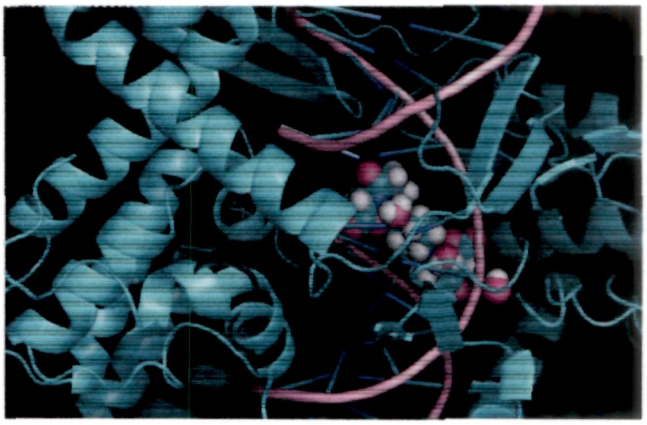

***Figure 48**. Molecular docked model of complex $[Cu_2(glygly)_2(ppz)(H_2O)_4].2H_2O$ in the cleavage site of human DNA topoisomerase I (PDB ID: 1SC7).*

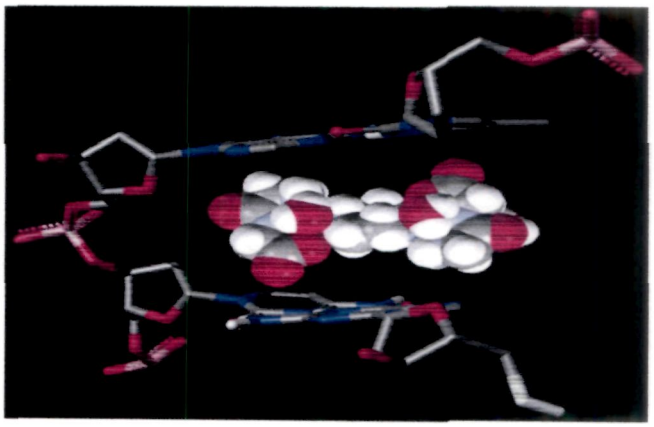

***Figure 49**. View is a cut–out of sequence 5′–AAAAAGACTTsX–GAAAATTTTT–3′ showing complex $[Cu_2(glygly)_2(ppz)(H_2O)_4].2H_2O$ (space filling model) docked in DNA sequence between C112, A113 and T10, TGP11.*

Molecular docking with superoxide dismutase

In order to further evaluate the SOD inhibitory assay obtained from experimental results, complex $[Cu_2(glygly)_2(ppz)(H_2O)_4].2H_2O$ was successively docked with an enzyme to search the targeted active–site (Arg141). The X–ray structure of the enzyme shows that a positively charged Arg141 is located in the outer sphere of the active site and is ~5.9 Å away from the copper ion which is coordinated by His44, His46, His61, His118, and a weakly bound water molecule which occupies the axial position of a distorted square pyramid and is directed toward the cavity opening. However, the zinc ion is completely buried in the protein, is bridged to the copper by the imidazolate side chain of His61 ion and plays a key structural role in maintaining active site structural integrity during the catalytic cycle [258,259]. Since the only access to the copper ion is from the active–site cavity, the chelators must enter the channel. This interaction would be facilitated by the positive residues lining the channel such as Arg141, Lys120, and Lys134 as illustrated in Figure 50. The resulting docked model clearly indicated that dipeptide carbonyl group of complex $[Cu_2(glygly)_2(ppz)(H_2O)_4].2H_2O$ can coordinate to the active–site copper as well as guanidyl cation of Arg141 and positively charged ammonia ion of Lys134 amino acid residues surrounding the active redox center of SOD (i.e., the Cu^{2+}) (Figure 51). In addition, the concentration of positive electrostatic potential around the channel facilitate the binding of anionic ligands in the cavity.

Hence, in design for SOD mimic using binuclear copper complexes with dipeptide ligands through the hydrogen bonding moiety near outer coordination sphere of the copper site may be essential for SOD activity.

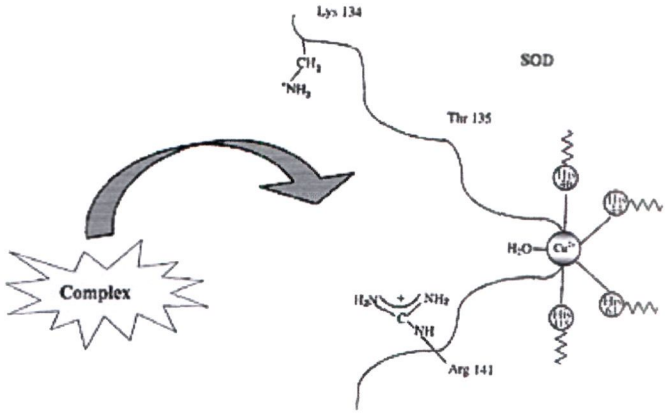

***Figure 50**. Schematic representation of the key–lock interaction between the CuZnSOD enzyme (PDB ID: 1SXA) and the complex $[Cu_2(glygly)_2(ppz)(H_2O)_4].2H_2O$.*

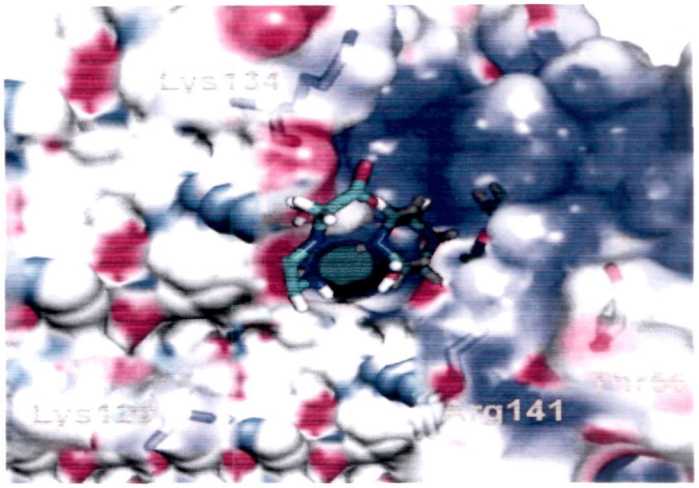

***Figure 51**. Docking of complex $[Cu_2(glygly)_2(ppz)(H_2O)_4].2H_2O$ into the active–site channel demonstrates that a carbonyl group of complex can access the active–site copper. An electrostatic loop consisting of the positively charged side chains of Arg141, Lys120, and Lys134 guides the anionic superoxide substrate to the copper center. Arg141 and Thr135 act as a "bottleneck" for the active site, limiting the access of bulky anions to the copper shown as a green sphere at the bottom of the active–site channel.*

Conclusions

In this work, we have designed and synthesized a new dinuclear copper(II) complex derived from the dipeptide (glygly) and piperazine as metallopeptide drug to examine its effect on the binding propensity of DNA and to elucidate the mechanism of action at the molecular target. The *in vitro* DNA binding studies of complex $[Cu_2(glygly)_2(ppz)(H_2O)_4].2H_2O$ revealed an electrostatic mode of binding as well as selective binding to minor groove of DNA. The complex $[Cu_2(glygly)_2(ppz)(H_2O)_4].2H_2O$ cleave supercoiled plasmid DNA through an oxidative (O_2–pathway) cleavage mechanism induced by reactive oxygen species (ROS). Furthermore, complex $[Cu_2(glygly)_2(ppz)(H_2O)_4].2H_2O$ exhibits significant inhibitory effects on Topo–I activity at a very low concentration ~12.5 μM, including excellent SOD mimics with an IC_{50} of 0.086 μM. Additionally, molecular docking studies was performed with molecular target DNA and the active site of enzymes in order to validate the experimental results. Therefore, it is concluded that present chemical entity can acts as potent drug binding to DNA minor groove and inhibit DNA–processing enzymes; which can be exploited as an important class of anticancer drugs.

CHAPTER III (b)

Interaction and Photo–induced Cleavage Studies of Copper based Chemotherapeutic Drug with Human Serum Albumin: Spectroscopic and Molecular Docking Study

Synthesis

The synthesis and single crystal X-rays crystallographic studies of a new metallopeptide complex of the formulation $[Cu_2(glygly)_2(ppz)(H_2O)_4].2H_2O$ was described previously [260].

Results and discussion

Electronic absorption studies

Electronic absorption spectroscopy is a reliable tool to understand the morphological changes in secondary structure of HSA *via* complex formation between drug and HSA. On addition of complex $[Cu_2(glygly)_2(ppz)(H_2O)_4].\ 2H_2O$ with incremental increase of concentration (0.67–2.33 x 10^{-5} M) to HSA of constant concentration (1.80 x 10^{-6} M), there was a sharp increase in absorption intensity, "hyperchromism" (Figure 52) of the intraligand band at 278 nm was observed which implicates that complex $[Cu_2(glygly)_2(ppz)(H_2O)_4].2H_2O$ interacts with HSA by non–covalent interaction by electrostatic attraction and could be facilitated by hydrogen–bond formation due to the molecular topology of peptide ligand scaffold of complex $[Cu_2(glygly)_2(ppz)(H_2O)_4].2H_2O$. In order to evaluate the binding propensity quantitatively with HSA, the intrinsic binding constant (K_b) of the complex $[Cu_2(glygly)_2(ppz)(H_2O)_4].2H_2O$ with HSA was calculated using Equation (3) and K_b value was found to be 1.48 x 10^4 M^{-1}. The K_b value of complex $[Cu_2(glygly)_2(ppz)(H_2O)_4].2H_2O$ suggests moderate binding propensity to HSA followed by conformational transition.

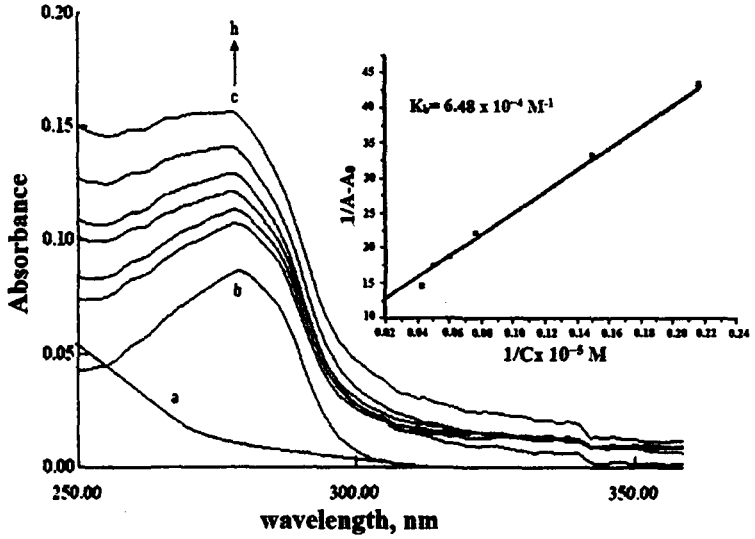

Figure 52. *UV absorption spectra of the HSA–complex $[Cu_2(glygly)_2(ppz)(H_2O)_4].2H_2O$ system obtained in 5 mM Tris–HCl/50 mM NaCl buffer, pH 7.4, at room temperature: (a) complex $[Cu_2(glygly)_2(ppz)(H_2O)_4].2H_2O$, 0.60 x 10^{-5} M; (b) HSA, 1.80 x 10^{-6} M; (c–h) complex $[Cu_2(glygly)_2(ppz)(H_2O)_4].2H_2O$–HSA, the complex concentrations were 0.67, 1.0, 1.33, 1.67, 2.00, 2.33 x 10^{-5} M, respectively. Arrows show the intensity changes upon increasing concentration of the complex $[Cu_2(glygly)_2(ppz)(H_2O)_4].2H_2O$. Inset: Plot of $1/A–A_o$ vs. 1/ [Complex].*

Fluorescence quenching mechanism

Fluorescent quenching techniques involves a variety of molecular interactions such as excited state reactions, molecular rearrangements, energy transfer, the formation of ground–state complex, collision, etc [261]. Therefore, fluorescence quenching experiments were undertaken to investigate the interaction between complex $[Cu_2(glygly)_2(ppz)(H_2O)_4].2H_2O$ and HSA. When HSA molecule is excited at 280 nm, both tryptophan and tyrosine amino acid residues give fluorescence emissions at an excitation wavelength of 295 nm in which tryptophan has strong fluorescence emissions while tyrosine does not absorb in this region [262]. The fluorescence spectra of HSA in the absence and presence of complex $[Cu_2(glygly)_2(ppz)(H_2O)_4].2H_2O$ as a quencher in Tris–HCl buffer (pH 7.4) were monitored with an excitation wavelength of 295 nm

(Figure 53). HSA exhibits a strong fluorescence emission with a peak at 370 nm due to the emission from the single tryptophan residue (Trp–214). However, intrinsic fluorescence intensity of HSA decreased regularly and no shift was observed in the emission wavelength with the increase in concentration of complex $[Cu_2(glygly)_2(ppz)(H_2O)_4].2H_2O$. The strong quenching of the HSA fluorescence implicated the existence of interaction between $[Cu_2(glygly)_2(ppz)(H_2O)_4].2H_2O$ and HSA which changes the local environment around Trp–214 residues [263].

In order to determine the fluorescence quenching mechanism, the fluorescence quenching data at different temperatures (299, 309 and 318 K) were analyzed using the classical Stern–Volmer equation (7). Figure 54 shows the Stern–Volmer plots of F_0/F versus $[Q]$ at three different temperatures and the calculated K_{sv} and k_q values are summarized in Table 6.

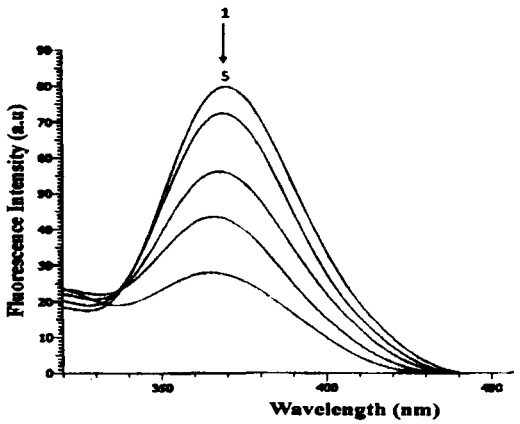

Figure 53. *The fluorescence quenching spectra of HSA by different concentrations of complex$[Cu_2(glygly)_2(ppz)(H_2O)_4].2H_2O$ with the excitation wavelength at 295 nm in 5 mM Tris–HCl/50 mM NaCl buffer, pH 7.4, at room temperature: [HSA], 1.0 x10^{-6} M; (1–5) the concentration of complex $[Cu_2(glygly)_2(ppz)(H_2O)_4].2H_2O$ corresponding to 0, 0.60, 1.00, 2.00, 3.33 x 10^{-5} M, respectively. Arrow shows the intensity changes upon increasing concentration of the quencher.*

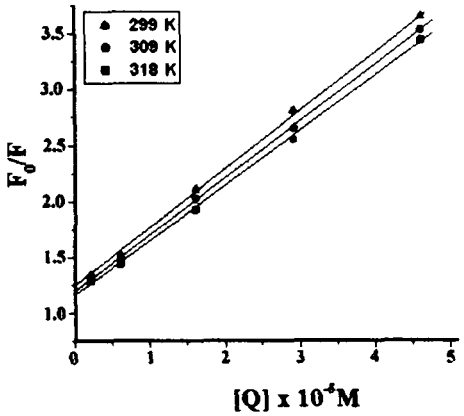

Figure 54. *Stern–Volmer plots showing HSA tryptophan quenching caused by complex* $[Cu_2(glygly)_2(ppz)(H_2O)_4].2H_2O$ *at three different temperatures (pH 7.40,* λ_{ex} *= 295 nm,* λ_{em} *= 370 nm).*

The results revealed that the Stern–Volmer quenching constant K_{SV} is inversely correlated with temperature and k_q is larger than the limiting diffusion constant K_{dif} of the biomolecule (K_{dif} = 2.0 x 10^{10} M-1 s^{-1}) [264], indicating that fluorescence quenching was caused by a specific interaction between HSA and complex $[Cu_2(glygly)_2(ppz)(H_2O)_4].2H_2O$, consistent with the static quenching mechanism (Scheme 2) [265].

Table 6. *Stern–Volmer quenching constant of the complex* $[Cu_2(glygly)_2(ppz)(H_2O)_4].2H_2O$*–HSA system at different temperatures*

pH	T (K)	K_{sv} (10^4M^{-1})	K_q ($10^{12}M^{-1}s^{-1}$)	R
	299	2.13	2.13	0.998
7.40	309	2.06	2.06	0.995
	318	1.94	1.94	0.981

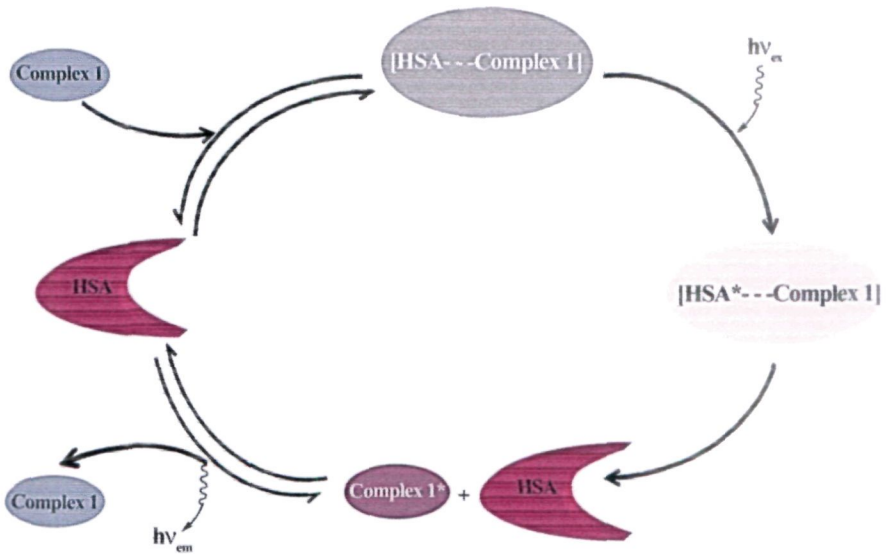

Scheme 2. Mechanism of fluorescence quenching.

For static quenching, the equation (10) was employed to calculate the binding constant and number of binding sites [266]. Thus, a plot of $\log[(F_0-F)/F]$ versus $\log[Q]$ was used to determine K as well as n. The binding data (K and n) at different temperatures were presented in Figure 55 and Table 7. It was found that the binding constant (K) decreased with the increase of temperature, resulting in a reduction of the stability between complex $[Cu_2(glygly)_2(ppz)(H_2O)_4].2H_2O$–HSA binding reaction. Literature reveals that Cu(II) metal ion most likely binds to the hydrophobic pocket located within subdomain IIA, Trp–214 which is near or within the binding site. These results were further validated by docking simulation studies.

***Table** 7. Binding constant (K) and the number of binding sites (n) for the complex $[Cu_2(glygly)_2(ppz)(H_2O)_4].2H_2O$–HSA system at different temperatures*

pH	T (K)	K($10^4 M^{-1}$)	n	R
	299	6.48	1.68	0.998
7.40	309	5.02	1.71	0.995
	318	3.62	2.10	0.981

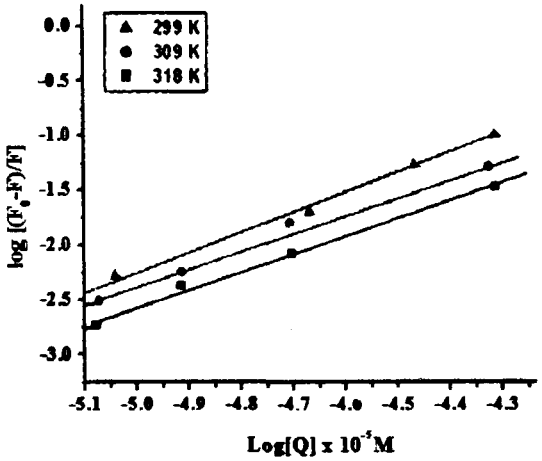

Figure 55. *Logarithmic plot of the fluorescence quenching of HSA at different temperatures.*

Energy transfer and Binding distance between $[Cu_2(glygly)_2(ppz)(H_2O)_4].2H_2O$ and HSA

Fluorescence energy transfer occurs *via* overlapping of a fluorophore (donor) with the absorption spectrum of molecule (acceptor). The overlap of the absorption spectrum of the complex $[Cu_2(glygly)_2(ppz)(H_2O)_4].2H_2O$ with the fluorescence emission spectra of HSA is shown in Figure 56. According to fluorescence resonance energy transfer theory [267], the rate of energy transfer depends on the extent of overlapping between fluorescence emission spectrum of donor with the absorption spectrum of acceptor, the relative orientation of the donor and acceptor transition dipoles, and the distance between donor and acceptor [268].

A Foster resonance energy transfer (FRET) mechanism (Figure 57) is involved in the quenching of Trp fluorescence by complex $[Cu_2(glygly)_2(ppz)(H_2O)_4].2H_2O$.

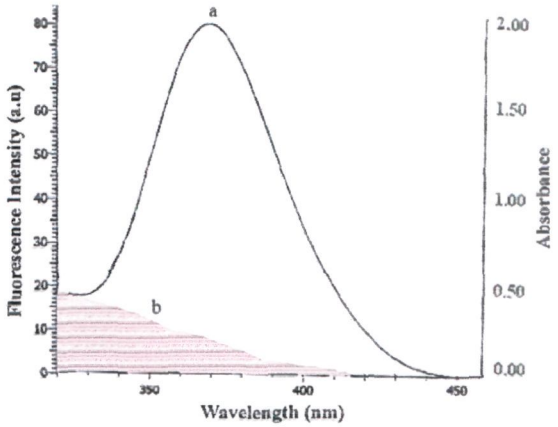

Figure 56. *The overlap of UV absorption spectra of complex 1 with the fluorescence emission spectra of HSA. (a) The fluorescence emission spectrum of HSA (1.0 x 10^{-6} M); (b) the UV absorption spectrum of complex [$Cu_2(glygly)_2(ppz)(H_2O)_4$].$2H_2O$ (0.60 x 10^{-5} M).*

Under the experimental condition, K^2 =2/3, N =1.336, ϕ= 0.188, according to Eqs. (13) – (15), the value of E, R_0, r and J were calculated and found to be 0.99, 2.5 nm, 3.7 nm and 1.6 x 10^{-14} M^{-1} cm^3, respectively. The donor to acceptor distance $r < 7$ nm indicated that the energy transfer from tryptophan residue in HSA to complex [$Cu_2(glygly)_2(ppz)(H_2O)_4$].$2H_2O$ occur with high probability [269].

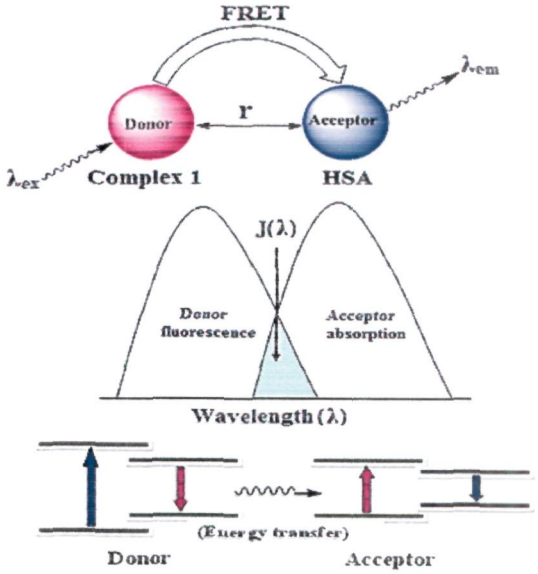

Figure 57. *Fluorescence resonance energy transfer (FRET) mechanism.*

Binding mode

The acting forces between a small molecule and bio–macromolecule are mainly include weak interactions such as hydrogen bonds, van der Waals forces, electrostatic and hydrophobic interactions [270]. The thermodynamic parameters, enthalpy change (ΔH), entropy change (ΔS) and free energy change (ΔG) are the main evidence to determine the binding mode. From the thermodynamic standpoint, $\Delta H > 0$ and $\Delta S > 0$ implies a hydrophobic interaction; $\Delta H < 0$ and $\Delta S < 0$ reflects the van der Waals force or hydrogen bond formation; and $\Delta H \approx 0$ and $\Delta S > 0$ suggests an electrostatic force. The thermodynamic temperatures chosen for measurements were 299, 309 and 318 K, so that HSA does not undergo any structural degradation. The thermodynamic parameters can be calculated from the Van't Hoff equation, in which ΔH and ΔS of reaction could be determined from the linear relationship between ln K and the reciprocal absolute temperature (Figure 58). The free energy change (ΔG) could be calculated by the Equation (12). As shown in Table 8, ΔG and ΔH were negative, and ΔS was positive. Therefore, the formation of complex $[Cu_2(glygly)_2(ppz)(H_2O)_4].2H_2O$–HSA was spontaneous and exothermic process. From the point of water structure, a positive ΔS value is frequently taken as evidence for a hydrophobic interaction. Furthermore, the negative ΔH value (-6.02 kJ mol^{-1}) observed cannot be mainly attributed to electrostatic interactions since for electrostatic interactions ΔH is very small, almost zero [271]. Therefore, the negative ΔH and positive ΔS values suggest that hydrophobic and hydrogen bond interactions play major roles in the complex $[Cu_2(glygly)_2(ppz)(H_2O)_4].2H_2O$–HSA binding reaction and contributed to the stability of the complex.

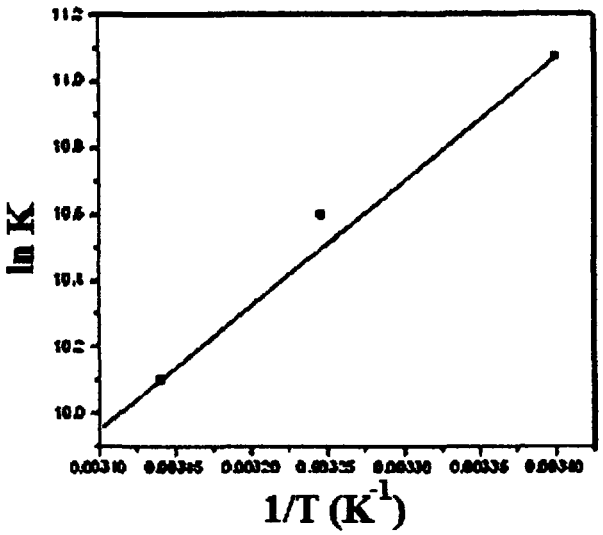

Figure 58. *Van't Hoff plot for the interaction of* $[Cu_2(glygly)_2(ppz)(H_2O)_4].2H_2O$ *and HSA.*

Table 8. *Thermodynamic parameters of complex* $[Cu_2(glygly)_2(ppz)(H_2O)_4].2H_2O$ *– (HSA) interaction at pH 7*

Complex	T (K)	ΔG (kJ/mole)	ΔH (kJ/mole)	ΔS (J/mole K)
Complex–HSA	299	–24.232	–6.062	+81.03
	309	–25.044		
	318	–25.773		

Ionic strength

In order to examine the electrostatic interaction between complex $[Cu_2(glygly)_2(ppz)(H_2O)_4].2H_2O$ and human serum albumin, fluorescence titrations were carried out under the conditions of increasing ionic strength through added amounts of NaCl at constant concentration of complex $[Cu_2(glygly)_2(ppz)(H_2O)_4].2H_2O$. The results were depicted in Table 9, which indicate that the binding constant decreases markedly with the increase in ionic strength due to the change of ionic environment and competition between coexistent ions and Cu(II) ions, leads to shortening of the storage time of complex $[Cu_2(glygly)_2(ppz)(H_2O)_4].2H_2O$ in blood plasma. Thus, we suggest that

the electrostatic and hydrophobic interactions exist between complex $[Cu_2(glygly)_2(ppz)(H_2O)_4].2H_2O$ and serum albumin, well corroborated by the thermodynamic data [272].

Table 9. *The binding constant according to Stern–Volmer curves at different NaCl concentrations in Tris–HCl buffer (pH 7.4)*

NaCl (mM)	T (K)	K_{sv}(HSA) ($10^4 M^{-1}$)	R
33	299	1.301	0.995
83	309	0.958	0.997
116	318	0.762	0.999

Investigations on the circular dichroism of HSA

To ascertain the possible influence of complex $[Cu_2(glygly)_2(ppz)(H_2O)_4].2H_2O$ binding on the secondary structure of HSA, CD measurement was also performed in the presence of complex $[Cu_2(glygly)_2(ppz)(H_2O)_4].2H_2O$ at different concentrations. As shown in Figure 59, CD spectra of free HSA (line a) exhibited two negative bands in the ultraviolet region at 208 and 222 nm attributed to $n\rightarrow\pi^*$ transfer for the peptide bond of α–helix [273]. It was observed that with the increase in complex $[Cu_2(glygly)_2(ppz)(H_2O)_4].2H_2O$ concentration, the CD signal of HSA increased, suggestive of the binding of complex $[Cu_2(glygly)_2(ppz)(H_2O)_4].2H_2O$ to HSA induces a significant conformational change in HSA (line b and c). However, the CD spectra of HSA in the presence or absence of complex $[Cu_2(glygly)_2(ppz)(H_2O)_4].2H_2O$ is similar in shape, indicating that the structure of HSA is also predominantly α–helical.

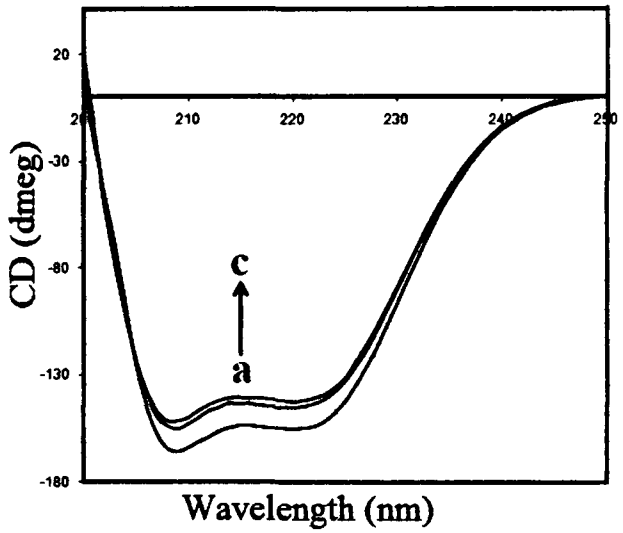

Figure 59. *CD Spectra of the HSA–complex $[Cu_2(glygly)_2(ppz)(H_2O)_4].2H_2O$ system. (a) 1.5 x 10^{-5} M HSA; (b) 1.5 x 10^{-5} M HSA + 3.0 x 10^{-5} M complex $[Cu_2(glygly)_2(ppz)(H_2O)_4].2H_2O$; (c) 4.5 x 10^{-5} M HSA + 3.0 x 10^{-5} M complex $[Cu_2(glygly)_2(ppz)(H_2O)_4].2H_2O$. pH 7.40, at room temperature.*

From Equation (17), the quantitative analysis results of the α–helix in the secondary structure of HSA were obtained. They differed from that of 59.79% in free HSA to 49.14% and 46.33% in the complex $[Cu_2(glygly)_2(ppz)(H_2O)_4].2H_2O$–HSA system at pH 7.4 and temperature 25 °C (curves a–c in Figure 59). The α–helix gradually decreases with the increase in concentration of complex $[Cu_2(glygly)_2(ppz)(H_2O)_4].2H_2O$, which reveals that interaction between complex $[Cu_2(glygly)_2(ppz)(H_2O)_4].2H_2O$ and HSA leads to a change in secondary structure of HSA [274].

Fourier transform infrared (FTIR) measurements

To further investigate the conformational change of HSA induced by complex $[Cu_2(glygly)_2(ppz)(H_2O)_4]. 2H_2O$, FT–IR experiment was performed. The spectrum in Figure 60a was obtained by subtracting the absorption of the Tris–HCl from the spectrum of the HSA solution. The spectrum in Figure 60b was obtained by subtracting the absorption of the complex $[Cu_2(glygly)_2(ppz)(H_2O)_4].2H_2O$–free form from that of the

complex $[Cu_2(glygly)_2(ppz)(H_2O)_4].2H_2O$–bound form. Infrared spectra of HSA exhibit a number of the amide bands, which represent different vibrations of the peptide moiety. The amide I peak observed in the range 1600–1700 cm^{-1} (mainly C=O stretch) and amide II band in the region 1500–1600 cm^{-1} (C–N stretch coupled with N–H bending mode). It is well known that the amide bands have a relationship with the secondary structure of HSA, and amide I is more sensitive than amide II for change of secondary structure of HSA. As shown in Figure 60, the peak position of amide I bands were shifted from 1633.9 cm^{-1} to 1641.4 cm^{-1}, indicating the secondary structure of the HSA was changed in presence of complex $[Cu_2(glygly)_2(ppz)(H_2O)_4].2H_2O$ [275].

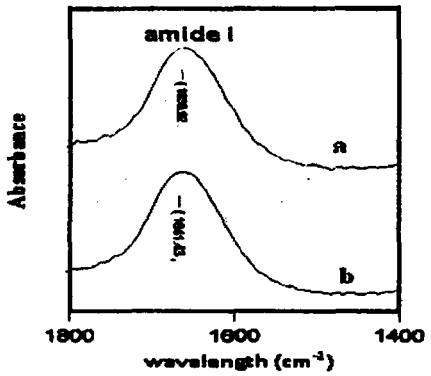

Figure 60. *FT-IR spectra of (a) free HSA; (b) different spectra [(HSA solution + complex $[Cu_2(glygly)_2(ppz)(H_2O)_4].2H_2O$ solution)–complex $[Cu_2(glygly)_2(ppz)(H_2O)_4].2H_2O$ solution)] in 5 mM Tris-HCl/50 mM NaCl buffer, pH 7.4, at room temperature in the region of 1750–1400 cm^{-1}, [HSA], 1.5 x 10^{-5} M; [complex], 3.0 x 10^{-5} M.*

3D–Fluorescence studies

3D fluorescence spectroscopy is a newly emerged analytical technique to investigate the conformational and structural changes of proteins by changing excitation and emission wavelength simultaneously [276]. By comparing the 3D fluorescence spectral changes of HSA in the absence and presence of complex $[Cu_2(glygly)_2(ppz)(H_2O)_4].2H_2O$, the

conformational and micro–environmental changes of HSA can be obtained. The 3D fluorescence spectra and contour ones of HSA and complex $[Cu_2(glygly)_2(ppz)(H_2O)_4].2H_2O$–HSA system are shown in Figure 61, respectively, and the corresponding characteristic parameters are shown in Table 10. Peak a was the Rayleigh scattering peak ($\lambda_{ex}=\lambda_{em}$). Peak b (280, 346 nm, λ_{ex}, λ_{em}) mainly reflected the spectral behavior of Trp residue, and the maximum emission wavelength and the fluorescence intensity of the residue associated with its microenvironment's polarity. Peak c was the second–ordered scattering peak ($\lambda_{em}=2\lambda_{ex}$) [277]. As shown in Figure 61 $[Cu_2(glygly)_2(ppz)(H_2O)_4].2H_2O$, it was observed that the fluorescence intensities of peak a and b both decreased significantly and the maximum emission wavelength of the peak was changed in the presence of complex $[Cu_2(glygly)_2(ppz)(H_2O)_4].2H_2O$ indicated the quenching of fluorescence of HSA. We can conclude that the interaction of complex $[Cu_2(glygly)_2(ppz)(H_2O)_4].2H_2O$ with HSA induced some conformational and micro–environmental changes in HSA, corroborated well with our spectroscopic results obtained from UV–vis, FT–IR and CD measurements.

Table 10. *3D fluorescence spectral characteristic parameters of HSA and HSA–complex* $[Cu_2(glygly)_2(ppz)(H_2O)_4].2H_2O$ *system*

HSA				HSA-complex 1			
	Peak position $\lambda_{ex}/\lambda_{em}$ (nm/nm)	$\Delta\lambda$	Intensity		Peak position $\lambda_{ex}/\lambda_{em}$ (nm/nm)	$\Delta\lambda$	Intensity
Peak a	280/280-360/360	0	4.43-62.69	Peak a	280/280-360/360	0	5.25-62.69
Peak b	280/344	64	48.23	Peak b	280/348	68	26.23

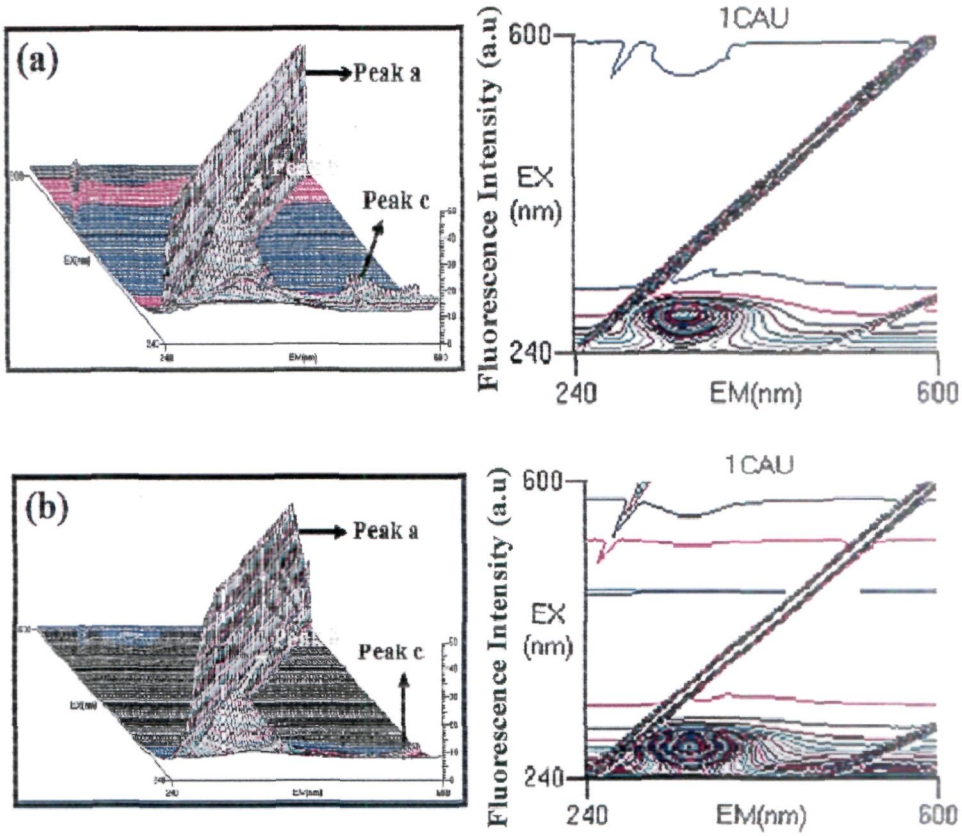

Figure 61. *3D fluorescence spectrum and corresponding contour diagrams of (a) HSA, and (b) complex* $[Cu_2(glygly)_2(ppz)(H_2O)_4].2H_2O$*–HSA conjugate system. The concentration of HSA is fixed at 2.5 μM and that of complex* $[Cu_2(glygly)_2(ppz)(H_2O)_4].2H_2O$ *is fixed at 22.5 μM. pH = 7.4, at room temperature.*

HSA photocleavage studies

There is a considerable interest in the development of synthetic chemical proteases that are activated by radical–generating metal complex. Such chemical proteases can be utilized for breaking large proteins into smaller fragments that are more amenable to sequencing. The ability of Cu(II) complexes to mediate protein cleavage is well established in literature [278,279] owing to the fact that these complexes show their own selectivity for a cleavage mechanism, it is therefore imperative to study the effect of

Cu(II) complex on HSA in presence of different concentration and reactive oxygen species.

In order to ascertain the ability of the complex $[Cu_2(glygly)_2(ppz)(H_2O)_4].2H_2O$ to serve as a synthetic metalloproteases, the HSA photocleavage activity of the complex $[Cu_2(glygly)_2(ppz)(H_2O)_4].2H_2O$ was studied using 4 μM HSA in 50 mM Tris–HCl buffer on exposure to UV–A1 light of 365 nm with different complex concentrations for 20 min and the extent of cleavage was compared with the untreated HSA band. The photoinduced protease activity of complex $[Cu_2(glygly)_2(ppz)(H_2O)_4].2H_2O$ was assayed by SDS–PAGE (12%3%) analysis. As shown in Figure 62a, it was observed that HSA alone (Lane 1) did not show any apparent cleavage under these conditions. However, upon increasing the concentration of complex $[Cu_2(glygly)_2(ppz)(H_2O)_4].2H_2O$ (100–250 μM), HSA showed significant smearing or fading of the band (Lane 2–5), indicating photocleavage of HSA under physiological reaction conditions. At the same time, when the concentration of complex $[Cu_2(glygly)_2(ppz)(H_2O)_4].2H_2O$ reached to 250 μM, HSA cleaved into smaller fragment that could not be observable by SDS–PAGE. The smearing of the band results from non–specific cleavage of the HSA by the highly diffusible $HO^{\bullet}$ radicals generated by the complex upon photoexcitation, leading to the cleavage of HSA into very small fragments. The complex $[Cu_2(glygly)_2(ppz)(H_2O)_4].2H_2O$ did not show any cleavage activity in the dark, thus ruling out any hydrolytic cleavage of HSA (Lane 6). To explore the mechanistic pathway of the cleavage activity, comparative HSA cleavage experiment of complex $[Cu_2(glygly)_2(ppz)(H_2O)_4].2H_2O$ was carried out in presence of standard radical scavengers such as DMSO and KI as hydroxyl radical scavenger ($HO^{\bullet}$) and sodium azide (NaN_3) as singlet oxygen ($^1O_2$) quencher were used

prior to the exposure to UV–A1 light. As shown in Figure 62b, the HSA cleavage mediated by complex $[Cu_2(glygly)_2(ppz)(H_2O)_4].2H_2O$ in the presence of DMSO and KI (Lane 3 and 4, respectively) show significant reduction in the HSA cleavage activity, indicating the involvement of hydroxyl radicals as the reactive species.

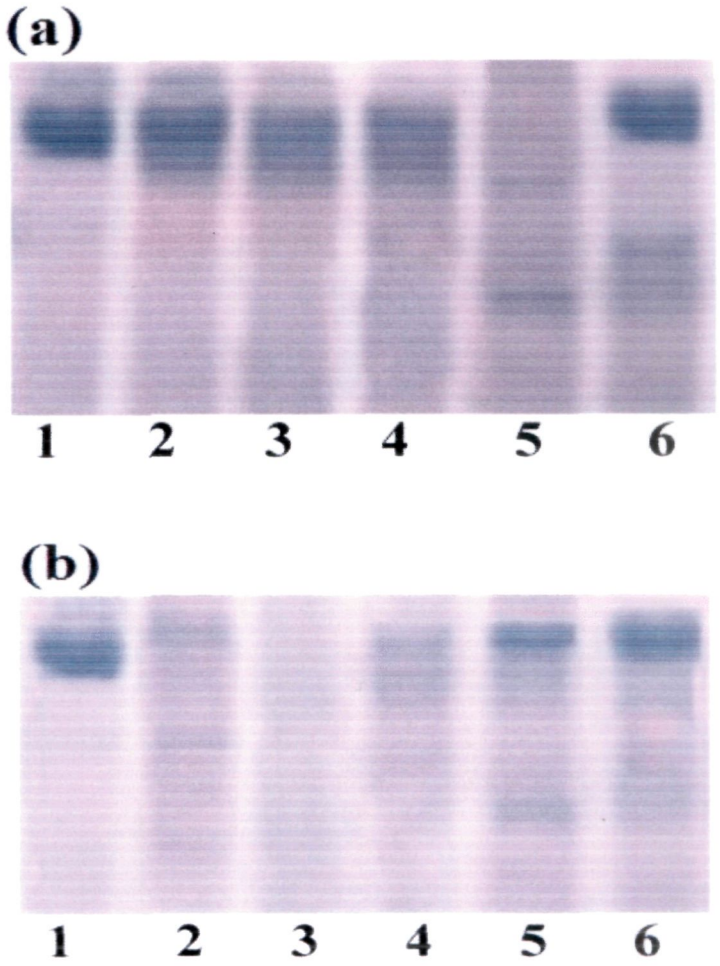

Figure 62. *SDS–PAGE electrophoresis of complex* $[Cu_2(glygly)_2(ppz)(H_2O)_4].2H_2O$ *in 12% polyacrylamide gel showing photocleavage of human serum albumin (HSA, 15 μM) with 20 min photoexposure to UV–A1 light at 365 nm Tris HCl buffer (pH 7.4), (a) at different concentration; lane–1, HSA control; lane–2, HSA + (100 μM); lane–3, HSA + (150 μM); lane–4, HSA + (200 μM); lane–5, HSA + (250 μM); lane–6, HSA + (250 μM, in dark) and (b) in presence of standard radical scavengers; lane–1, HSA + (250 μM, in dark); lane–2, HSA + (250 μM); lane–3, HSA + DMSO (20 μL) + (250 μM); lane–4, HSA + KI (3 mM) + (250 μM); lane–5, HSA +* NaN_3 *(3 mM) + (250 μM); lane–6, HSA + TEMP (3 mM)+ (250 μM).*

On the other hand, addition of $NaN_3$and TEMP (Lane 5 and 6, respectively) did not show any inhibition suggesting that the singlet oxygen quencher was not involved in the cleavage process. Since, the present complex $[Cu_2(glygly)_2(ppz)(H_2O)_4].2H_2O$ contains Lewis acid Cu(II) metal ion and coordinated water molecule, which facilitates the nucleophilic attack on amide bond mediating internal attack by a coordinated $Cu–OH_2$ molecule. So, it is clear that the delivery of high concentrations of metal ion to the HSA, in locally generating oxygen or hydroxide radicals, yields an efficient HSA cleavage reaction.

Antitumor activity assays

The results obtained from the previous biological studies, namely, DNA binding and cleavage, Topo–I inhibition, and antioxidative studies for complex $[Cu_2(glygly)_2(ppz)(H_2O)_4]$. $2H_2O$, encouraged us to evaluate their *in vitro* cytotoxic activity. The activity of complex $[Cu_2(glygly)_2(ppz)(H_2O)_4].2H_2O$ was evaluated in terms of GI_{50}, TGI and LC_{50} values against human carcinoma cell lines of different histological origin: 786–O, A498 (kidney), Zr–75–1 (Breast), SiHa (Cervix), A549, Hop–62 (Lung), SW620, HCT15 (Colon), MIAPACA2 (Pancreatic) by Sulforhodamine B test (SRB) assay [280]. The cytotoxic screening data (Table 11) shows that the complex $[Cu_2(glygly)_2(ppz)(H_2O)_4].2H_2O$ act as a potential selective anticancer agent with a significant GI_{50} values specifically towards MIAPACA2, A498, and A549 tumor cell lines.

Table 11. Summary of the screening data of complex $[Cu_2(glygly)_2(ppz)(H_2O)_4].2H_2O$ for the in vitro anti–tumor activity (in μg/ml)

Human Tissue of origin		Kidney	Breast	Cervix	Lung	Colon	Lung	Colon	Kidney	Pancreatic
Cell line		786-O	Zr-75-1	SiHa	Hop62	HCT15	A549	SW620	A498	MIAPACA2
GI_{50}	1	68.8	>80	>80	>80	62.4	41.6	>80	29.0	19.5
	ADR	<10	<10	<10	<10	<10	<10	<10	<10	<10
TGI	1	>80	>80	>80	>80	>80	80.7	>80	53.8	>80
	ADR	26.5	<10	14.9	10.1	37.0	42.1	17.0	13.9	20.4
LC_{50}	1	>80	>80	>80	>80	174.7	>80	>80	78.6	>80
	ADR	55.9	22.2	32.6	31.0	66.9	77.8	34.3	35.3	46.8

Where:

- GI_{50}= Growth inhibition of 50 % (GI_{50}) calculated from [(Ti–Tz)/(C–Tz)] x 100 = 50, drug concentration result in a 50% reduction in the net protein increase.
- ADR= Adriamycin (taken as positive control compound).
- TGI = Tumor growth inhibition
- LC_{50} = Lethal concentration of 50 % (LC_{50}).

Molecular docking study

In order to provide a considerable insight into the interactions of HSA with complex $[Cu_2(glygly)_2(ppz)(H_2O)_4].2H_2O$, molecular docking technique was employed to search the exact binding sites inside the molecular target HSA. From the 3–D structure of crystalline albumin, it is known that HSA comprises three homologous domains (denoted I, II, and III): I (residues 1–195) II (196–383) and III (384–585) that assemble to form heart shaped molecule. The principal region of complex $[Cu_2(glygly)_2(ppz)(H_2O)_4].2H_2O$ binding sites of HSA are located in hydrophobic cavities in subdomain IIA and IIIA, corresponding to site I and site II, respectively and tryptophan residue (Trp–214) of HSA in subdomain IIA. There is a large hydrophobic cavity in subdomain IIA to accommodate the complex $[Cu_2(glygly)_2(ppz)(H_2O)_4].2H_2O$. The resulting docked pattern (Figure 63a) indicates that complex $[Cu_2(glygly)_2(ppz)(H_2O)_4].2H_2O$ is located within the subdomain IIA of HAS [281], suggesting the existence of hydrophobic interaction between complex

$[Cu_2(glygly)_2(ppz)(H_2O)_4].2H_2O$and HSA, correlated with the binding mode observed by thermodynamic analysis and fluorescence quenching mechanism of HSA in presence of complex $[Cu_2(glygly)_2(ppz)(H_2O)_4].2H_2O$.

(a)

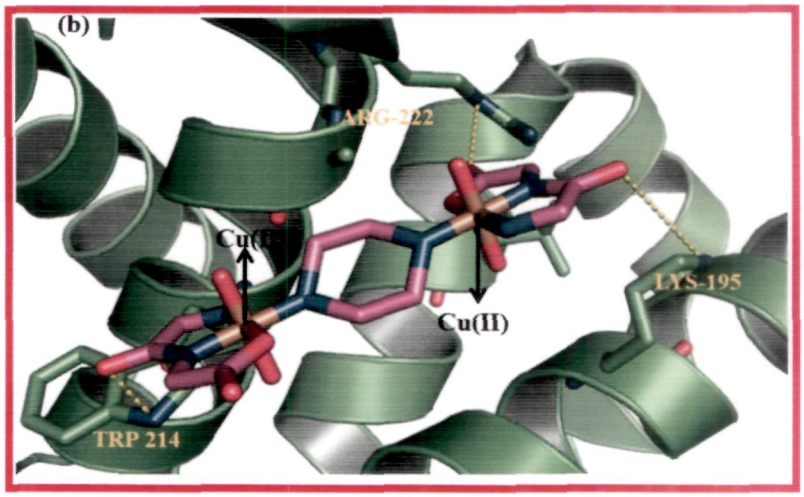

(b)

Figure 63. *(a) Molecular docked model of complex $[Cu_2(glygly)_2(ppz)(H_2O)_4].2H_2O$ (stick representation) located within the hydrophobic pocket in subdomain IIA of HSA; (b)the interaction mode between complex $[Cu_2(glygly)_2(ppz)(H_2O)_4].2H_2O$ (red colour) and HSA (green colour) were represented in a cartoon form and the yellow dashed line showing hydrogen bond interaction between them.*

Furthermore, there are also a number of specific electrostatic interactions and hydrogen bonds, because several ionic and polar residues in the proximity of the ligand play an important role in stabilizing the molecule H–bonds and electrostatic interactions. As shown in Figure 63b, there are hydrogen bond interactions between the main chain carbonyl oxygen of Arg–257 and terminal amino group of the complex $[Cu_2(glygly)_2(ppz)(H_2O)_4].2H_2O$ and another between carbonyl groups of $[Cu_2(glygly)_2(ppz)(H_2O)_4].2H_2O$ and Ala–291 and Arg–222 residues of HSA. These results suggest that formation of hydrogen bonds decreased the hydrophilicity and increased the hydrophobicity to keep complex $[Cu_2(glygly)_2(ppz)(H_2O)_4].2H_2O$–HSA system stable. The results obtained from molecular docking indicated that the interaction between complex $[Cu_2(glygly)_2(ppz)(H_2O)_4].2H_2O$ and HSA was dominated by hydrophobic forces.

Conclusions

In this work, we have explored the interaction studies of new dinuclear copper(II) complex derived from the dipeptide (glycyl glycine) and piperazine as metallopeptide drug to examine their effect on the binding propensity of HSA and to elucidate the mechanism of action at the molecular target. The interaction between complex $[Cu_2(glygly)_2(ppz)(H_2O)_4].2H_2O$ and HSA was investigated by employing different spectroscopic techniques (UV–visible, fluorescence, CD, FTIR) in accordance with molecular docking techniques. The results revealed that the secondary structure of HSA was affected upon interaction with the complex $[Cu_2(glygly)_2(ppz)(H_2O)_4].2H_2O$. Fluorescence results indicated the presence of static quenching mechanism upon binding of complex $[Cu_2(glygly)_2(ppz)(H_2O)_4].2H_2O$ to HSA. On the basis of spectroscopic results we have concluded that the complex $[Cu_2(glygly)_2(ppz)(H_2O)_4].2H_2O$ was bound to site I of protein, which was located within hydrophobic pocket of subdomain IIA. The complex $[Cu_2(glygly)_2(ppz)(H_2O)_4].2H_2O$ shows photo–induced degradation of HSA induced by hydroxyl radicals as the reactive species. Furthermore, complex $[Cu_2(glygly)_2(ppz)(H_2O)_4].2H_2O$ exhibits significant GI_{50} values specifically towards MIAPACA2, A498 and A549 tumor cell lines. Therefore, it is concluded that drugs that bind and cleave HSA will not only help the transportation and distribution of drug in blood plasma but also elucidate the valuable information to understand the mechanistic pathway of drug delivery and contribute to the molecular design of novel synthetic protein photo–degradation agents.

CHAPTER IV (a)

DNA binding and cleavage studies of sulfasalazine–derived dipeptide Zn(II) complex: Validation for specific recognition with 5′–TMP

Synthesis

Synthesis of [Zn(glygly)(ssz)(H_2O)].6H_2O

To a stirred methanolic solution (15 ml) of zinc nitrate hexahydrate (0.595g, 2mmol) was added an aqueous solution of glycyl glycine (0.264g, 2mmol) followed by dropwise addition of KOH (0.224g, 4mmol) and pH of the resulting solution was adjusted between 8–12. This reaction mixture was stirred for ca. 2 h at room temperature to obtain clear solution. A methanolic solution (20 ml) of sulfasalazine (0.80 g, 2mmol) was added to the above reaction mixture and stirred for another 3 h. The orange colored solid precipitate was filtered, thoroughly washed with ice cold methanol and dried in vacuo over anhydrous $CaCl_2$ (Yield: 0.610g, 71%). m.p. 206 ± 2°C, Anal. Calc. for $C_{22}H_{32}ZnN_6O_{15}S$ (%): C, 36.80; H, 4.49; N, 11.71; S, 4.46, Found: C, 36.08; H, 4.23; N, 11.79; S, 4.02. Selected IR data on KBr/nujol, cm^{-1}: 3424 ν(NH_2+H_2O); 1603 ν(C=O); 1388 ν(C–N); 424 ν(Zn–N); 460 ν(Zn–O). Molar Conductance, Λ_M (1 x 10^{-3} M, H_2O): 17 $\Omega^{-1}cm^2$ mol^{-1} (Non–electrolyte). UV–vis absorption: (H_2O, 10^{-4} M), λ_{max}/nm (ε/10^4 M^{-1} cm^{-1}) 231 (2.6); 256 (1.30); 370 (1.81). ESI–MS (m/z, H_2O): 716.4 $[M]^+$; 608.6 $[M–(6H_2O)]^+$.

^{1}H NMR (DMSO–d_6, 400 MHz) δ(ppm): 3.36 (NCH_2); 3.80 (CCH_2); 4.80 (H_2O); 6.86–8.35 (ArH). ^{13}C NMR (DMSO–d_6, 100 MHz) δ(ppm): 46.15–54.29 (CH_2); 118.59–150.06 (ArC); 178.86 (O–C=O); 158.09 (CO).

Results and discussion

In order to investigate the ability of complex towards molecular recognition and sequence specific cleavage of DNA by synthetic probes, new drug candidate, complex [Zn(glygly)(ssz)(H_2O)].6H_2O was synthesized and characterized. The synthesis of new Zn(II) complex [Zn(glygly)(ssz)(H_2O)].6H_2O was achieved by mixing stoichiometric

amounts of Zn(II) nitrate hexahydrate with glycyl glycine and sulfasalazine followed drop wise addition of KOH (Scheme 3), in a good yield. The composition of the complex $[Zn(glygly)(ssz)(H_2O)].6H_2O$ was ascertained by elemental analysis, IR, UV–vis, ESI–MS and NMR spectroscopy. The resulting complex $[Zn(glygly)(ssz)(H_2O)].6H_2O$ is stable towards air and moisture and readily soluble in H_2O. Molar conductance value of complex in H_2O ($1x10^{-3}$ M) at 25 °C suggest its non–electrolyte nature ($17\Omega^{-1}cm^2mol^{-1}$).

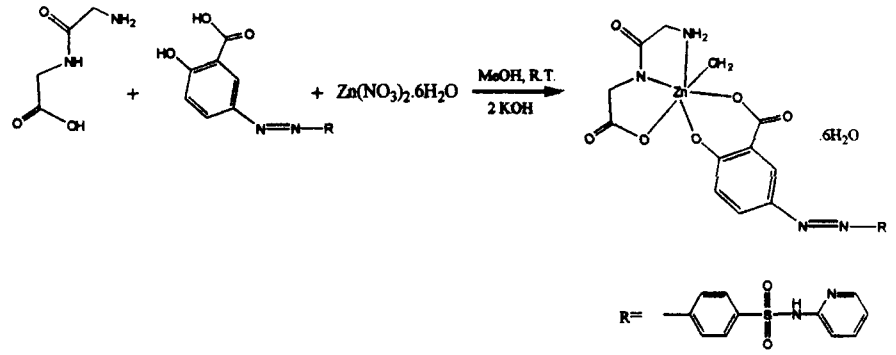

Scheme 3. Synthetic route for complex $[Zn(glygly)(ssz)(H_2O)].6H_2O$

Infrared spectra

The IR spectra of complex $[Zn(glygly)(ssz)(H_2O)].6H_2O$ was recorded in the region 4000–400 cm^{-1} and analyzed in comparison to the IR spectra of the free ligand. The bands around 1575 cm^{-1} and 1254 cm^{-1} observed in the free dipeptides attributed to amide II and III bands [due to δ(NH) + ν(C–N) in compound containing neutral secondary peptide groups] were replaced by a new absorption band at 1388 cm^{-1} in complex $[Zn(glygly)(ssz)(H_2O)].6H_2O$, which is characteristic for deprotonated secondary (in fact tertiary) peptide complex; the large shift towards low frequency region is typical of peptide N–bonding. Since, on removal of peptide proton the band becomes a pure C–N stretch [282]. The $\nu(CO)_{peptide}$ [amide I] band observed at ~1665 cm^{-1} in the free dipeptide was shifted to lower frequency at ~1603 cm^{-1} after complexation which

confirms the coordination of metal ion through peptide–N atom. The bands around 1586 and 1410 cm^{-1}, due to ν_{asym} (COO^-) and ν_{sym} (COO^-) of the amino acids appeared in the complex $[Zn(glygly)(ssz)(H_2O)].6H_2O$ at 1555 and 1476 cm^{-1} [283]. The shift of these two bands suggests the involvement of the carboxylic groups of the amino acids in complex formation. A broad band with strong–to–medium intensity in the 3400–3450 cm^{-1} region may be assigned to the OH stretching vibration for the coordinated water molecules in the complex. The shift in ν(CO) of phenolic group from 1281 cm^{-1} in the free sulfasalazine ligand to 1260 cm^{-1} in the complex $[Zn(glygly)(ssz)(H_2O)].6H_2O$ indicated the participation of the phenolic group in complex formation via deprotonation [284]. The medium intensity bands at 424 and 460 cm^{-1} were attributed to stretching vibration of Zn–N and Zn–O, respectively.

NMR spectroscopy

The ^1H and ^{13}C NMR spectra in D_2O solution show signals for aliphatic and aromatic protons with chemical shift values in accordance with their anticipated structure. In ^1H NMR spectrum of complex $[Zn(glygly)(ssz)(H_2O)].6H_2O$, signals due to free carboxylic (COOH), phenolic (OH) and amide linkage (–NH–) groups as expected in the range 12.0–10.0, 12.55 and 11.81 ppm, respectively were absent, which commensurate with the fact that coordination to the metal center takes place by the deprotonation of the functional groups [285,286]. Additionally, the characteristic resonance signals at 3.36, 3.80 and 4.80 ppm corresponding to the CH_2 proton adjacent to the amino group (NCH_2), CH_2 proton adjacent to the carboxylate group (CCH_2) of glycylglycine and coordinated H_2O molecules, respectively were observed. The aromatic protons of sulfasalazine appeared as a multiplet at 6.86–8.35 ppm [287]. The broadening of the spectrum in the aromatic region was due to the merging of $–SO_2NH$ and NH_2 protons in the same region [288]. The ^{13}C NMR spectrum of complex $[Zn(glygly)(ssz)(H_2O)].6H_2O$ exhibited

various resonances due to O–C=O, C–O–Zn and $-CH_2$ carbons at 178.86, 158.09 and 46.15–54.29 ppm, respectively. In addition, aromatic carbon signals were observed at 118.59–150.06 ppm (Figure 64).

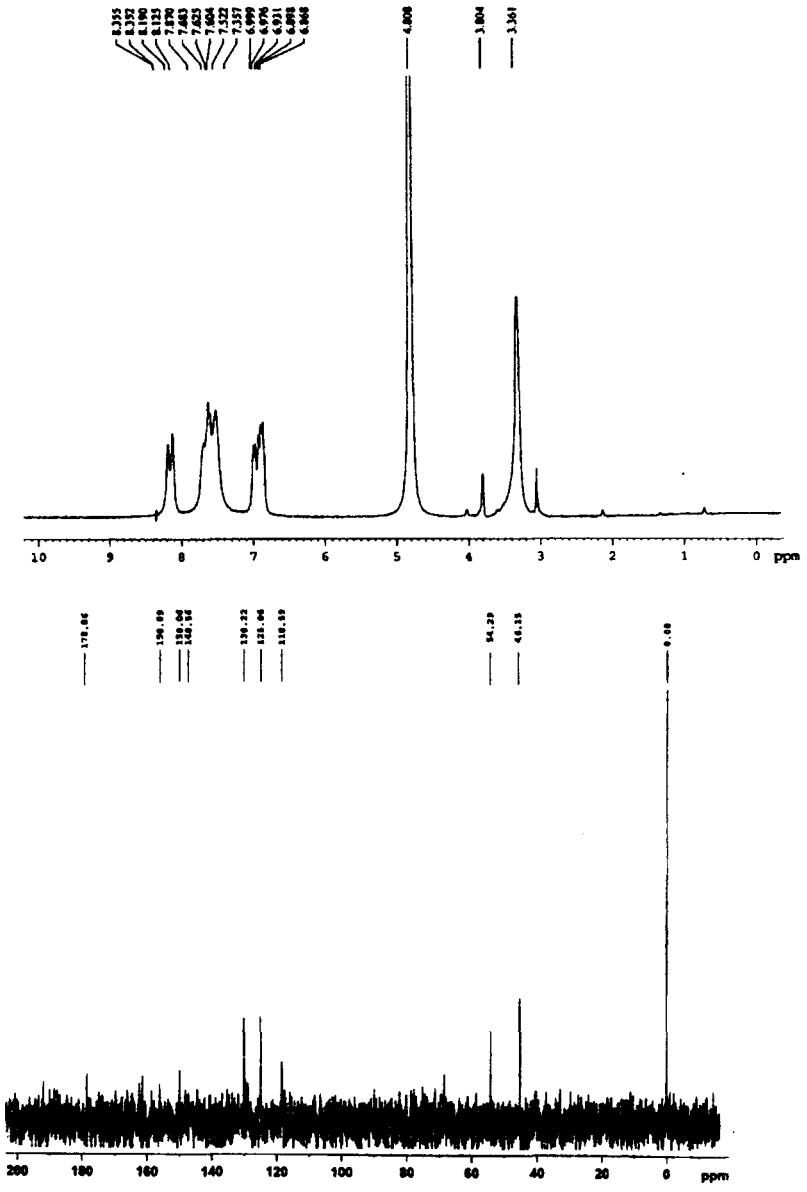

Figure 64. *^{1}H and ^{13}C NMR spectra of complex* [Zn(glygly)(ssz)(H_2O)].6H_2O *in D_2O solution.*

Electronic spectra

The electronic absorption spectrum of complex [Zn(glygly)(ssz)(H_2O)].6H_2O in freshly prepared aqueous solutions was carried out in the region 200–1100 nm at room temperature. The electronic spectrum of free dipeptide displayed an intense absorption bands at 220 nm due to n→π* transition which was shifted to 231 nm upon coordination with Zn(II) metal ion, and has been assigned to N^- →Zn(II) charge transfer (LMCT) transition [283]. A broad band at 256 and 370 nm were attributed to π–π* transitions of carboxylate group of peptide and n–π* transitions of the carboxylic –OH and phenolic –OH of sulfasalazine ligand to the metal ion, respectively. [284].

X–ray diffraction analysis

To obtain further evidence about the structure and lattice dynamics of the metal complex [Zn(glygly)(ssz)(H_2O)].6H_2O, X–ray powder diffraction was performed. The XRPD pattern (Figure 2) obtained for the metal complex [Zn(glygly)(ssz)(H_2O)].6H_2O shows well defined crystalline peaks indicating that the complex [Zn(glygly)(ssz)(H_2O)].6H_2O is crystalline in phase due to inherent crystalline nature. The X–ray diffractogram of the complex [Zn(glygly)(ssz)(H_2O)].6H_2O shows reflecting peaks at 2θ scattering angles of 31.72, 34.40, 36.21, 47.49, 56.51 and 76.82 assigned to (100), (002), (101), (102), (110) and (202) crystal planes respectively, characteristic of a well ordered hexagonal arrangement of Zn(II) atoms (JCPDF:80–0075). The lattice parameters found for complex [Zn(glygly)(ssz)(H_2O)].6H_2O are a = b = 3.23 and c = 5.19, which are consistent with the known lattice parameters a = b = 3.253 and c = 5.209, indicating that the complex particles have the same crystal structure as that of the bulk. A summary of the refined XRPD parameters of complex [Zn(glygly)(ssz)(H_2O)].6H_2O is given in Table 12.

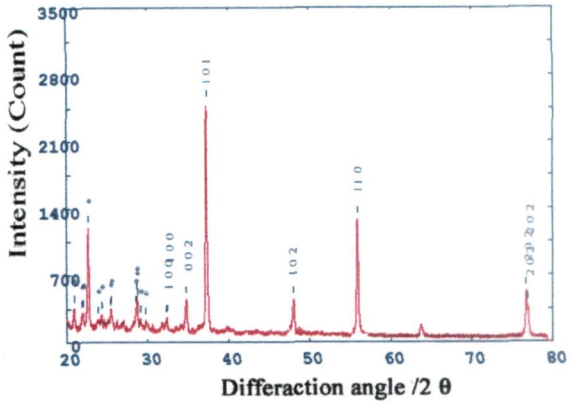

Figure 65. *The XRPD pattern of complex [Zn(glygly)(ssz)(H₂O)].6H₂O showing peaks at different scattered angles and their planes (miller indices).*

Table 12. *Summary of the XRPD data and the refinement parameters for complex [Zn(glygly)(ssz)(H₂O)].6H₂O*

Parameter	Complex *[Zn(glygly)(ssz)(H₂O)].6H₂O*
Formula	$C_{22}H_{32}ZnN_6O_{15}S$
FW	717.97
Temperature(K)	298
Method	Micro crystalline
Wavelength	1.540598
Radiation	Cu–Kα1
Crystal System	Hexagonal
Space group	P
Unit cell dimension	
a(Å)	3.23
b(Å)	3.23
c(Å)	5.19
α°	90
β°	90
γ°	120
2θ range	20–80
Limiting indices	$0 \leq h \leq 5$
Intensity (%)	14.29–100

DNA binding studies

Electronic absorption titration

Electronic absorption spectroscopy is one of the most convenient tools to examine the binding mode of DNA with metal complexes. Any interaction between the complexes and DNA is expected to perturb the ligand centered transitions of complex. Binding of

complexes with DNA by intercalation mode generally results in hypochromism and a red shift (bathochromism) of the absorption band due to a strong stacking interaction between an aromatic moiety of the ligand and the base pairs of the DNA [289,290]. On the other hand, the absorption intensity of a complex is increased (hyperchromism) upon increasing the concentration of CT DNA owing to the degradation of the DNA double–helix structure [291]. The extent of the hyperchromism is indicative of the partial or non–intercalative binding modes, such as electrostatic forces, van der Waals interactions, dative bonds, hydrogen bonds and hydrophobic interactions.

The absorption spectra of complex $[Zn(glygly)(ssz)(H_2O)].6H_2O$ in the absence and presence of CT DNA is shown in Figure 66. In the UV region, complex $[Zn(glygly)(ssz)(H_2O)].6H_2O$ displayed an intense absorption bands at 256 nm, attributed to intraligand π–π^* transition. Upon the addition of increasing amounts of CT DNA (0.0–3.33 x 10^{-5} M) to the complex $[Zn(glygly)(ssz)(H_2O)].6H_2O$ at constant concentration (1.00 x 10^{-5} M) showed an increase in the absorption spectral intensity of the intraligand "hyperchromism" absorption band with a red shift of 1–2 nm. These results suggest that interactions between the complex $[Zn(glygly)(ssz)(H_2O)].6H_2O$ and CT DNA occurs by non–intercalative binding modes either due to (i) external contact (surface binding) with the duplex through hydrogen–bonding interactions between coordinated $-NH_2$ and oxygen atoms of the ligand with DNA nucleobases which are accessible both in the major and minor grooves, (ii) covalent coordinate bonding with base pairs of DNA due to the replacement of the labile water molecule. Also, the presence of aromatic moieties could facilitate partial intercalation by insertion of the complexes into the adjacent base pairs of DNA. The intrinsic binding constant (K_b) value was calculated and found to be 2.67 x 10^4 M^{-1}. The K_b value suggested that complex $[Zn(glygly)(ssz)(H_2O)].6H_2O$ binds strongly to calf thymus DNA. Literature survey reveals that Zn(II) complexes in contrast to Cu(II)

and Ni(II) binds selectively to thymine, altering the local structure of the A–T base pairs of DNA helix by hydrogen bond breakage [292].

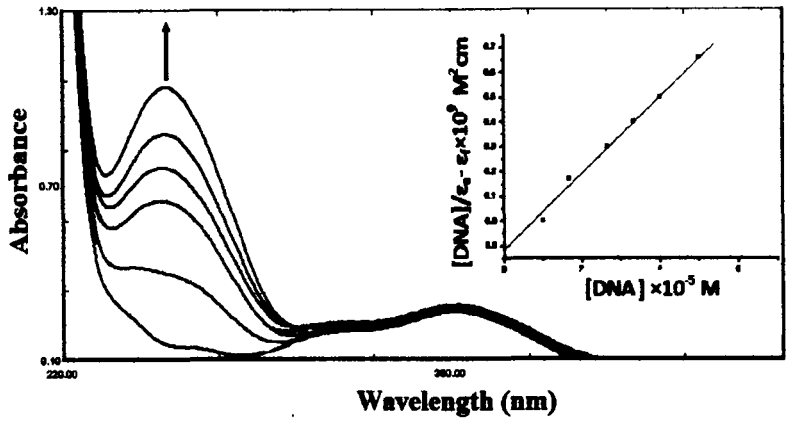

Figure 66. *Absorption spectral traces of complex [Zn(glygly)(ssz)(H₂O)].6H₂O in 5mM Tris HCl/ 50 mM NaCl buffer at pH 7.2 upon addition of CT DNA. Inset: Plots of [DNA]/ ε_a–ε_f (M^2 cm) vs. [DNA] for the titration of CT DNA with complexes ■, experimental data points; full lines, linear fitting of the data. [Complex] 1.00 x 10^{-5} M. [DNA] 0.0–3.33 x 10^{-5} M.*

Absorption titration with 5′–TMP and 5′–GMP

In order to gain support for selective binding of the zinc metal ion to thymine base of DNA helix selectively involving possibly N3 thymine coordination, the interaction of [Zn(glygly)(ssz)(H₂O)].6H₂O with DNA bases thymine and guanine was investigated using electronic absorption spectral technique. Addition of thymine to complex [Zn(glygly)(ssz)(H₂O)].6H₂O resulted in increase in absorbance (78% hyperchromism) in the intraligand bands with no blue or red shift (Figure 67). The hyperchromicity implies that the interaction between complex [Zn(glygly)(ssz)(H₂O)].6H₂O and the thymine could be due to coordination of Zn(II) metal ion after ligand dissociation or reorganization and hydrogen bonding with O2 and O4 oxygen atoms of thymine. However, on addition of guanine to the complex [Zn(glygly)(ssz)(H₂O)].6H₂O exhibited relatively small hyperchromic changes (61%) were observed in absorbance intensity (Figure 68). In order to evaluate the binding affinity of complex

[Zn(glygly)(ssz)(H_2O)].6H_2O with 5'–TMP and 5'–GMP, the intrinsic binding constant (K_b) values were determined and calculated to be 3.49 x 10^4 and 1.42 x 10^4 M^{-1}, respectively. These results revealed that complex [Zn(glygly)(ssz)(H_2O)].6H_2O has stronger binding affinity towards thymine in comparison to guanine due to two effects; when thymine binds, hydrogen bonds are formed between the NH_2 group of ligand and carbonyl groups of thymine, which stabilizes the complex and secondly, a significant stronger molecular orbital (MO) interaction is identified in thymine in comparison to guanine [293]. The presence of two electron withdrawing oxo groups C2 and C3 position of thymine ring lower the energy of the lone pair orbital at N3 of thymine base.

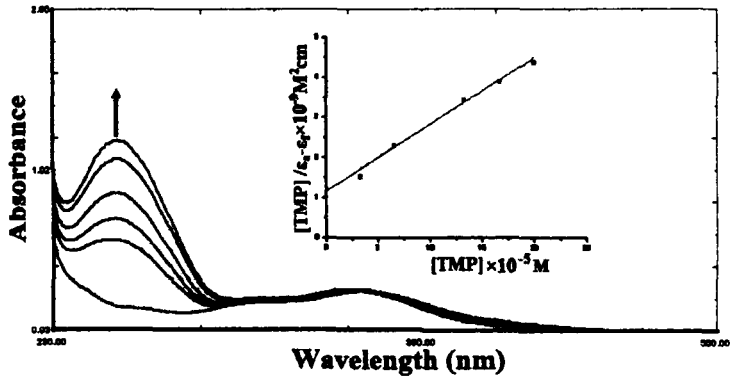

Figure 67. Absorption spectral traces of complex [Zn(glygly)(ssz)(H_2O)].6H_2O in 5 mM Tris-HCl/50 mM NaCl buffer upon addition of 5'–TMP Arrow shows the absorbance changes upon increasing concentration of the 5'–TMP.

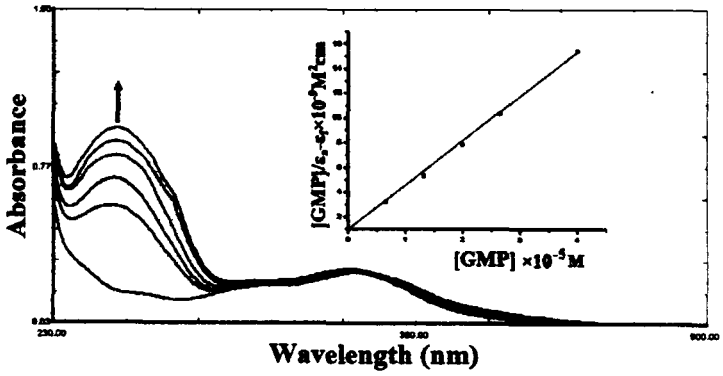

Figure 68. Absorption spectral traces of complex [Zn(glygly)(ssz)(H_2O)].6H_2O in 5 mM Tris-HCl/50 mM NaCl buffer upon addition of 5'–GMP Arrow shows the absorbance changes upon increasing concentration of the 5'–GMP.

NMR (^{1}H and ^{31}P) interaction studies with 5′–TMP

To validate our hypothesis, the preferential binding of complex [Zn(glygly)(ssz)(H_2O)].6H_2O towards 5′–TMP were carried out by employing ^{1}H and ^{31}P NMR techniques at physiological pH (7.4). The ^{1}H NMR of free 5′–TMP in D_2O solvent recorded the proton resonance of N3–H at 7.64 ppm and ribose H1′–H5′ at 3.8–5.8 ppm respectively. On interaction of complex [Zn(glygly)(ssz)(H_2O)].6H_2O with 5′–TMP, the N3 position was shifted downfield with a decrease in the peak intensity (Figure 69a) from 7.64 ppm to 8.22 ppm. However, the ribose proton H1′–H5′ signals were shifted upfield ~0.08 ppm, which indicate the presence of diamagnetic Zn(II) center in the proximity of these protons.

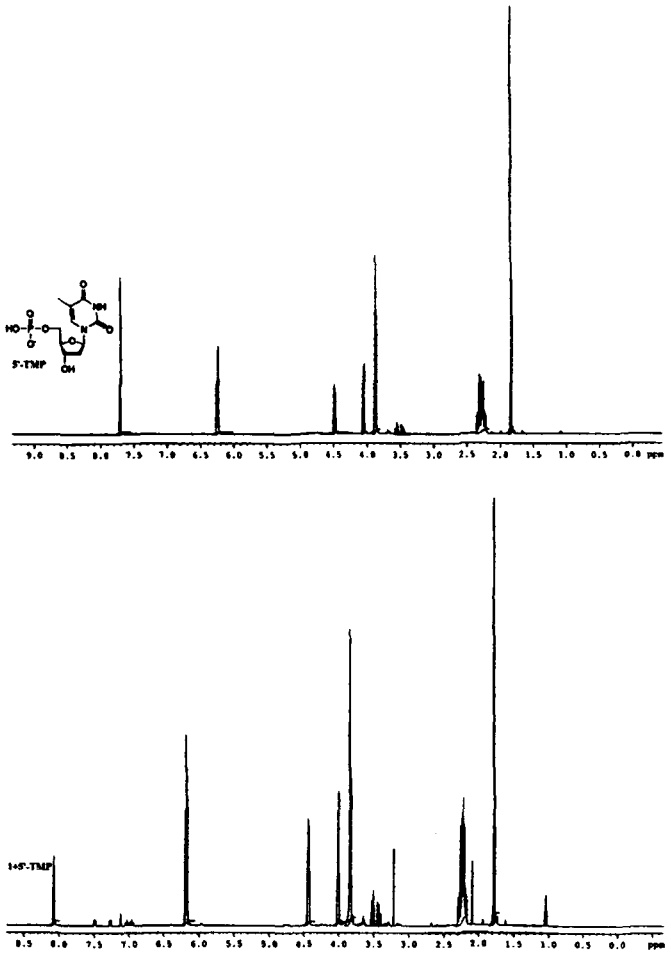

(a)

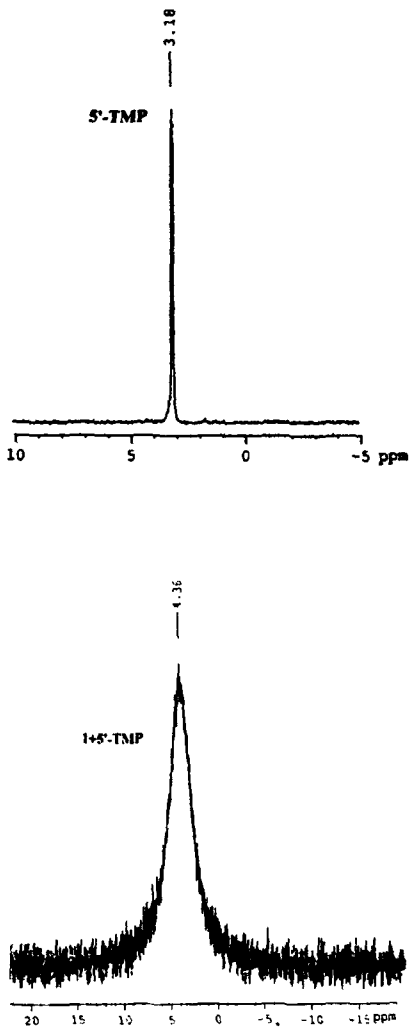

(b)

Figure 69. *(a) ^{1}H NMR spectra of 5'–TMP and the reaction of complex [Zn(glygly)(ssz)(H_2O)].6H_2O (2.5 mmol) with 5'–TMP (5 mmol) at 25 ^{0}C (b) ^{31}P NMR spectrum of 5'–TMP and the reaction of complex [Zn(glygly)(ssz)(H_2O)].6H_2O (2.5 mmol) with 5'–TMP (5 mmol) at 25 °C.*

The ^{31}P NMR spectrum of 5'–TMP reveals a signal at 3.67 ppm which was shifted downfield to 4.60 ppm on interaction with complex [Zn(glygly)(ssz)(H_2O)].6H_2O, indicative of electrostatic binding mode of the complex [Zn(glygly)(ssz)(H_2O)].6H_2O to the phosphate group of 5'–TMP (Figure 69b). Since there is a large downfield shift, it implies that the complex involves other non–covalent DNA binding modes in addition to

electrostatic binding. These observations are in corroboration with spectroscopic and molecular docking results.

Ethidium bromide displacement assay

To further investigate the mode of binding of the complex [Zn(glygly)(ssz)(H_2O)].6H_2O, the ethidium bromide displacement assay was carried out. The extent of quenching of the fluorescence of EthBr bound to DNA would reflect the extent of DNA binding of complex [Zn(glygly)(ssz)(H_2O)].6H_2O. EB (3,8–diamino–5–ethyl–6–phenylphenanthrium bromide), a phenanthridine fluorescence dye, is a typical probe for intercalation [294], form soluble complexes with nucleic acids and emits intense fluorescence when intercalated into the base pairs of DNA [295]. Upon addition of complex [Zn(glygly)(ssz)(H_2O)].6H_2O to CT DNA pretreated with EB ([DNA]/[EB] =1) solution caused appreciable reduction in emission intensities (Figure 70). Addition to the EB–DNA system induces notable fluorescence changes, which indicate that EB molecule, have been replaced by the complex [Zn(glygly)(ssz)(H_2O)].6H_2O. Further, the quenching extent was evaluated qualitatively by employing Stern–Volmer equation (4).

The K_{SV} value for the complex [Zn(glygly)(ssz)(H_2O)].6H_2O was found to be 2.56, indicating the strong affinity of the complex [Zn(glygly)(ssz)(H_2O)].6H_2O to CT DNA. Since EB was not completely displaced, partial intercalation in addition to the electrostatic mode of binding cannot be ruled out.

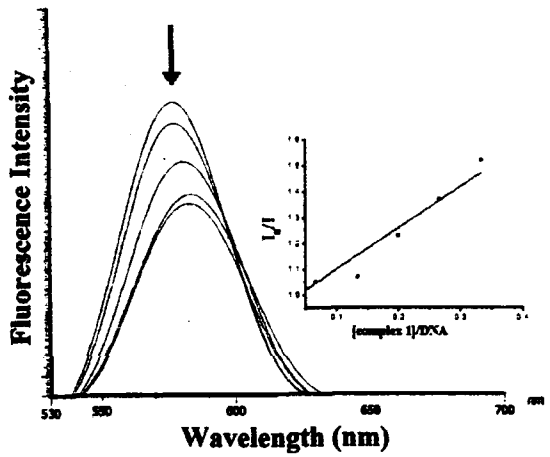

Figure 70. *Emission spectra of EB bound to DNA in the absence and presence complex [Zn(glygly)(ssz)(H₂O)].6H₂O in 5 mM Tris–HCl/50 mM NaCl buffer. Arrows show the intensity changes upon increasing concentration of the complex. Inset: Plots of I_0/I vs [complex]/[DNA]. (■) experimental data points; full lines, linear fitting of the data.*

Thermal denaturation

The binding of the complex [Zn(glygly)(ssz)(H_2O)].6H_2O to CT DNA was further distinguished by examining the thermal denature profile of DNA. When ds–DNA is heated slowly, the helix unfolds and the interaction between the base pairs of the helix decreases to give single stranded DNA. The mid–point temperature of this transition is the melting temperature (T_m) of the double strand DNA. The breakage of ds–DNA into single strand DNA can be detected by the "hyperchromic effect" in the UV absorption because the molar extinction coefficient at 260 nm of the DNA base pairs of ss–DNA is much higher than in ds–DNA. In general, groove binding or electrostatic binding along the phosphate backbone of DNA gives rise to only a small change in thermal denaturation temperature, while intercalation leads to a significant rise in thermal denaturation temperature of DNA due to the stabilization of the Watson–Crick base-paired duplex. The DNA melting curves in the absence and presence of complex [Zn(glygly)(ssz)(H_2O)].6H_2O is presented in Figure 71. The ΔT_m value of DNA in the

presence of complex [Zn(glygly)(ssz)(H_2O)].6H_2O is 3 °C, which is characteristic of electrostatic binding behavior [296].

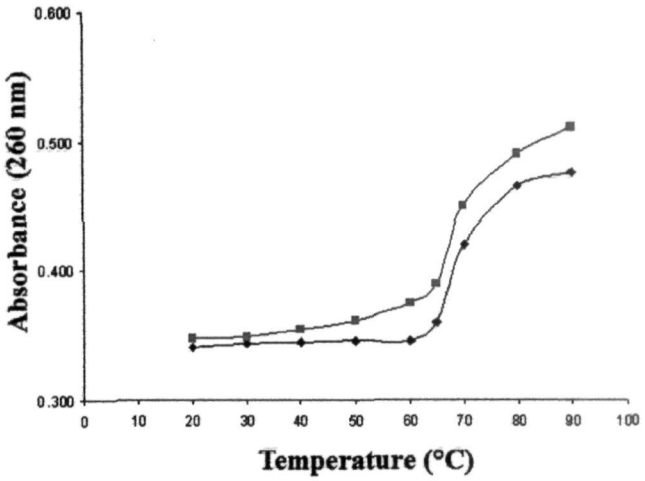

Figure 71. *Thermal melting curves of CT-DNA (pink) and DNA + complex [Zn(glygly)(ssz)(H_2O)].6H_2O (blue).*

Circular dichroism(CD) spectral study

CD spectroscopy is useful technique in diagnosing changes in DNA morphology during drug–DNA interactions. The CD spectrum of CT DNA exhibits a positive band at 275 nm (UV: λ_{max}, 260 nm) due to base stacking and a negative band at 245 nm due to the right–handed helicity of B–DNA form which are quite sensitive to the mode of DNA interactions with small molecules. Groove binding and electrostatic interaction of the complexes with DNA has been shown to bring about only marginal changes in the intensity of negative band as well as the positive band of DNA. On the other hand intercalators are known to enhance the intensities of both these bands [297]. Upon the addition of complex [Zn(glygly)(ssz)(H_2O)].6H_2O to CT DNA, the CD spectrum of DNA undergoes marginal changes both in its positive and negative bands (Figure 72). The intensities of both the bands decrease (negative band tending to zero levels). The decrease in ellipsticity is due to destabilization of DNA form attributed to the opening of DNA

structure by the formation of intra–strand DNA cross–linkings [298]. The decrease in the positive band suggests that the complex can unwind the DNA helix and lead to loss of helicity [299].

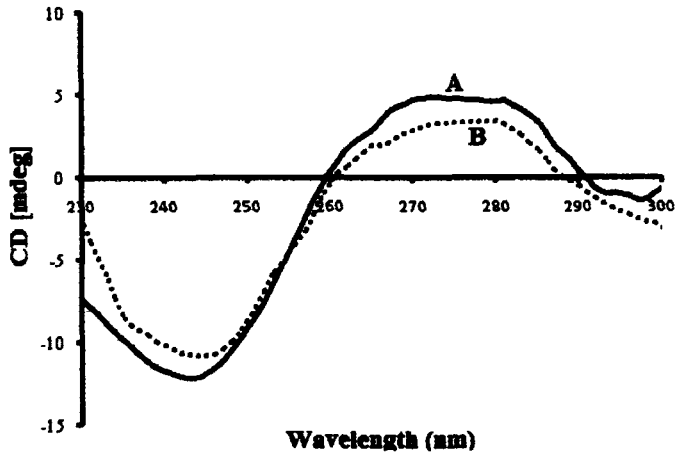

Figure 72. *CD spectra of (A) CT DNA alone (B) CT DNA in presence of complex [Zn(glygly)(ssz)(H_2O)].6H_2O in 5 mM Tris–HCl/50 mM NaCl buffer at 25 °C. [Zn(glygly)(ssz)(H_2O)].6H_2O 1.0 x 10^{-4} M, [DNA] 1.0 x 10^{-4} M.*

Chemical nuclease activity

DNA cleavage without added reductant.

There has been considerable interest in DNA endonucleolytic cleavages reactions activated by transition metal complexes. The delivery of high concentrations of metal ion to the helix, in locally generating oxygen or hydroxide radicals, yields an efficient DNA cleavage reaction. It is known that DNA cleavage is reflected by relaxation of the supercoiled circular form of pBR322 DNA resulting in nicked circular and/or linear forms. The ability of Zn(II) complexes to mediate DNA cleavage is well established in literature [300,301] owing to the fact that these complexes show their own selectivity for a cleavage mechanism, it is therefore imperative to study the effect of Zn(II) complex on pBR322 DNA in the presence of activators, DNA recognition elements (groove binding) and radical scavengers.

The DNA cleavage ability of complex [Zn(glygly)(ssz)(H_2O)].6H_2O was performed where pBR322 DNA (300ng) was incubated with increasing concentration of complex [Zn(glygly)(ssz)(H_2O)].6H_2O in aqueous buffer solution (5mM Tris–HCl/50mM NaCl, pH 7.2) for 45 min without addition of a reductant. As shown in Figure 73, it was observed that complex [Zn(glygly)(ssz)(H_2O)].6H_2O exhibits nuclease activity at 10 μM concentration, as evidenced by the conversion of supercoiled DNA from Form I to Form II (Lane 2). Further increase in the concentration of complex [Zn(glygly)(ssz)(H_2O)].6H_2O (20–30 μM), the amounts of Form I diminishes gradually, whereas those of Form II progressively increased (Lane 2–6) without the formation of Form III, suggesting single strand DNA cleavage. So, it is clear that cleavage of pBR322 DNA is highly dependent on metal ions concentration and intensified nicked (Form II) was observed. Since the nuclease efficiency of complexes is usually dependent on activators [302]. Therefore, DNA cleavage activity of [Zn(glygly)(ssz)(H_2O)].6H_2O in the presence of H_2O_2, ascorbate (Asc), 3–mercaptopropionic acid (MPA) and glutathione (GSH) was ascertained. As shown in Figure 74, the cleavage activity of [Zn(glygly)(ssz)(H_2O)].6H_2O follows the order H_2O_2 > MPA > GSH > Asc. Thus, complex [Zn(glygly)(ssz)(H_2O)].6H_2O exhibited a significant DNA cleavage activity in the presence of H_2O_2.

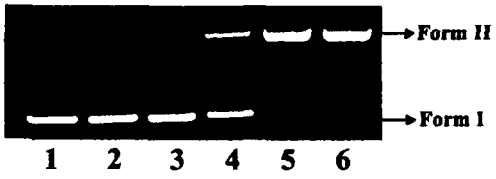

***Figure** 73. The cleavage patterns of the agrose Gel electrophoresis diagram showing cleavage of pBR322 supercoiled DNA (300 ng) by complex [Zn(glygly)(ssz)(H_2O)].6H_2O at 310 K after 45 min of incubation; Lane 1, DNA control; Lane 2, 10 μM of [Zn(glygly)(ssz)(H_2O)].6H_2O + DNA; Lane 3: 15 μM of [Zn(glygly)(ssz)(H_2O)].6H_2O + DNA; Lane 4: 20 μM of [Zn(glygly)(ssz)(H_2O)].6H_2O + DNA; Lane 5: 25 μM of [Zn(glygly)(ssz)(H_2O)].6H_2O + DNA; Lane 6: 30 μM of [Zn(glygly)(ssz)(H_2O)].6H_2O + DNA.*

Figure 74. *Agarose Gel electrophoresis pattern for the cleavage of pBR322 supercoiled DNA (300 ng) by complex [Zn(glygly)(ssz)(H₂O)].6H₂O in presence of different activating agents at 310 K after incubation for 45 min. Lane 1: DNA Control; Lane 2: 25 μM of [Zn(glygly)(ssz)(H₂O)].6H₂O + H₂O₂ (0.4 M) + DNA; Lane 3: 25 μM of [Zn(glygly)(ssz)(H₂O)].6H₂O + MPA (0.4 M) + DNA; Lane 4: 25 μM of [Zn(glygly)(ssz)(H₂O)].6H₂O + GSH (0.4 M) + DNA; Lane 5: 25 μM of [Zn(glygly)(ssz)(H₂O)].6H₂O + ASc (0.4 M) + DNA; Lane 6: 25 μM of [Zn(glygly)(ssz)(H₂O)].6H₂O + DMSO (0.4 M) + DNA; Lane 7: 25 μM of [Zn(glygly)(ssz)(H₂O)].6H₂O + EtOH (0.4 M) + DNA; Lane 8 : 25 μM of [Zn(glygly)(ssz)(H₂O)].6H₂O + sodium azide (0.4 M) + DNA Lane 9 : 25 μM of [Zn(glygly)(ssz)(H₂O)].6H₂O + SOD (15 units) + DNA.*

Effect of radical scavengers on DNA cleavage

In order to explore the mechanistic pathway of the cleavage activity, comparative DNA cleavage experiment of complex [Zn(glygly)(ssz)(H₂O)].6H₂O was carried out in presence of some standard radical scavengers such as DMSO and ethyl alcohol as hydroxyl radical scavenger (HO˙), sodium azide (NaN_3) as singlet oxygen ($^1O_2$) quencher and superoxide dismutase as superoxide anion radical ($O_2^{\cdot -}$) scavenger were used prior to the addition of complex [Zn(glygly)(ssz)(H₂O)].6H₂O to DNA solution. As shown in Figure 74, the DNA cleavage mediated by complex [Zn(glygly)(ssz)(H₂O)].6H₂O in the presence of DMSO (Lane 6) did not show any remarkable inhibition, whereas ethyl alcohol (Lane 7) even promotes the conversion of Form II to Form III, indicating that the freely diffusible hydroxyl radical is one of the reactive species involved in the DNA strand scission. On the other hand, addition of NaN_3 and SOD (Lane 8 and 9, respectively), also do not attenuate the DNA strand scission and even in presence of SOD the cleavage reaction was enhanced. These results suggest that hydroxyl radical, singlet

oxygen and superoxide anion radicals are not involved in the DNA cleavage system. Therefore, an oxidative cleavage pathway of DNA by complex [Zn(glygly)(ssz)(H_2O)].6H_2O has been excluded and evidently the cleavage proceeds by a hydrolytic mechanism.

The mechanistic pathway proposed for the present complex [Zn(glygly)(ssz)(H_2O)].6H_2O is depicted in Scheme 4. Complex [Zn(glygly)(ssz)(H_2O)].6H_2O contains coordinated water molecule, which facilitates the nucleophilic attack of water oxygen to phosphorus to give a five–coordinate phosphate intermediate and subsequent rearrangement of the phosphate, which allows the DNA to be cleaved readily. This hypothesis is consistent with previous literature reports which reveals that Zn(II) complexes generally cleave the DNA by hydrolytic pathway [303,304].

To ascertain the discernible hydrolytic DNA cleavage pathway mediated by complex [Zn(glygly)(ssz)(H_2O)].6H_2O, DNA religation experiment was further performed in which supercoiled pBR322 DNA was treated with T4 ligase enzyme and subjected to gel electrophoresis [305]. In our case, the nicked form (Form II) was religated to a large extent in the presence of T4 DNA ligase enzyme in comparison to control DNA alone in supercoiled form (Figure 75), providing a direct evidence in favor of hydrolytic mechanism. Therefore, complex [Zn(glygly)(ssz)(H_2O)].6H_2O could be useful not only in drug design but also in elucidating the precise role of metal ions in enzyme catalysis.

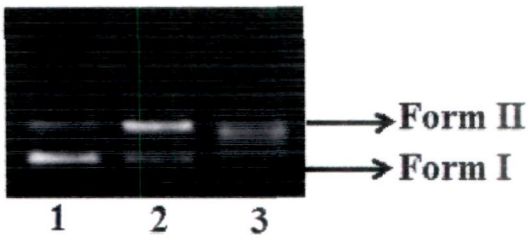

Figure 75. *Agarose Gel electrophoresis pattern for the ligation pBR322 plasmid DNA linearized by complex [Zn(glygly)(ssz)(H₂O)].6H₂O; Lane 1: DNA control; Lane 2: pBR322 plasmid DNA cleaved by complex [Zn(glygly)(ssz)(H₂O)].6H₂O; Lane 3: ligation of the cleaved pBR322 DNA by T4 DNA ligase.*

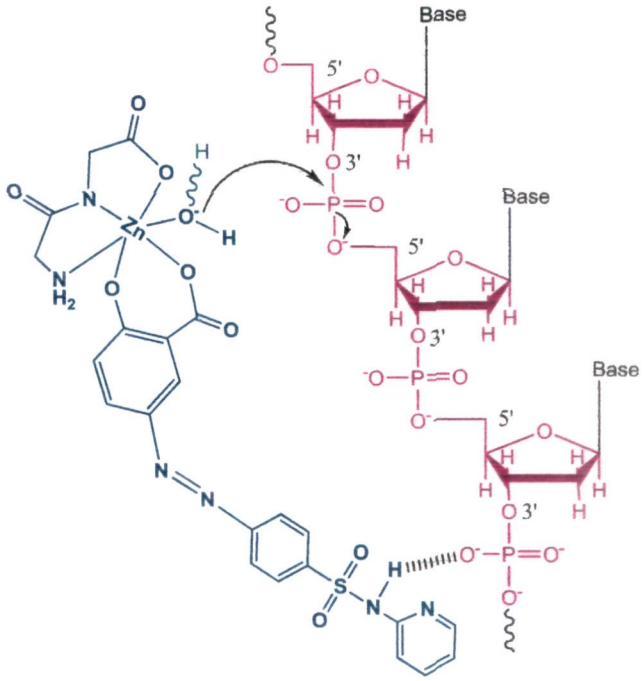

Scheme 4*. Proposed intermediate in the hydrolysis of DNA cleavage promoted by complex [Zn(glygly)(ssz)(H₂O)].6H₂O*

DNA cleavage in presence of recognition elements (Groove binding)

The potential interacting site of complex [Zn(glygly)(ssz)(H₂O)].6H₂O with pBR322 DNA was determine in presence of minor groove binding agent, DAPI and the major groove binding agent, methyl green. The supercoiled pBR322 DNA was treated with DAPI or methyl green prior to the addition of complex [Zn(glygly)(ssz)(H₂O)].6H₂O. As shown in Figure 76, the cleavage reaction mediated by complex

[Zn(glygly)(ssz)(H_2O)].6H_2O was quenched in presence of DAPI, however no apparent inhibition of DNA damage was observed in presence of methyl green, suggesting that minor groove is the preferred interacting site of complex [Zn(glygly)(ssz)(H_2O)].6H_2O which is further validated by molecular docking studies.

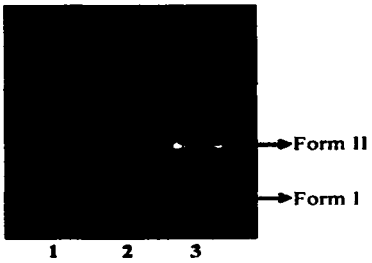

Figure 76. *Agarose Gel electrophoresis pattern for the cleavage of pBR322 supercoiled DNA (300 ng) by complex [Zn(glygly)(ssz)(H_2O)].6H_2O in presence of DNA minor binding agent DAPI and major binding agent methyl green at 310 K after incubation for 45 min. Lane 1, DNA control; Lane 2, 9 μM of complex [Zn(glygly)(ssz)(H_2O)].6H_2O + DNA + DAPI (8 μM); Lane 3, 9 μM of complex [Zn(glygly)(ssz)(H_2O)].6H_2O + DNA + methyl green (2.5 μL of a 0.01mg/ml solution).*

Molecular docking with DNA

In order to get more insight into the mode of binding, complex [Zn(glygly)(ssz)(H_2O)].6H_2O was successively docked with DNA duplex of sequence d(CGCGAATTCGCG)$_2$ dodecamer (PDB ID:1BNA) to search the chosen binding site along with preferred orientation of the ligand inside the DNA minor groove. In general, minor–groove binding molecules have aromatic rings connected by single bonds that allow for torsional rotation in order to facilitate into the curvature of groove with displacement of water molecules. The minimum energy docked pose (Figure 77) revealed that complex [Zn(glygly)(ssz)(H_2O)].6H_2O snuggly fitted into the curve contour of DNA minor groove in the A–T (~10.8 Å) regions compared to G–C (~13.2 Å) ones, and slightly bends the DNA in such a way that a part of the aromatic rings of sulfasalazine ligand makes more effective π–π stacking interactions between DNA base pairs and lead to van der Waals interaction with the DNA functional groups which define the stability of

groove [306]. On the other hand, the dipeptide moiety arranged in a parallel fashion with respect to the deoxyribose groove walls of the DNA and stabilized by hydrogen bonding (2.8–3.0 Å) between the amino group and C–2 carbonyl oxygen of T8 at a distance of 3.71 Å.

The resulting relative binding energy of docked structures of the complex [Zn(glygly)(ssz)(H_2O)].6H_2O with DNA was found to be –287.4 $KJmol^{-1}$, indicating the more potent the binding affinity between DNA and complex [Zn(glygly)(ssz)(H_2O)].6H_2O, correlating well with the experimental DNA binding studies and minor groove binder using DAPI assay. Thus, we can conclude that there is a mutual complement between spectroscopic and molecular docking techniques, which can substantiate our experimental results and provide valuable information about the mode of interaction between complex and DNA.

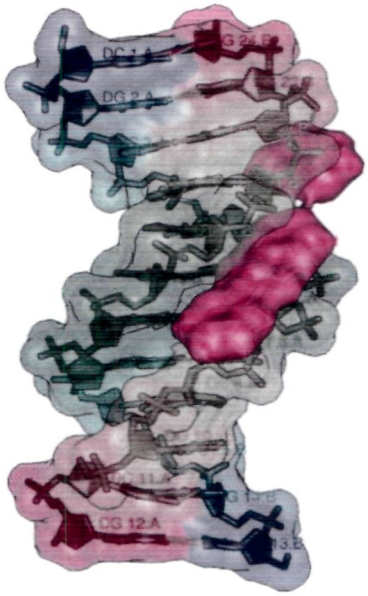

Figure 77. *Molecular docked model of complex [Zn(glygly)(ssz)(H_2O)].6H_2O revealing partial intercalation into adjacent A/T base pairs from minor groove side with DNA dodecamer duplex of sequence d(CGCGAATTCGCG)$_2$ (PDB ID: 1BNA).*

Conclusion

In this work, we have designed and synthesized a new zinc(II) complex possessing pharmacologically active and well–tailored pharmacophore derived from the glycyl glycine and sulfasalazine ligand. The *in vitro* DNA binding studies of complex [Zn(glygly)(ssz)(H_2O)].6H_2O were carried out to examine its effect on DNA binding propensity which reveals an electrostatic mode of binding, in addition to selective recognition towards the minor groove of DNA in A/T rich sequences. The complex [Zn(glygly)(ssz)(H_2O)].6H_2O binds supercoiled plasmid pBR322 DNA and cleave DNA through hydrolytic mechanism. This could be attributed to its high binding affinity which enhances local concentration of metal complexes around DNA and consequently, results in better cleavage activity. The hydrolytic cleavage mechanism of the complex [Zn(glygly)(ssz)(H_2O)].6H_2O is supported by evidence from DNA religation employing T4 DNA ligase assay and was validated from free radical quenching. Furthermore, molecular docking study was performed with DNA sequence d(ACCGACGTCGG)$_2$ in order to validate the experimental results. The significance of such studies provides the design of novel metal–based drugs with proven pharmacokinetic properties that could overcome the intrinsic or acquired resistance of several tumors to platinum drugs and role of metal ions in enzyme catalysis.

CHAPTER IV (b)

Synthesis, characterization and interaction studies of copper based drug with Human Serum Albumin (HSA): spectroscopic and molecular docking investigations

Synthesis

Synthesis of [Cu(glygly)(ssz)(H_2O)].6H_2O

To a stirred methanolic solution (15 ml) of copper nitrate hexahydrate (0.483g, 2mmol) was added an aqueous solution of glycyl glycine (0.262g, 2mmol) followed by drop wise addition of KOH (0.224g, 2 mmol) and pH of the resulting solution was adjusted between 8.0–12. This reaction mixture was stirred for ca 2 h at room temperature to obtain clear blue color solution. A methanolic solution (20 ml) of sulfasalazine (0.80 g, 2mmol) was added to the above reaction mixture and stirred for 3h. The light brown colored solid precipitate was filtered, thoroughly wash with ice cold methanol and dried in vacuo over anhydrous $CaCl_2$ (Yield: 0.510g, 65%). m.p. 250 ± 2 °C (dec.), Anal. Calc. for $C_{22}H_{32}CuN_6O_{15}S$ (%): C, 36.92; H, 4.51; N, 11.75; S, 4.47, Found: C, 36.64; H, 4.67; N, 11.95; S, 4.16. Selected IR data on KBr/nujol, cm^{-1}: 3399 ν(NH_2+H_2O); 1606 ν(C=O); 1387 ν(C–N); 580 (Cu–O); 441 (Cu–N). Molar Conductance, Λ_M (1 x 10^{-3} M, H_2O): 28 $\Omega^{-1}cm^2$ mol^{-1} (Non–electrolyte). UV–vis absorption: (H_2O, 10^{-4} M), λ_{max}/nm (ε/10^2 M^{-1} cm^{-1}) 236 (4.00); 255 (4.20); 376 (7.50); 660 (0.70). ESI–MS (m/z, H_2O): 714.7 $[M]^+$; 608.6 $[M–(6H_2O)]^+$.

Results and discussion

In order to improve delivery of active drugs to their specific site of action (Figure 78), new drug candidate, complex [Cu(glygly)(ssz)(H_2O)].6H_2O was designed, synthesized and characterized by various physico–chemical methods. The synthesis of [Cu(glygly)(ssz)(H_2O)].6H_2O complex was achieved by mixing stoichiometric amounts of Cu(II) nitrate trihydrate with glycyl glycine and sulfasalazine followed dropwise addition of KOH (Scheme 5), in a good yield. The resulting complex [Cu(glygly)(ssz)(H_2O)].6H_2O is stable towards air and moisture and readily soluble in H_2O. The complex [Cu(glygly)(ssz)(H_2O)].6H_2O was characterized by using elemental

analysis, IR, Uv–vis and EPR spectral studies. Molar conductance value of complex in H_2O (1 x 10^{-3} M) at 25 °C suggest its non–electrolyte nature (28 $\Omega^{-1}cm^2$ mol^{-1}).

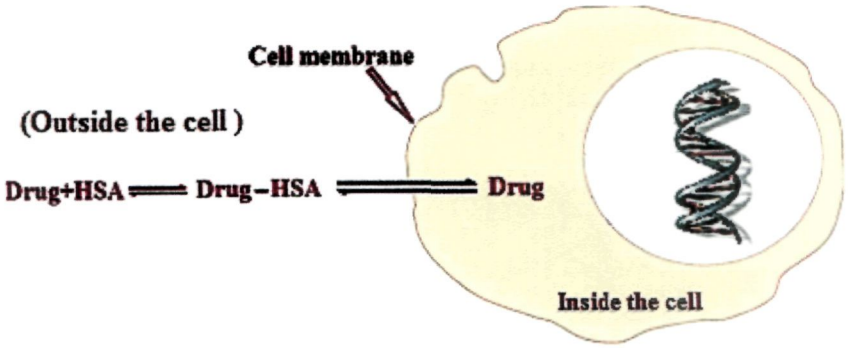

Figure 78. *Chemical equilibrium between the complex [Cu(glygly)(ssz)(H_2O)].6H_2O–HSA system towards targeted delivery.*

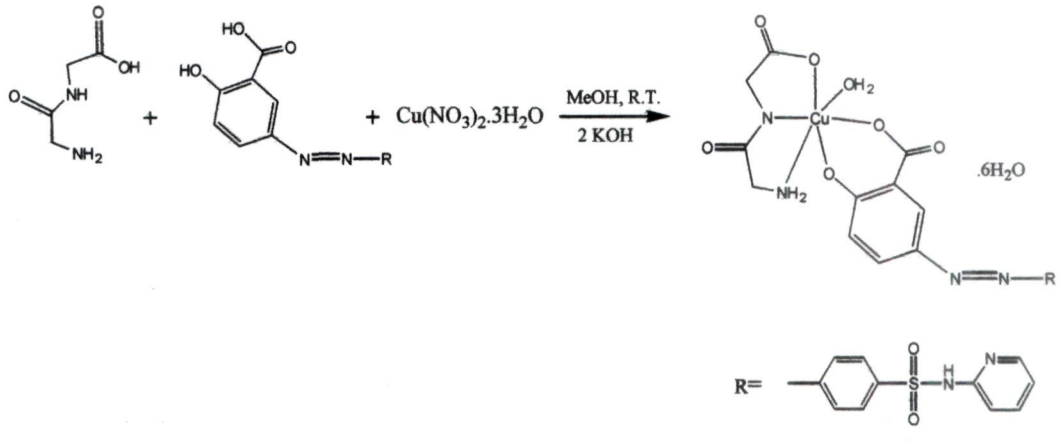

Scheme 5. *Synthetic route for complex [Cu(glygly)(ssz)(H_2O)].6H_2O*

Electronic Spectra

The electronic absorption spectrum of complex [Cu(glygly)(ssz)(H_2O)].6H_2O in freshly prepared aqueous solutions was carried out in the region 200–1100 nm at room temperature. The electronic spectra of free dipeptides displayed an intense absorption bands at 220 nm due to n→π* transition which was shifted to 236 nm upon coordination with Cu(II) metal ion, and has been assigned to $-N^-$→Cu(II) charge transfer (LMCT) transition [307]. The bands at 255 and 376 nm were attributed to π–π* transitions of

carboxylate group of peptide and n–π* transitions of the carboxylic–OH and phenolic–OH of sulfasalazine ligand to the metal ion, respectively, through deprotonation [308]. The low energy d–d band at 660 nm was assigned to $^2B_{1g} \rightarrow {}^2B_{2g}$ transitions suggesting an octahedral geometry around Cu(II) metal ion [309] which was also deduced by EPR.

IR spectra

The IR spectra of complex [Cu(glygly)(ssz)(H_2O)].6H_2O was recorded in the region 4000–400 cm^{-1} and analyzed in comparison to the IR spectra of the free ligands with its metal complex as described previously in our Chapter IV (a). The formation of complex [Cu(glygly)(ssz)(H_2O)].6H_2O was also deduced by the presence of new medium intensity bands around 441 and 580 cm^{-1} corresponding to Cu–N and Cu–O, respectively [311,312].

EPR studies

The X–band EPR spectra of the complex [Cu(glygly)(ssz)(H_2O)].6H_2O was recorded at room temperature in aqueous solution at a frequency of 9.1 GHz under the magnetic field strength 3000±1000 Gauss using tetracyanoethylene (TCNE) as field marker at LNT (Figure 79). The $g_{\|}$, $g_{\perp}$ and g_{av} values calculated from the expression $g_{av}^2 = (g_{\|}^2 + 2g_{\perp}^2)/3$ and were found to be 2.27, 2.04 and 2.11, respectively. These values are consistent with an octahedral geometry of copper with d^9 (Cu^{II}) configuration i.e. $(eg)^4$ $(a1g)^2$ $(b2g)^2$ $(b1g)^1$, occupied by an unpaired electron [312]. The trend $g_{\|} > g_{\perp} > g_e$ (2.0023) reveals that the unpaired electron is localized in the $d_{x^2-y^2}$ orbital. The values of $g_{\|}$ for covalent complex, $g_{\|} < 2.3$ and for an ionic environment, $g_{\|} = 2.3$ or more are reported in the literature. In the present complex $g_{\|} < 2.3$ indicates an appreciable metal–ligand covalent character [313].

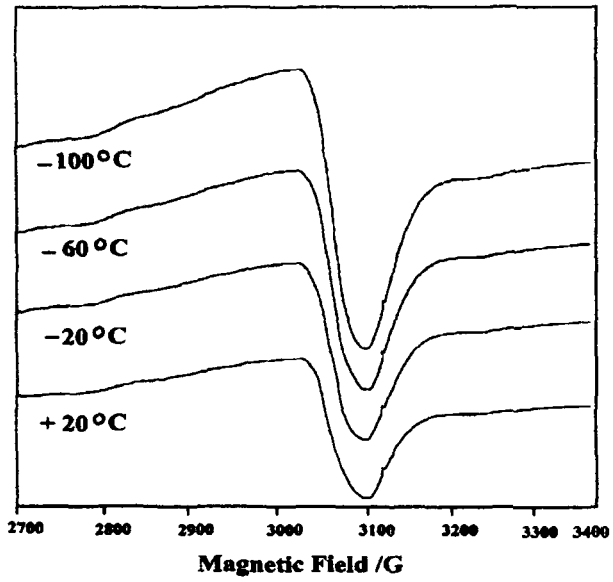

Figure 79. *EPR spectra of complex [Cu(glygly)(ssz)(H_2O)].6H_2O at variables temperature in aqueous solution.*

HSA binding studies

Fluorescence quenching of HSA by complex [Cu(glygly)(ssz)(H_2O)].6H_2O

Fluorescence spectroscopy is an effective method to explore the interaction between small molecules and biomacro–molecules. Literature reveals that fluorescence of HSA comes from the tryptophan, tyrosine and phenylalanine residues. Phenylalanine has a very low quantum yield and the fluorescence of tyrosine is almost totally quenched if it is ionized or present near to an amino group, a carboxyl group or a tryptophan. Thus, the fluorescence of HSA is dominated by the residue Trp–214 in subdomain IIA [314]. When small molecular substances bound to HSA, the changes of intrinsic fluorescence intensity of HSA are induced by the microenvironment of Trp residue. The fluorescence emission spectra of HSA at various concentration of complex [Cu(glygly)(ssz)(H_2O)].6H_2O is shown in Figure 80. HSA exhibits a strong fluorescence emission with a peak at 350 nm at λ_{ex} = 280 nm, while complex [Cu(glygly)(ssz)(H_2O)].6H_2O has no intrinsic fluorescence under the present experiment conditions. Upon increasing the concentration

of complex [Cu(glygly)(ssz)(H_2O)].6H_2O, caused a reduction of the fluorescence intensity. The strong quenching of HSA fluorescence clearly indicated complex [Cu(glygly)(ssz)(H_2O)].6H_2O was bound to HSA takes place and the interactions of HSA with complex [Cu(glygly)(ssz)(H_2O)].6H_2O changed the microenvironment around the Trp–214 residue and the tertiary structure of HSA [315].

The fluorescence intensity of a compound can be decreased by a variety of molecular interactions, such as excited–state reactions, molecular rearrangements, energy transfer, ground–state complex formation and collision quenching [207]. Collisional or dynamic quenching refers to a process that the fluorophore and the quencher come into contact during the lifetime of the excited–state, whereas static quenching refers to fluorophore–quencher complex formation [316].

In order to ascertain the fluorescence quenching mechanism, the fluorescence quenching data at different temperatures (299, 308 and 318 K, Figure 81) was analyzed using the classical Stern–Volmer equation. The results (Table 13) showed that the Stern–Volmer quenching constant K_{sv} is inversely correlated with temperature, and the values of k_q being larger than the limiting diffusion constant K_{dif} of the biomolecule ($K_{dif} = 2.0 \times 10^{10}$ $M^{-1}s^{-1}$), suggested that the fluorescence quenching was caused by a specific interaction between HSA and complex [Cu(glygly)(ssz)(H_2O)].6H_2O, and the quenching is not initiated by dynamic collision but arises mainly due to the complex formation.

Table 13. *Stern–Volmer quenching constant of the complex [Cu(glygly)(ssz)(H_2O)].6H_2O–HSA system at different temperatures*

pH	T (K)	K_{sv} ($10^5 M^{-1}$)	K_q ($10^{13} M^{-1}s^{-1}$)
7.40	299	3.08	3.08
	308	1.89	1.89
	318	1.59	1.59

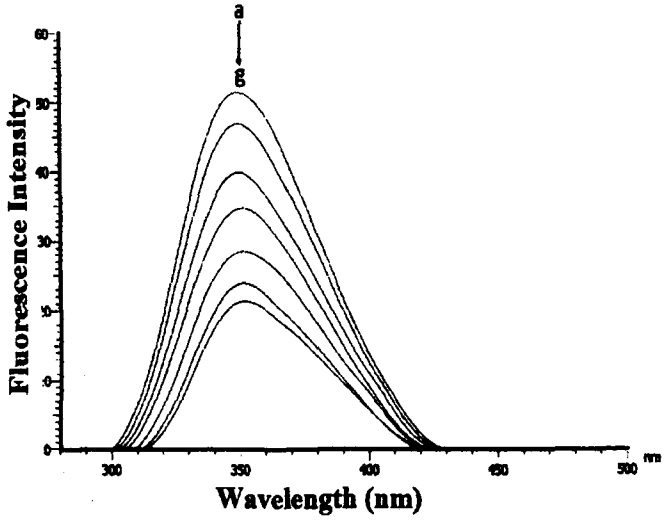

Figure 80. *The fluorescence quenching spectra of HSA by different concentrations of complex Cu(glygly)(ssz)(H_2O)].6H_2O with the excitation wavelength at 280 nm in 5 mM Tris–HCl/50 mM NaCl buffer, pH 7.4, at room temperature: [HSA], 1.0 x10^{-6} M; (a-g) the concentration of complex Cu(glygly)(ssz)(H_2O)].6H_2O corresponding to 0–3.33 x 10^{-5} M, respectively. Arrow shows the intensity changes upon increasing concentration of the quencher.*

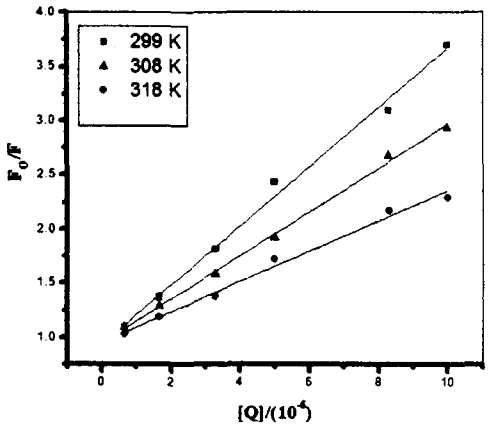

Figure 81. *Stern–Volmer plots showing HSA tryptophan quenching caused by complex [Cu(glygly)(ssz)(H_2O)].6H_2O at three different temperatures.*

Binding constants and the number of binding sites

For the static quenching process, the quenching data were analyzed according to the modified Stern–Volmer equation (Equation (9)). As shown in Figure 82, the binding constant decreased with increasing temperature (Table 14), which coincided with the Stern–Volmer quenching constant. As static quenching, the quenching constant can be

interpreted as the association constant of the complexation reaction since static quenching occurs from the formation of a ground state complex which is non–fluorescent or weakly fluorescent between fluorophore and quencher. When small molecules bind independently to a set of equivalent sites on a macromolecule, the equilibrium between free and bound molecules is given by the equation (10). The binding constants K and binding sites "n" were calculated by the slopes of the static quenching equation (log (F_0–F)/F versus log [Q]) curves as shown in Figure 83 and the results have been summarized in Table 14. The binding constants decreased with increasing temperature, which coincided with the Lineweaver–Burk, Stern–Volmer quenching constants.

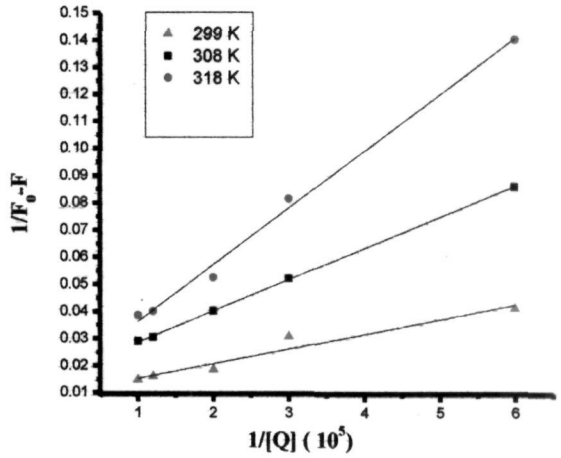

Figure 82. *The Linweaver–Burk plot for the binding of HSA with complex [Cu(glygly)(ssz)(H_2O)].6H_2O at different temperatures.*

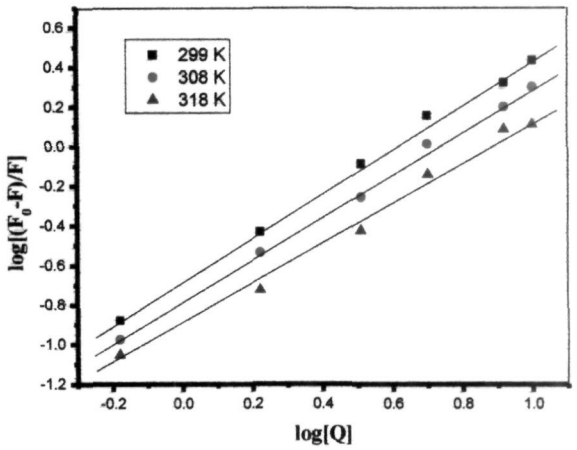

Figure 83. *Logarithmic plot of the fluorescence quenching of HSA at different temperatures.*

Table 14. *Binding constant (K_b), the number of binding sites (n) and ΔG values for the complex [Cu(glygly)(ssz)(H_2O)].6H_2O–HSA system at different temperatures*

pH	T (K)	$K_b(10^5M^{-1})$	n	ΔG (kJ/mole)
7.40	299	2.309	1.098	–30.713
	308	1.944	1.244	–31.997
	318	1.298	1.042	–31.136

Thermodynamic parameters and nature of the binding forces

The binding forces between [Cu(glygly)(ssz)(H_2O)].6H_2O complex and HSA exhibit weak interactions such as electrostatic forces, hydrophobic interaction, hydrogen–bond formation and van der Waals interaction etc. [317]. The thermodynamic parameters, enthalpy change (ΔH), entropy change (ΔS) and free energy change (ΔG) are the main evidence for confirming the binding modes. From the thermodynamic standpoint, $\Delta H > 0$ and $\Delta S > 0$ implies a hydrophobic interaction; $\Delta H < 0$ and $\Delta S < 0$ reflects the van der Waals force or hydrogen bond formation; and $\Delta H \approx 0$ and $\Delta S > 0$ suggests an electrostatic force. The positive ΔS value is frequently taken as evidence for hydrophobic interaction. Furthermore, the negative ΔH value observed cannot be mainly attributed to electrostatic

interactions since for electrostatic interactions ΔH is very small, almost zero. A negative ΔH value is observed whenever there is hydrogen bond on the binding site. It is not possible to account for the thermodynamic parameters of the complex [Cu(glygly)(ssz)(H_2O)].6H_2O–HSA coordination complex on the basis of a single intermolecular force. Consequently, the negative ΔH (–3.116 KJ/mole) and positive ΔS (+120.57 J/mole K) values suggest that both hydrophobic and hydrogen bond interactions could play major roles in the complex [Cu(glygly)(ssz)(H_2O)].6H_2O–HSA binding reaction and contribute to the stability of the complex. The negative value of ΔG reveals that the interaction process is spontaneous (Figure 84 and Table 14).

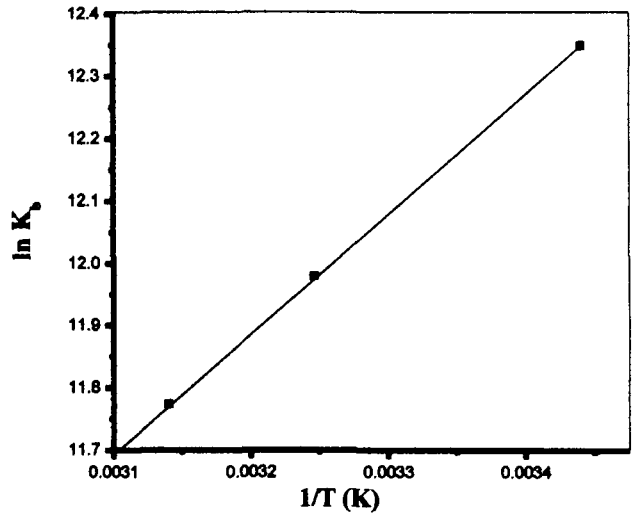

Figure 84. *Van't Hoff plot for the interaction of complex [Cu(glygly)(ssz)(H_2O)].6H_2O and HSA.*

Energy transfer between complex [Cu(glygly)(ssz)(H_2O)].6H_2O and HSA

Fluorescence energy transfer occurs *via* overlapping of emission spectrum of a fluorophore (donor) overlaps with the absorption spectrum of another molecule (acceptor). The overlap of the absorption spectrum of the complex [Cu(glygly)(ssz)(H_2O)].6H_2O with the fluorescence emission spectra of free HSA is shown in Figure 85. The rate of energy transfer depends on: (i) the extent of overlapping

between fluorescence emission spectrum of donor and the absorption spectrum of acceptor, (ii) the relative orientation of the donor and acceptor dipoles, and (iii) the distance between the donor and the acceptor. Here the donor and acceptor were HSA and the complex [Cu(glygly)(ssz)(H_2O)].6H_2O, respectively. From Equations (13)–(15), the value of E, R_0, r and J were calculated and found to be 0.99, 2.5 nm, 3.7 nm and 1.6×10^{-14} M^{-1} cm^3, respectively. The donor to acceptor distance r < 7 nm indicated that the energy transfer from tryptophan residue in HSA to complex [Cu(glygly)(ssz)(H_2O)].6H_2O occur with high probability [318], which is also in accordance with the conditions of FRET, indicating the static quenching interaction between complex [Cu(glygly)(ssz)(H_2O)].6H_2O and HSA.

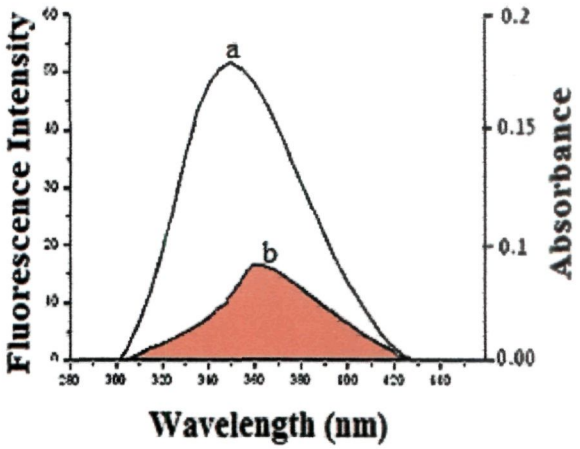

Figure 85. *The overlap of UV absorption spectra of complex [Cu(glygly)(ssz)(H_2O)].6H_2O with the fluorescence emission spectra of HSA. (a) The fluorescence emission spectrum of HSA (1.0×10^{-6} M) and (b) the UV absorption spectrum of complex [Cu(glygly)(ssz)(H_2O)].6H_2O (0.60×10^{-5} M).*

Changes of the protein's secondary structure induced by complex [Cu(glygly)(ssz)(H_2O)].6H_2O

To ascertain the possible influence of complex [Cu(glygly)(ssz)(H_2O)].6H_2O binding on the secondary structure of HSA, CD measurement was performed in the presence of complex [Cu(glygly)(ssz)(H_2O)].6H_2O at different concentrations. As shown in Figure

86, CD spectra of free HSA (line a) exhibit two negative bands in the ultraviolet region at 208 and 222 nm attributed to $n \rightarrow \pi^*$ transfer for the peptide bond of α–helix [319]. It was observed that in presence of $[Cu(glygly)(ssz)(H_2O)].6H_2O$ the CD signal of HSA increased. The increase of the CD signal indicates decrease of helical secondary structure content. This phenomenon is like with the interaction of HSA with complex $[Cu(glygly)(ssz)(H_2O)].6H_2O$. However, the CD spectra of HSA in the presence or absence of complex $[Cu(glygly)(ssz)(H_2O)].6H_2O$ is similar in shape, indicating that the structure of HSA is also predominantly α–helical. From above Equations (16) and (17), the quantitative analysis results of the α–helix in the secondary structure of HSA were obtained. They differed from that of 59.29% in free HSA to 56.54% in the complex $[Cu(glygly)(ssz)(H_2O)].6H_2O$–HSA conjugate at pH 7.4 and temperature 25 °C. The α–helix gradually decreased in the presence of complex $[Cu(glygly)(ssz)(H_2O)].6H_2O$, which reveals that the interaction between complex $[Cu(glygly)(ssz)(H_2O)].6H_2O$ and HSA leads to a change of the protein's secondary structure.

To further understand the structural alternations of HSA induced by the binding of complex $[Cu(glygly)(ssz)(H_2O)].6H_2O$ to HSA, FT–IR spectroscopy were performed on HSA and complex $[Cu(glygly)(ssz)(H_2O)].6H_2O$–HSA system (Figure 87a and b). The spectrum in Figure 87(a) was obtained by subtracting the absorption of the Tris–HCl from the spectrum of the protein solution. The spectrum in Figure 87(b) was obtained by subtracting the absorption of the complex $[Cu(glygly)(ssz)(H_2O)].6H_2O$–free form from that of the complex $[Cu(glygly)(ssz)(H_2O)].6H_2O$–bound form. Infrared spectra of proteins exhibit a number of the amide bands, which represent different vibrations of the peptide moiety. Among these amide bands of the protein, amide I peak position occur in the range 1600–1700 cm^{-1} (mainly C=O stretch) and amide II band in the region 1500–1600 cm^{-1} (C–N stretch coupled with N–H bending mode). The amide bands have a

relationship with the secondary structure of protein, and amide I is more sensitive than amide II for change of secondary of protein [320]. As shown in Figure 87, the peak position of amide I band was shifted from 1653.27 cm^{-1} to 1635.32 cm^{-1}, implicating that that the secondary structure of the HSA protein altered due to interaction of complex $[Cu(glygly)(ssz)(H_2O)].6H_2O$.

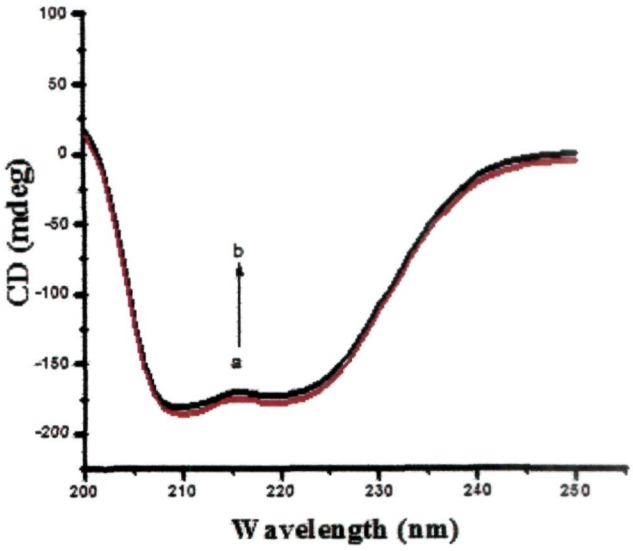

Figure 86. *CD Spectra of the HSA–complex $[Cu(glygly)(ssz)(H_2O)].6H_2O$ system (a) 1.5 x 10^{-5} M HSA and (b) 1.5 x 10^{-5} M HSA + 3.0 x 10^{-5} M [complex].*

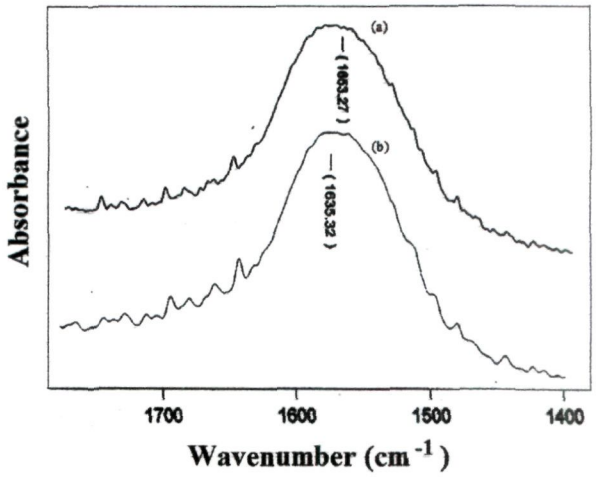

Figure 87. *FT–IR spectra of (a) free HSA and (b) different spectra [(HSA solution + $[Cu(glygly)(ssz)(H_2O)].6H_2O$ solution)–($[Cu(glygly)(ssz)(H_2O)].6H_2O$ solution)] in 5 mM Tris–HCl/50 mM NaCl buffer, pH 7.4, at room temperature in the region of 1750–1400 cm^{-1}, [HSA], 1.5 x 10^{-5} M; $[Cu(glygly)(ssz)(H_2O)].6H_2O$], 3.0 x 10^{-5} M.*

Molecular modeling study of the interaction between HSA and complex [Cu(glygly)(ssz)(H_2O)].6H_2O

Molecular docking technique was further employed to understand the interaction between complex [Cu(glygly)(ssz)(H_2O)].6H_2O and HSA. Descriptions of the 3D structure of crystalline albumin have revealed that that HSA comprises three homologous domains (denoted I, II, and III): I (residues 1–195) II (196–383) and III (384–585); each domain has two subdomains (A and B) that assemble to form heart shaped molecule (Figure 88). The principal region of drug binding sites of HSA are located in hydrophobic cavities in subdomain IIA and IIIA, which are corresponding to site I and site II, respectively and tryptophan residue (Trp–214) of HSA in subdomain IIA [321]. There is a large hydrophobic cavity in subdomain IIA to accommodate the complex [Cu(glygly)(ssz)(H_2O)].6H_2O, which play an important role in absorption, metabolism, and transportation of HSA. The results as depicted in (Figure 89) reveal that the complex [Cu(glygly)(ssz)(H_2O)].6H_2O was half–surrounded within subdomain IIA hydrophobic cavity, and it is in close proximity to hydrophobic residues, such as Lys195, Trp214, Ala215, Arg218, Leu219, Val216, Ala291, Glu292, etc., of subdomain IIA of HSA [48], suggesting the existence of hydrophobic interaction between them. Hence, this finding provides a good structural basis to explain the efficient fluorescence quenching of HSA emission in the presence of the complex [Cu(glygly)(ssz)(H_2O)].6H_2O. Furthermore, there are also a number of weak electrostatic interactions and hydrogen bonds, because several ionic and polar residues in the proximity of the ligand play an important role in stabilizing the molecule by forming hydrogen bonds and weak electrostatic interactions. As shown in Figure 90, there are hydrogen bond interactions between the main chain carbonyl oxygen of Arg–257 and terminal amino group of the complex [Cu(glygly)(ssz)(H_2O)].6H_2O and other between carbonyl and sulfone (O=S=O), groups

of the complex [Cu(glygly)(ssz)(H_2O)].6H_2O and the residues Ala–291, Arg–222 and Lys–195 of HSA. These results suggest that the formation of hydrogen bonds decreased the hydrophilicity and increased the hydrophobicity to enforce stability in [Cu(glygly)(ssz)(H_2O)].6H_2O–HSA system. On the other hand, the amino acid residues with benzene ring could match with that of the structure of [Cu(glygly)(ssz)(H_2O)].6H_2O complex in space in order to firm the conformation of the complex. The results obtained from molecular docking indicated that the interaction between complex [Cu(glygly)(ssz)(H_2O)].6H_2O and HSA was dominated by hydrophobic forces as well as hydrogen bonds, which is consistent with our experimental results.

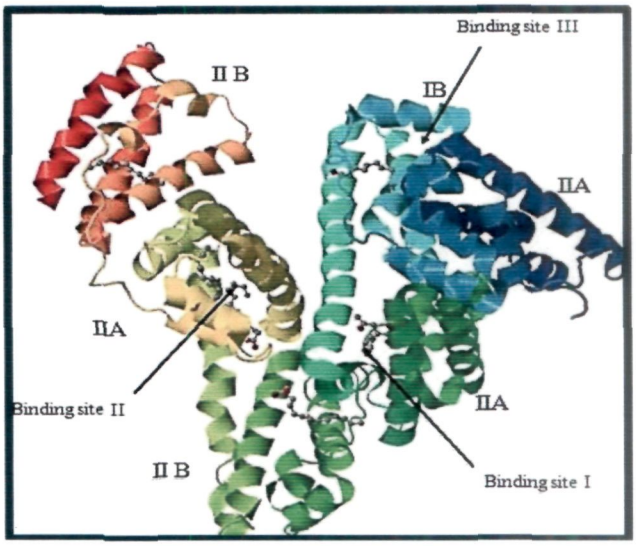

Figure 88. *Modeling of X–ray crystallographic structure of HSA (PDB ID: 1h9z). The domains and subdomains were displayed with different color, the every subdomain and classical binding site were marked in the corresponding location.*

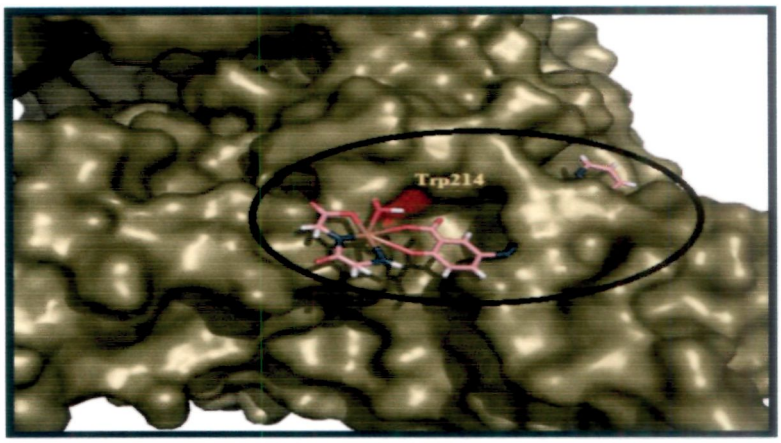

Figure 89. *Molecular docked model of complex [Cu(glygly)(ssz)(H_2O)].6H_2O (stick representation) located within the hydrophobic pocket in subdomain IIA of HSA.*

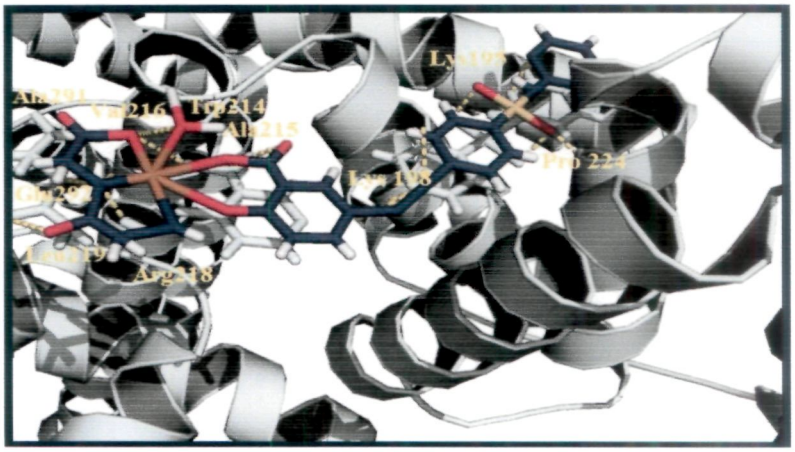

Figure 90. *The interaction mode between complex [Cu(glygly)(ssz)(H_2O)].6H_2O (showing stick representation) and HSA (cartoon form) and the yellow dashed line showing hydrogen bond interaction between them.*

Conclusion

In this work, we have designed, synthesized and characterized a new drug candidate; complex [Cu(glygly)(ssz)(H_2O)].6H_2O derived from the dipeptide (glycyl glycine anion) and sulfasalazine ligands to examine their effect on the binding propensity of HSA and to elucidate the mechanism of action at the molecular target. The interaction between complex [Cu(glygly)(ssz)(H_2O)].6H_2O and HSA was investigated employing different spectroscopic techniques (fluorescence, CD, FTIR) which was further validated by molecular docking study. The results revealed that the secondary structure of protein was affected upon interaction with the complex [Cu(glygly)(ssz)(H_2O)].6H_2O. Fluorescence results indicated the presence of static quenching mechanism upon binding of complex [Cu(glygly)(ssz)(H_2O)].6H_2O to HSA. On the basis of spectroscopic results, it is concluded that the [Cu(glygly)(ssz)(H_2O)].6H_2O complex was bound to site I of protein, which is located in the hydrophobic pocket of subdomain IIA, the distance between the donor (protein) and the acceptor (complex [Cu(glygly)(ssz)(H_2O)].6H_2O) was also calculated by using FRET. Our results may provide valuable information to understand the mechanistic pathway of drug delivery and to pharmacological behavior of drug.

CHAPTER V

Synthesis, characterization of metal complexes: comparative *in vitro* DNA binding profile, SOD mimics and molecular docking studies.

Synthesis

Synthesis of $[Cu_2(bipy)_2(im)_2(pip)(NO_3)_2].2NO_3$

The complex was prepared by a general synthetic method in which corresponding 2,2'–bipyridyl (0.312g, 2mmol) and imidazole (0.136g, 2mmol) in 15 mL methanol was added to a methanolic solution (10 mL) of $Cu(NO_3)_2 \cdot 3H_2O$ (0.482g, 2mmol) with stirring for ca. 2 hour followed by the addition of the piperazine solution (0.388g, 2 mmol) taken in 5 mL of methanol. The solution was refluxed for 2 hours at 60°C. On completion of the reaction, the reaction mixture was kept at room temperature which yielded a dark bluish product, washed with hexane and diethyl ether and dried in vacuo. (Yield: 0.682g, 75%). m.p. 165 ± 2°C, Anal. Calc. for $C_{30}H_{36}Cu_2N_{14}O_{12}$ (%) C, 39.52; H, 3.98; N; 21.51, Found: C, 38.63; H, 4.22; N, 21.41. Selected IR data on KBr/nujol, cm^{-1}: 3405–3275 ν(N–H); 2959 ν(CH); 1566 ν(C=C); 1444 ν(C=N); 1313 ν(C–N); 1384 ν(N–O); 1275 δ(imidazole N–H); 771 (Ar); 423 ν(Cu–N). UV-vis absorption: (H_2O, 10^{-4} M), λ_{max}/nm ($\varepsilon/10^3$ M^{-1} cm^{-1}): 299 (0.65); 311 (0.71); 590 (0.08). Λ_M (1×10^{-3} M, H_2O): 140 $\Omega^{-1}cm^2mol^{-1}$ (1:2 electrolyte). ESI–MS (m/z, H_2O): 661.1 $[(C_{30}H_{36}Cu_2N_{14}O_{12})–(4NO_3)]^+$; 436.3 $[(C_{30}H_{36}Cu_2N_{14}O_{12})–(C_{13}H_{13}CuN_7O_9)]^+$.

Synthesis of $[Zn_2(bipy)_2(im)_2(pip)].4Cl$

This complex was synthesized by a similar procedure as described for $[Cu_2(bipy)_2(im)_2(pip)(NO_3)_2].2NO_3$ with $ZnCl_2$ (0.272g, 2mmol). White coloured product was isolated. (Yield: 0.525g, 65%). m.p. 300 ± 2°C, Anal. Calc. for $C_{30}H_{36}Cl_4N_{10}Zn_2$ (%) C, 44.52; H, 4.48; N, 17.31, Found: C, 44.49; H, 4.46; N, 17.28. Selected IR data on KBr/nujol, cm^{-1}: 3403–3204 ν(N–H); 2972 ν(CH); 1559 ν(C=C); 1450 ν(C=N); 1350 ν(C–N); 1262 δ(imidazole N–H); 766 (Ar); 432 ν(Cu–N). UV–vis (1×10^{-4} M, H_2O),

λ_{max} / nm ($\varepsilon/10^3$ M^{-1} cm^{-1}): 294 (0.44); 306 (0.56). Λ_M (1×10^{-3} M, H_2O): 347 $\Omega^{-1}cm^2$ mol^{-1}(1:4 electrolyte). ^1H NMR (DMSO–d_6, 400 MHz) δ(ppm): 2.55 (CH_2–CH_2); 3.19 ($NHCH_2CH_2NH$); 6.97–7.34 (Ar–protons); 8.43 (NH imidazole). ^{13}C NMR (DMSO–d_6, 100 MHz) δ(ppm): 44.53 (Pip–C); 154.9 (C=N); 121.7–148.7 (Ar–C). ESI–MS (m/z, H_2O): 666.3 $[(C_{30}H_{36}Cl_2N_{10}Zn_2)–(4Cl)]^+$; 290.2 $[(C_{30}H_{36}Cl_2N_{10}Zn_2)–(C_{17}H_{24}N_6Cl_4Zn)]^+$.

Synthesis of $[Ni_2(bipy)_2(im)_2(pip)].4Cl$

This was synthesized by a similar procedure as described for $[Cu_2(bipy)_2(im)_2(pip)(NO_3)_2].2NO_3$ with $NiCl_2·6H_2O$ (0.467g, 2mmol). Light green coloured product was isolated. (Yield: 0.557g, 70%). m.p. 320 ± 2°C, Anal. Calc. for $C_{30}H_{36}Cl_4N_{10}Ni_2$ (%) C, 45.27; H, 4.56; N, 17.60, Found: C, 45.49; H, 4.11; N, 17.43. Selected IR data on KBr/nujol, cm^{-1}: 3398–3243 ν(N–H); 2959 ν(CH); 1562 (C=C); 1440 (C=N); 1314 ν(C–N); 1250 δ(imidazole N–H); 767 (Ar); 459 ν(Cu–N). UV–vis (1×10^{-4} M, H_2O), λ_{max} /nm ($\varepsilon/10^3$ M^{-1} cm^{-1}): 294 (0.50); 306 (1.50); 540 (0.06). Λ_M (1×10^{-3} M, H_2O): 326 $\Omega^{-1}cm^2$ mol^{-1} (1:4 electrolyte). ^1H NMR (DMSO–d_6, 400 MHz) δ(ppm): 2.97 (CH_2–CH_2); 3.20 ($NHCH_2CH_2NH$); 7.76–7.92 (Ar–protons); 8.37 (NH imidazole). ^{13}C NMR (DMSO–d_6, 100 MHz) δ(ppm): 42.62 (Pip–C); 116.6–149.6 (Ar–C); 166.82 (C=N). ESI–MS (m/z, H_2O): 655.7 $[(C_{30}H_{36}Cl_4N_{10}Ni_2)–(4Cl)]^+$; 279.9 $[(C_{30}H_{36}Cl_4N_{10}Ni_2)–(C_{17}H_{27}N_6Cl_4Ni)]^+$.

Results and discussion

All the complexes are stable towards air and moisture and soluble in H_2O. The coordination geometry of central metal ion Cu(II) was square pyramidal while the Zn(II) and Ni(II) atom was present in square planar environment (Scheme 6), which was proposed on the basis of analytical and spectroscopic data.

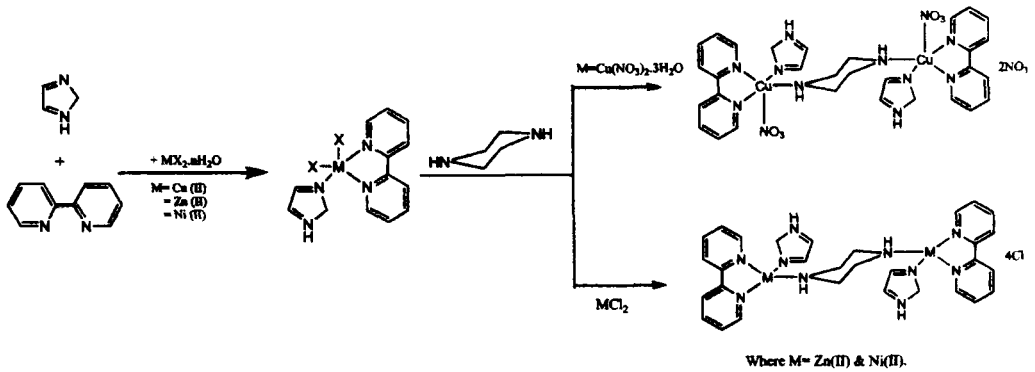

Scheme 6. Synthetic route for complexes

Infrared spectra

The IR spectra of complexes $[Cu_2(bipy)_2(im)_2(pip)(NO_3)_2].2NO_3$, $[Zn_2(bipy)_2(im)_2(pip)].4Cl$ and $[Ni_2(bipy)_2(im)_2(pip)].4Cl$ exhibited characteristic broad envelope at ~3405–3204 cm^{-1} attributed to ν(N–H) stretching vibrations. [322]. Other medium intensity bands observed at 1313–1350 cm^{-1} and 1275–1250 cm^{-1} were assigned to ν(C–N) and δ(N–H) vibration in the complexes [323]. The strong characteristic bands appearing between 1450–1440 cm^{-1} were attributed to ν(C=N) of the imidazole and bipyridyl rings [324]. The band at 1384 cm^{-1} in the complex $[Cu_2(bipy)_2(im)_2(pip)(NO_3)_2].2NO_3$ was assigned to ν(N–O) stretching vibrations, indicating the presence of NO_3 ions. The band observed at 2972–2959 cm^{-1} in the complexes were ascribed to $\nu_{as}(CH_2)$ and $\nu_s(CH_2)$ sreching vibrations. The formation of complexes $[Cu_2(bipy)_2(im)_2(pip)(NO_3)_2].2NO_3$, $[Zn_2(bipy)_2(im)_2(pip)].4Cl$ and $[Ni_2(bipy)_2(im)_2(pip)].4Cl$ were also revealed by the presence of medium intensity ν(M–N) stretching vibrations in the range 423–459 cm^{-1} [325].

NMR spectra

The ^{1}H and ^{13}C NMR spectra of complexes $[Zn_2(bipy)_2(im)_2(pip)].4Cl$ and $[Ni_2(bipy)_2(im)_2(pip)].4Cl$ exhibited well resolved signals and significant chemical shifts. The sharp signal at 8.80–8.41 ppm, is indicative of imidazole –NH. The resonance at 2.55–2.97 ppm and ~3.19 ppm was ascribed to H_2C–CH_2 and –NH protons of piperazine ring. The peaks observed in the range of 6.97–7.92 ppm were consistent with the aromatic protons [326]. The ^{13}C NMR spectra of complexes were characterized by various resonances attributed to the bridge Piperazine carbons at 42.62–44.53 ppm, respectively, The various resonances due to the aromatic carbons of imidazole and bipyridyl ring appeared in the range 116.66–149.56 ppm [327,328] (Figure 91a–d).

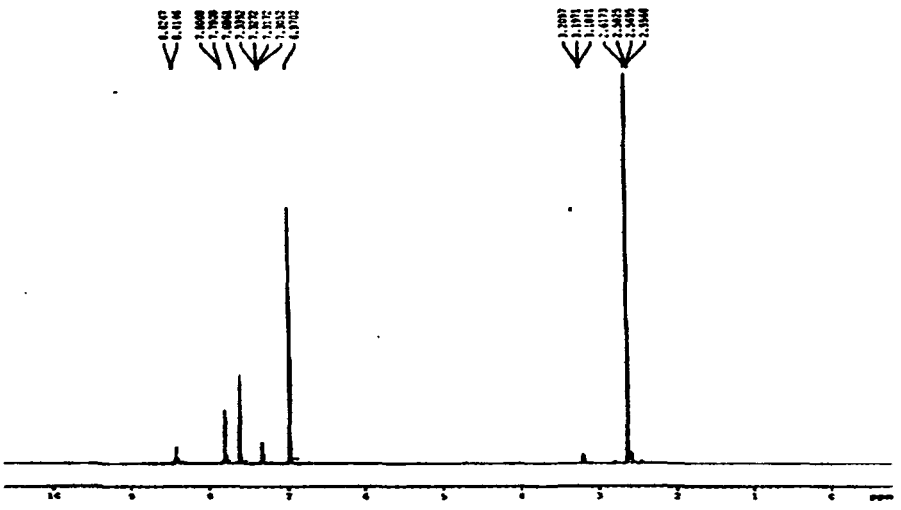

(a)

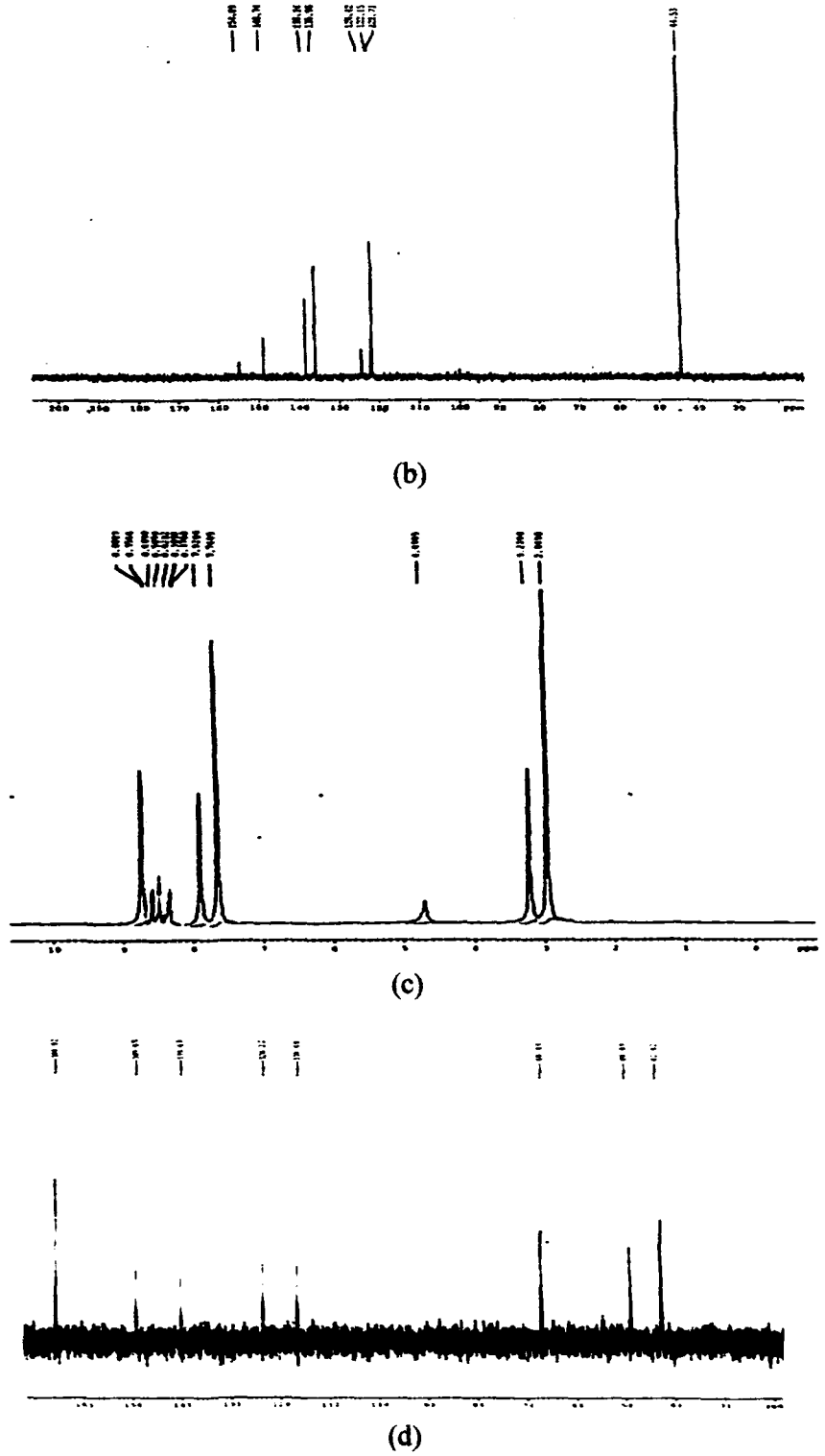

(b)

(c)

(d)

Figure 91. *^{1}H and ^{13}C NMR spectrum of complex $[Zn_2(bipy)_2(im)_2(pip)].4Cl$ (a and b) and $[Ni_2(bipy)_2(im)_2(pip)].4Cl$ (c and d) in D_2O solution.*

Electronic absorption spectra

The UV–visible spectra of complexes $[Cu_2(bipy)_2(im)_2(pip)(NO_3)_2].2NO_3$, $[Zn_2(bipy)_2(im)_2(pip)].4Cl$ and $[Ni_2(bipy)_2(im)_2(pip)].4Cl$ at room temperature were carried out in the region 190–1100 nm in H_2O exhibited broad and intense absorption maxima. The complexes exhibited sharp peaks observed in the range of 230–296 nm attributed to intraligand charge transfer (ILCT) transitions. However, the absorption bands at 306–311 nm, were assigned to a metal to ligand charge transfer (MLCT) transition. The complexes $[Cu_2(bipy)_2(im)_2(pip)(NO_3)_2].2NO_3$ and $[Ni_2(bipy)_2(im)_2(pip)].4Cl$ revealed a d–d transitions in the lower frequency region centered at 590 ($\varepsilon/10^3$ M^{-1} cm^{-1}, 0.08) and 540 nm ($\varepsilon/10^3$ M^{-1} cm^{-1}, 0.06), respectively, consistent with their square pyramidal and square planar geometry, respectively.

EPR spectra

The solid state X–band EPR spectrum of complex $[Cu_2(bipy)_2(im)_2(pip)(NO_3)_2].2NO_3$ was recorded at LNT with a magnetic field strength of 3000G. The EPR spectrum revealed an isotropic spectrum with a broad signal indicating that the copper ion in a distorted square pyramidal geometry with g_{iso} value of ~2.075 [329]. Thus, an unpaired electron of paramagnetic $3d^9$ copper(II) ion occupy $d(x^2–y^2)$ orbital in (B_1g) ground state configuration with an elongated square based pyramidal geometry (Figure 92).

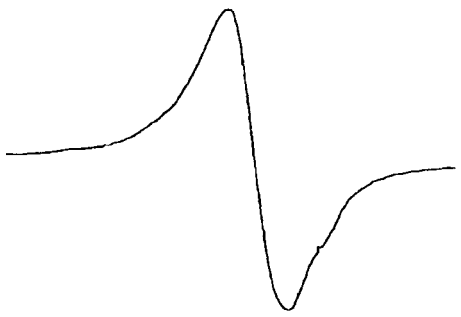

Figure 92. *EPR spectra of complex* $[Cu(bipy)_2(im)_2(pip)(NO_3)_2].2NO_3$ *at LNT.*

Mass spectral analysis

The formation of metal complexes and the speciation of various ionic forms in a H_2O solution were studied with ESI–MS. The spectra of the complexes displayed prominent peaks corresponding to the molecular ion fragment. The complex $[Cu_2(bipy)_2(im)_2(pip)(NO_3)_2].2NO_3$ showed three major peaks at m/z 661.1, 436.3, and 287.9 were assigned to $[C_{30}H_{36}Cu_2N_{10}]^+$, $[C_{17}H_{23}CuN_7O_3]^+$ and $[C_{13}H_{13}CuN_4]^+$, respectively. The complex $[Zn_2(bipy)_2(im)_2(pip)].4Cl$ exhibited two major peaks at m/z 666.3 and 290.2 attributed to $[C_{30}H_{36}N_{10}Zn_2]^+$ and $[C_{13}H_{12}N_4Zn]^+$, respectively. However, the appearance of two major peaks at m/z 655.7 and 279.9 for complex $[Ni_2(bipy)_2(im)_2(pip)].4Cl$ were ascribed to $[C_{30}H_{36}N_{10}Ni_2+H]^+$ and $[(C_{13}H_{13}N_4Ni)–4H]^+$, respectively. These observations indicate that the metal–ligated skeletons of these complexes are stable in solution.

Thermal Studies

Thermogravimeteric analysis of the complex $[Cu_2(bipy)_2(im)_2(pip)(NO_3)_2].2NO_3$ was carried out to study the pyrolysis pattern in temperature range 25–1000 ^{0}C. The thermogram of $[Cu_2(bipy)_2(im)_2(pip)(NO_3)_2].2NO_3$ exhibited weight loss in three steps over the temperature range 75–350, 400–680 and 700–1000 °C (Figure 93). The weight loss in the temperature range 75–350 °C confirmed the removal of the coordinated nitrate molecule (19 %) while at 400–680 °C (48 %), the noticeable weight loss indicated the removal of the aryl groups [330]. Finally, the TGA curve showed a plateau above 772°C corresponding to the formation of metal–oxide as the final products.

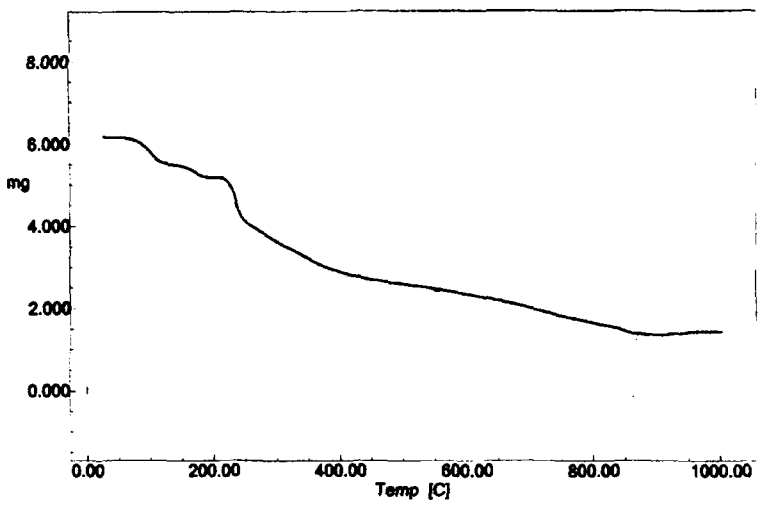

Figure 93. *TGA curve showing the degradation of bimetallic complex* $[Cu_2(bipy)_2(im)_2(pip)(NO_3)_2].2NO_3$.

X–ray diffraction analysis

To obtain further evidence about the structure of the metal complexes, X–ray powder diffraction studies of the complexes $[Cu_2(bipy)_2(im)_2(pip)(NO_3)_2].2NO_3$, $[Zn_2(bipy)_2(im)_2(pip)].4Cl$ and $[Ni_2(bipy)_2(im)_2(pip)].4Cl$ were performed as it was difficult to isolate single crystals suitable for single crystal X–ray crystallography. The diffractograms obtained for the metal complexes are given in Figure 94a–c. The XRPD patterns indicate crystalline nature for the complexes $[Cu_2(bipy)_2(im)_2(pip)(NO_3)_2].2NO_3$, $[Zn_2(bipy)_2(im)_2(pip)].4Cl$ and $[Ni_2(bipy)_2(im)_2(pip)].4Cl$. A summary of the refined XRPD parameters of complexes is given in Table 15.

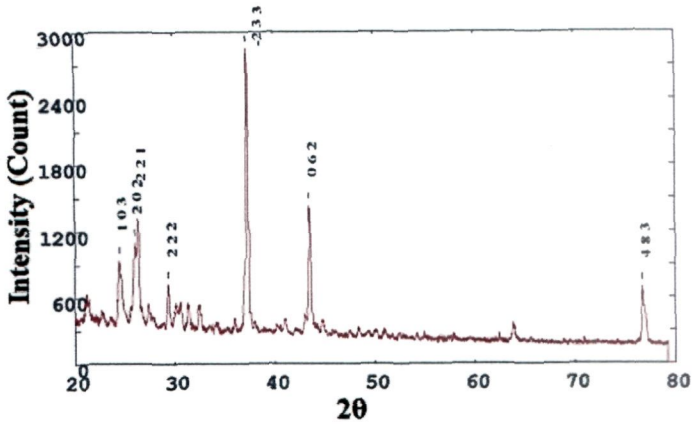

(a)

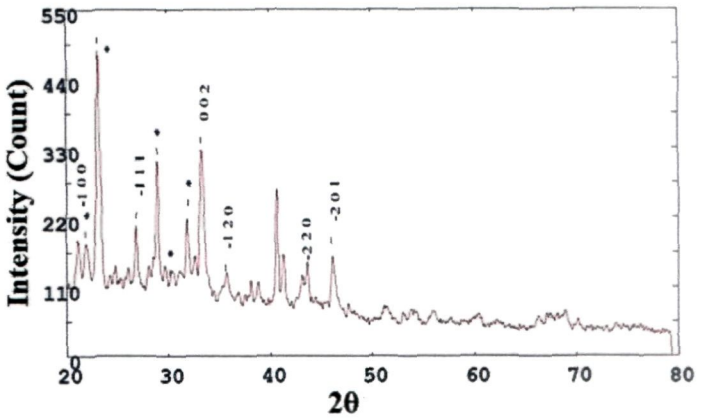

(b)

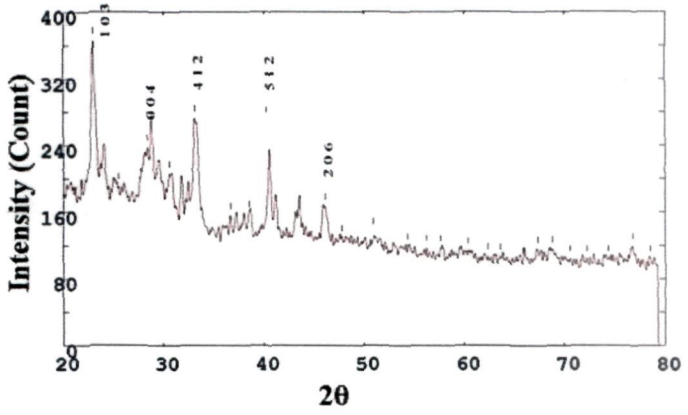

(c)

Figure 94. *X–ray powder diffraction patterns of (a) $[Cu_2(bipy)_2(im)_2(pip)(NO_3)_2].2NO_3$, (b) $[Zn_2(bipy)_2(im)_2(pip)].4Cl$ and (c) $[Ni_2(bipy)_2(im)_2(pip)].4Cl$ complexes.*

Table 15. *Summary of the XRPD data and the refinement parameters for complexes* $[Cu_2(bipy)_2(im)_2(pip)(NO_3)_2].2NO_3$, $[Zn_2(bipy)_2(im)_2(pip)].4Cl$ *and* $[Ni_2(bipy)_2(im)_2(pip)].4Cl$

Parameter	$[Cu_2(bipy)_2(im)_2(pip)(NO_3)_2].2NO_3$	$[Zn_2(bipy)_2(im)_2(pip)].4Cl$	$[Ni_2(bipy)_2(im)_2(pip)].4Cl$
Formula	$C_{30}H_{36}Cu_2N_{14}O_{12}$	$C_{30}H_{36}Cl_4N_{10}Zn_2$	$C_{30}H_{36}Cl_4N_{10}Ni_2$
FW	911.76	809.28	795.94
Temperature	298	298	298
Method	Micro crystalline	Micro crystalline	Micro crystalline
Wavelengt	1.540598	1.540598	1.540598
Radiation	Cu–Kα1	Cu–Kα1	Cu–Kα1
Crystal	Monoclinic	Triclinic	Triclinic
Space	P	P	P
Unit cell			
a(Å)	8.303	4.917	8.3700
b(Å)	13.382	4.916	10.520
c(Å)	11.876	5.407	10.831
α°	90	90	90
β°	90	90	90
γ°	90	90	90
2θ range	20–80	20–80	20–80
Limiting	$0 \leq h \leq 3$	$0 \leq h \leq 2$	$0 \leq h \leq 6$
Intensity	25.42–100	38.03–100	48.64–100

In vitro DNA binding Studies

Absorption titrations

The complexes $[Cu_2(bipy)_2(im)_2(pip)(NO_3)_2].2NO_3$, $[Zn_2(bipy)_2(im)_2(pip)].4Cl$ and $[Ni_2(bipy)_2(im)_2(pip)].4Cl$ displayed intense absorption bands at 235–270 nm in the UV region assigned to $\pi \rightarrow \pi^*$ transitions of aromatic chromophore and shows another band at 290–310 nm assigned to MLCT transition, respectively. On the addition of CT DNA, complexes $[Cu_2(bipy)_2(im)_2(pip)(NO_3)_2].2NO_3$, $[Zn_2(bipy)_2(im)_2(pip)].4Cl$ and $[Ni_2(bipy)_2(im)_2(pip)].4Cl$ show an increase in molar absorptivity (hyperchromism; 17–33%, Table 16) with a blue shift of 4–8 nm at 235–270 nm.

Table 16. *The binding constant (K_b) values of complexes $[Cu_2(bipy)_2(im)_2(pip)(NO_3)_2].2NO_3$, $[Zn_2(bipy)_2(im)_2(pip)].4Cl$ and $[Ni_2(bipy)_2(im)_2(pip)].4Cl$ with the DNA*

Complex	K(M^{-1})	% Hyperchromism	Blue Shift (nm)
$[Cu_2(bipy)_2(im)_2(pip)(NO_3)_2].2NO_3$	2.74×10^4	33	4
$[Zn_2(bipy)_2(im)_2(pip)].4Cl$	2.04×10^4	23	8
$[Ni_2(bipy)_2(im)_2(pip)].4Cl$	1.51×10^4	17	5

These changes are typical for complexes bound to DNA through non covalent interaction [331]. Hypochromism results from the contraction of DNA helix as well as the conformational changes on DNA, while hyperchromism results from the secondary damage of DNA double helix structure [332,333].

To quantify the extent of DNA binding, the intrinsic binding constant, K_b of the complexes were determined. The K_b values obtained follows the order: $[Cu_2(bipy)_2(im)_2(pip)(NO_3)_2].2NO_3 > [Zn_2(bipy)_2(im)_2(pip)].4Cl > [Ni_2(bipy)_2(im)_2(pip)].4Cl$ (Figure 95).

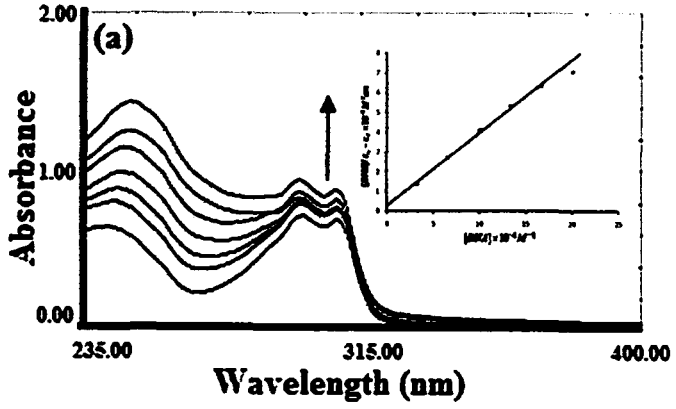

(a)

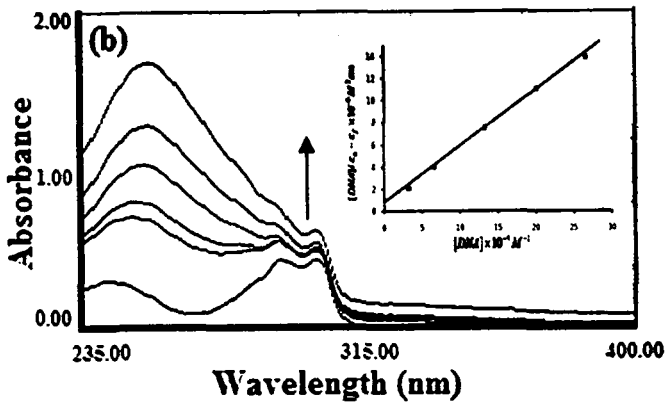

(b)

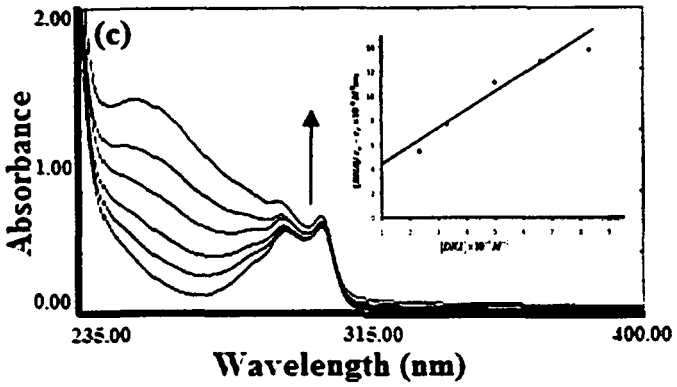

(c)

Figure 95. *Absorption spectral traces of complexes (a) $[Cu_2(bipy)_2(im)_2(pip)(NO_3)_2].2NO_3$, (b) $[Zn_2(bipy)_2(im)_2(pip)].4Cl$ and (c) $[Ni_2(bipy)_2(im)_2(pip)].4Cl$ in 5mM Tris HCl/ 50 mM NaCl buffer at pH 7.2 upon addition of CT DNA. Inset: Plots of [DNA]/ $\varepsilon_a-\varepsilon_f$ (M^2 cm) vs [DNA] for the titration of CT DNA with complexes ■, experimental data points; full lines, linear fitting of the data. [Complex] 0.67 x 10^{-4} M, [DNA] 0.00–0.33 x 10^{-4} M.*

An explanation for higher K_b value of copper complexes is apparently that copper complexes are 'borderline' metals which show high affinity for both nucleobases and phosphate. In particular, Cu(II) complexes bind specifically to N7 of guanine nucleobase of DNA helix [334]

Interaction with 5'–GMP

To obtain concrete information and to determine the coordination of the metal ion to the specific site, interaction with low molecular building blocks of large DNA molecules *viz*; guanosine 5'–monophosphate becomes mandatory. Cu(II) complexes, exhibits specificity towards guanine nucleotide of DNA. On addition of 5'–GMP to the complex $[Cu_2(bipy)_2(im)_2(pip)(NO_3)_2].2NO_3$, there is a sharp increase "hyperchromic" effect in the absorption bands at 235–280 nm (Figure 96). This observation supports the multiple binding events of the Cu(II) complex as observed in case of CT DNA and also provides an authentic proof for binding to 5'–GMP through electrostatic interaction *via* phosphate backbone of the DNA helix.

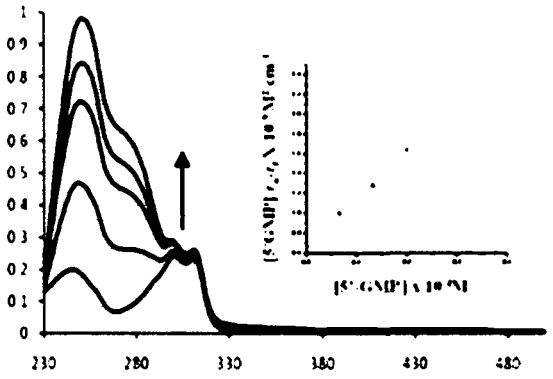

Figure 96. *Variation of UV–vis absorption for complex* $[Cu_2(bipy)_2(im)_2(pip)(NO_3)_2].2NO_3$ *with increase in the concentration of 5' GMP (0.067 x* 10^{-4}*–0.33 x* 10^{-4} *M) in buffer (5mM Tris–HCl/50 mM NaCl, pH= 7.2) at room temperature. Inset: plot of [5' GMP]/(*ε_a–ε_f*) vs [5' GMP] for the titration of 5' GMP.*

To obtain a concrete evidence of binding via electrostatic interaction, the binding of $[Cu_2(bipy)_2(im)_2(pip)(NO_3)_2].2NO_3$ to 5'–GMP was also validated by ^1H and ^{31}P NMR techniques. The free 5'–GMP exhibited H8 signal at 8.02 ppm, on addition of complex $[Cu_2(bipy)_2(im)_2(pip)(NO_3)_2].2NO_3$, there was a slight shift (~0.03 ppm) in H8 signal (Figure 97a & b), indicative of weak binding of $[Cu_2(bipy)_2(im)_2(pip)(NO_3)_2].2NO_3$ to the

5'–GMP. The ^{31}P NMR spectra of $[Cu_2(bipy)_2(im)_2(pip)(NO_3)_2].2NO_3$ in presence of 5'–GMP reveal a substantial downfield shift (3.67 ppm to 1.67ppm) to that of free nucleotide (without the added complex). The observations deduced from above studies demonstrate that complex $[Cu_2(bipy)_2(im)_2(pip)(NO_3)_2].2NO_3$ interacts strongly with the anionic phosphate backbone of the DNA helix (Figure 97c & b) [335,336].

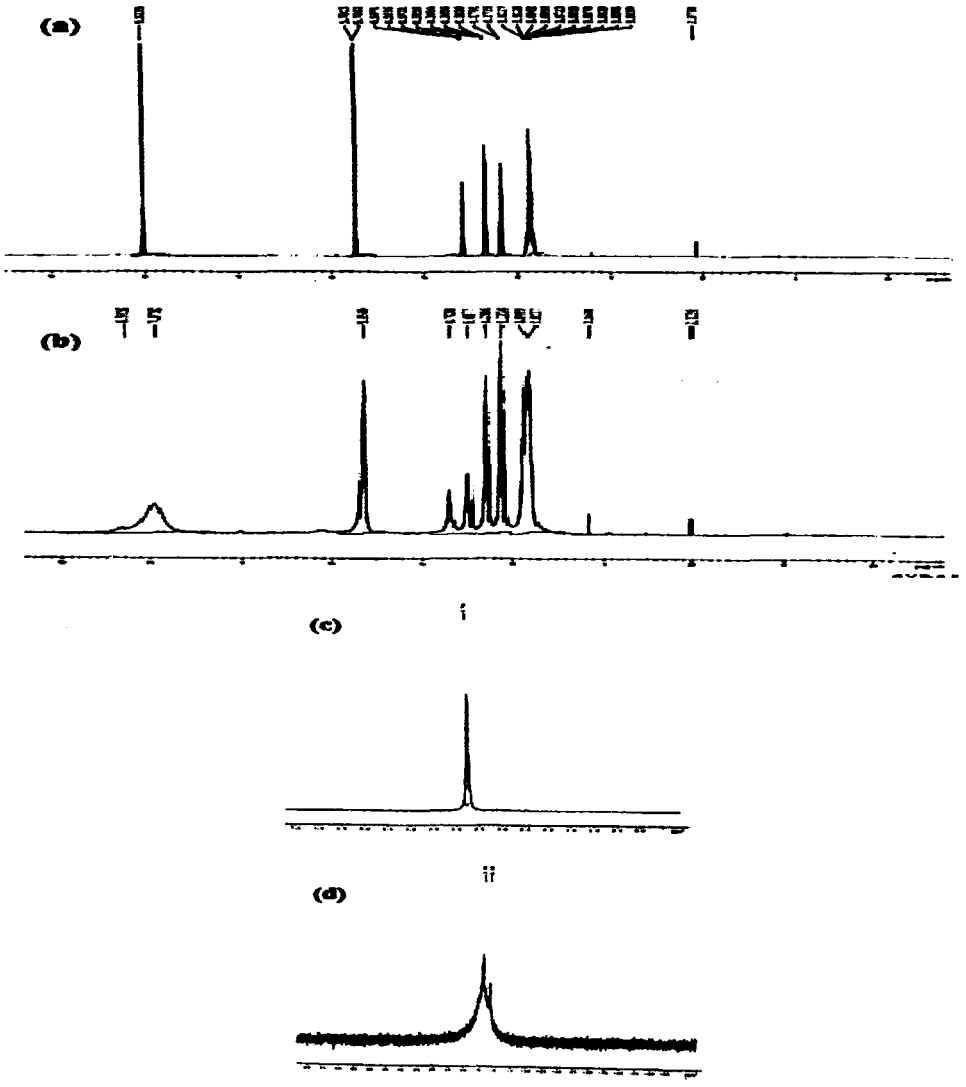

Figure 97. *(a) ^{1}H NMR spectra of 5'–GMP, (b) ^{1}H NMR spectra of complex $[Cu_2(bipy)_2(im)_2(pip)(NO_3)_2].2NO_3$ with 5'–GMP, (c) ^{31}P NMR spectra of 5'–GMP,and ^{31}P NMR spectra of complex $[Cu(bipy)_2(im)_2(pip)(NO_3)_2].2NO_3$ with 5'–GMP at 25 °C.*

Fluorescence studies

In the absence of CT–DNA, complexes $[Cu_2(bipy)_2(im)_2(pip)(NO_3)_2].2NO_3$, $[Zn_2(bipy)_2(im)_2(pip)].4Cl$ and $[Ni_2(bipy)_2(im)_2(pip)].4Cl$ emit weak luminescence in Tris–HCl buffer at room temperature, with a fluorescence maximum appearing at ~325 nm when excited at 260 nm. Upon addition of increasing concentration of CT–DNA over a range 0.00–3.33 x 10^{-5} M, to the fixed amount of complexes (0.33 x 10^{-5} M), the emission intensity of $[Cu_2(bipy)_2(im)_2(pip)(NO_3)_2].2NO_3$, $[Zn_2(bipy)_2(im)_2(pip)].4Cl$ and $[Ni_2(bipy)_2(im)_2(pip)].4Cl$ increased appreciably as illustrated in the Figure 98(a–c), respectively. The enhancement of the emission intensity is largely due to the change in the environment of the metal complex and related to the extent to which the complex gets into a hydrophobic environment inside the CT–DNA. Since, it is found that complexes with increased ligand hydrophobicities show greater increase in emission intensities upon binding to polyelectrolytes *via* DNA, therefore, such an increase in emission intensities is attributed to electrostatic association. Thus, we infer that the complexes are less deeply accommodated inside the hydrophobic pockets inside the DNA which is indicative of electrostatic mode of binding of the complex to the CT–DNA. The relative fluorescence intensity plotted as a function of DNA concentration (in terms of ([M]/[DNA]), (Figure 98a–c) showed larger increase in the emission intensity of complex $[Cu_2(bipy)_2(im)_2(pip)(NO_3)_2].2NO_3$ than the complex $[Zn_2(bipy)_2(im)_2(pip)].4Cl$ and $[Ni_2(bipy)_2(im)_2(pip)].4Cl$. This implies that complex $[Cu_2(bipy)_2(im)_2(pip)(NO_3)_2].2NO_3$ is bound to the DNA more strongly by means of surface binding with the DNA duplex (Table 17).

Table 17. *Emission properties of complexes* $[Cu_2(bipy)_2(im)_2(pip)(NO_3)_2].2NO_3$, $[Zn_2(bipy)_2(im)_2(pip)].4Cl$ *and* $[Ni_2(bipy)_2(im)_2(pip)].4Cl$ *bound to CT DNA*

Complex	Emission	Excitation	Monitored	K_b (M^{-1})
$[Cu_2(bipy)_2(im)_2(pip)(NO_3)_2].2NO_3$	220	260	329	1.87×10^4
$[Zn_2(bipy)_2(im)_2(pip)].4Cl$	220	260	324	1.24×10^4
$[Ni_2(bipy)_2(im)_2(pip)].4Cl$	220	260	325	1.09×10^4

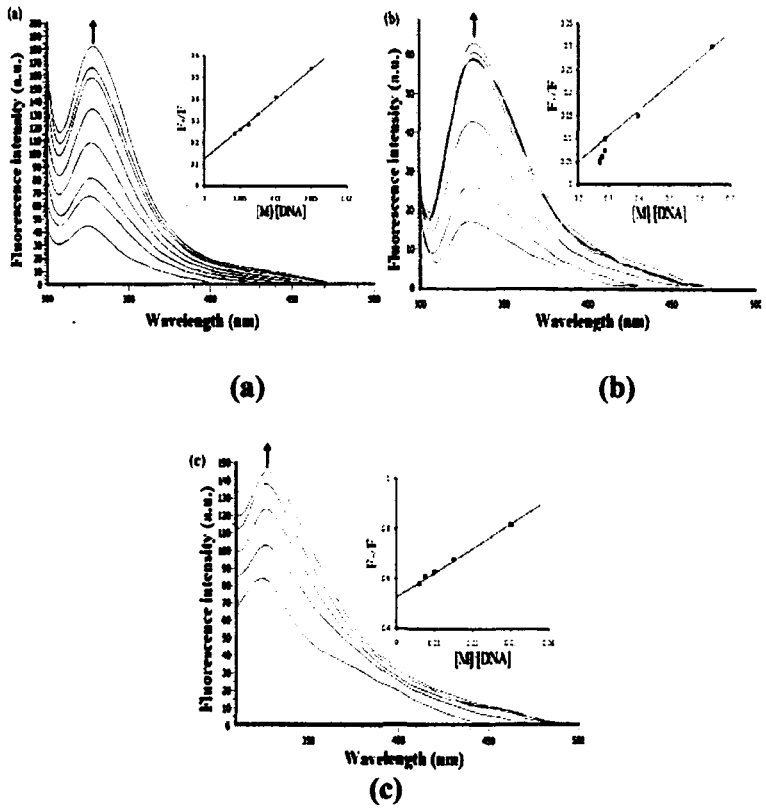

Figure 98. *Emission enhancement spectra of the complexes (a)* $[Cu_2(bipy)_2(im)_2(pip)(NO_3)_2].2NO_3$, *(b)* $[Zn_2(bipy)_2(im)_2(pip)].4Cl$ *and (c)* $[Ni_2(bipy)_2(im)_2(pip)].4Cl$ *in presence of CT–DNA. Arrow indicates the change in the intensity upon increasing DNA concentration.*

To demonstrate the interaction strength of the complexes $[Cu_2(bipy)_2(im)_2(pip)(NO_3)_2].2NO_3$, $[Zn_2(bipy)_2(im)_2(pip)].4Cl$ and $[Ni_2(bipy)_2(im)_2(pip)].4Cl$ with CT–DNA, steady state emission quenching experiments using $[Fe(CN)_6]^{4-}$ as quencher were also performed [337.338]. The propensity to CT–DNA for the complexes follows the order: $[Cu_2(bipy)_2(im)_2(pip)(NO_3)_2].2NO_3$ > $[Zn_2(bipy)_2(im)_2(pip)].4Cl$ > $[Ni_2(bipy)_2(im)_2(pip)].4Cl$ as evidenced by the binding constant K_{sv} values given in the Table 18.

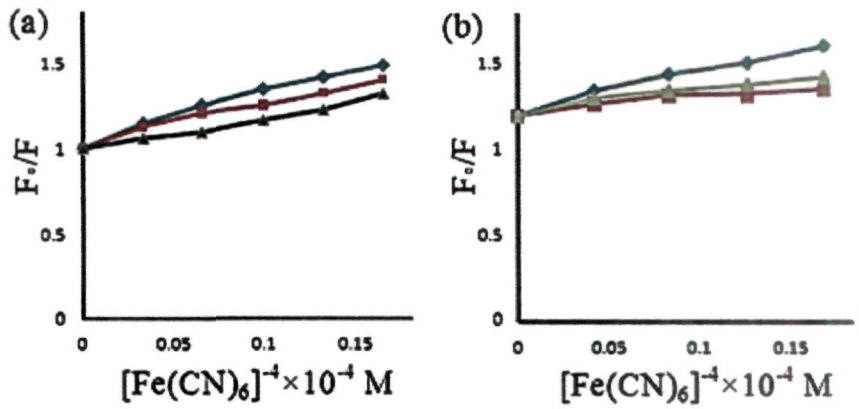

Figure 99. *Stern–Volmer quenching plots of complexes $[Cu_2(bipy)_2(im)_2(pip)(NO_3)_2].2NO_3$, $[Zn_2(bipy)_2(im)_2(pip)].4Cl$ and $[Ni_2(bipy)_2(im)_2(pip)].4Cl$ in the (a) absence and (b)Presence of CT–DNA.*

In the absence of CT–DNA, emission intensity of complex $[Cu_2(bipy)_2(im)_2(pip)(NO_3)_2].2NO_3$, $[Zn_2(bipy)_2(im)_2(pip)].4Cl$ and $[Ni_2(bipy)_2(im)_2(pip)].4Cl$ were efficiently quenched by $[Fe(CN)_6]^{4-}$ as shown in Figure 99a,b. The greater decrease of quenching for $[Cu_2(bipy)_2(im)_2(pip)(NO_3)_2].2NO_3$ as compared to $[Zn_2(bipy)_2(im)_2(pip)].4Cl$ and $[Ni_2(bipy)_2(im)_2(pip)].4Cl$ indicated higher DNA binding ability of $[Cu_2(bipy)_2(im)_2(pip)(NO_3)_2].2NO_3$.

Table 18. *Emission quenching of CT–DNA bound* $[Fe(CN)_6]^{4-}$ *by complexes* $[Cu_2(bipy)_2(im)_2(pip)(NO_3)_2].2NO_3$, $[Zn_2(bipy)_2(im)_2(pip)].4Cl$ *and* $[Ni_2(bipy)_2(im)_2(pip)].4Cl$

Complex	Emission	Excitation	Monitored	K_{sv}
$[Cu_2(bipy)_2(im)_2(pip)(NO_3)_2].2NO_3$	220	260	330	2.55×10^4
$[Zn_2(bipy)_2(im)_2(pip)].4Cl$	220	260	360	1.39×10^4
$[Ni_2(bipy)_2(im)_2(pip)].4Cl$	220	260	336	1.35×10^4

Circular dichroism studies

Circular dichroism (CD) is a powerful and sophisticated tool for identifying conformational changes of DNA. The secondary structure of DNA is greatly influenced by interaction of $[Cu_2(bipy)_2(im)_2(pip)(NO_3)_2].2NO_3$, $[Zn_2(bipy)_2(im)_2(pip)].4Cl$ and $[Ni_2(bipy)_2(im)_2(pip)].4Cl$ and changes in conformation of DNA from B→Z or B →A. The observed CD spectrum of CT DNA consists of a positive band at 275 nm due to base stacking and a negative band at 245 nm due to helicity, which are characteristic of DNA in right handed canonical B–form. Simple groove binding and electrostatic interaction of the complexes with DNA showed less or no perturbations on the base stacking and helicity bands while intercalator enhances the intensities of both the bands. On incubation of present complexes $[Cu_2(bipy)_2(im)_2(pip)(NO_3)_2].2NO_3$, $[Zn_2(bipy)_2(im)_2(pip)].4Cl$ and $[Ni_2(bipy)_2(im)_2(pip)].4Cl$ with CT DNA, the CD spectra of DNA undergoes changes in both positive and negative bands (Figure 100 a–c).

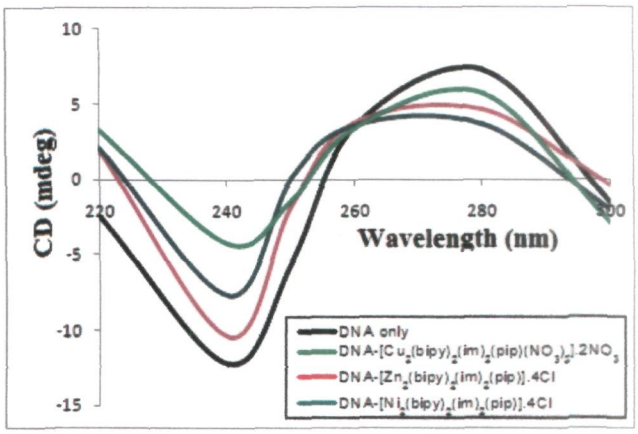

Figure 100. *CD spectrum of CT–DNA in the absence and presence of complexes, (a) ▬, DNA alone; (b) ▬,[$Cu_2(bipy)_2(im)_2(pip)(NO_3)_2$].$2NO_3$+DNA, (c)▬ [$Zn_2(bipy)_2(im)_2(pip)$].4Cl +DNA, and (d) ▬, [$Ni_2(bipy)_2(im)_2(pip)$].4Cl+DNA. [Complex] 1 x 10^{-4} M, [DNA] 1 x 10^{-4} M.*

In complex [$Cu_2(bipy)_2(im)_2(pip)(NO_3)_2$].$2NO_3$, [$Zn_2(bipy)_2(im)_2(pip)$].4Cl and [$Ni_2(bipy)_2(im)_2(pip)$].4Cl, after addition of CT DNA the CD spectra shows an decrease in positive and in negative bands without shift in the band position. Such results suggest that the CD spectra are closely correlated with DNA binding affinity [339].

DNA cleavage activity

DNA Cleavage without added reductant

The DNA cleavage ability of complex [$Cu_2(bipy)_2(im)_2(pip)(NO_3)_2$].$2NO_3$ was studied by agarose gel electrophoresis using supercoiled pBR322 plasmid DNA as a substrate. The activity of complex [$Cu_2(bipy)_2(im)_2(pip)(NO_3)_2$].$2NO_3$ was assessed by the conversion of DNA from Form I to Form II or Form III. A concentration-dependent DNA cleavage by complex [$Cu_2(bipy)_2(im)_2(pip)(NO_3)_2$].$2NO_3$ was first performed. Briefly, pBR322 DNA was mixed with different concentration of complex [$Cu_2(bipy)_2(im)_2(pip)(NO_3)_2$].$2NO_3$ and the mixture was incubated at 310 K for 45 min. With the increase of concentration of complex [$Cu_2(bipy)_2(im)_2(pip)(NO_3)_2$].$2NO_3$, DNA

was converted from Form I (Supercoiled Form) to more intense Form II was observed (shown in Lane 2–5, Figure 101) with the simultaneous reduction of Form I, whereas no conversion to Form III was observed. The reduction in the intensity of Form I and appearance of more intense Form II of pBR322 DNA on the gel shows the complex $[Cu_2(bipy)_2(im)_2(pip)(NO_3)_2].2NO_3$ are involved in an efficient double strand DNA cleavage pathway.

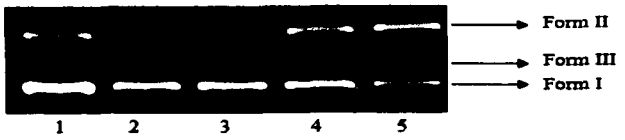

Figure 101. *The cleavage patterns of the agarose gel electrophoresis diagram showing cleavage of pBR322 supercoiled DNA (300 ng) by* $[Cu_2(bipy)_2(im)_2(pip)(NO_3)_2].2NO_3$ *at 25 °C after 45 minutes of incubation. Lane 1, DNA control; Lane 2, 5 μM of complex + DNA; Lane 3, 10 μM of complex + DNA; Lane 4, 20 μM of complex + DNA; Lane 5, 30 μM of complex. With the increase of concentration of* $[Cu_2(bipy)_2(im)_2(pip)(NO_3)_2].2NO_3$, *DNA was converted from Form I (Supercoiled Form) to Form II (Nicked Circular Form) and then to Form III (Linear Form).*

DNA cleavage in presence of activators

The nuclease activity of complex $[Cu_2(bipy)_2(im)_2(pip)(NO_3)_2].2NO_3$ markedly depends on different activators [192,193]. Thus, activators such as ascorbate (Asc), 3–mercaptopropionic acid (MPA), H_2O_2 and glutathione (GSH) (Lanes 2–5, Figure 102) were also used to investigate the DNA cleavage activity of complex $[Cu_2(bipy)_2(im)_2(pip)(NO_3)_2].2NO_3$ at a concentration of 20 μM. The cleavage activity of $[Cu_2(bipy)_2(im)_2(pip)(NO_3)_2].2NO_3$ was significantly enhanced by these activators and follows the order: H_2O_2>MPA>Asc≈GSH.

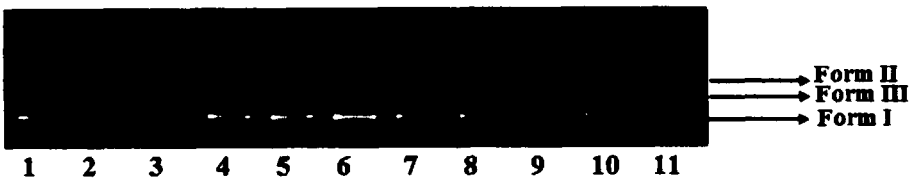

Figure 102. *Agarose gel electrophoresis pattern for the cleavage pattern of pBR322 plasmid DNA (300 ng) by complex $[Cu_2(bipy)_2(im)_2(pip)(NO_3)_2].2NO_3$ (0.25 mmol) in the presence of different activating agents at 37 °C after incubation for 45 min: Lane 1, DNA control; Lane 2, DNA + $[Cu_2(bipy)_2(im)_2(pip)(NO_3)_2].2NO_3$ + H_2O_2 (0.4 μM); Lane 3, DNA + $[Cu_2(bipy)_2(im)_2(pip)(NO_3)_2].2NO_3$ + MPA (0.4 μM); Lane 4, DNA + $[Cu_2(bipy)_2(im)_2(pip)(NO_3)_2].2NO_3$ + Asc (0.4 μM); Lane 5, DNA + $[Cu_2(bipy)_2(im)_2(pip)(NO_3)_2].2NO_3$ + GSH (0.4 μM); Lane 6, DNA + $[Cu_2(bipy)_2(im)_2(pip)(NO_3)_2].2NO_3$+ NaN3 (0.4 μM); Lane 7, DNA + 1 + Superoxide Dismutase (15 units); Lane 8, DNA + $[Cu_2(bipy)_2(im)_2(pip)(NO_3)_2].2NO_3$+ DMSO (0.4 μM); Lane 9, DNA + $[Cu_2(bipy)_2(im)_2(pip)(NO_3)_2].2NO_3$+ tert–butyl alcohol (0.4 μM); Lane 10, DNA + 1 + Methyl green (2.5 μL of a 0.01 mg/mL solution); Lane 11, DNA + $[Cu_2(bipy)_2(im)_2(pip)(NO_3)_2].2NO_3$+ DAPI (8 μM).*

DNA cleavage in presence of recognition elements (Groove binding)

Minor groove binding agent DAPI [340], and major groove binding agent methyl green [341] (Lane 10 and 11, Figure 102) were used to examine the potential interacting site of complex $[Cu_2(bipy)_2(im)_2(pip)(NO_3)_2].2NO_3$ with supercoiled plasmid DNA. The cleavage patterns, demonstrated that $[Cu_2(bipy)_2(im)_2(pip)(NO_3)_2].2NO_3$ prefers minor groove binding, which is further validated by molecular docking study.

Reactive oxygen species responsible for DNA cleavage

The interaction between metal complexes and dioxygen or redox reagents are believed to be a major cause of DNA damage [342]. To probe the potential mechanism of DNA cleavage mediated by complex $[Cu_2(bipy)_2(im)_2(pip)(NO_3)_2].2NO_3$, some standard radical scavengers were used prior to the addition of $[Cu_2(bipy)_2(im)_2(pip)(NO_3)_2].2NO_3$ to DNA solution. The complex $[Cu_2(bipy)_2(im)_2(pip)(NO_3)_2].2NO_3$ did not show any inhibition in presence of DMSO while DNA cleavage was inhibited significantly in presence of tert–butyl alcohol (Lane 7). The addition of sodium azide (Lane 8) as singlet

oxygen scavenger and SOD (Lane 9) as superoxide anion radical scavenger also did not attenuate the DNA strand scission and even in presence of SOD the cleavage reaction is enhanced. Therefore an oxidative cleavage pathway of DNA by complex $[Cu_2(bipy)_2(im)_2(pip)(NO_3)_2].2NO_3$ was excluded and evidently the cleavage proceeds by a hydrolytic mechanism.

Superoxide Dismutase Activity

The $O_2^{\bullet -}$ (superoxide radical) was generated using a non–enzymatic system in the presence or absence of test compounds, and $O_2^{\bullet -}$ was detected by monitoring reduction of nitroblue tetrazolium (NBT) to monoformazan dye at 560 nm. A plot of NBT percent inhibition with an increase in concentration of complex $[Cu_2(bipy)_2(im)_2(pip)(NO_3)_2].2NO_3$ is shown in Figure 103. The determined IC_{50} values for the complex $[Cu_2(bipy)_2(im)_2(pip)(NO_3)_2].2NO_3$ under investigation are given in Table 19. The IC_{50} value of complex $[Cu_2(bipy)_2(im)_2(pip)(NO_3)_2].2NO_3$ is 0.28 μM, which is considered to be an excellent SOD mimic among the most active bipy–Cu(II) complexes but it is somewhat less active than the IC_{50} value obtained for native enzyme (IC_{50} = 0.04 μM). Furthermore, the high superoxide dismutase activity of complex $[Cu_2(bipy)_2(im)_2(pip)(NO_3)_2].2NO_3$ may be possibly due to cooperation of two Cu(II) centers in close proximity, acting in concord in free radical binding and electron transfer. Also may be due to a vacant coordination site that permits the bonding of superoxide anion and the influence of ligand on SOD activity [343].

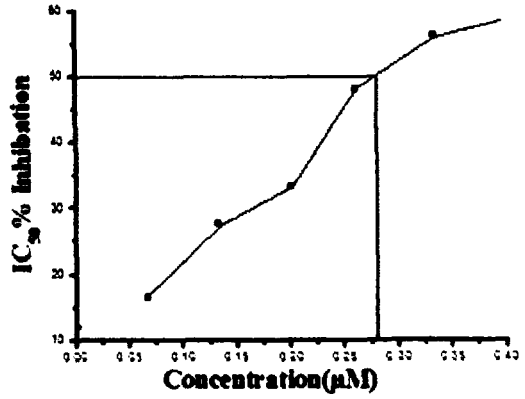

Figure 103. *A plot of percentage of NBT inhibition reduction with an increase in the concentration of complex* $[Cu_2(bipy)_2(im)_2(pip)(NO_3)_2].2NO_3$.

Table 19. IC_{50} *(μM) values of the complex* $[Cu_2(bipy)_2(im)_2(pip)(NO_3)_2].2NO_3$ *, some of the copper (II) complexes and the native Cu,ZnSOD enzyme*

Complexes	IC_{50} (μM)	References
$[Cu_2(bipy)_2(im)_2(pip)(NO_3)_2].2NO_3$	0.28	(This work)
$[Cu(stz)(py)_3Cl]$	1.31	[344]
$[Cu(Hstz)_2(MeOH)Cl_2]$	2.51	[344]
$[Cu(Cip)_2(bipym)_2(pip)].5H_2O$	0.058	[345]
$[Cu(stz)_2(1,2\text{–}dmHim)_2]$	1.03	[346]
$[Cu(stz)(py)_3Cl]$	1.586	[346]
Native Cu,Zn–SOD	0.045	

Molecular docking studies

In order to get more insight into the mode of binding, complexes $[Cu_2(bipy)_2(im)_2(pip)(NO_3)_2].2NO_3$, $[Zn_2(bipy)_2(im)_2(pip)].4Cl$ and $[Ni_2(bipy)_2(im)_2(pip)].4Cl$ were successively docked with DNA duplex of sequence $d(CGCGAATTCGCG)_2$ dodecamer (PDB ID:1BNA). The minimum energy docked pose (Figure 104a-c) revealed that complex $[Cu_2(bipy)_2(im)_2(pip)(NO_3)_2].2NO_3$, $[Zn_2(bipy)_2(im)_2(pip)].4Cl$ and $[Ni_2(bipy)_2(im)_2(pip)].4Cl$ snuggly fitted into the curve

contour of DNA minor groove, and slightly bends the DNA in such a way that a part of the aromatic rings of bipyridyl ligand makes more effective π–π stacking interactions between DNA base pairs and lead to van der Waals interaction with the DNA functional groups which define the stability of groove [347]. The resulting relative binding energy of docked structures of complexes $[Cu_2(bipy)_2(im)_2(pip)(NO_3)_2].2NO_3$, $[Zn_2(bipy)_2(im)_2(pip)].4Cl$ and $[Ni_2(bipy)_2(im)_2(pip)].4Cl$ with DNA were found to be –241.4, –220.1 and –202.3 $KJmol^{-1}$, respectively, indicating the more potent the binding affinity between DNA and complex $[Cu_2(bipy)_2(im)_2(pip)(NO_3)_2].2NO_3$, correlating well with the experimental DNA binding studies and minor groove binder using DAPI assay. Thus, we can conclude that there is a mutual complement between spectroscopic and molecular docking techniques, which can be substantiate our experimental results and provide valuable information about the mode of interaction between complex and DNA.

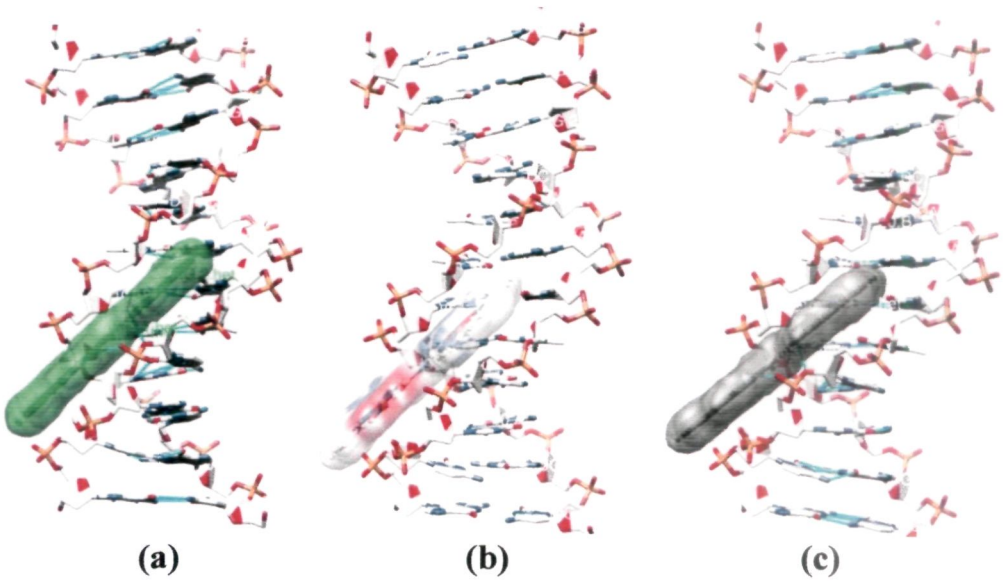

***Figure 104**. Molecular docked model of complex (a) $[Cu_2(bipy)_2(im)_2(pip)(NO_3)_2].2NO_3$ (b) $[Zn_2(bipy)_2(im)_2(pip)].4Cl$ and (c) $[Ni_2(bipy)_2(im)_2(pip)].4Cl$ with DNA dodecamer duplex of sequence $d(CGCGAATTCGCG)_2$ (PDB ID: 1BNA).*

Conclusion

In this work, we have described the synthesis and characterization of bimetallic complexes $[Cu_2(bipy)_2(im)_2(pip)(NO_3)_2].2NO_3$, $[Zn_2(bipy)_2(im)_2(pip)].4Cl$ and $[Ni_2(bipy)_2(im)_2(pip)].4Cl$ which can be explored as potential cancer chemotherapeutic agents. *In vitro* DNA binding studies of these complexes $[Cu_2(bipy)_2(im)_2(pip)(NO_3)_2].2NO_3$, $[Zn_2(bipy)_2(im)_2(pip)].4Cl$ and $[Ni_2(bipy)_2(im)_2(pip)].4Cl$ were carried out by using various biophysical and spectroscopic techniques. The binding affinity of these complexes followed the order $[Cu_2(bipy)_2(im)_2(pip)(NO_3)_2].2NO_3$ > $[Zn_2(bipy)_2(im)_2(pip)].4Cl$ > $[Ni_2(bipy)_2(im)_2(pip)].4Cl$. Experimental results indicate that the complexes bind to CT–DNA by electrostatic groove binding mechanism. The interaction of complex $[Cu_2(bipy)_2(im)_2(pip)(NO_3)_2].2NO_3$ with CT–DNA displays a higher binding propensity as compared to the rest of the complexes. As observed for gel electrophoretic mobility assay, the complex $[Cu_2(bipy)_2(im)_2(pip)(NO_3)_2].2NO_3$ displays efficient cleavage activity of plasmid pBR322 DNA converting the Form I to Form II and ultimately leading to the formation of linearized Form III with increasing concentrations of the complex. The complex $[Cu_2(bipy)_2(im)_2(pip)(NO_3)_2].2NO_3$ exhibited remarkable ability to affect DNA double strand scission in hydrolytic cleavage manner. SOD activity exhibited by $[Cu_2(bipy)_2(im)_2(pip)(NO_3)_2].2NO_3$ is the high activity with IC_{50} value equal ~ 0.28 μM.

CHAPTER VI

Synthesis, characterization of new bis–macrocyclic metal complexes: *in vitro* DNA binding and cleavage studies.

Synthesis

Synthesis of ethylene [O,O′–bis{5–{(1E)–(2 hydroxyphenyl)methylene]amino}–2–hydroxybenzoic acid] (L)

The salicylaldehyde derivative was synthesized according to the procedure reported earlier [348] which is described below (scheme 7).

To a stirred methanolic (30 mL) solution of 5–aminosalicylic acid (0.612g, 4mmol) was added dropwise salicylaldehyde derivative (0.54g, 2mmol) in methanol (20 mL). The reaction mixture was reflux for 4 hours to ensure the completion of reaction which yielded yellow colored solid product, washed with methanol (15 mL) and diethyl ether (30 mL). The yellow solid was then dried to afford ligand L. (Yield: 0.309g, 57.2%). m.p. 240 °C. Anal. Calc. for $C_{30}H_{24}N_2O_8$ (%): C, 66.66; H, 4.48; N, 5.18. Found: C, 66.69; H, 4.50; N, 5.21. Selected IR data on KBr/nujol, cm^{-1}: 3081 ν(Ar–CH); 1606 ν(C=N); 1677 ν(COO^-); 1483 ν(C=C); 1265; 1206 ν(Ar–O); 755 ν(Substituted benzene). ^1H NMR (DMSO–d_6, 400 MHz) δ (ppm): 8.78 (s, 2H, C(H)=N); 8.22 (s, 2H, C(H)=N); 6.75–7.97 (ov, m, 14H Ar); 5.58 (s, 2H, –OH); 3.20 (s, 4H, C_2H_5). ^{13}C NMR (DMSO–d_6, 100 MHz) δ(ppm): 171.7 (C=O); 159.6 (C=N); 158.4 (CO); 153.5 (CO); 112.9–142.8 (ArC).

Synthesis of bimetallic complexes

Complex $[Cu_2(L)_2]$

To a stirred methanolic (15 mL) solution of $Cu(NO_3)_2.3H_2O$ (0.241g, 1mmol) was added slowly ligand **L** (0.54 g, 1mmol) in methanol (25 mL). The resulting mixture was refluxed for ca 4 hours until a dark brown product was obtained and washed thoroughly with methanol and diethyl ether then dried in vacuo. (Yield: 0.453g, 74%). m.p. >300 °C. Anal. Calc. for $C_{60}H_{48}N_4O_{16}Cu_2$ (%): C, 59.65; H, 4.00; N, 4.64. Found: C, 59.45; H,

3.98; N, 4.61. Selected IR data on KBr/nujol, cm^{-1}: 3081 ν(Ar–CH); 1602 ν(C=N); 1677 ν(COO^-); 1486 ν(C=C); 1260, 1204 ν(Ar–O); 747 ν(Substituted benzene); 564 ν(Cu–O). Molar Conductance, Λ_M (1×10^{-3} M, DMSO): 51 Ω^{-1} cm^2 mol^{-1} (non–electrolyte). UV–vis absorption: (10^{-3} M, DMSO), λ_{max}/nm ($\varepsilon/10^3$ M^{-1} cm^{-1}): 270 (4.81); 375 (3.25); 538 (1.73).

Complex $[Ni_2(L)_2]$

The $[Ni_2(L)_2]$ complex was prepared by using $NiCl_2.6H_2O$ (0.237g, 1mmol) according to the method outlined for complex $[Cu_2(L)_2]$. The light yellow coloured product obtained was washed with methanol and dried in vacuo. (Yield: 0.308g, 51.4 %). m.p. 250 ±2 °C. Anal. Calc. for $C_{60}H_{48}N_4O_{16}Ni_2$ (%): C, 60.13; H, 4.04; N, 4.68. Found: C, 60.17; H, 3.99; N, 4.70. Selected IR data on KBr/nujol, cm^{-1}: 3073 ν(Ar–CH); 1602 ν(C=N); 1677 ν(COO^-); 1479 ν(C=C); 1265, 1202 ν(Ar–O); 749 ν(Substituted benzene); 543 ν(Ni–O). ^1H NMR (DMSO–d_6, 400 MHz) δ(ppm): 8.80 (s, 2H, C(H)=N); 6.81–8.00 (ov, m, 14H Ar); 4.58 (s, 2H, –OH); 3.26 (s, 4H, C_2H_4). ^{13}C NMR (DMSO–d_6, 100 MHz) δ(ppm): 171.81 (C=O); 159.7 (C=N); 158.5 (CO); 153.5 (CO); 112.8–142.8 (ArC). Λ_M (1×10^{-3} M, DMSO): 12 Ω^{-1} cm^2 mol^{-1} (non–electrolyte). UV–vis absorption: (10^{-3} M, DMSO), λ_{max}/nm ($\varepsilon/10^3$ M^{-1} cm^{-1}): 265 (2.40); 377 (1.35); 490 (0.95).

Complex $[Sn_2(L)_2.4Cl]$

The $[Sn_2(L)_2.4Cl]$ complex was prepared by using $SnCl_4.5H_2O$ (0.350g, 1mmol) according to the method outlined for complex $[Cu_2(L)_2]$. The light pink coloured product obtained was washed with methanol and dried in vacuo. (Yield: 0.459g, 63 %). m.p. 305 °C. Calc. for $C_{60}H_{48}Cl_4N_4O_{16}Sn_2$ (%): C, 49.35; H, 3.31; N, 3.84. Found: C, 49.44; H,

3.15; N, 3.81. Selected IR data on KBr/nujol, cm^{-1}: 3080 ν(Ar–CH); 1602 ν(C=N); 1649 ν(COO^-); 1482 ν(C=C); 1252 ν(Ar–O); 765 ν(Substituted benzene); 573 ν(Sn–O). ^1H NMR (DMSO–d_6, 400 MHz) δ(ppm): 8.90 (s, 2H, C(H)=N); 6.90–8.15 (ov, m, 14H Ar); 4.58 (s, 2H, –OH); 3.22 (s, 4H, C_2H_4). ^{13}C NMR (DMSO–d_6, 100 MHz) δ(ppm): 171.62 (C=O); 160.8 (C=N); 160.4 (CO); 160.2 (CO); 112.9–139.5 (Ar–C). ^{119}Sn NMR (DMSO–d_6, δppm): –625.8; –626.4. Λ_M(1×10^{-3} M, DMSO): 16 Ω^{-1} cm^2 mol^{-1} (non–electrolyte). UV–vis absorption: (10^{-3} M, DMSO), λ_{max}/nm (ε/10^3 M^{-1} cm^{-1}): 319 (0.99); 377 (0.62).

Results and discussion

The complexes $[Cu_2(L)_2]$, $[Ni_2(L)_2]$ and $[Sn_2(L)_2.4Cl]$ were synthesized as depicted in scheme 7. Empirical formulae and proposed structure were ascertained by elemental analysis, molar conductivity measurements, UV–vis, FTIR, NMR spectroscopy and XRPD studies. All complexes are soluble in organic polar solvents, DMSO and DMF. On the basis of UV–vis. and EPR data, the proposed geometry of the complexes $[Cu_2(L)_2]$ and $[Ni_2(L)_2]$ were assigned to be square planar (four–coordinated environment) while $[Sn_2(L)_2.4Cl]$ was in six coordinated environment.

IR spectroscopy

The IR spectrum of free ligand (L) exhibited characteristic stretch at ~1596 cm^{-1} attributed to the presence of free ν(OH) group of phenolic moiety. However, in complexes $[Cu_2(L)_2]$, $[Ni_2(L)_2]$ and $[Sn_2(L)_2.4Cl]$, ν(OH) stretching band shifted, indicating the coordination of the metal ions Cu(II), Ni(II) and Sn(IV) through the oxygen atom of both the phenolic groups. The Δν ($\nu_{as}(CO_2)$–$\nu_s(CO_2)$) value was used to determine the nature of binding of carboxylate to metal center. In general, the difference

3.98; N, 4.61. Selected IR data on KBr/nujol, cm^{-1}: 3081 ν(Ar–CH); 1602 ν(C=N); 1677 ν(COO^-); 1486 ν(C=C); 1260, 1204 ν(Ar–O); 747 ν(Substituted benzene); 564 ν(Cu–O). Molar Conductance, Λ_M (1×10^{-3} M, DMSO): 51 Ω^{-1} cm^2 mol^{-1} (non–electrolyte). UV–vis absorption: (10^{-3} M, DMSO), λ_{max}/nm ($\varepsilon/10^3$ M^{-1} cm^{-1}): 270 (4.81); 375 (3.25); 538 (1.73).

Complex $[Ni_2(L)_2]$

The $[Ni_2(L)_2]$ complex was prepared by using $NiCl_2.6H_2O$ (0.237g, 1mmol) according to the method outlined for complex $[Cu_2(L)_2]$. The light yellow coloured product obtained was washed with methanol and dried in vacuo. (Yield: 0.308g, 51.4 %). m.p. 250 ±2 °C. Anal. Calc. for $C_{60}H_{48}N_4O_{16}Ni_2$ (%): C, 60.13; H, 4.04; N, 4.68. Found: C, 60.17; H, 3.99; N, 4.70. Selected IR data on KBr/nujol, cm^{-1}: 3073 ν(Ar–CH); 1602 ν(C=N); 1677 ν(COO^-); 1479 ν(C=C); 1265, 1202 ν(Ar–O); 749 ν(Substituted benzene); 543 ν(Ni–O).

^{1}H NMR (DMSO–d_6, 400 MHz) δ(ppm): 8.80 (s, 2H, C(H)=N); 6.81–8.00 (ov, m, 14H Ar); 4.58 (s, 2H, –OH); 3.26 (s, 4H, C_2H_4). ^{13}C NMR (DMSO–d_6, 100 MHz) δ(ppm): 171.81 (C=O); 159.7 (C=N); 158.5 (CO); 153.5 (CO); 112.8–142.8 (ArC). Λ_M (1×10^{-3} M, DMSO): 12 Ω^{-1} cm^2 mol^{-1} (non–electrolyte). UV–vis absorption: (10^{-3} M, DMSO), λ_{max}/nm ($\varepsilon/10^3$ M^{-1} cm^{-1}): 265 (2.40); 377 (1.35); 490 (0.95).

Complex $[Sn_2(L)_2.4Cl]$

The $[Sn_2(L)_2.4Cl]$ complex was prepared by using $SnCl_4.5H_2O$ (0.350g, 1mmol) according to the method outlined for complex $[Cu_2(L)_2]$. The light pink coloured product obtained was washed with methanol and dried in vacuo. (Yield: 0.459g, 63 %). m.p. 305 °C. Calc. for $C_{60}H_{48}Cl_4N_4O_{16}Sn_2$ (%): C, 49.35; H, 3.31; N, 3.84. Found: C, 49.44; H,

in Δv between asymmetric ($\nu_{as}(CO_2)$) and symmetric ($\nu_s(CO_2)$) absorption frequency below 200 cm^{-1} suggests the bidentate carboxylate moiety while greater than 200 cm^{-1} implies the unidentate carboxylate moiety [349]. In complexes $[Cu_2(L)_2]$, $[Ni_2(L)_2]$ and $[Sn_2(L)_2.4Cl]$, the Δv values were 191, 198 and 169 cm^{-1}, respectively, indicative of bidentate carboxylate ligation through deprotonation. Other medium intensity bands at 747–765 cm^{-1} were attributed to the characteristic signatures of aromatic ring vibration. The complexes formation of $[Cu_2(L)_2]$, $[Ni_2(L)_2]$ and $[Sn_2(L)_2.4Cl]$ were also revealed by the presence of medium intensity (Cu–O), (Ni–O) and (Sn–O) bands around ~564, ~543 and ~577 cm^{-1}, respectively in the far IR region [350–352].

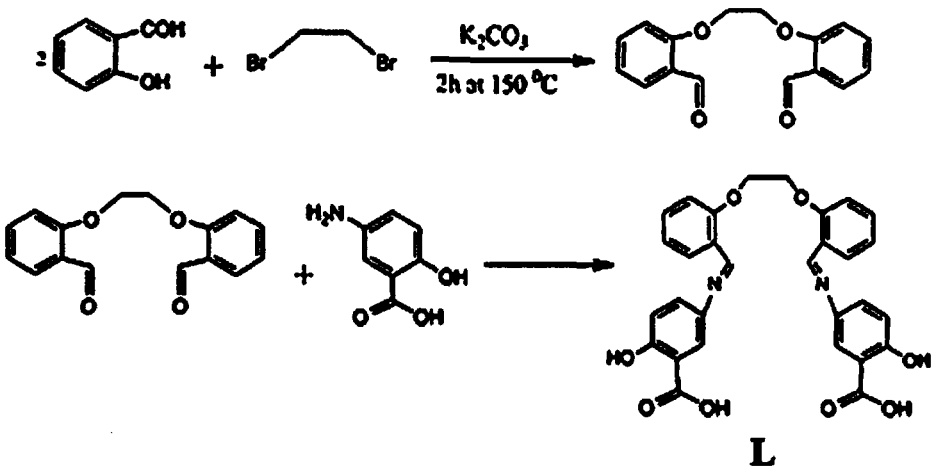

Scheme 7 (a). Synthesis of ligand (L).

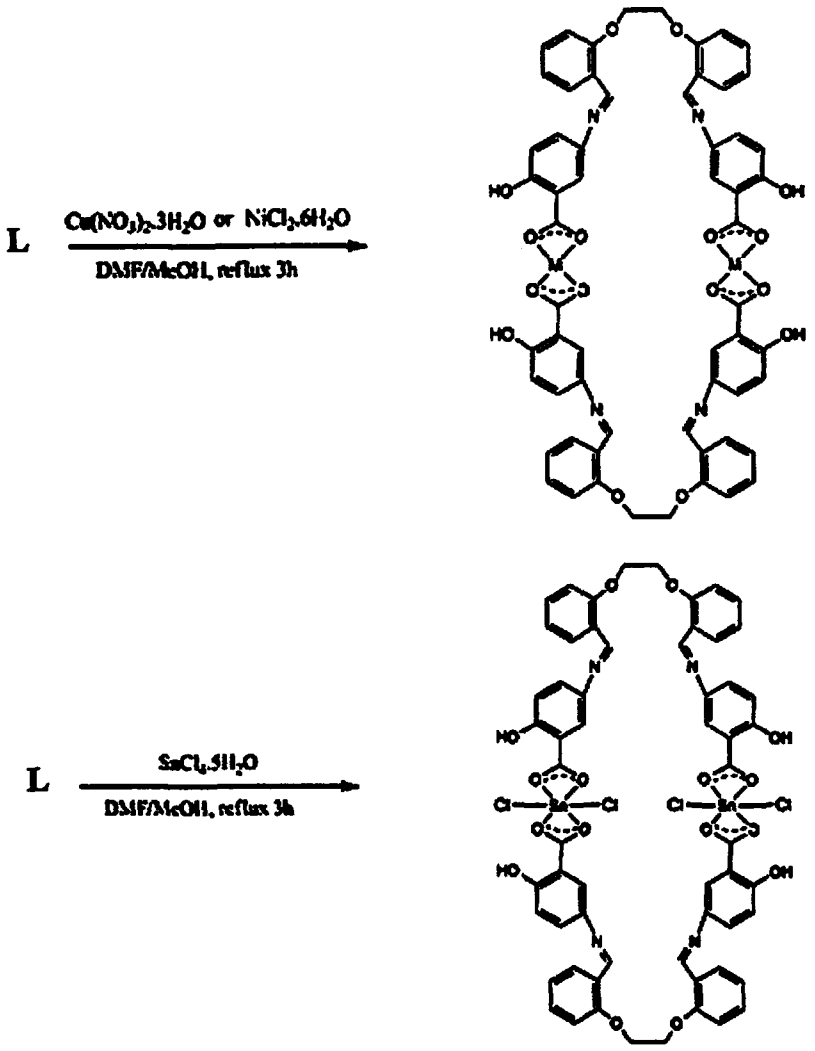

Scheme 7 (b). Synthesis of bimetallic complexes $[Cu_2(L)_2]$, $[Ni_2(L)_2]$ and $[Sn_2(L)_2.4Cl]$.

NMR spectral studies

The ^1H NMR spectrum of complex $[Ni_2(L)_2]$ and $[Sn_2(L)_2.4Cl]$ displayed several interesting features in comparison to the free ligand (L) as depicted in Figure 105. The complexes exhibit resonance signals appeared at 4.58 ppm is due to the presence of phenolic –OH group. However, the signals due to free carboxylic (–COOH) group at 12.0–10.0 were absent indicating the coordination of metal atoms *via* deprotonation. Coupled with these observations, the characteristic signals appeared at 8.80–8.90 and

6.81–8.15 corresponding to –CH=N, aromatic proton, respectively [353]. The complex $[Ni_2(L)_2]$ and $[Sn_2(L)_2.4Cl]$ exhibited ^{13}C NMR spectrum displaying various resonances due to O–C=O, CH=N, C–O–Ni and C–O–Sn carbons at 171.6–171.8, 159.7–162.2, 158.2 and 158.4 ppm, respectively. In addition, aromatic carbon signals of $[Ni_2(L)_2]$ and $[Sn_2(L)_2.4Cl]$ were observed at range 112.7–142.8 ppm (Figure 106). The ^{119}Sn chemical shift, $\delta(^{119}Sn)$ is sensitive to the chemical environments of the tin atom. ^{119}Sn NMR spectrum of the complex $[Sn_2(L)_2]$ displayed two sharp signals at –625.8 and –626.4 ppm, due to the presence of two tin centers (Figure 107) [354].

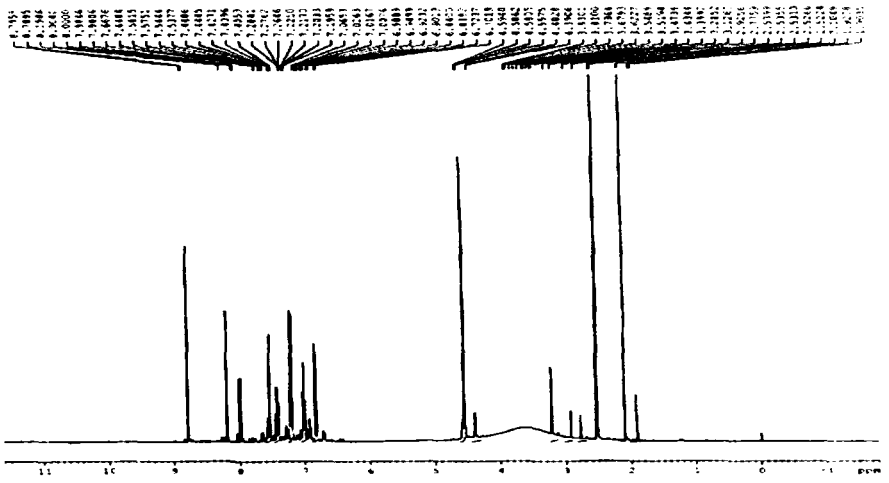

(a)

Figure 105(a). *^1H NMR spectrum of the complex $[Ni_2(L)_2]$.*

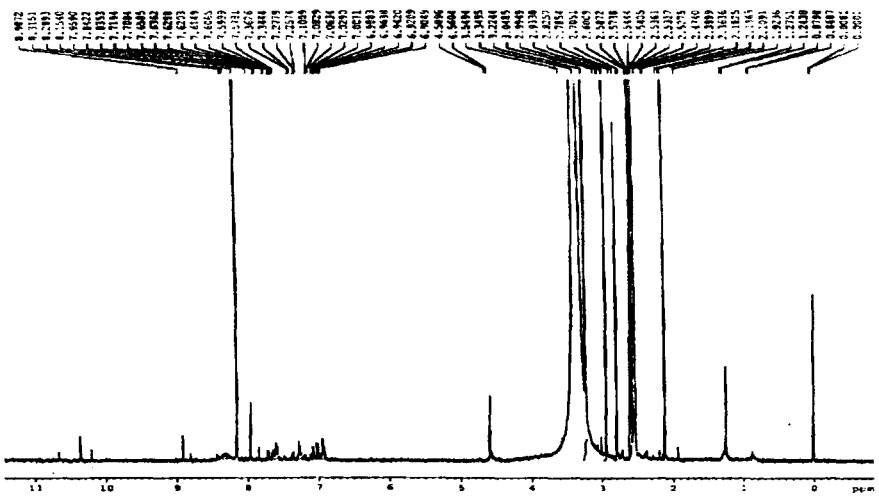

(b)

Figure 105(b). *^{1}H NMR spectrum of the complex $[Sn_2(L)_24Cl]$.*

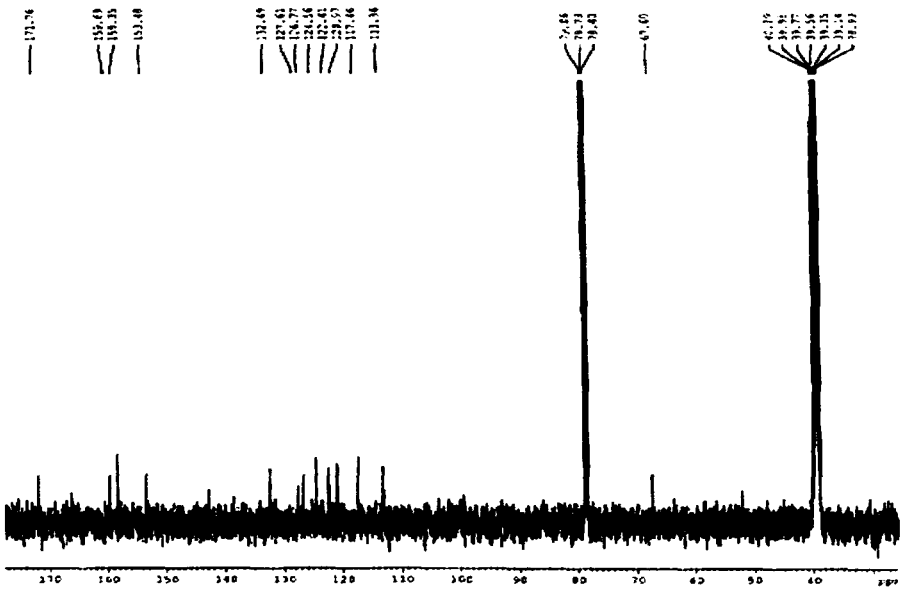

(a)

Figure 106(a). *^{13}C NMR spectrum of the complex $[Ni_2(L)_2]$.*

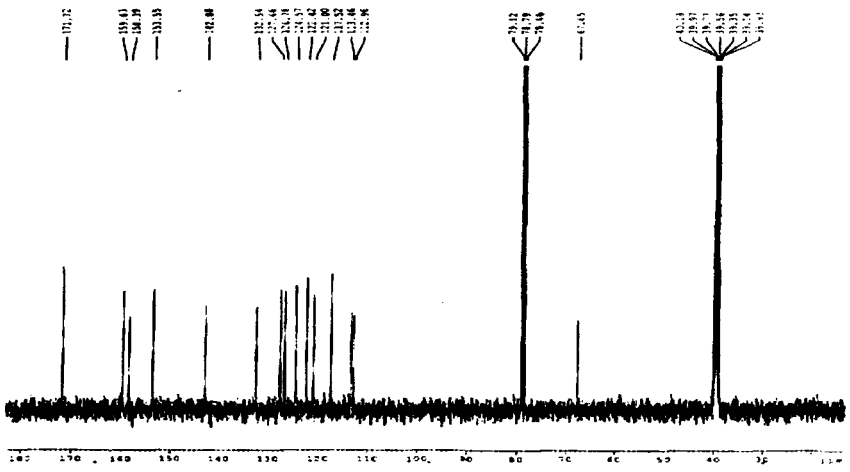

(b)

Figure 106(b). *^{13}C NMR spectrum of the complex $[Sn_2(L)_2.4Cl]$.*

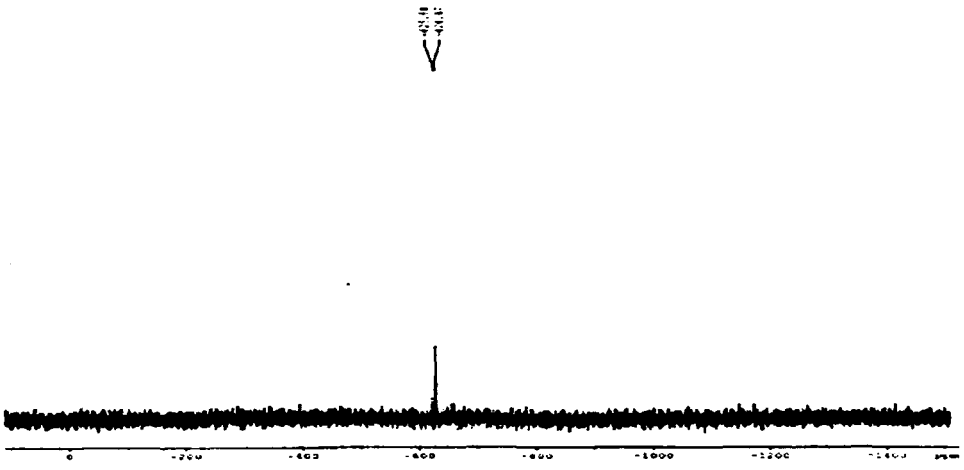

Figure 107. *^{119}Sn NMR spectrum of the complex $[Sn_2(L)_2.4Cl]$.*

EPR studies

The solid state X–band EPR spectrum (Figure 108) of polycrystalline complex $[Cu_2(L)_2]$ was recorded at room temperature with tetracyanoethylene (TCNE) as field marker (g = 2.0027). The spectrum displayed an isotropic signal and exhibits axial symmetrical line shape with $g_{\|}$=2.133 and $g_{\perp}$=2.055 and g_{av}=2.08 computed from the formula $g_{av}^2=g_{\|}^2+2g_{\perp}^2/3$. These parameters are consistent with the square planar

geometry of the copper(II) metal ion and are quite similar to the values reported for other related square planar copper(II) systems. The trend of g values ($g_{\parallel} > g_{\perp} > 2.0023$) observed for the copper(II) indicates that the unpaired electrons lies predominantly in the dx^2-y^2 orbital of Cu(II) ion (spectroscopic state $^2B_{1g}$). The exchange interaction parameter G = 2.42, suggesting presence of exchange coupling between the copper centers [355].

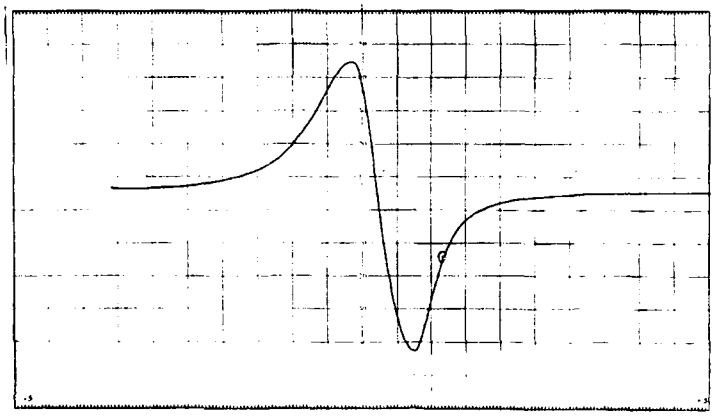

Figure 108. *X–band EPR spectrum of complex[$Cu_2(L)_2$] at LNT with g_{av}=2.08.*

Electronic Spectra

The absorption spectra of the complexes were recorded in DMSO solution. The complex $[Cu_2(L)_2]$ reveals bands at 270 nm and a broad band at 538 nm ($\varepsilon/10^3$ M^{-1} cm^{-1}: 4.81 and 1.73, respectively), which were assigned to ($\pi \rightarrow \pi^*$) and d–d transitions, respectively while the absorption spectrum of complex $[Ni_2(L)_2]$ revealed two bands at 265 nm and 490 nm ($\varepsilon/10^3$ M^{-1} cm^{-1}: 2.40 and 0.95, respectively) due to LMCT and d–d transitions, respectively. The complex $[Sn_2(L)_2.4Cl]$ revealed two bands at 319 nm and 377 nm ($\varepsilon/10^3$ M^{-1} cm^{-1}: 0.99 and 0.62, respectively), which were assigned to intraligand and LMCT transitions, respectively. These results are consistent with the square planar environment around Cu(II) and Ni(II) ions [356].

X–ray powder diffraction analysis

To obtain further evidence about the structure of the metal complexes, X–ray powder diffraction studies of the complexes $[Cu_2(L)_2]$, $[Ni_2(L)_2]$ and $[Sn_2(L)_2.4Cl]$ were performed as it was difficult to isolate single crystals suitable for X–ray crystallography could not be obtained. The crystalline nature of the complex was authenticated by XRPD measurements. Figure 109a–c showed the XRPD patterns indicate crystalline nature for the complexes $[Cu_2(L)_2]$, $[Ni_2(L)_2]$ and $[Sn_2(L)_2.4Cl]$. A summary of the refined XRPD parameters of complexes is given in Table 20.

Table 20. *Summary of the XRPD data and the refinement parameters for complexes* $[Cu_2(L)_2]$, $[Ni_2(L)_2]$ *and* $[Sn_2(L)_2.4Cl]$

Parameter	$[Cu_2(L)_2]$	$[Ni_2(L)_2]$	$[Sn_2(L)_2.4Cl]$
Formula	$C_{60}H_{48}N_4O_{16}Cu_2$	$C_{60}H_{48}N_4O_{16}Ni_2$	$C_{60}H_{48}Cl_4N_4O_{16}Sn_2$
FW	1208.12	1198.48	1460.28
Temperature (K)	298	298	298
Method	Micro crystalline	Micro crystalline	Micro crystalline
Wavelength	1.540598	1.540598	1.540598
Radiation	Cu–Kα1	Cu–Kα1	Cu–Kα1
Crystal System	Monoclinic	Triclinic	Triclinic
Space group	P	P	P
Unit cell			
a(Å)	7.550	7.615	4.329
b(Å)	7.042	10.574	11.192
c(Å)	10.228	10.401	3.983
α°	90	90	90
β°	90	90	90
γ°	90	90	90
2θ range	20–80	20–80	20–80
Limiting	$0 \leq h \leq 8$	$0 \leq h \leq 4$	$0 \leq h \leq 1$
Intensity (%)	17.79–100	20.68–100	33.95–100

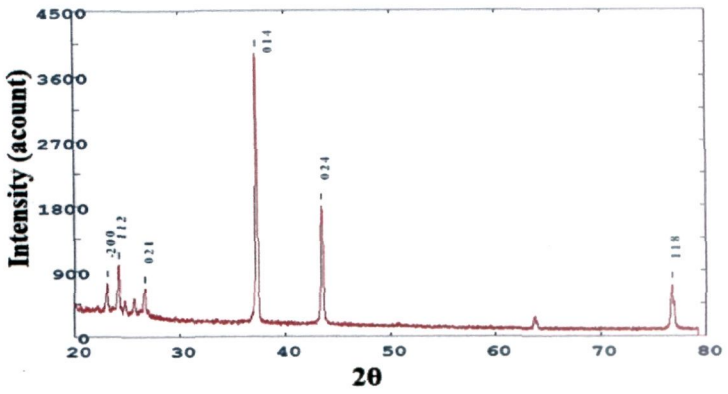

Figure 109. *X–ray powder diffraction patterns of (a) $[Cu_2(L)_2]$ (b) $[Ni_2(L)_2]$ and (c) $[Sn_2(L)_2.4Cl]$ complexes.*

Interaction studies with CT DNA

Absorption titrations

The comparative DNA binding ability of ligand L, complexes $[Cu_2(L)_2]$, $[Ni_2(L)_2]$ and $[Sn_2(L)_2.4Cl]$ and cisplatin drug were evaluated using metal complex–DNA interactions. Figure 110 illustrates the respective absorption spectral changes of the ligand and its complexes in absence and the presence of CT–DNA. Upon addition of increasing amount of CT–DNA (0.00–1.66 x 10^{-5}M) to the fixed amount of complexes/ligand, a significant "hyperchromic" effect with a small bathochromic shift was observed. Complexes $[Cu_2(L)_2]$, $[Ni_2(L)_2]$ and $[Sn_2(L)_2.4Cl]$ and ligand [L] displayed a substantial bathochromic shift of 2–4 nm which supports a higher degree of binding for this complex towards CT–DNA. Thus, from these spectral changes, we deduce that the complexes bind to the CT–DNA by a strong electrostatic interaction mode. The complexes $[Cu_2(L)_2]$, $[Ni_2(L)_2]$ and $[Sn_2(L)_2.4Cl]$ show greater propensity for DNA as compared to free ligand due to the presence of metal centers which is attributed to its strong tendency for phosphate binding.

To study quantitatively, the binding ability of complexes with CT–DNA, the intrinsic binding constant K_b values determined as given in Table 21. The binding constant K_b values follows the order $[Cu_2(L)_2]$ > Cisplatin > $[Ni_2(L)_2]$ > $[Sn_2(L)_2.4Cl]$ > [L]. This relative difference in the K_b values might be the result of different binding mode of the complexes and cisplatin. Cisplatin binds to the CT–DNA *via*, base specific interactions forming 1,2–intrastrand crosslinks between adjacent N7 atoms of guanine (GpG) and adenine nucleobase (ApG) and secondary interaction with phosphate backbone, which obscure the DNA helix to a much larger extent (Figure 110a). Moreover, the K_b values of

the complexes were slightly higher than that of classical minor groove binder 4′,6–diamino–2–phenylindole (DAPI–DNA, 8.90 x $10^3 M^{-1}$ in 2 mM Tris–0.2 mM EDTA containing 30 mM NaCl buffer, pH 8) [357].

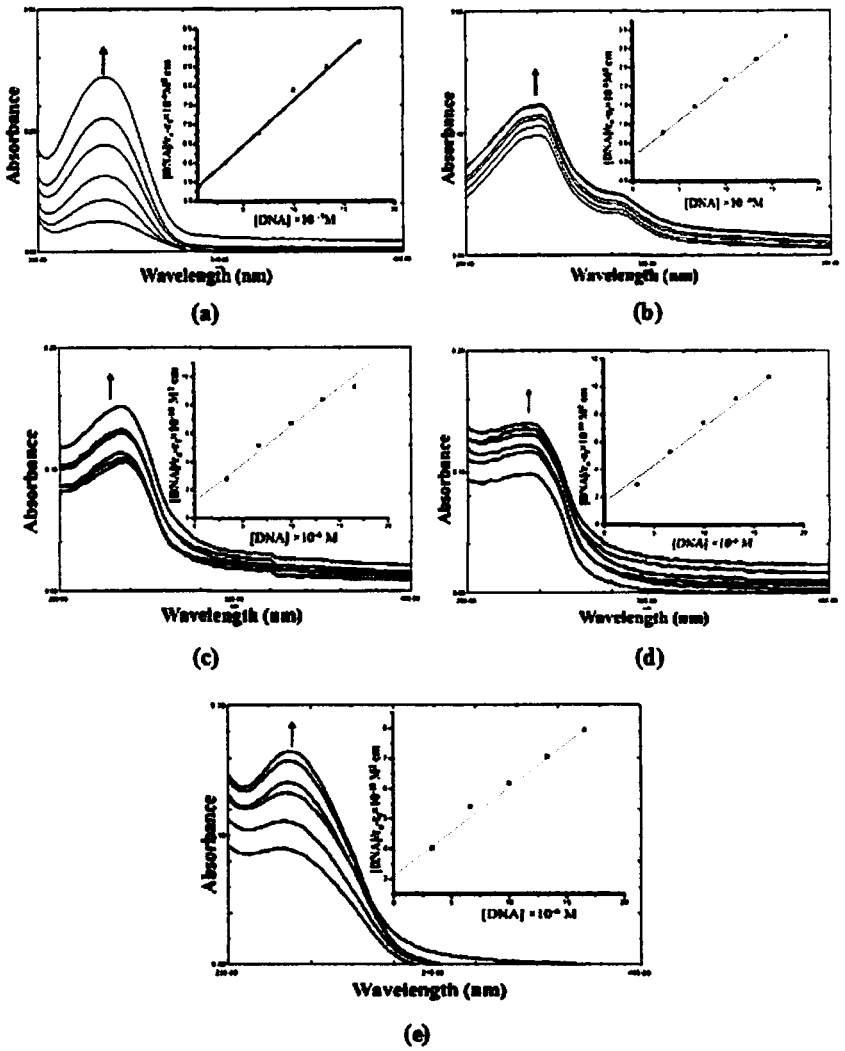

Figure 110. *Absorption spectra of (a) complex $[Cu_2(L)_2]$ (b) complex and $[Ni_2(L)_2]$ and (c) complex $[Sn_2(L)_2.4Cl]$ in Tris–HCl buffer (pH= 7.2) in the absence and presence of increasing amount of CT–DNA. Inset: Plots of [DNA]/(ε_a–ε_f) vs [DNA] for the titration of CT–DNA with complexes. Arrow indicates the increase in the absorbance upon increasing CT–DNA concentration. Plots of [CT–DNA]/ ($\varepsilon_a - \varepsilon_f$) vs. [CT–DNA].*

Table 21. The binding constant (K_b) values of complexes with the CT–DNA

Complexes	K_b (x $10^4 M^{-1}$)	Monitored at(nm)	%Hyperchromism	Bathochromic (nm)
Ligand (L)	1.15	269	22.0	2
$[Cu_2(L)_2]$	3.38	276	37.5	3
$[Ni_2(L)_2]$	2.40	271	38.8	4
$[Sn_2(L)_2.4Cl]$	1.93	258	67.6	2
Cisplatin	2.96	251	60.0	2

NMR studies

To validate our hypothesis the binding of complexes $[Ni_2(L)_2]$ and $[Sn_2(L)_2.4Cl]$ towards DNA, ^1H and ^{31}P NMR techniques at physiological pH were carried out. The ^1H NMR of free oligonucleotide in D_2O showed aromatic base resonances appear between 8.0 and 8.09 ppm, the cytosine H5 and sugar H1′resonances 5.14–5.68 ppm, the sugar H3′ resonances 4.68–5.14 ppm, the sugar H4′/H5′/H5″ resonances 3.88–4.68 ppm and the sugar H2′/H2″ and thymine methyl resonances 1.75–3.24 ppm. The base resonances are usually well resolved, and their assignment to an adenine, guanine, cytosine or thymine is relatively straight forward. The adenine H8 resonances are generally found furthest down field, due to experiencing only small ring current shifts from neighbouring bases, while guanine H8 resonances appear upfield (8.09 ppm). On interaction of complex $[Ni_2(L)_2]$ and $[Sn_2(L)_2.4Cl]$ with DNA, the H8 signal was shifted downfield with a slight decrease in the peak intensity (Figure 111) from 8.09 ppm to 7.49 and 8.21ppm, respectively. However, the ribose proton H1′–H5′ signals for complex $[Ni_2(L)_2]$ and $[Sn_2(L)_2.4Cl]$ were shifted upfield ~1.6 and 0.12 ppm, respectively, which indicate the preference for ribose sugar due to the presence of Ni(II) and Sn(IV) hard Lewis acid center [358].

To confirm the involvement of electrostatic interaction, the ^{31}P signals was appeared at 1.59 ppm (between 1.7 and 2 ppm), are shifted upfield at 0.41 and 0.38 ppm, respectively for $[Ni_2(L)_2]$ and $[Sn_2(L)_2.4Cl]$. The broad signal at 1.59 ppm was attributed to phosphodiester resonance in the DNA. The upfield shift (~1.0 ppm) observed during binding with Ni(II)/Sn(IV) complexes (Figure 112) were attributed to bound metals centers to polyanionic phosphate backbone in DNA [359].

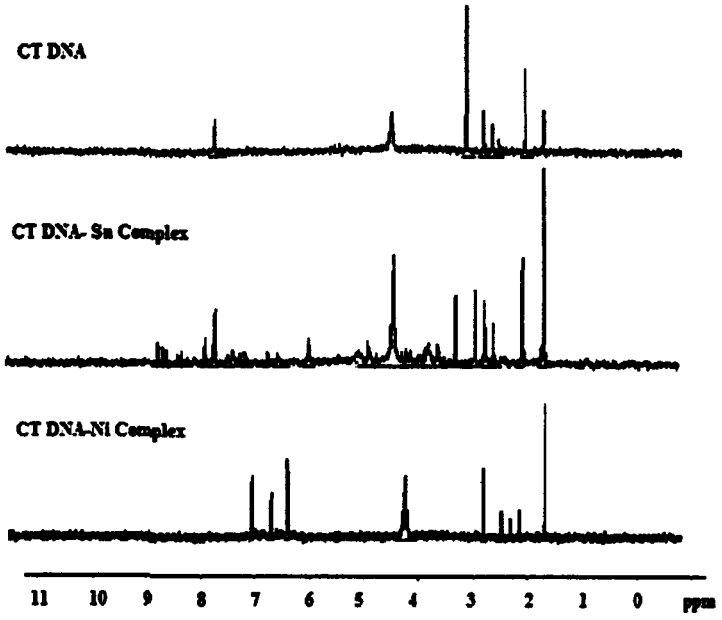

Figure 111. *^1H NMR spectra of (a) DNA alone (b) $[Ni_2(L)_2]$ with DNA and (c) $[Sn_2(L)_2.4Cl]$ with DNA at 25 °C.*

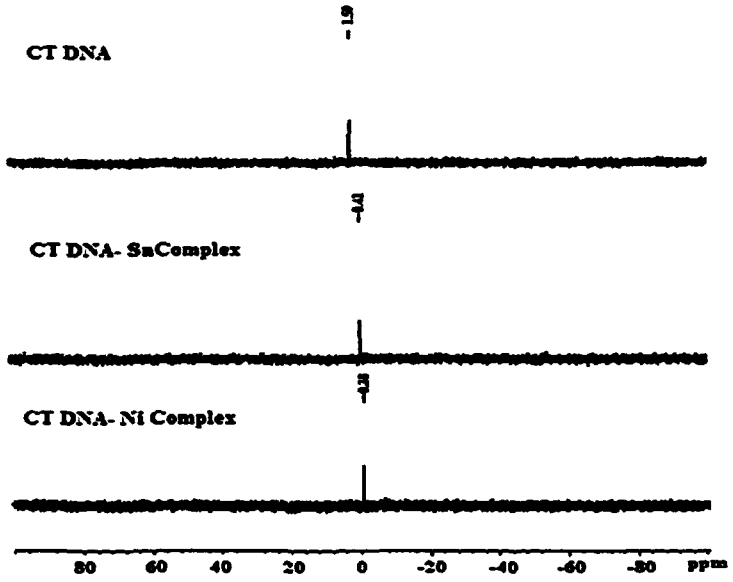

Figure 112. *^{31}P NMR spectra of (a) DNA alone (b) $[Ni_2(L)_2]$ with DNA and (c) $[Sn_2(L)_2.4Cl]$ with DNA at 25 °C.*

Fluorescence spectroscopic studies

The complexes $[Cu_2(L)_2]$, $[Ni_2(L)_2]$ and $[Sn_2(L)_2.4Cl]$ exhibited luminescence either in DMSO or in presence of CT DNA. Hence, binding studies of all metal complexes to CT DNA were carried out by fluorescence spectral titration in absence of any fluorophore [360]. Fixed volumes (1.0×10^{-5} M) of the studied complexes were titrated, respectively with increasing concentration of DNA in the range from ($0.00–1.66 \times 10^{-5}$M). As seen from the Figure 113(a–c), the intensity of emission increased appreciably in the presence of DNA. The observed enhancement could be due to relatively non–polar environment of the bound metal complex in the presence of DNA, such that the complexes were less deeply inserted inside the hydrophobic pockets or grooves of CT–DNA [361]. Cationic complexes usually bind to DNA non–covalently as the cationic core of the complexes exerts a strong electrostatic attraction to the anionic phosphate backbone of DNA thus precluding substantial overlap with the base pairs leading to higher emission intensity

indicative of electrostatic binding of the probe to the DNA. The binding constant (K) estimated for complexes $[Cu_2(L)_2]$, $[Ni_2(L)_2]$ and $[Sn_2(L)_2.4Cl]$ by Scatchard equation were 3.06 x 10^4 M^{-1}, 1.82 x 10^4 M^{-1} and 1.20 x 10^4 M^{-1}, respectively. The binding constant K values were of the order $[Cu_2(L)_2]$ > $[Ni_2(L)_2]$ > $[Sn_2(L)_2.4Cl]$. These results are consistent with the findings obtained from UV–vis spectral studies.

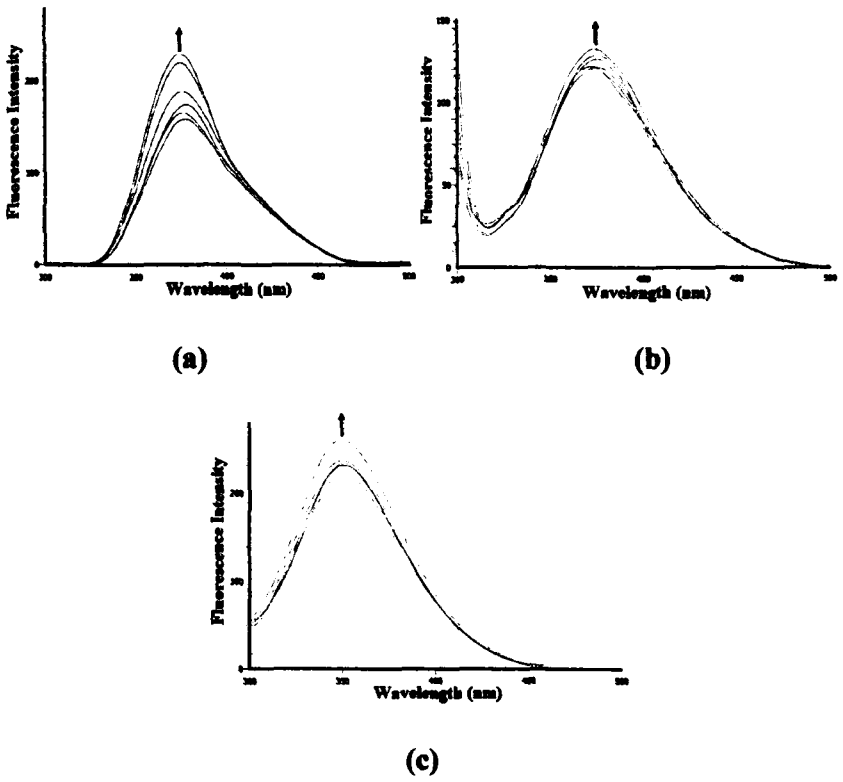

Figure 113. *Emission spectra of (a) complex $[Cu_2(L)_2]$ (b) complex $[Ni_2(L)_2]$ and (c) complex $[Sn_2(L)_2.4Cl]$ in Tris–HCl buffer the absence and presence of CT–DNA. Arrow shows the intensity change upon increasing CT–DNA concentration.*

To demonstrate the interaction strength of the complexes $[Cu_2(L)_2]$, $[Ni_2(L)_2]$ and $[Sn_2(L)_2.4Cl]$ with CT–DNA, steady state emission quenching experiments using $[Fe(CN)_6]^{4-}$ as quencher were also performed [362,363]. The propensity to CT–DNA for the complexes follows the order: $[Cu_2(L)_2]$ > $[Ni_2(L)_2]$ > $[Sn_2(L)_2.4Cl]$ as evidenced by the K_{sv} values given in the Table 22.

Table 22. *Stern Volmer quenching constant of complexes[$Cu_2(L)_2$], [$Ni_2(L)_2$] and [$Sn_2(L)_2$.4Cl] in absence of DNA (K_{sv1}) and in presence of DNA (K_{sv2}) with increasing concentration of quencher[$Fe(CN)_6$]$^{4-}$*

Complex	Emission	Excitation	Monitored at	K_{SV1}	K_{SV2}
$[Cu_2(L)_2]$	377	260	340	4.50	1.50
$[Ni_2(L)_2]$	378	260	320	0.90	0.68
$[Sn_2(L)_2.4Cl]$	355	260	303	0.70	0.61

In the absence of CT–DNA, emission intensity of complex $[Cu_2(L)_2]$ > $[Ni_2(L)_2]$ > $[Sn_2(L)_2.4Cl]$ were efficiently quenched by $[Fe(CN)_6]^{4-}$ as shown in Figure 114. The greater decrease of the K_{sv} value for $[Cu_2(L)_2]$ as compared to $[Ni_2(L)_2]$ and $[Sn_2(L)_2.4Cl]$ indicated higher DNA binding ability of $[Cu_2(L)_2]$. These results are consistent with the electronic absorption titration (Table 22).

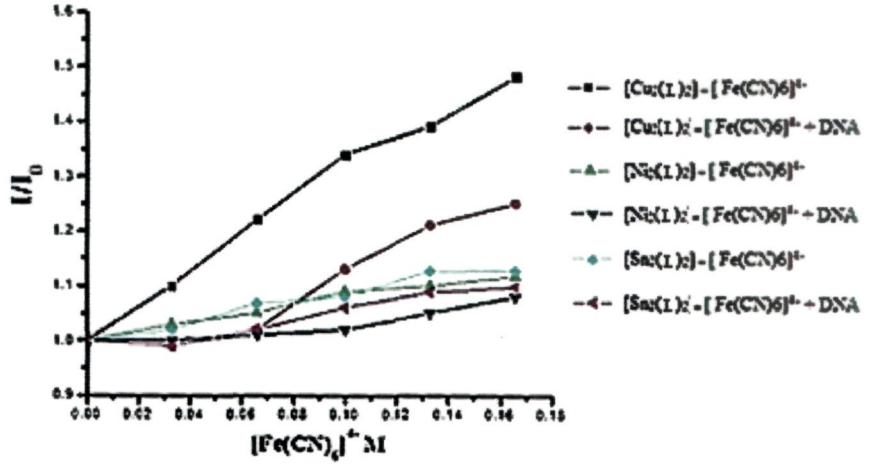

Figure 114. *Emission quenching curves of [$Cu_2(L)_2$], [$Ni_2(L)_2$] and [$Sn_2(L)_2$.4Cl] in absence of CT–DNA and in the presence of CT–DNA. [Complex] = 1.0 x 10^{-5} M.*

Circular dichroic studies

The circular dichroism pattern observed for CT–DNA provide further and definitive confirmation of the probable mode of CT–DNA binding of complexes $[Cu_2(L)_2]$ > $[Ni_2(L)_2]$ > $[Sn_2(L)_2.4Cl]$ which is depicted by the perturbation induced in the DNA morphology upon the binding of complexes to CT–DNA (Figure 115). Complexes $[Cu_2(L)_2]$ > $[Ni_2(L)_2]$ > $[Sn_2(L)_2.4Cl]$ displays increase in the positive band with respect to DNA accompanied by a large increase in the negative band. This corroborates well with the hypothesis in literature that simple groove binding and electrostatic interaction of the complexes with DNA shows less or no perturbation on the base stacking and helicity bands while intercalator enhances the intensities of both the bands [364]. These results support groove binding nature of the complexes $[Cu_2(L)_2]$ > $[Ni_2(L)_2]$ > $[Sn_2(L)_2.4Cl]$ probably due to some partial intercalative interactions which modifies the CT–DNA morphology during drug–DNA interactions.

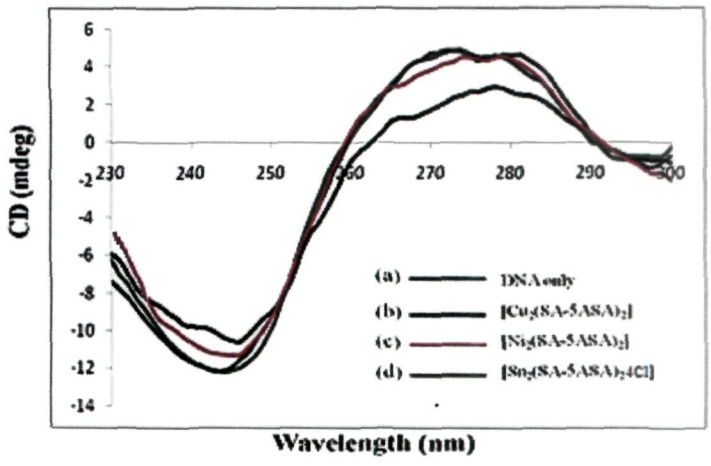

Figure 115. *CD spectrum of CT–DNA in the absence and presence of complexes (1.0 x 10^{-5}M), (a) —, DNA alone; (b) —,$[Cu_2(L)_2]$ +DNA, (c)— $[Ni_2(L)_2]$+DNA, and (d) —, $[Sn_2(L)_2.4Cl]$ +DNA.*

Gel electrophoresis

The complex $[Cu_2(L)_2]$ showed maximum binding propensity with CT–DNA, therefore, the cleavage activity has been evaluated for complex $[Cu_2(L)_2]$. It has been well established in literature that copper(II) complexes are selective for the cleavage of DNA either through oxidative or hydrolytic mechanism. The nuclease activity of complex $[Cu_2(L)_2]$ was studied using supercoiled pBR322 DNA as a substrate (Figure 116). To ascertain the DNA cleavage ability of complex, supercoiled pBR322 DNA was incubated with different concentration of complex in aqueous buffer solution (5mM Tris–HCl/40 mM NaCl, pH 7.4) without addition of any reductant.

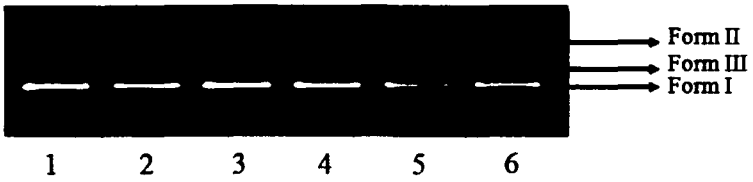

***Figure 116.** The cleavage patterns of the agarose gel electrophoresis for pBR322 plasmid DNA (300ng) by $[Cu_2(L)_2]$; Lane 1: DNA control; Lane 2: 10 μM complex + DNA; Lane 3: 15 μM complex + DNA; Lane 4: 20 μM complex + DNA; Lane 5: 30 μM complex + DNA; Lane 6: 40 μM complex + DNA.*

As shown in Figure 116, there was a gradual decrease in the amount of Form I with a simultaneous increase in Form II (Lanes 2 and 4) on increasing the concentration of the complex. A notable cleavage feature observed for this complex is the appearance of Form III before the disappearance of Form I (Lanes 5 and 6). The reduction in the intensity of Form I and appearance of more intense Form II of pBR322 DNA on the gel shows that the complex $[Cu_2(L)_2]$ is involved in an efficient double strand DNA cleavage pathway. In the presence of activators *viz*; glutathione (GSH), ascorbic acid (Asc), hydrogen peroxide (H_2O_2) and mercaptopropionic acid (MPA), the complex $[Cu_2(L)_2]$ showed

significant increase in the cleavage of the DNA and follows the order H_2O_2> MPA >GSH ≈Asc (Figure 117).

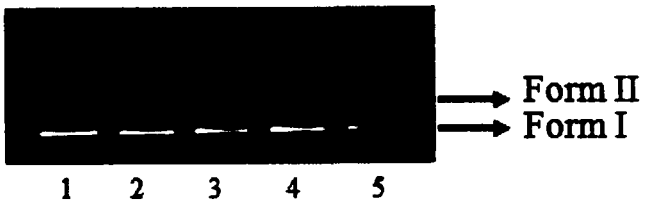

Figure 117. *Agarose gel electrophoresis pattern for the cleavage pattern of pBR322 plasmid DNA (300ng) by complex [$Cu_2(L)_2$] (30 μM) in presence of different activating agent at 37 °C after incubation for 45 min. Lane 1, DNA control; Lane 2, DNA + [$Cu_2(L)_2$] + Asc (40 μM); Lane 3, DNA + [$Cu_2(L)_2$]+ H_2O_2 (40 μM); Lane 4, DNA + [$Cu_2(L)_2$]+ GSH (40 μM);*); *Lane 5, DNA + [$Cu_2(L)_2$]+ MPA (40 μM).*

Minor groove binding agent (DAPI) [365] and major groove binding agent (Methyl Green) [366] were used to probe the potential interacting sites of complex [$Cu_2(L)_2$] with pBR322 DNA (Figure 118). The cleavage patterns, demonstrated that in presence of methyl green DNA cleavage activity is affected significantly, suggesting that minor groove are involved in the complex–DNA interactions.

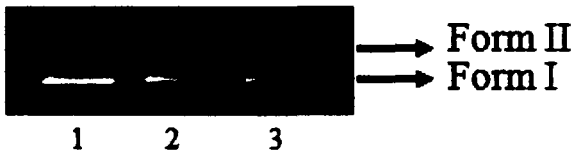

Figure 118. *Agarose gel electrophoresis pattern for the cleavage of pBR322 plasmid DNA (300ng) by complex [$Cu_2(L)_2$] (30 μM) in the presence of DNA minor binding agent DAPI and major binding agent methyl green at 37 °C after incubation for 30 min. Lane 1, DNA control; Lane 2, DNA + [$Cu_2(L)_2$]+ DAPI (8 μM); Lane 3, DNA + [$Cu_2(L)_2$]+ Methyl green (2.5 μL of a 0.01mg/ml solution).*

In order to identify the reactive oxygen species that are responsible for the DNA cleavage reaction, experiments in the presence different common scavengers such as DMSO and Ethyl alcohol (hydroxyl radical scavengers), NaN_3 (singlet oxygen scavenger) and SOD (superoxide oxygen scavenger) were carried out, respectively with [$Cu_2(L)_2$].

As shown in Figure 119. The cleavage activity of $[Cu_2(L)_2]$ is reduced dramatically by the presence of hydroxyl radical scavengers ethyl alcohol and DMSO (Figure 119, lanes 2,3), indicating that the freely diffusible hydroxyl radical is one of the intermediates involved in the DNA scission process. On the other hand, addition of sodium azide (singlet oxygen scavenger) decreases the cleavage efficiencies, this reveals that $^1O_2$ is also the activated oxygen intermediate responsible for the cleavage (Figure 119, Lane 5). Addition of superoxide dismutase (superoxide scavenger) to the reaction mixture reveals no significant quenching of the cleavage reaction indicating that superoxide anion is not the active species responsible for the cleavage (Figure119, Lane 4) [367]. Thus, freely diffusible oxygen intermediate or hydroxyl radical may be involved in the strand scission and hence a simple diffusible radical mechanisms applicable. Since the complex $[Cu_2(L)_2]$ are able to cleave DNA in the absence of any reducing agent, it may be assumed that DNA might be cleaved by a discernible hydrolytic path.

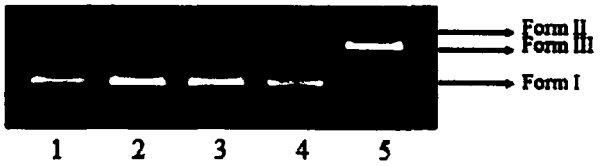

Figure 119. *Agarose gel electrophoresis pattern for the cleavage pattern of pBR322 plasmid DNA (300 ng) in the presence of different activating agents at 310 K after 45 min of incubation in buffer (5mM Tris–HCl/50 mM NaCl, pH = 7.2) by $[Cu_2(L)_2]$ (30 μM), Lane 1, DNA control; Lane 2, DNA+metal complex+DMSO (0.4 μM); Lane 3, DNA+metal complex+EtOH (0.4 μM); Lane 4, DNA+metal complex+NaN_3 (0.4 μM);Lane 5, DNA+metal complex+Superoxide Dismutase (15 Units).*

Conclusion

An analogous parallel series of complexes of metals {Cu(II)/Ni(II) and Sn(IV)} was designed and synthesized to ascertain structure–activity relationship of these complexes towards cellular target DNA. The synthesis of macrocyclic–Schiff base ligand derived from salicylaldehyde derivative and 5–aminosalicylic acid was carried out and sub equally, the ligand was allowed to react with metal ions to yield binuclear complexes in the solid form and their structure was proposed by various physico–chemical and spectroscopic data.

The *in vitro* DNA binding studies *viz*; absorption titrations, fluorescence, NMR and circular dichorism in free complexes and in presence of DNA supported that the complexes $[Cu_2(L)_2]$, $[Ni_2(L)_2]$ and $[Sn_2(L)_2.4Cl]$ bind to DNA by noncovalent mode of binding by electrostatic interaction *via* phosphate backbone of the helix.

The complex $[Cu_2(L)_2]$ exhibited highest DNA binding affinity and Cu(II) complex $[Cu_2(L)_2]$ binds DNA more avidly than the other metal complexes Ni(II) and Sn(IV), respectively, which was quantified by their intrinsic binding constant K_b values. Interaction between complex $[Cu_2(L)_2]$ and pBR322 DNA has also been investigated by agarose gel electrophoresis, noticeably, the Cu(II) complex $[Cu_2(L)_2]$ exhibited an outstanding ability to affect DNA double strand scission in hydrolytic cleavage.

References

[1] C. Sanchez–Cano and M. J. Hannon, *Dalton Trans.*, (2009), 10702.

[2] P.C.A. Bruijnincx and P.J. Sadler, *Curr. Opin. Chem. Biol.*, (2008), **12**, 197.

[3] C. Orvig and M.J. Abrams, *Chem. Rev.*, (1999), **99**, 2201.

[4] C.X. Zhang and S.J. Lippard, *Curr. Opin. Chem. Biol.*, (2003), 7, 481.

[5] L. Kelland, *Nature Rev.*, (2007), 7, 573.

[6] K.L. Haas and K.J. Franz., *Chem. Rev.*, (2009), **109**, 4921.

[7] Z. Guo and P.J. Sadler, *Angew. Chem. Int. Ed.*, (1999), **38**, 1512.

[8] P. Caravan, J.J. Ellison, T.J. McMurry and R.B. Lauffer, *Chem. Rev.*, (1999), **99**, 2293.

[9] S.M. Cohen, *Curr. Opin. Chem. Biol.*, (2007), **11**, 115.

[10] L.H. Hurley, *J. Med. Chem.*, (1989), **32**, 2027.

[11] P.D. Garimella, A. Datta, D.W. Romanini, K.N. Raymond and M.B. Francis, *J. Am. Chem. Soc.*, (2011), **133**, 14704.

[12] (a) J. Xu, D.G. Churchill, M. Botta and K. N. Raymond, *Inorg. Chem.*, (2004), **43**, 5492. (b) S. Liu and D.S. Edwards, *Chem. Rev.*, (1999), **99**, 2235.

[13] (a) V. Sharma and D. Piwnica–Worms, *Chem. Rev.*, (1999), **99**, 2545. (b) S.S. Jurisson and J.D. Lydon, *Chem. Rev.*, (1999), **99**, 2205.

[14] A.L. Noffke, A. Habtemariam, A.M. Pizarro and P.J. Sadler, *Chem. Commun.*, (2012), **48**, 5219.

[15] I. Ahn and J. Park, *BioSystems*, (2011), **106**, 121.

[16] S.H. van Rijt and P.J. Sadler, *Drug Discovery Today*, (2009), **14**, 1089.

[17] A.M. Pizarro and P.J. Sadler, *Biochimie*, (2009), **91**, 1198.

[18] S. Shivharel and M.D. Gautam, *J. Curr. Pharma.Res.*, (2011), **6**, 16.

[19] M. Sönmez, İ. Berber and E. Akbaş, *Eur. J. Med. Chem.*, (2006), **41**, 101.

[20] A. Bacchi, M. Carcelli, C. Compari, E. Fisicaro, N. Pala, G. Rispoli, D. Rogolino, T. W. Sanchez, M. Sechi, V. Sinisi and N. Neamati, *J. Med. Chem.*, (2011), **54**, 8407.

[21] X. Li and R. Vince, *Bioorg. Med. Chem.*, (2006), **14**, 5742.

[22] S.K. Bharti and Sushil K. Singh, *Der Pharmacia Lett.*, (2009), **1**, 39.

[23] S.P. Fricker, *Dalton Trans.*, (2007), 4903.

[24] K.H. Thompson and C. Orvig, *Dalton Trans.*, (2006), 761.

[25] L.R. Kelland, S.Y. Sharp, C.F.O'Neill, F.I. Raynaud, P.J. Beale and I.R. Judson, *Inorg. Biochem.*, (1999), **77**, 111.

[26] S. van Zutphen and J. Reedijk, *Coord. Chem. Rev.*, (2005) **249**, 2845.

[27] E. Reisner, V.B. Arion, B.K. Keppler and A.J.L. Pombeiro, *Inorg. Chim. Acta*, (2008), **361**, 1569.

[28] M.D. Hall and T.W. Hambley, *Coord. Chem. Rev.*, (2002), **232**, 49.

[29] L. Feng, A. De Dille, V.J. Jameson, L. Smith, W.S. Dernell and M.C. Manning, *Cancer Chemother. Pharmacol.*, (2004), **54**, 441.

[30] Q.–S. Ye, W.–P. Liu, X.–Z. Chen, Y. Yu, Q.–W. Chang and S.–Q. Hou, *Arch. Pharm. Res.*, (2010), **33**, 807.

[31] X. Wang, Y. Wang, Z.G. Chen and D.M. Shin, *Cancer Res. Treat.*, (2009), **41**, 1.

[32] C. Bokemeyer, C.C. Berger, J.T. Hartmann, C. Kollmannsberger, H.–J. Schmoll, M. A. Kuczyk and L. Kanz, *British J. Cancer*, (1998), **77**, 1355.

[33] I. Ott and R. Gust, *Arch. Pharm. Chem. Life Sci.*, (2007), **340**, 117.

[34] S.H. van Rijt and P.J. Sadler, *Drug Discov Today*, (2009), **14**, 1089.

[35] R. Bakhtiar and E.–I. Ochiai, *Gen. Pharma.*, (1999) **32**, 525.

[36] N. Kamaly, Z. Xiao, P.M. Valencia, A.F. Radovic–Moreno and O.C. Farokhzad, *Chem. Soc. Rev.*, (2012), **41**, 2971.

[37] B. Lippert, *Coord. Chem. Rev.*, (2000), **200 – 202**, 487.

[38] G.J. Puppels, C. Otto and J. Greve, *Biochemistry*, (1994), **33**, 3386.

[39] A.M. Macmillan, *pure. Appl. Chem.*, (2004), **76**, 1521.

[40] A. H.–J. Wang, G. J. Quigley, F.J. Kolpak, J.L. Crawford, J.H. van Boom, G. van der Marel and A. Rich, *Nature (London)*, (1979), **282**, 680.

[41] G. Song and J. Ren, *Chem. Commun.*, (2010), **46**, 7283.

[42] W. Zacharias, A. Jaworski, J.E. Larson and R.D. Wells, *Proc. Nati. Acad. Sci. USA*, (1988), **85**, 7069.

[43] (a) R. Martinez and L.C. Garcia, *Curr. Med. Chem.*, (2005), **12**, 127. (b) S. Biagini, A. Bianchi, T. Biver, A. Boggioni, I.V. Nikolayenko, F. Secco and M. Venturini, *J. Inorg. Biochem.*, (2011), **105**, 558.

[44] (a) E. Tuite, U. Shehlstedt, P. Hagmer, B. Norden and M. Takahashi, *Euro. J. Biochem.*, (1997), **243**, 482. (b) S. Rajkalashmi, T. Weyhemuller, A.J. Freddy, H.R. Vasanthi and B.U. Nair, *Euro. J. Med. Chem.*, (2011), **46**, 608.

[45] (a) M.J. Hannon, *Chem. Soc. Rev.*, (2007), **36**, 280. (b) F. Arjmand and M. Ghauhan, *J. Organomet. Chem.*, (2007), **692**, 5156.

[46] N. Grover, T.W. Welch, T.A. Fairley, M. Cory and H.H. Thorp, *Inorg. Chem.*, (1994), **33**, 3544.

[47] M.–H David–Cordonnier, W. Laine, A. Lansiaux, F. Rosu, P. Colson, E. de Pauw, S. Michel, F. Tillequin, M. Koch, J.A. Hickman, A. Pierre′ and C. Bailly, *Mol Cancer Ther.*, (2005), **4**, 71.

[48] B.M. Zeglis, Valerie C. Pierre and J.K. Barton, *Chem. Comm.*, (2007), 4565.

[49] M.Ortiz–Lombardia, A. Gonzalez, R. Eritja, J. Aymami, F. Azorin and M. Coll, *Nat. Struct. Biol.*, (1999), **6**, 913.

[50] D.R. Boer, A. Canals and M. Coll, *Dalton Trans.*, 2009, 399.

[51] (a) L.R. Kelland and N.P. Farrell (Eds.), *Platinum–Based Drugs in Cncer Therapy*, Humana Press, Totowa, (2000), 321. (b) E. Rosenberg, F. Spada, K. Sugden, B. Martin, R. Gobetto, L. Milone, A. Viale and J. Fiedler, *J. Organomet. Chem.*, (2003), **668**, 51.

[52] L.J.K. Boerner and J.M. Zaleski, *Curr. Opin. Chem. Biol.*, (2005), **9**, 135.

[53] J.K. Borton, A. Danishefsky and J. Goldberg, *J. Am. Chem. Soc.*, (1984), **106**, 2172.

[54] S.S. Bhat, A.A. Kumbhar, H. Heptullah, A.A. Khan, V.V. Gobre, S.P. Gejji and V.G. Puranik, *Inorg. Chem.*, (2011), **50**, 545.

[55] J.L. Nitiss, *Nat. Rev. Cancer*, (2009), **9**, 338.

[56] K.–J. Du, J.–O. Wang, J.–F. Kou, G.–Y. Li, L.–L. Wang, H. Chao and L.–N. Ji, *Eur. J. Med. Chem.*, (2011), **46**, 1056.

[57] C.–M. Che and F.–M. Siu, *Curr. Opin. Chem. Biol.*, (2010), **14**, 255.

[58] B. Rosenberg, L.V. Camp and T. Krigas, *Nature*, (1965), **205**, 698.

[59] B.J. Thompson, *Curr. Opin.Cell Biol.*, (2010), **22**, 788.

[60] C.T. Jordan, *Curr. Opin. Cell Biol.*, (2004), **16**, 708.

[61] R.R. Langley and I.J. Fidler, *Endo. Rev.*, (2007), **28**, 297.

[62] J.J. Tyson, K. Chen and B. Novak, *Reviews*, (2001), **2**, 908.

[63] J.M. Brown and A.J. Giaccia, *Cancer Res.*, (1998), **58**, 1408.

[64] T.W. Hambley, *Dalton Trans.*, (2007), 4929.

[65] G. Gasser, I. Ott and N. Metzler–Nolte, *J. Med. Chem.*, (2011), **54**, 3.

[66] M.D. Hall, T.W. Failes, N. Yamamotoa and T.W. Hambley, *Dalton Trans.*, (2007), 3983.

[67] T.W. Failes, C. Cullinane, C.I. Diakos, N. Yamamoto, J.G. Lyons and T.W. Hambley, *Chem. Eur. J.*, (2007), **13**, 2974.

[68] P.J. Blower, J.R. Dilworth, R.I. Maurer, G.D. Mullen,C.A. Reynolds, Y. Zheng, *J. Inorg. Biochem.*, (2001) **85**, 15.

[69] J.L.J. Dearling, J.S. Lewis, G.E.D. Mullen, M.T. Rae, J. Zweit and P.J. Blower, *Eur. J. Nucl. Med.*, (1998), **25**, 788.

[70] N. Graf and S.J. Lippard, *Adv. Drug Delivery Rev.*, (2012) in press.

[71] H. Tapiero and K.D. Tew, *Biomed. Pharmacother.*, (2003), **57**, 399.

[72] N. Ferrell, *Coord. Chem. Rev.*, (2002), **232**, 1.

[73] E. Ho, *J. Nut.Biochem.*, (2004), **15**, 572.

[74] M.D. Vaira, C. Bazzicalupi, P. Orilioli, L. Messori, B Bruni and P. Zatta, *Inorg. Chem.*, (2004), **43**, 3795.

[75] A. Tarushi, C.P. Raptopoulou, V. Psycharis, A. Terzis, G. Psomas and D.P. Kessissoglou, *Bioorg. Med. Chem.*, (2010), **18**, 2678.

[76] F. Arjmand and S. Parveen, *RSC Adv.*, (2012), **2**, 6354.

[77] F. Yao, J. He, X. Li, H. Zou, Z. Yuan, *Sensors and Actuators B*, (2012), **161**, 886.

[78] R. Nair, A. Shah, S. Baluja and S. Chanda, *J. Serb. Chem. Soc.*, (2006), **71**, 733.

[79] P. Lemoine, B. Viossat, N.H. Dung, A. Tomas, G. Morgant, F.T. Greenaway and J.R.J. Sorenson, *J. Inorg. Biochem.*, (2004), **98**, 1734.

[80] H. Sakurai, Y. Kojima, Y. Yoshikawa, K. Kawabe and H. Yasui, *Coord. Chem. Rev.*, (2002), **226**, 187.

[81] C.T. Dillon, T.W. Hambley, B.J. Kennedy, P.A. Lay, Q. Zhou, N.M. Davies, J.R. Biffin and H.L. Regtop, *Chem. Res. Toxicol.*, 2003, **16**, 28.

[82] A.A.Osowole, I. Ott and O.M. Ogunlana, *Int. J. Inorg. Chem.*, (2012), **2012**, 1.

[83] D.K. –Demertzi, P.N. Yadav, J. Wiecek, S. Skoulika, T. Varadinova and M.A. Demertzis, *J. Inorg. Biochem.*, (2006), **100**, 1558.

[84]A. Tarushi, G. Psomas, C. P. Raptopoulou and D. P. Kessissoglou, *Inorg.Biochem.*, (2009), **103**, 898.

[85] F.M. Pohl, T.M. Jovin, W. Baehr, and J.J. Holbrook, *Proc. Nat. Acad. Sci. USA*, (1972), **69**, 3805.

[86] C.G. Reinhardt and T.R. Krugh, *Biochemistry*, (1978), **17**, 4845.

[87] G. Zhao, H. Lin, S. Zhu, H. Sun and Y. Chen, *Inorg. Biochem.*, (1998), **70**, 219.

[88] S. Tabassum, S. Mathur, F. Arjmand, K. Mishra and K. Banerjee, *Metallomics*, (2012), **4**, 205.

[89] A.R. Timerbaev, C.G. Hartinger and B.K. Keppler, *Trends in Analytical Chemistry*, (2006), **25**, 868.

[90] Z. Jakopin, E. Corsini, M. Gobec, I. Mlinarič–Raščan and M.S. Dolenc, *Eur. J. Med. Chem.*, (2011), **46**, 3762.

[91] S. Traub, N. Kubasch, S. Morath, M. Kresse, T. Hartung, R.R. Schmidt and C. Hermann, *J. Biol. Chem.*, (2004), **279**, 8694.

[92] K. Dzierzbicka and A.M. Kołodziejczyk, *Polish J. Chem.*, (2003), 77, 373.

[93] K. Dzierzbicka and A.M. Kołodziejczyk, *J. Med. Chem.*, (2003), **46**, 183.

[94] K. Dzierzbicka, A.M. Kołodziejczyk, B. Wysocka–Skrzela, A. Myśliwski and D. Sosnowska, *J. Med. Chem.*, (2001), **44**, 3606.

[95] J. Turanek, M. Ledvina, A. Kasna, A.Vacek, V. Hrıbalova, J. Krejcı and A. D. Miller, *Vaccine*, (2006), **24S2**, S2/90.

[96] C.D. Leclerc, F.M. Audibert, L.A. Chedid, E.J. Deriaud, N.K. Masihi and E. Lederer, *Infect.Immun.*, (1984), **43**, 870.

[97] Z. Zidek, *Agents Actions*, (1994), **42**, 163.

[98] D. Kikelj, S. Pečar, V. Kotnik, A. Štalc, B. Wraber–Herzog, S. Simčič, A. Ihan, L. Klamfer, L. Povšič, R. Grahek, E. Suhadolc, M. Hočevar, H. Hönig and R. Rogi–Kohlenprath, *J. Med. Chem.*, (1998), **41**, 530.

[99] U. Urleb, A. Krbavčič, M. Sollner, D. Kikelj, S. Pečar, *Arch.Pharm. (Weinheim)*, (1995), **328**, 113.

[100] C. Ochi, N. Norisada, M. Moriguchi, A. Štalc, U. Urleb and S. Muraoka, *Drug Res.*, (1999), **49**, 72.

[101] M. Moriguchi, N. Norisada, C. Ochi, A. Štalc, U. Urleb and S. Muraoka, *Drug Res.*, (1999), **49**, 184.

[102] J.C. Mai, Z. Mi, S.–H, Kim, B. Ng and P.D. Robbins, *Cancer Res.*, (2001), **61**, 7709.

[103] S. Kim, S.S. Kim, Y.–J. Bang, S.–J. Kim and B.J. Lee, *Peptides*, (2003), **24**, 945.

[104] J. Molnar, H. Engi, Y. Mandi, C. Somlai, B. Penke, A. Szabo and A. Orosz, *in vivo*, (2007), **21**, 429.

[105] F.J. Sharom, G. DiDiodota, X. Yu and K.J.D. Ashbourne, *J. Biol. Chem.*, (1995), **270**, 10334.

[106] C.A. Claussen and E.C. Long, *Chem. Rev.*, (1999), **99**, 2797.

[107] C. Achim, B.A. Armitage, D.H. Ly and J.W. Schneider, *Wiley Encyclopedia of chemical biology*, (2008), 1.

[108] K. Harford and B. Sarkar, *Acc. Chem. Res.*, (1997), **30**, 123.

[109] K. Karidi, J. Reedijk, N. Hadjiliadis and A. Garoufis, *J. Inorg. Biochem.*, (2007), **101**, 1483–1491.

[110] M.P. Fitzsimons and J.K. Barton, *J. Am. Chem. Soc.*, (1997), **119**, 3379.

[111] C.A. Hastings and J.K. Barton, *Biochemistry*, (1999), **38**, 10042.

[112] J.B. Blanco, V.I. Dodero, M.E. Vázquez, M. Mosquera, L. Castedo and J.L. Mascareñas, *Angew, Chem., Int. Ed.*, (2006), **45**, 8210.

[113] Y. Jin, M.A. Lewis, N.H. Gokhale, E.C. Long and J.A. Cowan, *J. Am. Chem. Soc.*, (2007), **129**, 8353.

[114] E. Kimoto, H. Tanaka, J. Gyotoku, F. Morishige and L. Pauling, *Cancer Res.*, (1983), **43**, 824.

[115] S.–H. Chiou, *J. Biochem.*, (1983), **94**, 1259.

[116] (a) D.P. Mack and P.B. Dervan, *Biochemistry*, (1992), **31**, 9399. (b) D.P. Mack and P.B. Dervan, *J. Am. Chem. Soc.*, (1990), **112**, 4604. (c) D.P. Mack, B.L. Iverson and P.B. Dervan, *J. Am. Chem. Soc.*, (1988), **110**, 7572.

[117] (a) M. Nagaoka, M. Hagihara, J. Kuwahara and Y. Sugiura, *J. Am. Chem. Soc.*, (1994), **116**, 4085. (b) C. Harford, S. Narindrasorasak and B. Sarkar, *Biochemistry*, (1996), **35**, 4271.

[118] G. Facchin, M.H. Torre, E. Kremer, O.E. Piro, E.E. Castellano and E.J. Baran, *Inorg. Biochem.*, (2002), **89**, 174.

[119] N.A. Roberts and P.A. Robinson, *Br. J. Rheumatol.*, (1985), **24**,128.

[120] S.L. Lippard and J.M. Berg, *Principles of Bioinorganic Chemistry*, University Science Books, Mill Valley, CA, USA, (1994). p.p.175.

[121] J.J. Goto, H. Zhu, R.J. Sanchez, A. Nersissian, E.B. Gralla and J.S. Valentine, *J. Biol. Chem.*, (2000), **275**, 1007.

[122] S. Fukahori, T. Fujiwara, Ryusei Ito and N. Funamizu, *Desalination*, (2011), **275**, 237.

[123] R.C. Maurya and S. Rajput, *J.Mol. Struct.*, (2006), **794**, 24.

[124] M.R. Caira, *Mol. Pharma.*, (2007), **4**, 310.

[125] Z. Xu, C. Song, Y. Hu and G. Li, *Talanta*, (2011), **85**, 97.

[126] G.G. Mohamed, M.A.M. Gad–Elkareem, *Spectrochim. Acta A*, (2007), **68**, 1382.

[127] A.M. Bayly and I.G. Macreadie, *Rends in Parasitology*, (2002), **18**, 49.

[128] D. Mandloi, S. Joshi, P.V. Khadikarc and N. Khosla, *Bioorg. Med. Chem. Lett.*, (2005), **15**, 405.

[129] H. Akgün, I. Karamelekoğlu, B. Berk, I. Kurnaz, G. Sarıbıyık, S. Öktem and T Kocagöz, *Bioorg. Med. Chem.*, (2012), **20**, 4149.

[130] A. Hangan, A. Bodoki, L. Oprean, G. Alzuet, M. Liu–González and J. Borrás, *Polyhedron*, (2010), **29**, 1305.

[131] H. Schiff, *Ann. Chem. Pharm.*, (1864), **131**, 118.

[132] S. Adsule, V. Barve, D. Chen, F. Ahmed, Q. Ping Dou, S. Padhye and F.H. Sarkar, *J. Med. Chem.*, (2006), **49**, 7242.

[133] I. Sakiyan, E. Logoglu, S. Arslan, N. Sari and N. Sakiyan, *Biometals*, (2004), **17**, 115.

[134] R. Karmakar, C. R. Choudhury, S. Mitra and L. Dahlenburg, *Struct. Chem*, (2005), **16**, 611.

[135] P. More, R. B. Bhalvankar and S.C. Patter, *J. Indian Chem. Soc.*, (2001), **78**, 474.

[136] Z.H. Chohan, M. Praveen and A. Ghaffar, *Metal– Based Drugs*, (1997), **4**, 267.

[137] M. Nath, S. Pokharia and R. Yadav, *Coord. Chem. Rev.*, (2001), **215**, 99.

[138] A. Pal, B. Biswas, S.K. Mondal, C.–H. Lin, R. Ghosh, *Polyhedron*, (2012), **31**, 671.

[139] H.–J Yu, S.–M. Huang, L.–Y. Li, H.–N. Jia, H. Chao, Z.–W. Mao, J.–Z. Liu, and L.–N. Ji, *J. Inorg. Biochem.*, (2009), **103**, 881.

[140] E. Rüba, J.R. Hart, and J.K. Barton, *Inorg. Chem.*, (2004), **43**, 4570.

[141] C. Hiort, P. Lincoln and B. Norden, *J. Am. Chem. Soc.*, (1993), **115**, 3448.

[142] J. Liu, W.J. Mei, L.J. Lin, K.C. Zheng, H. Chao, F.C. Yun and L.N. Ji, *Inorg. Chim. Acta*, (2004), **357**, 285.

[143] S.–P. Tang, L. Hou, Z.–W. Mao and L.–N. Ji, *Polyhedron*, (2009), **28**, 586.

[144] V. Uma, A. Castineiras and B.U. Nair, *Polyhedron*, (2007), **26**, 3008.

[145] J.A. Cowan, *Curr. Opin. Chem. Biol.*, (2001), **5**, 634.

[146] A. Sreedhara and J.A. Cowan, *J. Biol. Inorg. Chem.*, (2011), **6**, 337.

[147] F. Arjmand and M. Muddassir, *Chirality*, (2011), **23**, 250.

[148] J.K. Barton and A.L. Raphael, *J. Am. Chem. Soc.*, (1984), **106**, 2466.

[149] K. Ghosh, P. Kumar, N. Tyagi, U.P. Singh and N. Goel, *Inorg. Chem.Comm.*, (2011), **14**, 489.

[150] J. Chen, X. Wang, Y. Shao, J. Zhu, Y. Zhu , Y. Li, Q. Xu and Z. Guo, *Inorg. Chem.*, (2007), **46**, 3306.

[151] K. Ghosh, P. Kumar, N. Tyagi, U.P. Singh, V. Aggarawal, M.C. Baratto, *Eur. J. Med. Chem.*, (2010), **45**, 3770.

[152] F. Gao and H. Chao, L.–N. Ji, *Chem. Biodivers.*, (2008), **5**, 1962.

[153] W. Feng, M. Satyanarayana, Y.–C Tsai, A.A. Liu, L.F. Liu and E.J. LaVoie, *Eur. J. Med. Chem.*, (2009), **44**, 3433.

[154] (a) M.L. Rothenberg, *Ann. Oncol.*, (1997), **8**, 837. (b) B.A. Teicher, *Biochem. Pharmacol.*, (2008), **75**, 1262.

[155] J.M. Fortune, L. Valea, D.E. Graves, T. Utsugi, Y. Yamada and N. Osheroff, *Biochemistry*, (1999), **38**, 15580.

[156] K.–J. Du, J.–Q. Wang , J.–F. Kou, G.–Y. Li , L.–L. Wang , H. Chao and L.–N. Ji, *Eu. J. Med. Chem.*, (2011), **46**, 1056.

[157] M.N. Drwal, K. Agama, L.P.G. Wakelin, Y. Pommier and R. Griffith, *PLoS ONE*, (2011), **6**, e25150.

[158] M. Ferraroni, W. Rypniewski, K.S. Wilson, M.S. Viezzoli, L. Banci, I. Bertini and S. Mangani, *J. Mol. Biol.*, (1999), **285**, 413.

[159] K.D. Carugo, A. Battistoni, M.T. Carri, F. Polticelli, A. Desideri, G. Rotilio, A. Coda and M. Bolognesi, *FEBS Lett.*, (1994), **349**, 93.

[160] M. Ye and A. M. English, *Biochemistry*, (2006), **45**, 12723.

[161] F. Kratz, *J. Control Release*, (2008), **132**, 171.

[162] T. Sen, S. Mandal, S. Haldar, K. Chattopadhyay and A. Patra, *J. Phys. Chem.*, (2011), **115**, 24037.

[163] M. Yokoyama, *J. Artif. Organs*, (2005), **8**, 77.

[164] V.T.G. Chuang, and U. Kragh–Hansen and M. Otagiri, *Pharm. Res.*, (2002), **19**, 569.

[165] R.K. Jain, *Cancer. Res.*, (1987), **47**, 3039.

[166] R. Haag and F. Kratz, *Angew., Chem., Int. Ed.*, (2006), **45**, 1198.

[167] B. Elsadek and F. Kratz, *Controlled Release*, (2012), **157**, 4.

[168] N. Shahabadi and M. Maghsudi, *J. Mol. Struc.*, (2009), **929**, 193.

[169] L. Trynda–Lemiesz, *Bioorg. Med. Chem.*, (2004), **12**, 3269.

[170] L.Z. Benet, and B.–A. Hoener, *Clin. Pharmacol. Ther.*, (2002), **71**, 115.

[171] W.H. Ang, E. Daldini, L. Juillerat–Jeanneret, and P.J. Dyson, *Inorg. Chem.*, (2007), **46**, 9048.

[172] (a) W.H. Ang, E. Daldini, C. Scolaro, R. Scopelliti, L. Juillerat–Jeannerat and P. Dyson, *J. Inorg. Chem.*, (2006), **45**, 9006 (b) W.H. Ang and P.J. Dyson, *Eur. J. Inorg. Chem.*, (2006), 4003. (c) P.J. Dyson and G. Sava, *Dalton Trans.*, (2006), 1929. (d) C. Gossens, A. Dorcier, P.J. Dyson and U. Rothlisberger, *Organometallics*, (2007), **26**, 3969.

[173] C.–Q. Jiang, M.–X. Gao, X.–Z. Meng, *Spectrochim. Acta Part A*, (2003), **59**, 1605.

[174] K. Abdi, S. Nafisi, F. Manouchehri, M. Bonsaii and A. Khalaj, *J. Photochem. Photobiol. B*, (2012), **107**, 20.

[175] M.–Y. Tian, X.–F. Zhang, L. Xie, J.–F. Xiang, Y.–L. Tang and C.–Q. Zhao, *J. Mol. Struct.*, (2008), **892**, 20.

[176] J. Tang, F. Luan and X. Chen, *Bioorgan. Med. Chem.*, (2006), **14**, 3210.

[177] A. Hanaki and A. Odani, *J. Inorg. Biochem.*, (2007), **101**, 1428.

[178] C.–Q. Jiang, M.–X. Gao and X.–Z. Meng, *Spectrochim. Acta A*, (2003), **59**, 1605.

[179] S. Hu, L. Zhang and N.J. Dovichi, *J. Chromatogr. A*, (2001), **924**, 369.

[180] S.F. Sun, S.W. Kuo and R.A. Nash, *J. Chromatogr.*, (1984), **288**, 377.

[181] Y. Yue , X. Chen, J. Qin and X. Yao, *Colloids Surf. B*, (2009), **69**, 51.

[182] T. Lemma and J. Pawliszyn, *J. Pharma. Biomed. Anal.*, (2009), **50**, 570.

[183] C.D. Geddes, *Meas. Sci. Technol.*, (2001), **12**, R53.

[184] T. Chatterjee, A. Pal, S. Dey, B.K. Chatterjee and P. Chakrabarti, *PLoS ONE,* (2012), **7**, e37468.

[185] T. Wang, B. Xiang, Y. Wang, C. Chen, Y. Dong, H. Fang and M. Wang, *Colloids Surf. B*, (2008), **65**, 113.

[186] W.K. Surewicz, J.H.H. Mantsch and D. Chapman, *Biochemistry,* (1993), **32**, 389.

[187] T. Förster, *Discuss. Faraday Soc.*, (1959) **27** ,7.

[188] S.S. Kalanur , J. Seetharamappa and V.K.A. Kalalbandi, *J. Pharma. Biomed. Analy.*, (2010), **53**, 660.

[189] B. Valeur and J. C. Brochon, *New Trends in Fluorescence Spectroscopy*, Springer, Berlin, (2001).

[190] F. Deng, C. Dong and Y. Liu, *Mol. BioSyst.*, (2012), **8**, 1446.

[191] J. Liu, Y. Yue, M. Liu, N. Zhang and K. Zhuo, *Spectrochim. Acta A*, (2011), **82**, 299.

[192] F.F. Tian, F.L. Jiang, X.L. Han, C. Xiang, Y.S. Ge, J.H. Li, Y. Zhang, R. Li, X.L. Ding and Y. Liu, *J. Phys.Chem. B*, (2010), **114**, 14842.

[193] J. Juárez, S.G. López, A. Cambón, P. Taboada and V. Mosquera, *J. Phys. Chem. B*, (2009), **113**, 10521.

[194] M.C.B. de Oliveira, M. Scarpellini, A. Neves, H. Terenzi, A.J. Bortoluzzi, B. Szpoganics, A. Greatti, A.S. Mangrich, E.M. de Souza, P.M. Fernandez and M.R. Soares, *Inorg. Chem.*, (2005), **44**, 921.

[195] F.J. Fard, Z.M. Khoshkhoo, H. Mirtabatabaei, M.R. Housaindokht, R. Jalal, H.E. Hosseini, M.R. Bozorgmehr, A.A. Esmaeili and M.J. Khoshkholgh, *Spectrochim .Acta A*, (2012), **97**, 74.

[196] V.C. da Silveira, G.F. Caramori,; M.P. Abbott, M.B. Gonçalves, H.M. Petrilli and A.M.C. Ferreira, *J. Inorg. Biochem.*, (2009), **103**, 1331.

[197] C. Piguet, G. Bernardinelli and G. Hopfgartner, *Chem. Rev.*, (1997), **97**, 2005.

[198] Siemens. SMART and SAINT, *Area Detector Control and Integration Software*., Siemens Analytical X–Ray Systems, Inc., Madison, Wisconsin, USA, (1996).

[199] Siemens, SHELXTL, Version 5 Reference Manual, Siemens Analytical X–ray Systems, Inc., Madison, Wisconsin, USA, (1996).

[200] G.M. Sheldrick, *Acta Cryst A.*, (2008), **64**,112.

[201] L.J. Farrugia, *J. Appl. Cryst.*, (1997), **30**, 565.

[202] J. Marmur, *J. Mol. Biol.*, (1961), **3**, 208.

[203] M.E. Reicmann, S. A. Rice, C. A. Thomas and P. Doty, *J. Am.Chem. Soc.*, (1954), **76**, 3047.

[204] S. Tabassum, W.M. Al–Asbahy, M. Afzal and F. Arjmand, *J. Photochem. Photobiol. B*, (2012), **114**, 132.

[205] A. Wolfe, G. H. Shimer and T. Meehan, *Biochemistry*, (1987), **26**, 6392.

[206] J.J. Stephanos, *J. Inorg. Biochem.*, (1996), **62**, 155.

[207] C. Liu, J. Zhou and H. Xu, *J. Inorg. Biochem.*, (1998), **71**, 1.

[208] G.D. Liu, J. P. Liao, Y.Z. Fang, S.S. Huang, G.L. Sheng and R.Q. Yu, *Anal. Sci.*, (2002), **18**, 391.

[209] E.F. Healy, *J. Chem. Educ.*, (2007), **84**, 1304.

[210] J.R. Lakowicz, *Principles of fluorescence spectroscopy*, 3rd ed., springer, USA, (2006) pp. 278.

[211] Y.H. Pang, L.L. Yang, S.M. Shuang, C. Dong and M.Thompson, *J. Photochem. Photobiol. B*, (2005), **80**, 139.

[212] P. Rajdev, T. Mondol, A. Makhal and S.K. Pal, *J. Photochem. Photobiol. B*, (2011), **103**, 153.

[213] J. Chakraborty, N. Das and U.C. Halder, *J. Photochem. Photobiol. B*, (2011), **102**, 1.

[214] A. Ray, B. Koley Seth, U. Pal and S. Basu, *Spectrochim. Acta A*, (2012), **92**, 164.

[215] T. Zohoorian–Abootorabi, H. Sanee, H. Iranfar, M.R. Saberi and J. Chamani, *Spectrochim. Acta A*, (2012), **88**, 177.

[216] (a) C.V. Kumar, A. Buranaprapuk, G.J. Opiteck, M.B. Moyer, S. Jockusch, N.J. Turro, *Proc. Natl. Acad. Sci. USA*, (1998), **95**, 10361 (b) A. Buranaprapuk, S.P. Leach, C.V. Kumar and J.R. Bocarsly, *Biochim. Biophys. Acta*, (1998), **1387**, 309.

[217] X.–Q. Chen, X.–J. Peng, J.–Y. Wang, Yan Wang, S. Wu, L.–Z. Zhang, T. Wu and Y.–K. Wu, *Eur. J. Inorg. Chem.*, (2007), 5400.

[218] S.H. van Rijt, A.F.A. Peacock, R.D.L. Johnstone, S. Parsons and P.J. Sadler, *Inorg. Chem.*, (2009), **48**, 1753.

[219] F. Caruso, C. Pettinari, F. Paduano, R. Villa, F. Marchetti, E. Monti and M. Rossi, *J. Med. Chem.*, (2008), **51**, 1584.

[220] T. Imanari, M. Hirota, M. Miyazaki, K. Hakayama and Z. Tamura, *Igaku–no–ayumi*, (1977), **101**, 496.

[221] D. Mustard and D.W. Ritchie, *Proteins*, (2005), **60**, 269.

[222] Y. Fujii, T. Kiss, T. Gajda, X.S.T.T. Sato, Y.N.Y. Hayashi and M. Yashiro, *J. Biol. Inorg. Chem.*, (2002), 7, 843.

[223] A.R. Paital, D. Mandal, X. Huang, J. Li, G. Aromı and D. Ray, *Dalton Trans.*, (2009), 1352.

[224] M. Bera, J. Ribas, W. T. Wong and D. Ray, *Inorg. Chem. Commun.*, (2004), 7, 1242.

[225] M.D.P. Brandi–Blanco, D. Choquesillo–Lazarte, A. Domínguez–Martín, J. M. González–Pérez, A. Castiñeiras and J. Niclós–Gutiérrez, *J. Inorg. Biochem.*, (2011), **105**, 616.

[226] J. Dehand, J. Jordanov, F. Keck, A. Mosset, J.J. Bonnet and J. Galy, *Inorg. Chem.*, (1979), **18**, 1543.

[227] M. Tiliakos, E. Katsoulakou, V. Nastopoulos, A. Terzis, C. Raptopoulou, P. Cordopatis and E. Manessi–Zoupa, *J. Inorg. Biochem.*, (2003), **93**, 109.

[228] E. Manessi–Zoupa, S.P. Perlepes, V. Hondrellis and J. M. Tsangaris, *J. Inorg. Biochem.*, (1994), **55**, 217.

[229] M. Tiliakos, E. Katsoulakou, V. Nastopoulos, A. Terzis, C. Raptopoulou, P. Cordopatis and E. Manessi–Zoupa, *J. Inorg. Biochem.*, (2003), **93**, 109.

[230] I.A. Koval, M. Sgobba, M. Huisman, M. Luken, E. Saint–Aman, P. Gamez, B Krebs and J. Reedijk, *Inorg. Chim. Acta.*, (2006), **359**, 4071.

[231] G. Verquin, G. Fontaine, E. Abi–Aad, E. Zhilinskaya, A. Aboukaıs and J.–L. Bernier, *J. Photochem. Photobiol. B*, (2007), **86**, 272.

[232] D. Kivelson and R. Neiman, *J. Chem. Phys.*, (1961), **35**, 149.

[233] S. Chandra and X. Sangeetika, *Spectrochim. Acta. Part A.*, (2004), **60**, 147.

[234] H. L. Chan, H.–Q. Liu, B.–C. Tzeng, Y.–S. You, S.–M. Peng, M. Yang and C.–M. Che, *Inorg. Chem.*, (2002), **41**, 3161.

[235] Y. Iwasaki, M. Kimura, A. Yamada, Y. Mutoh, M. Tateishi, H. Arii, Y. Kitamura and M. Chikira, *Inorg. Chem. Comm.*, (2011), **14**, 1461.

[236] J.K. Barton, A.T. Danishefsky and J.M. Goldberg, *J. Am. Chem. Soc.*, (1984), **106**, 2172.

[237] J. Olmsted III and D. R. Kearns, *Biochemistry.*, (1977), **16**, 3647.

[238] B.C. Baguley and M. L. Bret, *Biochemistry.*, (1984), **23**, 937.

[239] R. Indumathy, S. Radhika, M. Kanthimathi, T. Weyhermuller and B.U. Nair, *J. Inorg. Biochem.*, (2007), **101**, 434.

[240] V.I. Ivanov, L.E. Minchenkova, A.K. Schyolkina and A.I. Poletayer, *Biopolymers.*, (1973), **12**, 89.

[241] J. Rajesh, A. Gubendran, G. Rajagopal and P. Athappan, *J. Mol. Struct.*, (2012), **1010**, 169.

[242] S. Mahadevan and M. Palaniandavar, *Inorg. Chem.*, (1998), **37**, 693.

[243] D.–D. Li, J.–L. Tian, W. Gu, X. Liu, H.–H. Zeng and S.–P. Yan, *J. Inorg. Biochem.*, (2011), **105**, 894.

[244] D.–D. Li, J.–L. Tian, W. Gu, X. Liu, H.–H. Zeng and S.–P. Yan, *J. Inorg. Biochem.*, (2011), **105**, 894.

[245] V.G. Vaidyanathan and B.U. Nair, *J. Inorg. Biochem.*, (2003), **93**, 271.

[246] B. Montaner, W. Castillo–Avila, M. Martinell and R. Ollinger, J. Aymami, E. Giralt and R. Perez–Tomas, *Toxicol. Sci.*, (2005), **85**, 870.

[247] L.F. Chin, S.M. Kong, H.L. Seng, K.S. Khoo, R. Vikneswaran, S.G. Teoh, M. Ahmad, S.B.A. Khoo, M.J. Maah and C.H. Ng, *J. Inorg. Biochem.*, (2011), **105**, 339.

[248] I. Fridovich, *Annu. Rev. Biochem.*, (1975), **44**, 147.

[249] G. Facchin, M.H. Torre, E. Kremer, O.E. Piro, E.E. Castellano and E.J. Baran, *J. Inorg. Biochem.*, (2002), **89**, 174.

[250] A.L. Abuhijleh, *J. Inorg. Biochem.*, (1997), **68**,167.

[251] R. Rohs, I. Bloch, H. Sklenar and Z. Shakked, *Nucleic Acids Res.*, (2005), **33**, 7048.

[252] L.F.P.D. Castro and M. Zacharias, *J. Mol. Recognit.*, (2002), **15**, 209.

[253] R. Filosa, A. Peduto, S. Di Micco, P. de Caprariis, M. Festa, A. Petrella, G. Capranico and G. Bifulco, *Bioorg. Med. Chem.*, (2009), **17**, 13.

[254] B.L. Staker, M.D. Feese, M. Cushman, Y. Pommier, D. Zembower, L. Stewart and A.B. Burgin, *J. Med. Chem.*, (2005), **48**, 2336.

[255] H.T.M. Van and W.–J. Cho, *Bioorg. Med. Chem. Lett.*, (2009), **19**, 2551.

[256] X.S. Xiao and M. Cushman, *J. Am. Chem. Soc.*, (2005), **127**, 9960.

[257] Y. Pommier, *Nat. Rev. Cancer.*, (2006), **6**, 789.

[258] W.R. Rypniewski, S. Mangani, B. Bruni, P.L. Orioli, M. Casati and K.S.Wilson, *J. Mol. Biol.*, (1995), **251**, 282.

[259] J. A. Tainer, E. D. Getzoff, J. S. Richardson and D. C. Richardson, *Nature.*, (1983), **306**, 284.

[260] S. Tabassum, W.M. Al–Asbahy, M. Afzal, F. Arjmand and V. Bagchi, *Dalton Trans.*, (2012), **41**, 4955.

[261] Y.–J. Hu, Y. Liu and L.–X. Zhang, R.–M. Zhao and S.–S. Qu, *J. Mol. Struct.*, (2005), **750**, 174.

[262] O. K. Abou–Zied and O. I. K. Al–Shihi, *J. Am. Chem. Soc.*, (2008), **130**, 10793.

[263] X.Z. Feng, C.L. Bai and Z. Lin, *Anal. Chem.*, (1998), **26**, 154.

[264] W. Song, M.Z. Ao, Y. Shi, L.F. Yuan, X.X. Yuan and L.J. Yu, *Spectrochim. Acta A*, (2012), **85**, 120.

[265] Y. Sun, Z. Ji, X. Liang, G. Li, S. Yang, S. Wei, Y. Zha, X. Hu and J. Fan, *Spectrochim. Acta A*, (2012), **87**, 171.

[266] G. Zhang, Q. Que, J. Pan and J. Guo, *J. Mol. Struct.*, (2008), **881**, 132.

[267] S. Bi, L. Ding, Y. Tian, D. Song, X. Zhou, X. Liu and H. Zhang, *J. Mol. Struct.*, (2004), **703**, 37.

[268] T. Förster, *Annalen der Physik*, (1948), **437**, 55.

[269] B. Honore and A. Perdersen, *Biochem. J.*, (1989), **258**, 199.

[270] J.–L. Yuan, Z. lv, Z.–G. Liu, Z. Hu and G.–L. Zou. *J. Photochem.Photobiol. A.*, (2007), **191**, 104.

[271] W. He, Y. Li, C. Xue, Z. Hu, X. Chen and F. Sheng, *Bioorg. Med. Chem.*, (2005), **13**, 1837.

[272] T. Maruyama, C.C. Lin, K. Yamasaki, T. Miyoshi, T. Imai, M. Yamasaki and M. Otagiri, *Biochem. Pharm.*, (1993), **45**, 1017.

[273] L. Trynda–Lemiesz, A. Karaczyn, B.K. Keppler and H. Kozlowski, *J. Inorg. Biochem.*, (2000), **78**, 341.

[274] X. Wu, J. Liu, Q. Wang, W. Xue, X. Yao, Y. Zhang and J. Jin, *Spectrochim.Acta A*, (2011), **79**, 1202.

[275] Y. Li, W.Y. He, Y.M. Dong, F. Shenga and Z.D. Hu, *Bioorg. Med. Chem.*, (2006), **14**, 1431.

[276] M.J. Rigueguez–Cuesta, R. Boqué,; F.X. Rius, D.P. Zamora, M.M. Galera and A.G. Frenich, *Anal. Chim. Acta*, (2003), **491**, 47.

[277] Y.–Z .Zhang,; B. Zhou, Y.–X. Liu, C.–X. Zhou, X.–L. Ding and Y. Liu, *J. Fluoresc.*, (2008), **18**, 109.

[278] (a) M.C.B. de Oliveira, M. Scarpellini, A. Neves, H. Terenzi, A.J. Bortoluzzi, B. Szpoganics, A. Greatti, S. Hangrich, E.M. de Souza, P.M. Fernandez and M.R. Soares, *Inorg. Chem.*, (2005), **44**, 921. (b) V. Rajendiran,; M. Palaniandavar, P. Swaminathan and L.Uma, *Inorg. Chem.*, (2007), **46**, 10446.

[279] G.K. Goswami, M. Roy, M. Nethaji and A.R. Chakravarty, *Organometallics*, (2009), **28**, 1992.

[280] T. Lammers, P. Peschke, V. Ehemann, J. Debus, B. Slobodin, S. Lavi and P. Huber, *Molecular Cancer*, (2007), **6**, 65.

[281] J. Tang, F. Luan and X. Chen, *Bioorg. Med. Chem.*, (2006), **14**, 3210.

[282] R.J.H. Clark and C.S. Williams, *Inorg. Chem.*, (1965), **4**, 350.

[283] J. Dehand, J. Jordanov, F. Keck, A. Mosset, J. J. Bonnet and J. Galy, *Inorg. Chem.*, (1979), **18**, 1543.

[284] M.S. Refat and S. F. Mohamed, *Spectrochim. Acta A*, (2011), **82**, 108.

[285] A.A. Soliman, *Spectrochim. Acta A*, (2006), **65**, 1180.

[286] H.–D. Yin, Q.–B. Wang and S.–C. Xue, *J. Organmet. Chem.*, (2004), **689**, 2480.

[287] D. Arish and M.S. Nair, *J. Mol. Struct.*, (2010), **983**, 112.

[288] M.T.B. Luiz, B. Szpoganicz, M. Rizzoto, M.G. Basallote and A.E. Martell, *Inorg. Chim. Acta*, (1999), **287**, 134.

[289] J. Liu, T. Zhang, T. Lu, L. Qu, H. Zhou, Q. Zhang and L. Ji, *J. Inorg. Biochem.*, (2002), **91**, 269.

[290] U. Chaveerach, A. Meenongwa, Y. Trongpanich, C. Soikum and P. Chaveerach, *Polyhedron*, (2010), **29**, 731.

[291] Q. Li, P. Yang and H. Wang, M. Guo, *J. Inorg. Biochem.*, (1996), **64**, 181.

[292] T. Matsubara and K. Hirao, *J. Mol. Struct. (Theochem.)*, (2002), **581**, 203.

[293] F. Arjmand and M. Muddassir, *J. Photochem. Photobiol. B*, (2010), **101**, 37.

[294] M. Chauhan and F. Arjmand, *J. Organomet. Chem.*, (2007), **692**, 5156.

[295] C.G. Reinhardt and T.R. Krugh, *Biochemistry*, (1978), **17**, 4845.

[296] J.G. Duguid, V.A. Bloomfield, J.M. Benevides and G.J. Thomas, Jr, *Biophy. J.*,(1995), **96**, 2623.

[297] A.M. Polyanichko, V.V. Andrushchenko, E.V. Chikhirzhina, V.Vorobev and H. Wieser, *Nucleic Acids Res.*, (2004), **32**, 989.

[298] J. Mier–Vinue, J. Lorenzo, A.M. Montana, V. Moreno and F.X. Aviles, *J. Inorg. Biochem.*, (2008), **102**, 973.

[299] K. Karidi, A. Garoufis, N. Hadjiliadis and J. Reedijk, *Dalton Trans.*, (2005), 728.

[300] J.–H. Li, J.–T. Wang, L.–Y.Zhang, Z.–N. Chen, Z.–W. Mao and L.–N. Ji, *Inorg. Chim. Acta*, (2009), **362**, 1918.

[301] N. Raman, R. Jeyamurugan, R. Senthilkumar, B. Rajkapoor and S.G. Franzblau, *Eur. J. Med. Chem.*, (2010), **45**, 5438.

[302] C.A. Detmer III, F.V. Pamatong and J.R. Bocarsly, *Inorg. Chem.*, (1997), **36**, 3676.

[303] M. Komiyama, N. Takeda and H. Shigekawa, *Chem. Commun.*, (1999) 1443.

[304] P.U. Maheswari, S. Barends, S. Ozalp–Yaman, P. de Hoog, H. Casellas, S.J. Teat, C. Massera, M. Lutz, A.L. Spek, G.P. van Wezel, P. Gamez and J. Reedijk, *Chem. Eur. J.*, (2007), **13**, 5213.

[305] D. Mandal, M. Chauhan, F. Arjmand, G. Aromi and D. Ray, *Dalton Trans.*, (2009), 9183.

[306] G.M. Morris, D. S. Goodsell, R.S. Halliday, R. Huey, W.E. Hart, R.K. Belew and A.J.J. Olson, *Comp. Chem.*, (1998), **19**, 1639.

[307] V.M. Miskowski, J.A. Thich, R. Solomon and H.J. Schugar, *J. Am. Chem. Soc.*, (1976), **98**, 8344.

[308] M.R. Udupa and B. Krebs, *Inorg. Chim. Acta*, (1978), **31**, 251.

[309] D.W. Smith, *Coord. Chem. Rev.*, (1976), **21**, 93.

[310] J.F. Pearson and M. A. Slifkin, *Spectrochim. Acta A*, (1972), **28**, 2403.

[311] G.B. Deacon and R.J. Phillips, *Coord. Chem. Rev.*, (1980), **33**, 227.

[312] J. Moncol, M. Mudra, P. Lönnecke, M. Hewitt, M. Valko, H. Morris, J. Svorec, M. Melnik, M. Mazur and M. Koman, *Inorg. Chim. Acta,* (2007), **360**, 3213.

[313] D. Kivelson and R. Neiman, *J. Chem. Phys.*, (1961), **35**, 149.

[314] A. Sułkowska, B. Bojko, J. Rownicka and W.W. Sułkowski, *J. Mol. Struct.*, (2006), **792–793**, 249.

[315] L. Trynda–Lemiesz, B.K. Keppler and H. Koztowski, *J. Inorg. Biochem.*, (1999), **73**, 123.

[316] D. Silva, C.M. Cortez, J.C. Bastos and S.R.W Louro, *Toxicol. Lett.*, (2004), **147**, 53.

[317] P.D. Ross and S. Subramanian, *Biochemistry,* (1981), **20**, 3096.

[318] Z. Hongwei, G. Min, Z. Zhaoxia, W. Wenfeng and W. Guozhong, *Spectrochim. Acta A*, (2006), **65**, 811.

[319] P.B. Kandagal, S. Ashoka, J. Seetharamappa, S.M.T. Shaikh, Y. Jadegoud, O.B. Ijare, *J. Pharm. Biomed. Anal.*, (2006), **41**, 393.

[320] I. Matei and M. Hillebrand, *J. Pharma. Biomed. Anal.*, (2010), **51**, 768.

[321] Z. Cheng, *Spectrochim. Acta A*, (2012), **93**, 321.

[322] R.S. Kumar, K. Sasikala and S. Arunachalam, *J. Inorg. Biochem.*, (2008), **102**, 234.

[323] A.S. Potapov and A.I. Khlebnikov, *Polyhedron*, (2006), **25**, 2683.

[324] K.H. Thebo, H.A. Shad, M.A. Malik and M. Helliwell, *J. Mol. Struct.*, (2010), **970**, 75.

[325] K. Nakamoto, *John Wiley and Sons*, New York, N Y., (2008).

[326] M. Hong, K. Zhang, Y.–Z. Li and J. Zhu, *Polyhedron*, (2009), **28**, 445.

[327] D.C. Onwudiwe, P.A. Ajibade and B. Omondi, *J. Mol. Struct.*, (2011), **987**, 58.

[328] I.H. Bhat and S. Tabassum, *Spectrochim. Acta A*, (2009),**72**, 1026.

[329] S. Youngme, N. Wannarit, C. Pakawatchai, N. Chaichit, E. Somsook, U. Turpeinen and I. Mutikainen, *Polyhedron*, (2007), **26**, 1459.

[330] N. Dixit, R.K. Koiri, B.K. Maurya, S.K. Trigun, C. Höbartner and L. Mishra, *J. Inorg. Biochem.*, (2011), **105**, 256.

[331] R. Eshkourfu, B. Čobeljić, M. Vujčić, I. Turel, A. Pevec, K. Sepčić, M. Zec, S. Radulović, T. Srdić–Radić, D. Mitić, K. Andjelković and D. Sladić, *J. Inorg. Biochem.*, (2011), **105**, 1196.

[332] F. Arjmand and F. Sayeed, *J. Mol. Struct.*, (2010), **965**, 14.

[333] C.S. Chow, J. K. Barton, *Methods Enzymol.*, (1992), **212**, 219.

[334] A. Raja, V. Rajendiran, P.U. Maheswari, R. Balamurugan, C.A. Kilner, M.A. Halcrow and M. Palaniandavar, *J. Inorg. Biochem.*, (2005), **99**, 1717.

[335] F. Arjmand, F. Sayeed and S. Parveen, *J. Organomet. Chem.*, (2011), **696**, 3836.

[336] P. Yang and M. Guo, *Metal–Based Drugs*, (1998), **5**, 41.

[337] A.E. Friedman, C.V. Kumar, N.J. Turro and J.K. Barton, *Nucleic Acids Res.*, (1991), **19**, 2595.

[338] F. Liu, K. Wang, G. Bai, Y. Zhang and L. Gao, *Inorg. Chem.* (2004), **43**, 1799.

[339] X. Lu, K. Zhu, M. Zhang, H. Liu and J. Kang, *J. Biochem. Biophys. Methods,* (2002), **52**, 189

[340] S.M. Nelson, L.R. Ferguson and W.A. Denny, *Mutation Research*, (2007), **623**, 24.

[341] B. Selvakumar, V. Rajendiran, P.U. Maheswari, H.S. Evans and M. Palaniandavar, *J. Inorg.Biochem.*, (2006), **100**, 316.

[342] V. Brabec and O. Novakova, *Drug Resist. Updates,* (2006), **9**, 111.

[343] A. Klanicová, J.D. Houck, P.Baran and Z. Trávnícek, *Inorg. Chim. Acta*, (2012), **384**, 47.

[344] L. Naso, A.C.G. Baró, L. Lezama, T. Rojo, P.A.M. Williams and E.G. Ferrer, *J. Inorg. Biochem.*, (2009), **103**, 219.

[345] R.N. Patel, N. Singh, K.K. Shukla, U.K. Chauhan, J. Niclos–Gutierrez and A. Castineiras, *Inorg. Chim. Acta*, (2004), **357**, 2469.

[346] K. Midorikawa and S. Kawanishi, *FEBS Lett.*, (2001), **495**, 187.

[347] N.V. Nagy, T. Szabo–Planka, G. Tircso, R. Kiraly, Z. Arkosi, A. Rockenbauer and E. Brucher, *J. Inorg. Biochem.*, (2004), **98**, 1655.

[348] S. Ilhan and H. Temel, *J. Mol. Struct.*, (2008), **891**, 157.

[349] (a) B.Y.K. Ho and J.J. Zuckerman, *Inorg. Chem.*, (1973), **12**, 1552. (b) K. Moore and G.S. Vigee, *Inorg. Chim. Acta*, (1984), **91**, 53.

[350] A.A. Jarzeücki, A.D. Anbar and T.G. Spiro, *J. Phys. Chem. A*, (2004), **108**, 2726.

[351] C.A. Bolos, G.S. Niokolov, L. Ekateriniadou, A. Kortsaris and D.A. Kyriakadis, *Metal Based Drugs*, (1998), **5**, 323.

[352] C. Ma, Y. Han and R. Zhang, D. Wang, *Dalton Trans.*, (2004), 1832.

[353] L. Yao, L. Wang, J. Zhang, N. Tang and J. Wu, *J. Mol. Catal. A*, (2012), **352**, 57.

[354] D.K. Dey, M.K. Saha, M.K. Das, N. Bhartiya, R.K. Bansal, G. Rosair and S. Mitra, *Polyhedron*, (1999), **18**, 2687.

[355] G. Verquin, G. Fontaine, E. Abi–Aad, E. Zhilinskaya, A. Aboukaıs and J.–L. Bernier, *J. Photochem. Photobiol. B*, (2007), **86**, 272.

[356] P.U. Maheswari, F. Hartl, M. Quesada, F. Buda, M. Lutz, A.L. Spek, P. Gamez and J. Reedijk, *Inorg. Chim. Acta*, (2011), **374**, 406.

[357] (a) Y. Mantri, S. J. Lippard and M–H. Baik, *J. Am. Chem. Soc.*, (2007), **129**, 5023. (b) P.M. Krishna, K.H. Reddy, P.G. Krishna and G.H. Phillip, *Ind. J. Chem.*, (2007), **46A**, 904.

[358] (a) R.M. Scheek, R. Boelens, N. Russo, J.H. van Boom and R. Kaptein, *Biochemistry*, (1984), **23**, 1371. (b) M. Piotto, V. Saudek and V. Sklenar, *Biomol NMR.*, (1992), **2**, 661.

[359] G. Gasmi, M. Pasdeloup, G. Pratviel, M. Pitie, J. Bernadou and B. Meunier, *Nucl. Acids Res.*, (1991), **19**, 2835.

[360] G.–D. Liu, J.–P. Liao, S.–S. Huang, G.–L. Shen and R.–Q. Yu, *Anal. Sci.*, (2001), **17**, 1031.

[361] J.–H. Xu, F.–J. Chen, P.–X. Xi, X.–H. Liu and Z.–Z. Zeng, *J. Photochem. Photobiol. A.*, (2008), **196**, 77.

[362] F. Arjmand, S. Parveen, M. Afzal, L. Toupet and T.B. Hadda, *Eur. J. Med. Chem.*, (2012), **49**, 141.

[363] J.–Z. Wu, L. Yuan and Jian–Fang Wu, *J. Inorg. Biochem.*, (2005), **99**, 2211.

[364] K. Karidi, A. Garoufis, A. Tsipis, N. Hadjiliadis, H. Dulk and J. Reedijk, *Dalton Trans.*, (2005), 1176.

[365] E. Trotta, N.D. Grosso, M. Erba and M. Paci, *Biochemistry*, (2000), **39**, 6799.

[366] P. Wittung, P. Nielsen and B. Norden, *J. Am. Chem. Soc.*, (1996), **118**, 7049.

[367] K.J. Humphreys, K.D. Karlin and S.E. Rokita, *J. Am. Chem. Soc.*, (2002), **124**, 8055.